

The Official Journal of the Chinese Stomatological Association (CSA)



Chinese Journal of Dental Research

CJDR

V
O
L
U
M
E

26

**2
0
2
3**

N
U
M
B
E
R

4



ANCORA
IMPARO

all rights reserved

向世界巅峰大师学习

**NAZARIY
MYKHAYLYUK**

纳扎利·米哈伊留克

NUNO SOUSA DIAS
努诺·索撒·迪亚斯

GUSTAVO GIORDANI
古斯塔沃·乔尔达尼

**GIOVANNI
ZUCHELLI**

乔瓦尼·祖凯利

OTTO ZUHR
奥托·祖尔

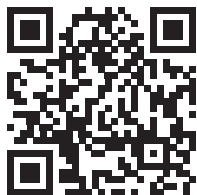
王鸿烈

HOM LAY WANG

三大师峰会

22 - 27 FEB 2024 | KL CONVENTION CENTRE

THE 3 MASTERS™



**SCAN FOR
MORE INFO**

<https://rb.gy/oqf13>



QUINTESSENCE PUBLISHING



straumann



HENRY SCHEIN®



Chinese Journal of Dental Research

The Official Journal of the Chinese Stomatological Association (CSA)



Chinese Journal of Dental Research

The Official Journal of the Chinese Stomatological Association (CSA)

Review

- 195 Research Models in Dentine Development and Regeneration
Ya Lu SUN, Xi Heng LI, Shuang Shuang WANG, Hu En LI, Bei CHANG, Hong Chen SUN
- 209 Mouse Models of Orofacial Clefts: SHH and TGF- β Pathways
Yu Chen LI, Le Ran LI, Zi Han GAO, Yi Ran YANG, Qian Chen WANG, Wei Yu ZHANG, Li Qi ZHANG, Tian Song XU, Feng CHEN

Original Article

- 227 Effect of Intact Periosteum on Alveolar Ridge Contour Stability after Horizontal Guided Bone Regeneration in the Posterior Region: a Retrospective and Radiographical Cohort Study
Deng Hui DUAN, Hom Lay WANG, En Bo WANG
- 235 Sixteen Cellular Senescence-associated DNA Methylation Signature Predicts Overall Survival in Patients with Head and Neck Squamous Cell Carcinoma
Ming Han YE, Xin Yi HUANG, Chun Jie LI, Qian Ju WU, Fei LIU
- 249 Evaluation of Sealer Remnants Using a Bioceramic Sealer Single-cone Technique after Post Space Preparation and its Influence on the Adhesion of Fibre Posts in vitro
Di QIAO, Meng Meng ZHU, Jie PAN
- 257 Comparison of Powered versus Manual Tooth Brushing for Safety and Efficacy in Patients with Gingivitis: A Randomised, Multicentre Clinical Trial in China
Dan Ying TAO, Yan SI, Tao HU, Shu Guo ZHENG, Han JIANG, Ye TAO, Yan ZHOU, Fang Zhi ZHU, Bao Jun TAI, Xi Ping FENG



Case report

- 265 Clear Cell Renal Cell Carcinoma Metastatic to the Mandible: a Unique Case Report and Literature Review
Xiao Fei HUANG, Zi Li YU

CSA guideline

- 271 Guideline for the Diagnosis and Clinical Management of Oral Submucous Fibrosis
Society of Oral Medicine, Chinese Stomatological Association

Chinese Journal of Dental Research

CN 10-1194/R • ISSN 1462-6446 • eISSN 1867-5646 • Quarterly

The Official Journal of the Chinese Stomatological Association

Co-sponsor: Peking University School of Stomatology, Quintessenz Verlag

Editor-in-Chief

Chuan Bin GUO Beijing, P.R. China

Chief-Editor Emeritus

Zhen Kang ZHANG Beijing, P.R. China
Xing WANG Beijing, P.R. China
Xu Chen MA Beijing, P.R. China
Guang Yan YU Beijing, P.R. China
Xue Dong ZHOU Chengdu, P.R. China

Executive Associate Editor

Qian Ming CHEN Hangzhou, P.R. China

Executive Editors

Ye Hua GAN Beijing, P.R. China
Hong Wei LIU Beijing, P.R. China

Associate Editors

Li Juan BAI Beijing, P.R. China
Zhuan BIAN Wuhan, P.R. China
Fa Ming CHEN Xi'an, P.R. China
Bin CHENG Guangzhou, P.R. China
Xu Liang DENG Beijing, P.R. China
Xin Quan JIANG Shanghai, P.R. China
Tie Jun LI Beijing, P.R. China
Hong Chen SUN Changchun, P.R. China
Song Ling WANG Chengdu, P.R. China
Ling YE Beijing, P.R. China
Zhi Yuan ZHANG Shanghai, P.R. China
Yi Min ZHAO Xi'an, P.R. China
Yong Sheng ZHOU Beijing, P.R. China

Editorial Board

Tomas ALBREKTSSON

Gothenburg, Sweden

Conrado APARICIO

Barcelona, Spain

Daniele BOTTICELLI

Rimini, Italy

Lorenzo BRESCHI

Bologna, Italy

Francesco CAIRO

Florence, Italy

Tong CAO

Singapore

Jack G. CATON

Rochester, USA

Yang CHAI

Los Angeles, USA

Wan Tao CHEN

Shanghai, P.R. China

Zhi CHEN

Wuhan, P.R. China

Bruno CHRCANOVIC

Malmö, Sweden

Kazuhiro ETO

Tokyo, Japan

Bing FAN

Wuhan, P.R. China

Zhi Peng FAN

Beijing, P.R. China

Alfio FERLITO

Udine, Italy

Roland FRANKENBERGER

Marburg, Germany

Xue Jun GAO

Beijing, P.R. China

Sufyan GAROUSHI

Turku, Finland

Reinhard GRUBER

Vienna, Austria

Gaetano ISOLA

Catania, Italy

Søren JEPSEN

Bonn, Germany

Li Jian JIN

Hong Kong SAR, P.R. China

Yan JIN

Xi'an, P.R. China

Newell W. JOHNSON

Queensland, Australia

Thomas KOCHER

Greifswald, Germany

Ralf-Joachim KOHAL

Freiburg, Germany

Niklaus P. LANG

Bern, Switzerland

Junying LI

Ann Arbor, USA

Yi Hong LI

New York, USA

Wei LI

Chengdu, P.R. China

Huan Cai LIN

Guangzhou, P.R. China

Yun Feng LIN

Chengdu, P.R. China

Hong Chen LIU

Beijing, P.R. China

Yi LIU

Beijing, P.R. China

Edward Chin-Man LO

Hong Kong SAR, P.R. China

Jeremy MAO

New York, USA

Tatjana MARAVIC

Bologna, Italy

Claudia MAZZITELLI

Bologna, Italy

Mark MCGURK

London, UK

Li Na NIU

Xi'an, P.R. China

Jan OLSSON

Gothenburg, Sweden

Gaetano PAOLONE

Milan, Italy

No-Hee PARK

Los Angeles, USA

Peter POLVERINI

Ann Arbor, USA

Lakshman SAMARANAYAKE

Hong Kong SAR, P.R. China

Keiichi SASAKI

Miyagi, Japan

Zheng Jun SHANG

Wuhan, P.R. China

Song SHEN

Beijing, P.R. China

Song Tao SHI

Guangzhou, P.R. China

Richard J. SIMONSEN

Downers Grove, USA

Manoel Damião de

SOUSA-NETO

Ribeirão Preto, Brazil

John STAMM

Chapel Hill, USA

Lin TAO

Chicago, USA

Tiziano TESTORI

Ann Arbor, USA

Cun Yu WANG

Los Angeles, USA

Hom-Lay WANG

Ann Arbor, USA

Zuo Lin WANG

Shanghai, P.R. China

Heiner WEBER

Tuebingen, Germany

Xi WEI

Guangzhou, P.R. China

Yan WEI

Beijing, P.R. China

Ray WILLIAMS

Chapel Hill, USA

Jie YANG

Philadelphia, USA

Quan YUAN

Chengdu, P.R. China

Jia Wei ZHENG

Shanghai, P.R. China

Publication Department

Production Manager: Megan Platt (London, UK)

Managing Editor: Xiao Xia ZHANG (Beijing, P.R. China)

Address: 4F, Tower C, Jia 18#, Zhongguancun South Avenue, HaiDian District, 100081, Beijing, P.R. China.

Tel: 86 10 82195785, **Fax:** 86 10 62173402

Email: editor@cjdrcsa.com

Manuscript submission: Information can be found on the Guidelines for Authors page in this issue. To submit your outstanding research results more quickly, please visit: <http://mc03.manuscriptcentral.com/cjdr>

Administrated by: China Association for Science and Technology

Sponsored by: Chinese Stomatological Association and Popular Science Press

Published by: Popular Science Press

Printed by: Beijing ARTRON Colour Printing Co Ltd

Subscription (domestically) by Post Office

Chinese Journal of Dental Research is indexed in MEDLINE.

For more information and to download the free full text of the issue, please visit www.quint.link/cjdr
<http://www.cjdrcsa.com>

Acknowledgements

We would like to express our gratitude to the peer reviewers for their great support to the journal in 2022.

- | | | |
|--|-------------------------------------|-----------------------------------|
| Abi Rached-Junior, Fuad Jacob (Brazil) | Hajeer, Mohammad Y. (Syrian Arab) | Özel, Şelale (Turkiye) |
| Al-Nuaimi, Nassr (United States) | Hou, Ben Xiang (China) | Pan, Shao Xia (China) |
| Ashour, Hossam M. (United States) | Huang, Ding Ming (China) | Pertek Hatipoglu, Fatma (Turkiye) |
| Baeza, Mauricio (Chile) | Huang, Xiao Bin (United States) | Piagkou, M. (Greece) |
| Banoon, Shaima (Iraq) | Huang, Xiao Jing (China) | Pradies, Guillermo (Spain) |
| Baraka, Osama (Egypt) | Jiang, Xin Quan (China) | Rong, Qi Guo (China) |
| Benson, Philip E. (United Kingdom) | Jin, Zuo Lin (China) | Saito, Hanae (United States) |
| Bolbolian, Marjan (Iran) | Kau, Chung How (United States) | Sarialioglu Gungor, Ayça (Turkey) |
| Bulut, Sule (Turkiye) | Kavitha G. (India) | Shao, Jin Long (China) |
| Cai, Zhi Gang (China) | Kou, Xiao Xing (China) | Si, Yan (China) |
| Canullo, Luigi (Switzerland) | Kurtulmus-Yilmaz, Sevcan (Turkiye) | Silva, Erick Ricardo (Brazil) |
| Cao, Huojun (United States) | Lai, Wen Li (China) | Sun, Yu Chun (China) |
| Chen, Fa Ming (China) | Lapinska, Barbara (Poland) | Tallarico, Marco (Italy) |
| Chen, Feng (China) | Lee, Jong-Ho (Korea) | Tosun, Büsra (Turkiye) |
| Chen, Ji Hua (China) | Li, Gang (China) | Tzanetakakis, Giorgos N. (Greece) |
| Chen, Peng (China) | Li, Guo Ju (China) | Uzunoglu-Ozyurek, Emel (Turkey) |
| Cheng, Yong (China) | Li, Tie Jun (China) | Wang, Chin-Wei (United States) |
| Chrcanovic, Bruno Ramos (Sweden) | Li, Xuefeng (United States) | Wang, Chun Xiao (China) |
| Clark, Wendy Auclair (United States) | Li, Ze Han (China) | Wang, Xiao Yan (China) |
| Contreras, Adolfo (Colombia) | Li, Zhi Min (China) | Wang, Yi Xiang (China) |
| Dede, Dogu Omur (Turkiye) | Liu, Da Wei (China) | Xie, Hai Feng (China) |
| Deng, Peng (United States) | Liu, Deng Gao (China) | Xu, Li (China) |
| Deng, Xu Liang (China) | Liu, Xue Nan (China) | Xu, Tian Min (China) |
| Du, Rennan Yanlin (China) | Liu, Yan (China) | Yang, Jie (United States) |
| El-Abd, Mohammed (Kuwait) | Liu, Yao (China) | Yang, Yan Qi (China) |
| Erdemir, Uğur (Turkiye) | Luan, Qing Xian (China) | Yu, Xi Jiao (China) |
| Fan, Yuan (China) | Mashyakhy, M (Saudi Arabia) | Zhang, Cheng Fei (China) |
| Fang, Bing (China) | Mei, Lei (China) | Zhang, Lei (China) |
| Faustino-Silva, Daniel Demetrio (Brazil) | Meng, Jia Lin (China) | Zhang, Lei (China) |
| Gao, Xue Jun (China) | Menini, Maria (Italy) | Zhang, Ling Lin (China) |
| Gao, Xue Mei (China) | Micheline, Daniela (United Kingdom) | Zhang, Wei Guang (China) |
| Gao, You Shui (China) | Niu, Li Na (China) | Zhao, Irene Shuping (China) |
| Gu, Yan (China) | Ocak, Mevlüt Sinan (Turkiye) | Zheng, Ning Bo (China) |
| | Oktay, Husamettin (Turkiye) | Zheng, Shu Guo (China) |
| | | Zhou, Shuang Ying (China) |

Editorial Office
Chinese Journal of Dental Research

Research Models in Dentine Development and Regeneration

Ya Lu SUN^{1#}, Xi Heng LI^{1#}, Shuang Shuang WANG², Hu En LI¹, Bei CHANG¹,
Hong Chen SUN¹

Dentine is a major component of teeth and is responsible for many of their functions, such as mastication and neural sensation/transduction. Over the past decades, numerous studies have focused on dentine development and regeneration using a variety of research models, including in vivo, ex vivo and in vitro models. In vivo animal models play a crucial role in the exploration of biochemical factors that are involved in dentine development, whereas ex vivo and in vitro models contribute mainly to the identification of biophysical factors in dentine regeneration, of which mechanical force is most critical. In the present review, research models involved in studies related to dentine development and regeneration were screened from publications released in recent years and summarised comprehensively, particularly in vivo animal models including prokaryotic microinjection, Cre/LoxP, CRISPR/Cas9, ZFN and TALEN, and scaffold-based in vitro and ex vivo models. The latter were further divided by the interactive forces. Summarising these research models will not only benefit the development of future dentine-related studies but also provide hints regarding the evolution of novel dentine regeneration strategies.

Key words: dentine development, dentine regeneration, research models, scaffolding system, transgenic mice
Chin J Dent Res 2023;26(4):195–208; doi: 10.3290/j.cjdr.b4784033

As the major component of teeth, dentine is responsible for various functions such as enamel support, pulp protection, neural sensation and transduction; however, due to caries lesions, trauma and abrasion, dentine loss has become one of the most common issues in den-

tal clinical work, leading to dentine hypersensitivity, occlusion deficiency and even changes in countenance. To deal with these problems, artificially synthesised materials such as resins or ceramic prostheses are usually employed, but although these materials manage to restore the appearance and some of the functions of dentine, they fail to reconstruct the sensation of the dentine–pulp complex, and their long-term effects are not guaranteed^{1,2}. Therefore, functional regeneration of dentine is still required and is of critical importance.

To perform functional dentine regeneration, it is vital to recognise the key factors involved in dentine development. Dentine development is known to be a complicated and delicate biological process. At different stages, regulatory biochemical factors vary regarding their types, expression patterns and rendered effects. For example, Runx2 is upregulated in the early stages of dentine development and downregulated in the later stages, whereas osterix is continuously and highly expressed at all stages of dentine development³. Thus, dentine development involves a series of genetic

-
- 1 Jilin Provincial Key Laboratory of Tooth Development and Bone Remodelling, Hospital of Stomatology, Jilin University, Changchun, P.R. China.
 - 2 Department of Oral Pathology, School and Hospital of Stomatology, China Medical University, Shenyang, P.R. China.
- # These two authors contributed equally to this work.

Corresponding authors: Dr Bei CHANG and Dr Hong Chen SUN, Hospital of Stomatology, Jilin University, #763 Huguang Road, Changchun 130021, Jilin Province, P.R. China. Tel: 86-431-85579567. Email: bchang@jlu.edu.cn; hcsun@jlu.edu.cn

This work is supported by the Young Elite Scientists Sponsorship Programme by CAST (YESS20210407), Natural Science Foundation of China (82101075), China Postdoctoral Science Foundation (2022M711301) and the Science and Technology Project of Jilin Provincial Department of Finance (JCSZ2021893-27).

modulations and activation/inactivation of signalling pathways that comprise an elaborate regulatory network. A careful illustration of this network will aid not only the prevention and treatment of dentine-related developmental diseases but also the functional reparation or regeneration of dentine.

In addition to biochemical cues, understanding of the fact that biophysical factors also contribute to dentine development and regeneration has increased in recent decades. It is widely known that in regenerative strategies, the biophysical characteristics of a scaffold determine the accommodating niche of stem cells and the release profiles of growth factors⁴. Meanwhile, during dentine development, the biophysical cues also participate in the commitment of the dental mesenchyme. For example, a study proposed that mesenchyme condensation in the dental papilla initiated odontogenesis⁵.

Research models are generally divided into *in vivo*, *ex vivo* and *in vitro*. Exploration of the biochemical network usually requires a combination of animal models and subsequent *in vitro* or *ex vivo* confirmation, among which animal models play the most vital role. Numerous studies focusing on dentine development have employed this approach and proven the effects of dentine sialophosphoprotein (DSPP), bone morphogenetic proteins (BMPs) and transforming growth factors (TGFs), etc. In the meantime, studies of biophysical cues in dentine regeneration and reparation depend largely on *ex vivo* and *in vitro* approaches. In particular, the development of novel biofabrication approaches such as micropatterning⁶ and mathematical modelling approaches^{7,8} have vastly facilitated these studies.

Thus, all three models supplement each other and work together to improve knowledge regarding dentine development and reparation; however, to the best of the present authors' knowledge, no systematic review of these approaches has been carried out to date. To fill this knowledge gap, approaches employed in the literature relating to dentine development or regeneration were screened and summarised in this review. First, animal models used to identify biochemical factors in studies relating to dentine development are introduced, including their history, basic theories and applications. Second, the exploration of biophysical factors via *ex vivo* and *in vitro* approaches is illustrated, focusing on the design of the systems and their application in studies relating to dentine regeneration. This review aims to provide insight regarding the tools for future studies concerning dentine development and reparative endodontics.

Biochemical cues: animal models

Of the three types of experimental models, *in vivo* animal models are considered the gold standard for speculating human responses because of animals' similarities to humans in terms of biological structures and genes. In particular, they are more reliable in the exploration of the dynamics of biochemical factors including genes and regulatory molecules compared to *in vitro* or *ex vivo* methods⁹.

Laboratory animals are a group of standardised animals that are used extensively in various experimental studies, both basic science and preclinical, owing to their accuracy, reproducibility and rationality¹⁰. In order to fulfil predetermined experimental aims, researchers employ laboratory animals and construct specific animal models. Among these, genetically modified animal models, which have marked a significant breakthrough, are relatively advanced models that are powerful and customisable. Researchers use various gene editing approaches to modify the genome of laboratory animals by inserting or deleting target DNA segments, resulting in customised models with specific biological, pathological and cellular characteristics that imitate those of human diseases.

In 1980, Gordon et al¹¹ created the first transgenic mouse via prokaryotic microinjection of fertilised eggs. Subsequently, the combination of the gene targeting technique based on homologous recombination devised by Thomas and Capecchi¹² and Smithies et al¹³, and the embryonic stem cell technique created by Evans and Kaufman¹⁴ led to the first gene knockout mice in 1989¹⁵. Over the subsequent decades, the booming development of transgenic mice and gene manipulation approaches have provided powerful tools for biological exploration and disease-related studies.

To date, commonly used gene-modified approaches include prokaryotic microinjection, Cre/LoxP, CRISPR/Cas9, ZFN and TALEN. Although each approach has its inherent advantages and disadvantages, they all contribute to the exploration of tooth development and related diseases (Fig 1).

Prokaryotic microinjection

Prokaryotic microinjection is the earliest transgenic technology that was developed to construct transgenic animals¹¹, and it has been used widely and successfully in numerous explorations. The general steps include acquisition of exogenous target genes, acquisition of fertilised eggs, prokaryotic microinjection, embryo transfer and genotype identification¹⁶. Specifically,

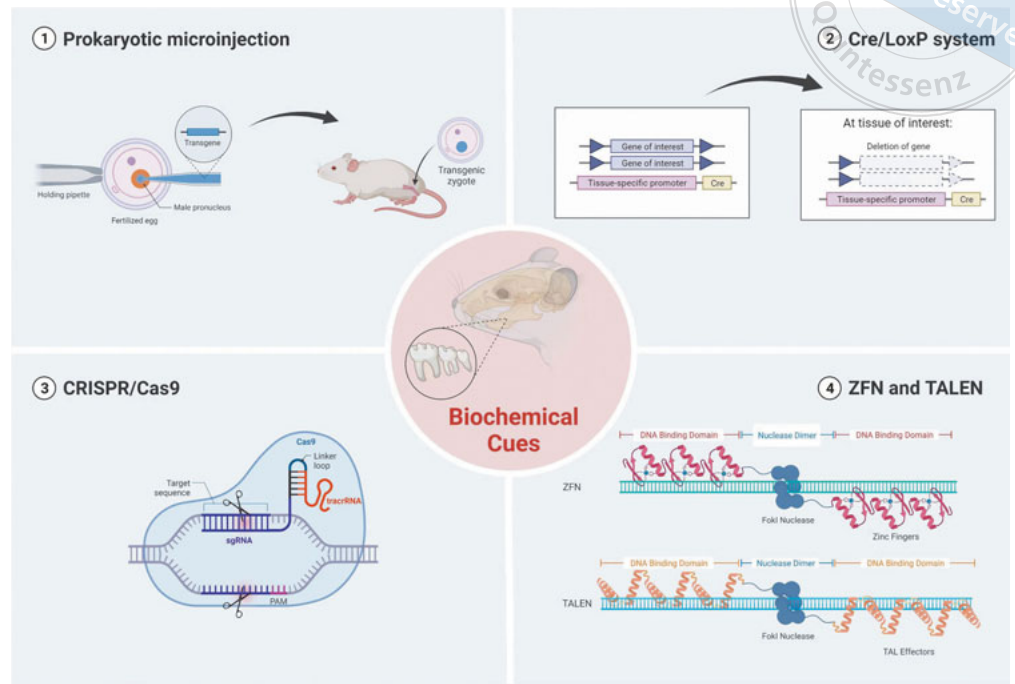


Fig 1 In vivo approaches commonly used in the identification of biochemical cues in dentin development-related and dentin regeneration-related studies: prokaryotic microinjection, Cre/LoxP, CRISPR/Cas and ZFN and TALEN.

gene expression vectors are first constructed using DNA recombination technology to obtain exogenous target genes that exist stably and can be inherited by offspring cells. Then, using prokaryotic microinjection techniques, the plasmid vector containing the target gene fragment is linearised and injected into the male pronucleus of fertilised mouse eggs to randomly integrate them into the host genome. Subsequently, the integrated fertilised eggs are implanted into the oviduct of a pseudopregnant female mouse of the same strain through embryo transfer techniques¹⁷. Finally, the target transgenic mice are generated by crossbreeding after transgenic founder mice are screened out.

To illustrate the importance and contribution of the prokaryotic microinjection technique in studies related to dentine development, the present authors summarised its applications in identifying the most critical components of dentine, the DSPP/dentine sialoprotein (DSP)/dentine phosphophoryn (DPP) system.

DSPP is a member of the non-collagenous small integrin-binding ligand N-linked glycoprotein family (SIBLING), which play critical roles in bone and dentine mineralisation¹⁸. Veis and Perry¹⁹ discovered DPP protein in 1967, and Butler et al²⁰ discovered DSP protein in 1981. The two proteins were studied irrelevantly until 1997 when MacDougall et al²¹ found the DNA sequence encoding DPP was right downstream of that encoding DSP via cDNA cloning and mRNA sequencing, thus

illustrating that DSP and DPP originated from a mutual gene *Dspp*. Subsequently, Steiglitz et al²², Sun et al²³ and von Marschal et al²⁴ found that DSPP was a non-functional precursor protein that was cleaved into DSP and DPP at the G447 | D448 site in odontoblasts, which were then released into the extracellular matrix; however, the respective functions of DSP and DPP remained ambiguous. With the help of prokaryotic microinjection techniques, researchers used a stepwise approach to explore the function of DSP and DPP in dentine development.

Zhang et al²⁵ constructed a cDNA encoding DPP and haemagglutinin (HA-DPP cDNA) as the target gene, in which HA was present as a tag to detect DPP expression. The pBC-KS vector containing the HA-DPP with a 3.6 kb *Col1a1* promoter was constructed, and the linearised plasmid vector was injected into the pronucleus of fertilised C57BL/6J mouse eggs, and *Col1a1*-HA-*Dpp* transgenic mice were generated after embryo transfer. Subsequently, this strain of mice was crossed with *Dspp*^{-/-} mice (*Dsp*^{-/-};*Dpp*^{-/-} mice) to obtain *Dspp*^{+/-}; *Dpp*^{Tg} mice, which were then crossed with *Dspp*^{-/-} mice (*Dsp*^{-/-};*Dpp*^{-/-} mice) to obtain *Dspp*^{+/-}; *Dpp*^{Tg} mice (*Dsp*^{-/-};*Dpp*⁺ mice) that expressed only the *Col1a1*-HA-*Dpp* gene but not endogenous *Dspp*. Compared to *Dsp*^{-/-};*Dpp*^{-/-} mice that manifested abnormal widening of predentine, irregular dentinal tubules and decreased mineralisation, the *Dsp*^{-/-};*Dpp*⁺ mice possessed dentine with relatively

increased thickness, volume and mineralised density. Moreover, scanning electron microscopy (SEM) examination and calcein-alizarin red double labelling assays in the *Dsp-;Dpp+* mice showed that the unmineralised and hypo-mineralised areas of dentine decreased, and the dentinal tubules were more regularly aligned and dispersed. Thus, this all implied that the expression of DPP exerted reparative effects on dentine dysplasia caused by *Dspp* deletion.

Based on the aforementioned and relevant studies, researchers inferred that after DPP was synthesised in mature odontoblasts and secreted towards the mineralisation front, it bound not only to collagen fibres but also to large amounts of calcium ions owing to their high content of aspartic acid and serine²¹, and as a result, the crystal nucleus of mineralising hydroxyapatite was formed²⁶. Thus, DPP played a role in the initial mineralisation of the dentine matrix and the maturation of mineralised dentine by adjusting the size and morphology of the crystal.

In the meantime, the functions of DSP remain relatively ambiguous. Gibson et al²⁷ injected the pBC KS+ plasmid vector containing DSP cDNA into the pronucleus of fertilized C57BL/6J mouse eggs and obtained *Dspp*^{-/-}; *Dsp*^{Tg} mice (*Dsp+*; *Dpp-* mice) expressing only the *Dsp* gene but not endogenous *Dspp*. Radiographic, micro-computed tomography (microCT), SEM and histological analysis showed that compared to *Dsp-;Dpp-* mice, the *Dsp+*; *Dpp-* mice possessed larger pulp chambers, thinner dentine and thicker predentine; meanwhile, the dentinal tubules were more disorganised, irregularly dispersed and in a significantly smaller amount. Besides, biglycan, which was supposed to be found solely in predentine in normal mice, was shown to be expressed in the whole predentine-dentine layer²⁸, implying that dentine mineralisation barely occurred in *Dsp+*; *Dpp-* mice. Thus, this work indicated that DSP functioned as a suppressor of the early mineralisation of predentine.

However, in another study that also used prokaryotic microinjection to study the role of DSP, Suzuki et al²⁹ drew an opposite conclusion. They enzymatically linearised the pIRES-DsRed vector containing the DSP expression fragment to obtain the corresponding target DNA solution and injected it into the fertilized eggs of FVB/NJ mice to obtain *Dsp*^{Tg} mice, and then crossed them as described above to obtain *Dspp*^{-/-}; *Dsp*^{Tg} mice (*Dsp+*; *Dpp-* mice). SEM and microCT showed that compared to *Dsp-;Dpp-* mice, the *Dsp+*; *Dpp-* mice displayed thinner predentine and thicker dentine and were thus more resistant to abrasion and unlikely to have pulp exposure. Therefore, the detailed roles of DSP need to be explored further.

Although prokaryotic microinjection techniques can be used to generate transgenic mice effectively, they also possess disadvantages including the need for expensive and sophisticated equipment, high sensitivity to personnel and technology, and uncontrollable integration sites or copy numbers of exogenous genes, which often result in mutations such as the deletion or misrecombination of DNA fragments and cause serious pathological defects³⁰. In recent years, precise gene editing technologies such as Cre/LoxP, CRISPR/Cas9, ZFN and TALEN have flourished and have addressed these challenges to some extent.

Cre/LoxP

The Cre/LoxP system is a powerful method for manipulating biological genetic information, and transgenic animal models based on this technique have become one of the most commonly used tools for tooth development studies^{31,32}. The Cre/LoxP system is composed of two LoxP sites, which are 34bp DNA segments comprising two 13bp palindromic sequences and an 8bp core sequence, and a Cre-recombinase that identifies loxP sites and mediates the deletion of DNA segments between the adjacent homotropic LoxP sites³³. Two mice are required to breed a Cre/LoxP mouse, one with the expression of Cre-recombinase and one with two LoxP sites inserted upstream and downstream of the target gene. When the two types of mice mate, the DNA segments between the LoxP sites are sheared and deleted in cells or tissues expressing Cre-recombinase. Since Cre-recombinase is expressed under the control of promoters, by selecting promoters that are uniquely expressed in specific cells or at specific developmental stages, the Cre-recombinase is intentionally activated and deletion of target genes is achieved³¹.

Growth factors play critical roles in the development of individuals, and the TGF- β superfamily³⁴, which includes TGF- β , activin, BMPs and growth differentiation factors (GDFs), has received increasing attention in recent years. Among these, BMPs are reported to be most closely related to dentine development^{35,36}. The present authors described the application of the Cre-LoxP system in studies on dentine development by introducing the BMP-Smad signalling pathway.

When odontoblasts start to differentiate, BMP2 is expressed in the dental mesenchyme. Malik et al³⁷ conditionally knocked out *Bmp2* in neural crest cells based on the Cre-LoxP system using *Wnt1* as the promoter to investigate the role of BMP2 in early odontogenesis. In *Wnt1-cre*; *Bmp2*^{fl/fl} mice, thinner dentine, disorganised dentinal tubules and ectopic mineralisation in the pulp

cavity were observed via microCT and SEM. Meanwhile, DSPP expression was significantly downregulated as shown by immunofluorescence staining and polymerase chain reaction (PCR), suggesting that a BMP2 deficiency caused abnormalities during early tooth development and resulted in dentine dysplasia.

BMP receptors are classified as type I and type II according to their cytoplasmic regions. Type I receptors include BMPR1A, ACVR1 and BMPR1B, and type II receptors include BMPR-II, ACVR-II and ACVR-IIB³⁸. Among them, the roles of BMPR1A and ACVR1 in tooth development have been investigated to the best of the present authors' knowledge, whereas the effects of other receptors such as BMPR1B and BMPR-II have only been explored in osteogenesis. For example, Zhang et al³⁹ used the Cre-LoxP system to conditionally knock out *Acvr1* in mesenchymal cells using *Osterix* as the promoter, and generated *Osterix-Cre;Acvr1^{fl/-}* mice. Haematoxylin and eosin (HE) staining and microCT displayed thinner crown dentine and thicker predentine in the molars and osteodentine in the incisors, in which a transition from *Dsp* to *Bsp* expression was detected. Moreover, Wnt antagonists *Dkk1* and *Sost* were downregulated, and β -catenin was upregulated in the cKO incisors but remained unchanged in molars. Therefore, it was suggested that ACVR1 played different roles, promoting the differentiation of dental mesenchyme to odontoblasts in molars but inducing a cell fate shift of odontoblasts to osteoblasts in incisors. Feng et al⁴⁰ and Liu et al⁴¹ used *Gli1*, *Nestin* and *OC* as promoters to knock out *Bmpr1a*, and found that all mice lines exhibited dentine defects including thinner dentine and changed morphologies of odontoblasts, although the degree of defect varied.

Smad4 is the only Co-Smad protein that has been discovered to date, which is one of the downstream signalling factors of the TGF- β /BMP signalling pathway⁴². Since previous studies had identified *Col1* and *Osteocalcin (OC)* as early marker genes and *Dspp* as a late marker gene in odontogenesis^{43,44}, Kim et al⁴⁵ used *Col1*, *OC* and *Dspp* as promoters and knocked out *Smad4* at different stages to obtain *Smad4*-cKO mouse lines. In all three strains, the mice were found to exhibit dwarf odontoblasts, thinning coronal dentine and decreased expression of *Col1a1*, *OC* and *Dsp* by HE, immunohistochemistry (IHC) and microCT. Among them, the phenotypes were more significant in the *Smad4^{OC}* and *Smad4^{Col}* mice and relatively mild in *Smad4^{Dspp}* mice. These results suggest that *Smad4* is required during dentine development in a stage- and site-dependent manner.

Using the same techniques, researchers also explored the roles of numerous other factors including DMP1⁴⁶,

DLX3⁴⁷ and TGF- β ⁴⁸, and found that knockout or knock-down of these factors usually led to similar phenotypes, such as disrupted odontoblast polarity and thinner dentine, implying the participation of various signalling pathways in dentine development.

Compared with the knockout mice constructed via traditional prokaryotic microinjection, the conditional knockout mice constructed via the Cre-loxP system can largely avoid embryonic or neonatal death of mice and effectively decrease the chances of blind or random integration of gene fragments. Moreover, genes can be removed in specific tissues or at particular stages, which is crucial for studying the spatial and temporal expression pattern of target genes.

CRISPR/Cas9

In 2012, Jinek et al⁴⁹ integrated the crRNA (CRISPR RNA) and tra-crRNA (trans-activating crRNA) from the natural CRISPR/Cas system into a single strand (single guide RNA, sgRNA) and developed the CRISPR/Cas9 technique. With this advanced approach, accurate DNA editing was achieved successively in both animals and cells⁵⁰. From then on, the CRISPR/Cas9 technique received a blowout spurt and has become one of the most popular tools in gene editing.

The CRISPR/Cas9 system is composed of two components: the gRNA that recognises a specific DNA sequence and the Cas9 protein that cuts the DNA sequence⁵¹. The gRNA and Cas9 bind and form a ribonucleoprotein (RNP) complex. The customised gRNA recognises the protospacer adjacent motif (PAM) and binds to the target DNA sequence, which enables Cas9 to cut the double-stranded DNA efficiently. Afterwards, DNA recombination via non-homologous end joining (NHEJ) or homology-dependent repair (HDR) is achieved, leading to targeted gene editing. Generally, cells will repair the broken DNA via NHEJ; however, mismatches such as base insertions or losses occur frequently. As a result, the downstream sequence of the cut site loses its function and gene deletion is obtained. Moreover, by introducing an extra gene repair template that contains the target gene sequence to be inserted and corresponding homologous arms at either side, the DNA double-strand can also be repaired via HDR and the target sequence can be inserted.

Because of its non-absolute specificity, gRNA may recognise other similar sequences in the genome, leading to off-target editing. Still, compared to the traditional Cre/LoxP system that requires gene targeting and is full of complexities and uncertainties, CRISPR/Cas9 possesses higher targeting accuracy and other

advantages including simple construction, easy operation, short trial cycle, low expense, high adaptability, efficient capability and simultaneous targeting of multiple genes. It is a revolutionary technique that has been employed successfully in various biomedical studies⁵². For example, this novel technique has made it possible to explore the role of *Dspp* in dentine development further in a more precise and competent way.

Based on clinical and radiographic appearance, hereditary dentine disorders can be divided into two types: dentinogenesis imperfect (DGI), which is further divided into DGI-I, DGI-II and DGI-III, and dentine dysplasia (DD), which is further divided into DD-I and DD-II. Among them, DGI-II is the most common. It is known that *Dspp* is the gene responsible for these diseases except for DGI-I. Further analysis of the mutations in *Dspp* that lead to hereditary dentine disorders suggests that they can be generally divided into two types: missense or nonsense mutations at the 5' end that encodes DSP segment, and frameshift mutations at the 3' end that encodes the DPP segment⁵³.

The missense mutation of *Dspp* at site 17 where leucine replaces proline (c.50C>T, p.P17L, g.50C>T) was found to lead to both DGI-II⁵⁴ and DGI-III⁵⁵ phenotypes. To identify the underlying mechanism, Liang et al⁵⁶ designed an sgRNA that was located on the antisense strand directly opposite to codon 19 of the mouse *Dspp* gene, which was equivalent to codon 17 of the human *Dspp* gene, and a typical PAM sequence (AGG) was immediately adjacent to its 3' end, as well as a single-stranded oligodeoxynucleotide as a repair template that contained the centrally located desired pathogenic mutation (CCG>CTG) as well as a silent mutation (GCC>GCG) flanked by two arms of homologous genomic sequence, respectively. Radiographic, microCT and SEM examinations showed that young *Dspp*^{P19L} mice displayed phenotypes similar to those of DGI-III, including larger pulp chambers, thinner dentine at the chamber roof and thicker dentine at the chamber floor. In contrast, aged *Dspp*^{P19L} mice exhibited phenotypes similar to those of DGI-II, including smaller pulp chambers and heavier abrasion. Moreover, the odontoblast processes in *Dspp*^{P19L} mice retracted and peritubular dentine was deposited continuously with aging. Thus, mutations of the *Dspp* gene at different stages present with different phenotypes.

In addition, it was found that compared to normal mice, DSP/DSPP signals increased significantly in odontoblasts but were weakly expressed in dentine extracellular matrix in *Dspp*^{P19L} mice. Besides, DSPP normally colocalises with GM130, a Golgi apparatus matrix protein, whereas the P19L-DSPP colocalised

mainly with calreticulin, an ER matrix protein, indicating that P19L-DSPP failed to be efficiently transported from ER to Golgi, leading to its accumulation in ER and damage in DSPP secretion. Moreover, considering that DSPP contains large amounts of aspartic acid and glutamate residues, its accumulation may result in ER stress and pathological unfolded protein responses⁵⁷.

Two years later, Liang et al⁵³ again employed the CRISPR/Cas9 technique to knock out the guanine right after the fourth amino acid in the DPP coding sequence and generated DSPP-1fs mice with a -1 frameshift. Compared to *Dspp*^{P19L} mice in which the morphology of odontoblasts remained normal while dentine became thinner with a rough inner surface, SEM, nanohardness testing and histological staining revealed that the DSPP-1fs mice displayed more severe dentine abnormalities. Phenotypes observed in the DSPP-1fs mice included the loss of the columnar morphology of odontoblasts and the dentinal tubules, which were similar to the appearance of reparative dentine formed after odontoblast death.

The development of CRISPR/Cas9 enables precise editing of *Dspp*. By illustrating the changes resulting from mutations of single base pairs, researchers are gaining a much deeper understanding of dentine dysplasia caused by *Dspp* mutations, which offers enormous potential and hope of clarifying the underlying mechanism and preventing the occurrence of these diseases.

Zinc finger nucleases (ZFN) and transcription activator-like effector nucleases (TALEN)

Unlike the CRISPR/Cas9 system that relies on sgRNA to recognise target sequences, the zinc finger nucleases (ZFN) technique and transcription activator-like effector nucleases (TALEN) technique recognise proteins.

ZFN is composed of two parts: the zinc finger proteins (ZFs) that recognise and bind to specific gene sequences, and the Fok I endonucleases that cut the genes. ZFs have three independent repeats that each recognise three bases; thus, a ZF DNA binding motif can recognise a 9bp gene sequence, and two ZFs recognise an 18bp gene sequence⁵⁸. After either ZF recognises the specific sequence on one of the two DNA strands, Fok I endonucleases cut the target gene by forming a dimer⁵⁹, leading to the breakage of DNA strands at particular sites, followed by DNA reparation via NHEJ or HDR⁶⁰. In this way, the genome is manipulated.

Chiba et al⁶¹ cut a base pair at specific sites via the ZFN technique, leading to a frameshift mutation of AmeloD, a transcription factor of the bHLH family,

and bringing the stop codon forward, which generated conditional *AmeloD* knockout mice. MicroCT examination in combination with HE staining showed that its deletion caused decreases in dentine volume and thickness, and dysplasia in the development of both the crown and root⁶¹.

The merits of ZFN include the lack of exogenous DNA introduction and wide application in various models, as NHEJ and HDR exist in basically all species⁶⁰; however, since the assembly of the ZFN sequence relies on current databases, its application is limited. Furthermore, the design of ZFN is intricate. Off-target effects also occur because of the low specificity and affinity of ZF motif when binding with DNA. When there are extensive off-target occurrences that DNA breakage outweighs repair, cells or animals may die, and these problems need to be solved in further studies⁶².

Similar to ZFN, TALEN is formed by Fok I and a protein that recognises and binds to specific DNA sequences, the transcription activator-like (TAL) effector. Similarly, Fok I cuts the DNA strands, which get repaired by NHEJ and HDR⁶³. The difference lies in the DNA-binding motifs. The recognition motif of TAL contains 34 amino acids with conservative sequences except for the twelfth and thirteenth ones, which are called repeat variable diresidue (RVD)^{64,65}. Each RVD corresponds to four different types of base pairs^{66,67}, as a result, the specific TAL recognises and binds to target DNA bases. Thus, by connecting different TAL motifs based on target sequences, and the sequence that encodes FokIendonuclease, a customised TALEN is constructed.

SIX1 (Sine Oculis Homeobox 1) is a transcription factor and belongs to the homologous box gene family. It plays a critical role in the development of sensory organs and craniofacial tissue. Takahashi et al⁶⁸ employed the TALEN technique and generated *Six1*-cKO mice. It was observed that odontoblast differentiation in mandibular incisors was damaged and DSPP expression in dentine matrix was decreased. Besides, the pre-odontoblast marker DKK1 which is normally expressed only in the labial side was observed at both labial and lingual sides in *Six1*-cKO mice. These phenotypes indicated that *Six1*/DKK1 participated in odontogenesis and dentine formation.

Although the TALEN technique also has off-target effects, it is easier to design compared to ZFN. Theoretically, it is possible to design and construct a specific TALEN nuclease for a random DNA sequence. Besides, the cytotoxicity and expense are lower. However, since a TALEN recognition motif is required for each base pair on the target sequence, significant

work needs to be performed for TALEN construction, and the delivery into cells is also challenging^{63,69,70}.

From the abovementioned examples, it can be seen that animal models play fundamental roles in studies relating to dentine development; however, dentine development is such an intricate process that it is regulated by thousands of genes and proteins among which extremely complicated interactions exist within the niche. This intricacy has made it somewhat challenging to identify and explore the role of one single component using only animal models. Thus, ex vivo or in vitro examinations are generally required following in vivo studies to confirm the conclusions. Compared to animal models, ex vivo or in vitro approaches have outstanding merits like relative simplicity, convenience of use, quick response to stimuli and the capacity to explore specific genes or regulatory molecules. Since such work has been thoroughly summarised previously, an in-depth discussion was not included in the present study.

Biophysical cues: ex vivo/in vitro approaches

It is not only various biochemical factors participate in dentine development and regeneration; so too do biophysical factors. In particular, the importance of mechanical stimuli from inherent or exogenous microenvironments has been increasingly proven in recent decades. Due to the limitations of current in vivo techniques, using them to explore the effects of biophysical factors remains an overwhelming challenge. Thus, researchers have turned to ex vivo and in vitro approaches. Traditionally, scaffolds or substrates of specific features are designed to explore the role of a concerned biophysical factor, and numerous scaffolding systems have been developed in recent decades. Excellent reviews summarising these systems based on scaffold types or features have been published previously, to which the present group also contributed^{71,72}. Therefore, in the present study, ex vivo and in vitro approaches will not be redundantly reviewed according to scaffold types.

In recent years, researchers have increasingly come to the agreement that biophysical factors indeed function by exerting mechanical forces on cells or tissues cultured within the niches. Cells respond to the forces via transmembrane mechanosensation receptors and intracellular mechanotransduction signalling pathways. Thus, in this section, approaches commonly used to identify biophysical factors in studies related to dentine development or regeneration were systematically interpreted according to the interactive forces between the scaffolds and cells (Fig 2).

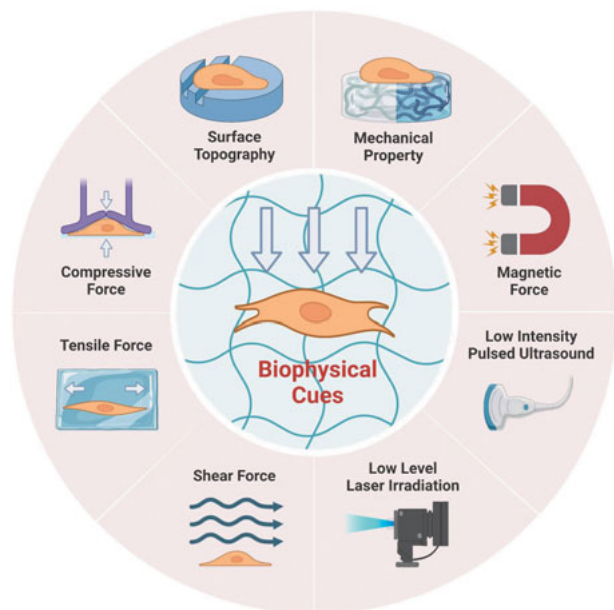


Fig 2 Ex vivo or in vitro approaches commonly used in the identification of biophysical cues in studies relating to dentine development and regeneration. Approaches are illustrated according to the interactive forces.

Stationary force

Surface topography

The surface topography of a scaffold indicates the features it presents to the accommodating cells, and it has been proven to play critical roles in cell fate determination. Of these, two inseparable features, the superficial morphology and the residing area/volume of a scaffold, have mainly been explored with regard to the regulation of dental stem cell behaviours.

Concerning the residing area/volume, Bachhuka et al⁷³ constructed gradients of different-sized gold nanoparticles to simultaneously examine the influence of nanoparticle density and size on dental pulp stem cells (DPSCs) on a single substrate and found the density of nanotopography features was positively correlated to DPSC adherence and proliferation. In addition, Du et al⁷⁴ constructed a bilayer poly(lactide-co-glycolide) (PLGA) scaffold with small pores on the closed side (1 to 5 μm) and large pores on the open side (45 μm) via the diffusion-induced phase separation technique and found that DPSCs showed improved F-actin stress fibre alignment, increased spreading area, elongated appearance, predominant nuclear YAP localisation and spontaneous osteogenic differentiation on the closed side. Graziano et al⁷⁵ generated PLGA membranes and treated them with N-metil-pyrrolidone to create

hierarchic concave pits (primary pits: 80 to 120 μm in diameter and 40 to 100 μm in depth, and secondary pits: 10 to 20 μm in diameter and 3 to 10 μm in depth) where cell-matrix interactions increased. They found that DPSCs seeded on the concave-rich PLGA substrates exhibited nuclear polarity, released greater amounts of BMP-2 and vascular endothelial growth factor (VEGF), expressed higher alkaline phosphatase (ALP) activity, and resulted in better osteogenesis compared to smooth substrates.

As to superficial morphology, DPSCs are generally believed to exert better differentiation potential on rough or extrusive surfaces. For example, *Dspp* was upregulated on the printed (rough) polylactic acid (PLA) scaffold compared to moulded (smooth) substrates⁷⁶. Portone et al⁷⁷ generated graphene oxide-coated polycaprolactone (PCL) nanofibres (mean diameter 500 nm) with different orientations, and found that randomly orientated nanofibres were able to revert neuronal pre-commitment and trigger osteoblastic differentiation, whereas uniaxially aligned fibres were fibroblast-directed. Similarly, Ha et al⁷⁸ generated gelatine methacryloyl hydrogels with microgrooves and ridges of 60 μm and 120 μm via photolithography. They found that the micropatterned hydrogels guided the self-alignment of SCAPs and promoted a higher degree of odontogenic differentiation than non-patterned hydrogels⁷⁸. In addition, Alksne et al⁷⁹ fabricated 3D printed scaffolds with wavy and porous topographies. The wavy ones were formed by closely assembled PLA threads (188 μm in diameter) with grooves, whereas the porous ones were formed by PLA threads (500 μm in diameter) with 300- μm -wide pores⁷⁹. DPSC morphology was modulated and spontaneous osteogenic differentiation was observed on both surfaces without biochemical induction⁷⁹.

In tooth development, odontogenesis is comprised of an odontoblast polarisation (morphology transformation) process and an odontoblast differentiation (function maturation) process. Nowadays, most work is focused on the differentiation process, whereas the polarisation process, which determines the formation of the tubular architecture of dentine, remains largely unclear due to the lack of appropriate research models.

To address this challenge, a series of studies were conducted recently in an attempt to solve this mystery⁸⁰⁻⁸². First, Ma et al⁸⁰ created bioinspired 3D nanofibrous matrices with highly organised tubular architecture via a laser-drilling technique. With the maskless micropatterning technology, this 3D tubular hierarchical scaffold successfully induced the regeneration of tubular dentine that possessed a well-organised microstructure as its natural counterpart⁸⁰. In contrast,

the non-tubular control group only induced osteodentine formation, indicating the decisive role of the 3D tubular structure⁸⁰. Chang et al⁸¹ further improved this system by establishing a nanofibrous tubular 3D micropatterning system that confined one single cell on each microisland for single DPSC polarisation. They found that DPSC polarisation was a dynamic and sequential process and that the nanofibrous tubular architecture was another critical factor in initiating DPSC polarisation⁸¹. Furthermore, cytoskeletal rearrangements were found to modulate DPSC polarisation and cell tension was involved. Chang et al⁸² continued to employ this scaffold as a platform and proved that nanofibrous architecture, tubule size and microisland area all contributed to the initiation of DPSC polarisation by regulating the formation of DPSC processes and the translocation of Golgi apparatus, while microisland geometry exerted negligible effects and gravity accelerated the polarisation process.

Niu et al⁸³ obtained similar conclusions with a distinct approach. They developed a microfluidic chip with microchannels that mimicked dentinal tubules and interconnected sites that were used to culture odontoblasts. The 2- μm channels were found to successfully induce the growth of odontoblast processes, while the 4- μm or larger channels only promoted the migration of odontoblasts into the microchannels, confirming the role of tubule size in odontoblast polarisation.

Mechanical properties

The stiffness of the substrate also plays an important role in regulating the behaviour of DPSCs. Qu et al⁸⁴ showed that DPSCs on nanofibrous gelatine scaffold of high stiffness had a more organised cytoskeleton, larger spreading area, higher expression of odontogenic differentiation marker genes and more mineral deposition than those of low stiffness. By further integrating matrices of the two stiffness into a single scaffold for pulp-dentine regeneration, they observed that biomineralisation only occurred in the high-stiffness peripheral area and formed a ring-like structure that surrounded the non-mineralised central area; thus, a complete construct similar to natural pulp-dentine complex was regenerated successfully⁸⁴.

Chuang et al⁸⁵ found that adjustment in the modulus of polyisoprene substrates by changing coating thickness or incorporating inorganic particles influenced DPSC differentiation. Upregulation of osteocalcin (OCN) and COL1a1 and increased biomineralisation without the induction of dexamethasone were observed on hard substrates, including both spun-cast thin poly-

isoprene substrates and filled thick polyisoprene substrates⁸⁵. Minerals were aggregated into large clusters on thin substrates and uniformly distributed on filled thick substrates, and intracellular modulus of DPSCs also changed to accommodate to changes in the modulus of interactive substrates⁸⁵. Similarly, a study showed that DPSCs were more likely to undergo osteoblastic/odontogenic differentiation and proliferation when seeded on stiff substrates, which involved the Wnt signalling pathway⁸⁶.

Compressive force

During embryo development, mesenchyme condensation triggers the organogenesis of many tissues including cartilage, bone, muscles, kidneys and lungs. It was believed that mesenchyme condensation also initiated odontogenesis. Researchers proposed that odontoblast polarisation and differentiation were the result of rapid proliferation and condensation of dental papilla mesenchymal cells, which generated mechanical compaction among the cells; however, this hypothesis could hardly be verified via *in vivo* approaches. The rapid development of *ex vivo* tissue culture methods, bioengineering techniques and mathematic models have recently made it possible to explore the role of compression on dentine development.

Mammoto et al⁵ created a mechanical compression device to explore the effect of compaction on the mesenchyme. The polydimethylsiloxane (PDMS) device had a soft base and piston and was permeable to air and water, and thus created a suitable microenvironment for *ex vivo* culture. Mesenchymal tissues from the first pharyngeal arch freshly isolated from embryonic day 10 were placed within the chamber of the device and compacted with a force of 1 kPa by a 30-g metal cube on the PDMS piston⁵. Compared to the uncompacted group, the mRNA expression of *Pax9*, *Msx1* and *BMP4* of the compacted tissues was significantly increased, indicating that mechanical compression enhanced mesenchyme differentiation⁵.

Miyashita et al⁸⁷ cultured hDPSCs on a customised silicone membrane with microchannels that were 10 μm in depth, 5 μm in diameter and 10 μm in pitch, resembling the morphology of dentinal tubules, and employed a compression bioreactor to exert cyclic loading force on the membrane. They found that the odontogenic markers *Bmp7* and *Wnt10* were upregulated and the phosphorylation levels of ERK1/2 and p38 were increased, implying that the MAPK signalling pathway was involved in promoting odontogenesis by mechanical compaction⁸⁷. They also found that DPSCs formed

odontoblast-like cellular processes within the microchannels, displaying a polarised morphology similar to *in vivo* conditions⁸⁷. Together, these results proved that mechanical compaction was capable of directing the odontogenic differentiation and polarisation of DPSCs.

Mammoto et al⁸⁸ confirmed the effect of mechanical compaction on odontogenesis based on micropatterning method. To recapitulate the mesenchyme condensation process of the dental papilla in the initial stage of dentine development, they generated micropatterns via a photolithography technique and cultured undifferentiated dental mesenchymal cells (E10) within the fibronectin-coated micropatterns in different densities⁸⁸. They found that *Pax9* was highly expressed on the high-density micropatterns compared to the low-density group, and that when the cells originally cultured with a high density were replated in a low density, *Pax9* was downregulated, indicating that the maintenance of mesenchyme condensation was a prerequisite for odontoblast differentiation⁸⁸. In addition, they proved that the microfilament cytoskeleton played a critical role in regulating dental mesenchyme condensation and noted that cell condensation led to changes in intracellular microfilament arrangement and activation of p38/MAPK pathway, which subsequently activated the SP1 transcriptional factor and promoted the synthesis of type VI collagen⁸⁸. As a result, the condensed status of cells was maintained and odontogenesis was stabilised⁸⁸.

Hashmi et al⁸⁹ reinforced this conclusion by employing a bioengineering scaffold. They generated a 3D thermosensitive GRGDS-modified PNIPAAm hydrogel that shrank in volume and displayed smaller interconnected micropores when heated from 34°C to 37°C, and cultured BMSCs within the hydrogel⁸⁹. Afterwards, the cell-scaffold complex was implanted under the mice subrenal capsules⁸⁹. ALP activity, calcium nodule formation and DSP expression were improved in the experimental group, and the mineralisation level of the newly formed tissues was significantly higher as examined by elemental map and SEM scanning⁸⁹. This indicated that compressive force generated from the scaffold transition induced odontogenic differentiation and mineralisation of BMSCs⁸⁹.

Tensile force

Clinical studies have found that tensile forces generated by orthodontic treatment induce ectopic dentine mineralisation in the pulp chamber⁹⁰. To understand the underlying mechanisms, researchers have adopted devices like Flexcell to explore the relationship between odontogenesis and tensile stress.

Liao et al⁹¹ employed the Flexcell system to exert tensile force on human pulp-derived odontoblast-like cells (hOBs) and found that while the odontogenic markers including *Dspp*, *Opn*, *Ocn* and *Runx2* were upregulated, the expression level of intracellular sclerostin was decreased. To further identify the influence of tension-relevant sclerostin on odontogenesis, they overexpressed sclerostin in hOB cells via plasmid transfection and found the odontogenic markers were downregulated with the STAT3 pathway involved, indicating that sclerostin impacted odontogenic differentiation⁹¹. When inhibitors that specifically target the ERK1/2 and proteasome pathways were utilised, tensile stress downregulated sclerostin via ERK1/2 and proteasome pathways, respectively⁹¹. Other researchers also generated *Sost*^{-/-} mice using the Cre/LoxP technique⁹², which displayed lower pulp volume and accelerated reparative dentine formation; meanwhile, the DPSCs derived from *Sost*^{-/-} mice had increased mineralisation. These results further confirmed the effect of tensile force and sclerostin on odontogenic differentiation.

With a similar Flexcell approach, Lee et al⁹³ concluded that tension promoted the odontogenic differentiation of hDPCs via the HO-1 pathway. Compared to the control group, hDPCs that underwent tensile stress within the Flexcell system exhibited increased expression of *Ho-1*, *Dspp*, *Dmp-1* and *Opn*, and this increase disappeared when a HO-1 siRNA was used⁹³. Moreover, tensile force induced the nuclear translocation of Nrf2, which was hindered when hDPCs were processed with inhibitors targeting PI3K and NF-κB, implying that mechanical tension induced odontogenic differentiation via Nrf2 and HO-1⁹³.

Cai et al⁹⁴ drew a contrasting conclusion regarding the role of tension on odontogenesis. Applying a uniaxial circulating tensile force of 2000 με and 1 Hz on isolated DPSCs, they detected decreased expression of DSPP and BSP via q-PCR and immunocytochemistry staining, suggesting tension played an inhibitory role on odontogenesis⁹⁴. The reason for such discrepancy remains unclear, and further in-depth studies are required.

Apart from Flexcell, other appliances were also used. For example, Chen et al⁹⁵ generated aligned polyglycolic acid (PGA) fibrous scaffolds that were applied with static tension via a dental arch expansion appliance and observed that when DPSCs were seeded into the scaffolds, tendon-related markers were significantly upregulated and tendon-like constructs were formed in a mouse model, implying that tensile force also encouraged DPSCs to differentiate towards tenocytes.

Shear force

Within dentinal tubules, odontoblast processes are constantly immersed in dentinal fluids. When exogenous stimuli like sudden temperature changes or mechanical operations are exerted on dentine, dentinal fluid flow occurs instantaneously⁹⁶. Thus, odontoblasts undergo shear stress frequently.

Sun et al⁹⁷ constructed a model that stimulated odontoblasts with fluid flow shear stress within a customized parallel plate flow chamber. With the shear force, the intracellular calcium content increased rapidly within odontoblasts, whereas this phenomenon disappeared when GsMTx4, a specific blocker of the mechanosensitive Piezo1 ion channel, was added to the culture system⁹⁷. When cells were cultured in an extracellular microenvironment where calcium ions were deprived, the shear force failed to trigger increase in calcium content; this indicated that shear stress promoted calcium influx via Piezo1 and confirmed the mechanosensation function of odontoblasts⁹⁷. Moreover, it was shown that odontoblasts released adenosine triphosphate (ATP) under fluid flow, which activated not only trigeminal neurons but also adjacent odontoblasts via P2Y and phospholipases C-coupled ATP/ADP receptors, modulating both mechanotransduction and odontogenesis of odontoblasts⁹⁸. Thus, a signalling network that enabled rapid communication was generated at the dentine-pulp complex.

Honda et al⁹⁹ further confirmed the effect of shear stress in tooth development with heterogenous cell clusters. They isolated, minced and enzymatically dissociated developing tooth tissues including dental epithelium, dental papilla and dental follicle into pieces, then cultured the heterogenous cells on PGA fibrous mesh pre-coated with type I collagen⁹⁹. The cell-PGA complex was placed on a Bio-shaker where the two-way flow of the culture medium produced shear stress, then the complex was implanted under the submentum of immune-deficient rats⁹⁹. In the experimental group, the protein levels of BSP and Vimentin and the mRNA expression of *Runx2*, *Col1a*, *Opn*, *Ocn* and *Dspp* were enhanced significantly⁹⁹. Organised columnar cells and mineralised structures resembling dentinal tubules, enamel and bone were detected, and tooth development was much faster than in the control group⁹⁹. All these results indicated that shear stress promoted tooth development.

Other forces

With advancements in physics, recent years have witnessed the creation and development of many novel

machines and technologies. Some of these technologies, for example ultrasound and lasers, have been adopted in the dental field and shown great potential in the treatment and therapy of dental diseases. They have also influenced dental tissues or dental stem cells via forces, but since these forces cannot be simply described as compression, tension or shear forces, they are only summarised briefly in the present study.

Low-intensity pulsed ultrasound (LIPUS)

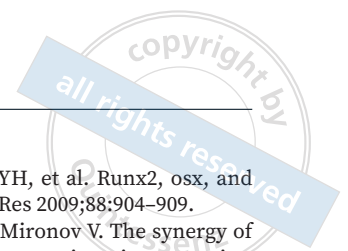
As a mild physiotherapy, low-intensity pulsed ultrasound (LIPUS) has been reported to accelerate wound healing and tissue regeneration by generating continuous and superposed shockwaves. In the dental field, LIPUS has been widely explored in dentine reparation. Zuo et al¹⁰⁰ treated mice molar defects with LIPUS and found that the disrupted odontoblast layer was repaired and tertiary dentine with orderly aligned, spindle odontoblast-like cells in the periphery was formed, indicating that LIPUS possessed the capacity to repair early dentine defects.

Low-level laser irradiation (LLLI)

Compared to other types of lasers that generate enormous amounts of heat and traumatise tissues, low-level laser irradiation (LLLI) barely causes any photothermal phenomena owing to its low capacity. Currently, LLLI is widely used in dental clinics to treat wounds, temporomandibular disorder, pain and swelling after tooth extraction, dentine hypersensitivity and mucosal diseases. With regard to odontogenesis, Theocharidou et al¹⁰¹ found that LLLI promoted the expression of biomarkers including DSP, BMP-2 and *Runx2* in DPSCs, and increased cell proliferation on porous Mg²⁺-based bioceramic scaffolds.

Magnetic forces

The precise assembly of cytoskeletons is a prerequisite for cell polarisation and tissue regeneration. In recent years, researchers have managed to modulate cell polarisation by controlling the organisation of cytoskeletal elements intracellularly. For example, Zhang et al¹⁰² constructed a MS-ABPAda α HACD complex that promoted the directional polymerisation of microfilaments. This complex was comprised of β -CD-modified hyaluronic acid polymers and magnetic nanospheres that were modified with actin-binding peptides (ABPs) and adamantane (Ada). The ABPs could efficiently target actin, whereas β -CD and Ada promoted self-assembly



of the nanofibres via non-covalent forces. It was shown by a confocal microscope and transmission electron microscope that this complex determined the organisation of microfilaments by promoting actin self-assembly in parallel to the magnetic field, and thus induced the directional extension of DPSC processes and cell polarisation.

Conclusion

Commonly used animal models including prokaryotic microinjection, Cre/LoxP, CRISPR/Cas9 and ZFN and TALEN were described in detail in the present study. However, *in vivo* models are complex systems considering that signalling factors interact with and compensate each other intimately, and it is impossible to isolate one signalling factor and explore its role. Meanwhile, the effects of biophysical factors cannot be studied using these models. *Ex vivo* or *in vitro* models present advantages in overcoming limitations of *in vivo* models; however, *ex vivo* or *in vitro* models also have unavoidable deficiencies. A major one is that cells or tissues used *in vitro* or *ex vivo* are often artificially modulated or transformed, leading to unpredictable changes in biological functions. To summarise, although each model has its own merits and disadvantages, they all contribute enormously to studies relating to dentine development and regeneration.

Conflicts of interest

The authors declare no conflicts of interest related to this study.

Author contribution

Drs Ya Lu SUN, Xi Heng LI, Shuang Shuang WANG and Hu En LI searched the literature and drafted the manuscript; Dr Bei Chang organised the structure and revised the manuscript; Dr Hong Chen SUN proposed the idea and revised the manuscript.

(Received May 26, 2023; accepted Aug 04, 2023)

References

- Wei Y, Lyu P, Bi R, et al. Neural regeneration in regenerative endodontic treatment: An overview and current trends. *Int J Mol Sci* 2022;23:15492.
- Huang GT, Liu J, Zhu X, et al. Pulp/dentin regeneration: It should be complicated. *J Endod* 2020;46:S128–S134.
- Chen S, Gluhak-Heinrich J, Wang YH, et al. Runx2, osx, and dspp in tooth development. *J Dent Res* 2009;88:904–909.
- Ovsianikov A, Khademhosseini A, Mironov V. The synergy of scaffold-based and scaffold-free tissue engineering strategies. *Trends Biotechnol* 2018;36:348–357.
- Mammoto T, Mammoto A, Torisawa YS, et al. Mechanochemical control of mesenchymal condensation and embryonic tooth organ formation. *Dev Cell* 2011;21:758–769.
- Théry M. Micropatterning as a tool to decipher cell morphogenesis and functions. *J Cell Sci* 2010;123:4201–4213.
- Foy BH, Gonçalves BP, Higgins JM. Unraveling disease pathophysiology with mathematical modeling. *Annu Rev Pathol* 2020;15:371–394.
- Lin M, Xu F, Lu TJ, Bai BF. A review of heat transfer in human tooth—Experimental characterization and mathematical modeling. *Dent Mater* 2010;26:501–513.
- Saeidnia S, Manayi A, Abdollahi M. From *in vitro* experiments to *in vivo* and clinical studies; Pros and cons. *Curr Drug Discov Technol* 2015;12:218–224.
- Robinson NB, Krieger K, Khan FM, et al. The current state of animal models in research: A review. *Int J Surg* 2019;72:9–13.
- Gordon JW, Scangos GA, Plotkin DJ, Barbosa JA, Ruddle FH. Genetic transformation of mouse embryos by microinjection of purified DNA. *Proc Natl Acad Sci U S A* 1980;77:7380–7384.
- Thomas KR, Capecchi MR. Introduction of homologous DNA sequences into mammalian cells induces mutations in the cognate gene. *Nature* 1986;324:34–38.
- Smithies O, Gregg RG, Boggs SS, Koralewski MA, Kucherlapati RS. Insertion of DNA sequences into the human chromosomal beta-globin locus by homologous recombination. *Nature* 1985;317:230–234.
- Evans MJ, Kaufman MH. Establishment in culture of pluripotential cells from mouse embryos. *Nature* 1981;292:154–156.
- Joyner AL, Skarnes WC, Rossant J. Production of a mutation in mouse *En-2* gene by homologous recombination in embryonic stem cells. *Nature* 1989;338:153–156.
- Wong RW, Sham MH, Lau YL, Chan SY. An efficient method of generating transgenic mice by pronuclear microinjection. *Mol Biotechnol* 2000;15:155–159.
- Ittner LM, Götz J. Pronuclear injection for the production of transgenic mice. *Nat Protoc* 2007;2:1206–1215.
- Fisher LW, Torchia DA, Fohr B, Young MF, Fedarko NS. Flexible structures of SIBLING proteins, bone sialoprotein, and osteopontin. *Biochem Biophys Res Commun* 2001;280:460–465.
- Weis A, Perry A. The phosphoprotein of the dentin matrix. *Biochemistry* 1967;6:2409–2416.
- Butler WT, Bhowm M, Dimuzio MT, Linde A. Noncollagenous proteins of dentin. Isolation and partial characterization of rat dentin proteins and proteoglycans using a three-step preparative method. *Coll Relat Res* 1981;1:187–199.
- MacDougall M, Simmons D, Luan X, Nydegger J, Feng J, Gu TT. Dentin phosphoprotein and dentin sialoprotein are cleavage products expressed from a single transcript coded by a gene on human chromosome 4. Dentin phosphoprotein DNA sequence determination. *J Biol Chem* 1997;272:835–842.
- Steiglitz BM, Ayala M, Narayanan K, George A, Greenspan DS. Bone morphogenetic protein-1/Tolloid-like proteinases process dentin matrix protein-1. *J Biol Chem* 2004;279:980–986.
- Sun Y, Lu Y, Chen S, et al. Key proteolytic cleavage site and full-length form of DSPP. *J Dent Res* 2010;89:498–503.
- von Marschall Z, Fisher LW. Dentin sialophosphoprotein (DSPP) is cleaved into its two natural dentin matrix products by three isoforms of bone morphogenetic protein-1 (BMP1). *Matrix Biol* 2010;29:295–303.

25. Zhang H, Xie X, Liu P, Liang T, Lu Y, Qin C. Transgenic expression of dentin phosphoprotein (DPP) partially rescued the dentin defects of DSPP-null mice. *PLoS One* 2018;13:e0195854.
26. Boskey AL, Maresca M, Doty S, Sabsay B, Veis A. Concentration-dependent effects of dentin phosphophoryn in the regulation of in vitro hydroxyapatite formation and growth. *Bone Miner* 1990;11:55–65.
27. Gibson MP, Liu Q, Zhu Q, et al. Role of the NH2-terminal fragment of dentin sialophosphoprotein in dentinogenesis. *Eur J Oral Sci* 2013;121:76–85.
28. Matsuura T, Duarte WR, Cheng H, Uzawa K, Yamauchi M. Differential expression of decorin and biglycan genes during mouse tooth development. *Matrix Biol* 2001;20:367–373.
29. Suzuki S, Sreenath T, Haruyama N, et al. Dentin sialoprotein and dentin phosphoprotein have distinct roles in dentin mineralization. *Matrix Biol* 2009;28:221–229.
30. Ohtsuka M, Miura H, Sato M, Kimura M, Inoko H, Gurumurthy CB. PITT: pronuclear injection-based targeted transgenesis, a reliable transgene expression method in mice. *Exp Anim* 2012;61:489–502.
31. Kos CH. Cre/loxP system for generating tissue-specific knockout mouse models. *Nutr Rev* 2004;62:243–246.
32. Ray MK, Fagan SP, Brunicardi FC. The Cre-loxP system: a versatile tool for targeting genes in a cell- and stage-specific manner. *Cell Transplant* 2000;9:805–815.
33. Kim H, Kim M, Im SK, Fang S. Mouse Cre-LoxP system: General principles to determine tissue-specific roles of target genes. *Lab Anim Res* 2018;34:147–159.
34. Chang H, Brown CW, Matzuk MM. Genetic analysis of the mammalian transforming growth factor-beta superfamily. *Endocr Rev* 2002;23:787–823.
35. Coin R, Haïkel Y, Ruch JV. Effects of apatite, transforming growth factor beta-1, bone morphogenetic protein-2 and interleukin-7 on ameloblast differentiation in vitro. *Eur J Oral Sci* 1999;107:487–495.
36. Wang XP, Suomalainen M, Jorgez CJ, Matzuk MM, Werner S, Thesleff I. Follistatin regulates enamel patterning in mouse incisors by asymmetrically inhibiting BMP signaling and ameloblast differentiation. *Dev Cell* 2004;7:719–730.
37. Malik Z, Alexiou M, Hallgrímsson B, Economides AN, Luder HU, Graf D. Bone morphogenetic protein 2 coordinates early tooth mineralization. *J Dent Res* 2018;97:835–843.
38. Yadin D, Knaus P, Mueller TD. Structural insights into BMP receptors: Specificity, activation and inhibition. *Cytokine Growth Factor Rev* 2016;27:13–34.
39. Zhang X, Shi C, Zhao H, et al. Distinctive role of ACVR1 in dentin formation: Requirement for dentin thickness in molars and prevention of osteodentin formation in incisors of mice. *J Mol Histol* 2019;50:43–61.
40. Feng J, Jing J, Li J, et al. BMP signaling orchestrates a transcriptional network to control the fate of mesenchymal stem cells in mice. *Development* 2017;144:2560–2569.
41. Liu W, Sun X, Braut A, et al. Distinct functions for Bmp signaling in lip and palate fusion in mice. *Development* 2005;132:1453–1461.
42. Derynck R, Zhang YE. Smad-dependent and Smad-independent pathways in TGF-beta family signalling. *Nature* 2003;425:577–584.
43. Bleicher F, Couble ML, Farges JC, Couble P, Magloire H. Sequential expression of matrix protein genes in developing rat teeth. *Matrix Biol* 1999;18:133–143.
44. Hao J, Zou B, Narayanan K, George A. Differential expression patterns of the dentin matrix proteins during mineralized tissue formation. *Bone* 2004;34:921–932.
45. Kim TH, Bae CH, Lee JY, et al. Temporo-spatial requirement of Smad4 in dentin formation. *Biochem Biophys Res Commun* 2015;459:706–712.
46. Ye L, MacDougall M, Zhang S, et al. Deletion of dentin matrix protein-1 leads to a partial failure of maturation of predentin into dentin, hypomineralization, and expanded cavities of pulp and root canal during postnatal tooth development. *J Biol Chem* 2004;279:19141–19148.
47. Duverger O, Zah A, Isaac J, et al. Neural crest deletion of Dlx3 leads to major dentin defects through down-regulation of Dspp. *J Biol Chem* 2012;287:12230–12240.
48. Oka S, Oka K, Xu X, Sasaki T, Bringas P Jr, Chai Y. Cell autonomous requirement for TGF-beta signaling during odontoblast differentiation and dentin matrix formation. *Mech Dev* 2007;124:409–415.
49. Jinek M, Chylinski K, Fonfara I, Hauer M, Doudna JA, Charpentier E. A programmable dual-RNA-guided DNA endonuclease in adaptive bacterial immunity. *Science* 2012;337:816–821.
50. Jinek M, East A, Cheng A, Lin S, Ma E, Doudna J. RNA-programmed genome editing in human cells. *Elife* 2013;2:e00471.
51. Doudna JA, Charpentier E. Genome editing. The new frontier of genome engineering with CRISPR-Cas9. *Science* 2014;346:1258096.
52. Zhang F, Wen Y, Guo X. CRISPR/Cas9 for genome editing: Progress, implications and challenges. *Hum Mol Genet* 2014;23:R40–R46.
53. Liang T, Hu Y, Zhang H, et al. Mouse Dspp frameshift model of human dentinogenesis imperfecta. *Sci Rep* 2021;11:20653.
54. Li D, Du X, Zhang R, et al. Mutation identification of the DSPP in a Chinese family with DGI-II and an up-to-date bioinformatic analysis. *Genomics* 2012;99:220–226.
55. Lee SK, Lee KE, Song SJ, Hyun HK, Lee SH, Kim JW. A DSPP mutation causing dentinogenesis imperfecta and characterization of the mutational effect. *Biomed Res Int* 2013;2013:948181.
56. Liang T, Zhang H, Xu Q, Wang S, Qin C, Lu Y. Mutant dentin sialophosphoprotein causes dentinogenesis imperfecta. *J Dent Res* 2019;98:912–919.
57. Verdelis K, Szabo-Rogers HL, Xu Y, et al. Accelerated enamel mineralization in Dspp mutant mice. *Matrix Biol* 2016;52:246–259.
58. Pavletich NP, Pabo CO. Zinc finger-DNA recognition: Crystal structure of a Zif268-DNA complex at 2.1 Å. *Science* 1991;252:809–817.
59. Smith J, Bibikova M, Whitby FG, Reddy AR, Chandrasegaran S, Carroll D. Requirements for double-strand cleavage by chimeric restriction enzymes with zinc finger DNA-recognition domains. *Nucleic Acids Res* 2000;28:3361–3369.
60. Carroll D. Genome engineering with zinc-finger nucleases. *Genetics* 2011;188:773–782.
61. Chiba Y, He B, Yoshizaki K, et al. The transcription factor AmeloD stimulates epithelial cell motility essential for tooth morphology. *J Biol Chem* 2019;294:3406–3418.
62. Alwin S, Gere MB, Guhl E, et al. Custom zinc-finger nucleases for use in human cells. *Mol Ther* 2005;12:610–617.
63. Miller JC, Tan S, Qiao G, et al. A TALE nuclease architecture for efficient genome editing. *Nat Biotechnol* 2011;29:143–148.
64. Gaj T, Gersbach CA, Barbas CF 3rd. ZFN, TALEN, and CRISPR/Cas-based methods for genome engineering. *Trends Biotechnol* 2013;31:397–405.
65. Joung JK, Sander JD. TALENs: A widely applicable technology for targeted genome editing. *Nat Rev Mol Cell Biol* 2013;14:49–55.
66. Moscou MJ, Bogdanove AJ. A simple cipher governs DNA recognition by TAL effectors. *Science* 2009;326:1501.

67. Boch J, Scholze H, Schornack S, et al. Breaking the code of DNA binding specificity of TAL-type III effectors. *Science* 2009;326:1509–1512.
68. Takahashi M, Ikeda K, Ohmura M, et al. Six1 is required for signaling center formation and labial-lingual asymmetry in developing lower incisors. *Dev Dyn* 2020;249:1098–1116.
69. Christian M, Cermak T, Doyle EL, et al. Targeting DNA double-strand breaks with TAL effector nucleases. *Genetics* 2010;186:757–761.
70. Nemudryi AA, Valetdinova KR, Medvedev SP, Zakian SM. TAL-EN and CRISPR/Cas genome editing systems: Tools of discovery. *Acta Naturae* 2014;6:19–40.
71. Chang B, Ahuja N, Ma C, Liu X. Injectable scaffolds: Preparation and application in dental and craniofacial regeneration. *Mater Sci Eng R Rep* 2017;111:1–26.
72. Li Q, Chang B, Dong H, Liu X. Functional microspheres for tissue regeneration. *Bioact Mater* 2022;25:485–499.
73. Bachhuka A, Delalat B, Ghaemi SR, Gronthos S, Voelcker NH, Vasilev K. Nanotopography mediated osteogenic differentiation of human dental pulp derived stem cells. *Nanoscale* 2017;9:14248–14258.
74. Du Y, Montoya C, Orrego S, et al. Topographic cues of a novel bilayered scaffold modulate dental pulp stem cells differentiation by regulating YAP signalling through cytoskeleton adjustments. *Cell Prolif* 2019;52:e12676.
75. Graziano A, d'Aquino R, Cusella-De Angelis MG, et al. Concave pit-containing scaffold surfaces improve stem cell-derived osteoblast performance and lead to significant bone tissue formation. *PLoS One* 2007;2:e496.
76. Feng KC, Pinkas-Sarafova A, Ricotta V, et al. The influence of roughness on stem cell differentiation using 3D printed polylactic acid scaffolds. *Soft Matter* 2018;14:9838–9846.
77. Portone A, Moffa M, Gardin C, et al. Lineage-specific commitment of stem cells with organic and graphene oxide-Functionalized nanofibers. *Adv Funct Mater* 2019;29:1806694-n/a.
78. Ha M, Athirasala A, Tahayeri A, Menezes PP, Bertassoni LE. Micropatterned hydrogels and cell alignment enhance the odontogenic potential of stem cells from apical papilla in-vitro. *Dent Mater* 2020;36:88–96.
79. Alksne M, Simoliunas E, Kalvaityte M, et al. The effect of larger than cell diameter polylactic acid surface patterns on osteogenic differentiation of rat dental pulp stem cells. *J Biomed Mater Res A* 2019;107:174–186.
80. Ma C, Qu T, Chang B, Jing Y, Feng JQ, Liu X. 3D maskless micropatterning for regeneration of highly organized tubular tissues. *Adv Healthc Mater* 2018;7:10.1002/adhm.201700738.
81. Chang B, Ma C, Liu X. Nanofibrous tubular three-dimensional platform for single dental pulp stem cell polarization. *ACS Appl Mater Interfaces* 2020;12:54481–54488.
82. Chang B, Ma C, Feng J, Svoboda KKH, Liu X. Dental pulp stem cell polarization: Effects of biophysical factors. *J Dent Res* 2021;100:1153–1160.
83. Niu L, Zhang H, Liu Y, et al. Microfluidic chip for odontoblasts in vitro. *ACS Biomater Sci Eng* 2019;5:4844–4851.
84. Qu T, Jing J, Ren Y, et al. Complete pulpodentin complex regeneration by modulating the stiffness of biomimetic matrix. *Acta Biomater* 2015;16:60–70.
85. Chuang YC, Yu Y, Wei MT, et al. Regulating substrate mechanics to achieve odontogenic differentiation for dental pulp stem cells on TiO₂ filled and unfilled polyisoprene. *Acta Biomater* 2019;89:60–72.
86. Liu N, Zhou M, Zhang Q, et al. Stiffness regulates the proliferation and osteogenic/odontogenic differentiation of human dental pulp stem cells via the WNT signalling pathway. *Cell Prolif* 2018;51:e12435.
87. Miyashita S, Ahmed NE, Murakami M, et al. Mechanical forces induce odontoblastic differentiation of mesenchymal stem cells on three-dimensional biomimetic scaffolds. *J Tissue Eng Regen Med* 2017;11:434–446.
88. Mammoto T, Mammoto A, Jiang A, Jiang E, Hashmi B, Ingber DE. Mesenchymal condensation-dependent accumulation of collagen VI stabilizes organ-specific cell fates during embryonic tooth formation. *Dev Dyn* 2015;244:713–723.
89. Hashmi B, Mammoto T, Weaver J, et al. Mechanical induction of dentin-like differentiation by adult mouse bone marrow stromal cells using compressive scaffolds. *Stem Cell Res* 2017;24:55–60.
90. Maikhuri B, Sahoo N, Jena S, Dash BP, Dash S. Prevalence of pulp stones after orthodontic treatment-A review. *J Pharm Negat* 2023;14:71–77.
91. Liao C, Ou Y, Wu Y, Zhou Y, Liang S, Wang Y. Sclerostin inhibits odontogenic differentiation of human pulp-derived odontoblast-like cells under mechanical stress. *J Cell Physiol* 2019;234:20779–20789.
92. Collignon AM, Amri N, Lesieur J, et al. Sclerostin deficiency promotes reparative dentinogenesis. *J Dent Res* 2017;96:815–821.
93. Lee SK, Lee CY, Kook YA, Lee SK, Kim EC. Mechanical stress promotes odontoblastic differentiation via the heme oxygenase-1 pathway in human dental pulp cell line. *Life Sci* 2010;86:107–114.
94. Cai X, Zhang Y, Yang X, Grottkau BE, Lin Y. Uniaxial cyclic tensile stretch inhibits osteogenic and odontogenic differentiation of human dental pulp stem cells. *J Tissue Eng Regen Med* 2011;5:347–353.
95. Chen YY, He ST, Yan FH, et al. Dental pulp stem cells express tendon markers under mechanical loading and are a potential cell source for tissue engineering of tendon-like tissue. *Int J Oral Sci* 2016;8:213–222.
96. Magloire H, Couble ML, Thivichon-Prince B, Maurin JC, Bleicher F. Odontoblast: A mechano-sensory cell. *J Exp Zool B Mol Dev Evol* 2009;312B:416–424.
97. Sun XF, Qiao WW, Meng LY, Bian Z. PIEZO1 ion channels mediate mechanotransduction in odontoblasts. *J Endod* 2022;48:749–758.
98. Sato M, Furuya T, Kimura M, et al. Intercellular odontoblast communication via ATP mediated by pannexin-1 channel and phospholipase C-coupled receptor activation. *Front Physiol* 2015;6:326.
99. Honda MJ, Shinohara Y, Sumita Y, Tonomura A, Kagami H, Ueda M. Shear stress facilitates tissue-engineered odontogenesis. *Bone* 2006;39:125–133.
100. Zuo J, Zhen J, Wang F, Li Y, Zhou Z. Effect of low-intensity pulsed ultrasound on the expression of calcium ion transport-related proteins during tertiary dentin formation. *Ultrasound Med Biol* 2018;44:223–233.
101. Theocharidou A, Bakopoulou A, Kontonasaki E, et al. Odontogenic differentiation and biomineralization potential of dental pulp stem cells inside Mg-based bioceramic scaffolds under low-level laser treatment. *Lasers Med Sci* 2017;32:201–210.
102. Zhang B, Yu Q, Liu Y. Polarization of stem cells directed by magnetic field-manipulated supramolecular polymeric nanofibers. *ACS Appl Mater Interfaces* 2021;13:9580–9588.

Mouse Models of Orofacial Clefts: SHH and TGF- β Pathways

Yu Chen LI^{1#}, Le Ran LI^{1#}, Zi Han GAO¹, Yi Ran YANG¹, Qian Chen WANG¹,
Wei Yu ZHANG¹, Li Qi ZHANG¹, Tian Song XU¹, Feng CHEN¹

Birth defects have always been one of the most important diseases in medical research as they affect the quality of the birth population. Orofacial clefts (OFCs) are common birth defects that place a huge burden on families and society. Early screening and prevention of OFCs can promote better natal and prenatal care and help to solve the problem of birth defects. OFCs are the result of genetic and environmental interactions; many genes are involved, but the current research has not clarified the specific pathogenesis. The mouse animal model is commonly used for research into OFCs; common methods of constructing OFC mouse models include transgenic, chemical induction, gene knockout, gene knock-in and conditional gene knockout models. Several main signal pathways are involved in the pathogenesis of OFCs, including the Sonic hedgehog (SHH) and transforming growth factor (TGF)- β pathways. The genes and proteins in each molecular pathway form a complex network to jointly regulate the formation and development of the lip and palate. When one or more genes, proteins or interactions is abnormal, OFCs will form. This paper summarises the mouse models of OFCs formed by different modelling methods, as well as the key pathogenic genes from the SHH and TGF- β pathways, to help to clarify the pathogenesis of OFCs and develop targets for early screening and prevention.

Key words: mouse models, orofacial clefts, Sonic hedgehog pathway, transforming growth factor- β pathway.

Chin J Dent Res 2023;26(4):209–226; doi: 10.3290/j.cjdr.b4784053

As a result of socioeconomic progress and development, the mean age of the childbearing population is gradually increasing, leading to a rise in the incidence of birth defects and placing huge burdens on families and society for medical care as well as other influences¹⁻³. Orofacial clefts (OFCs) account for a large proportion of birth defects, with an average of 1 in 600 to 800 newborns

suffering from cleft lip and palate⁴. OFCs not only seriously affect the appearance of the face, but also directly impact development of the mouth and nose, often leading to upper respiratory tract infections and otitis media and causing serious psychological trauma to children and parents. It is therefore important to screen for and prevent birth defects.

OFCs are the most common congenital malformation in the oral and maxillofacial region. They can be regarded as a symptom of many syndromes or can occur independently and can be divided into two types: cleft lip with or without cleft palate (CL/P) and cleft palate only (CPO). An OFC is a gap formed by the improper fusion of facial prominences during early embryonic development. Studies have found that a combination of genetic and environmental factors lead to this occurrence, which is regulated by complex mechanisms⁵. Multiple signalling pathways and genes are involved. Lip and palatal development involve a series of highly coordinated, genetically programmed morphogenetic events. Gene mutations lead to palate shelf elevation,

1 Central Laboratory, Peking University School and Hospital of Stomatology, Beijing, P.R. China.

These two authors contributed equally to this work.

Corresponding authors: Dr Feng CHEN and Dr Tian Song XU, Central Laboratory, Peking University School and Hospital of Stomatology, #22 Zhongguancun South Avenue, HaiDian District, Beijing 100081, P.R. China. Tel: 86-10-82195773. Email: chenfeng2011@hsc.pku.edu.cn; willmaxu@163.com

This study was supported by grants from the National Natural Science Foundation of China (nos. 81870747 and 82170916), and the Fundamental Research Funds for the Central Universities (PKU2022XGK001).

epithelial–mesenchymal transformation and epithelial apoptosis abnormalities, which result in abnormal development of the lip and palate. In addition, an increasing number of studies have found that epigenetic mechanisms may be involved in the pathogenesis of OFCs, mainly including deoxyribonucleic acid (DNA) methylation, non-coding ribonucleic acid (ncRNA) and histone modification^{6–8}. MicroRNAs (miRNAs) play a crucial role in silencing the expression of specific genes^{8,9}. Environmental factors such as nutrition and smoking have a significant impact on DNA methylation patterns¹⁰.

Animal models are important for understanding the pathogenesis of OFCs. Because the early embryonic craniomaxillofacial development of *Xenopus*, zebrafish and mice is very similar to that of humans, they are suitable animal models for the study of OFCs. The mouse is the most commonly used animal model in OFC studies; advantages include its small size, rapid reproduction, high similarity with human genes, stable genetic background and clear gene sequence¹¹, which make it suitable for a variety of experiments. The existing methods for constructing OFC mouse models include transgenesis, chemical induction, gene knockout (KO), gene knock-in and conditional gene knockout (CKO).

In the existing mouse model of OFCs, hundreds of genes have been studied. The pathogenesis of OFCs is complex, and multiple genes and signalling pathways are involved, such as fibroblast growth factor (FGF), bone morphogenetic protein (BMP), Wnt, Sonic hedgehog (SHH) and transforming growth factor (TGF)- β signalling¹². Of the many different pathways, SHH and TGF- β play an important role in growth and development. These signalling pathways affect embryonic differentiation, tissue development and organ formation in early developmental stages, and perturbation of signalling pathways may underlie many human craniofacial abnormalities^{12–14}. The mouse models of CL/P and CPO have been introduced in detail in previous reviews^{15,16}. This paper focuses on the mouse models of the SHH and TGF- β pathways and provides supplements and updates to the previous models. Research on the genes and mechanisms involved in cleft lip and palate is conducive to understanding its pathogenesis and further developing methods for prevention and treatment, thus reducing its incidence rate.

SHH signalling pathway

Hedgehog proteins are a family of secreted signal proteins that jointly regulate many aspects of animal development, tissue homeostasis and regeneration¹⁷.

The persistently activated SHH signalling pathway is involved in lung cancer cell proliferation, apoptosis, epithelial–mesenchymal transformation, angiogenesis and drug resistance recurrence. The pathway is composed of the Shh, Ptc, Smo, PKA and Gli proteins. Shh ligand can be produced by secretory cells of multiple organs and is an extracellular ligand (Fig 1).

The hedgehog pathway is relevant to many congenital diseases. Shh and Indian hedgehog (Ihh) are closely related to craniofacial development. Shh is expressed in the craniofacial ectoderm and regulates the development of the neural crest. It is significant for formation of the upper lip and secondary palate^{18–20}. Downregulation of this signal in the palate and medial nasal processes (MNPs) will lead to CL/P. During palatal fusion, however, if the signal is not downregulated in time, the medial marginal epithelium will fail to fuse, causing cleft palate (Fig 1).

Transgenic

In the early stage, transgenesis (the use of vectors to transfer specific foreign genes into a genome to increase, prevent or change the expression of a gene to study its functions) was widely used in the construction of OFC mouse models²¹ (Table 1). Transgenesis used in the SHH pathway mainly targets *Ptch1* and Hedgehog acyltransferase (Hhat).

As an important factor in the initial transmembrane process of SHH signalling, *Ptch1* is a negative regulator that inhibits the transmembrane protein Smo. Upon binding to Shh, *Ptch1* is degraded. *Ptch1* expression is essential for formation of the primitive nose and upper lip. Transfer of K14-Shh into embryos leads to overexpression of Shh in epithelial cells, similar to *Ptch1* knockout. This model results in CPO²².

In addition to the important role played by *Ptch1* in transmembrane processes, multimerisation, distribution and activity of Hedgehog protein are also significant. Autoproteolytic cleavage of Hedgehog (Hh) precursor molecules generates an N-terminal fragment (Hh-N) referred to as the mature form. Hh-N is then modified via the addition of a cholesterol moiety to its C-terminus, and then a palmitoyl moiety to its N-terminus. These lipid modifications are required for Hh protein multimerisation, distribution and activity. Mouse embryos engineered with AP2-Cre inserted into Hedgehog acyltransferase (Hhat) showed small size, craniofacial hypoplasia and limb defects. The mice displayed a defect in vertical extension and medial growth of the palatal shelves towards the midline, resulting in cleft palate. Hhat loss-of-function should disrupt the palmitoylation of Shh. The

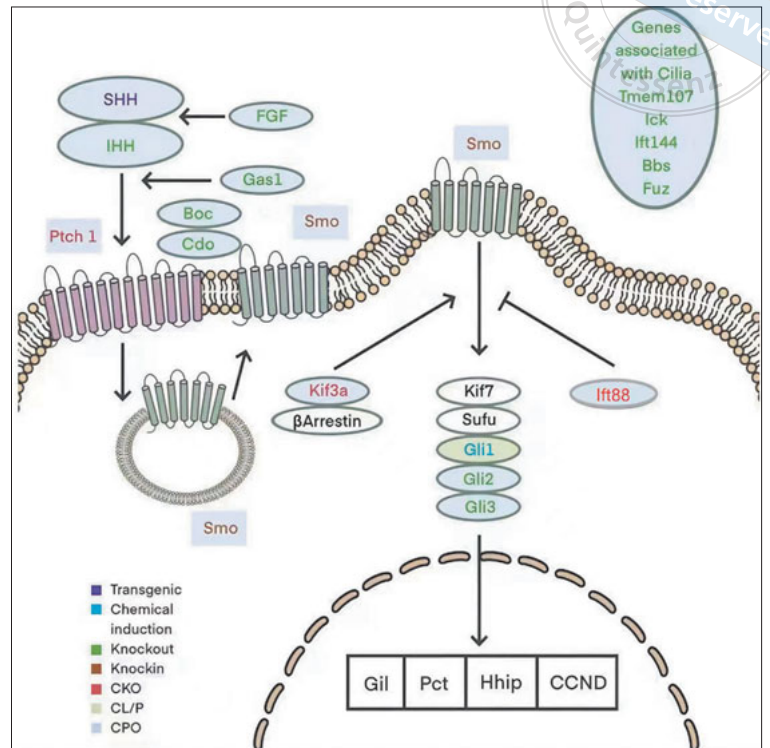


Fig 1 Genes associated with orofacial clefts in the SHH pathway.

signal gradient of Shh in the tissue is destroyed, resulting in abnormal SHH signal strength²³.

Chemical induction

Chemical induction methods use chemicals such as retinoic acid to induce an OFC phenotype in mice²⁴. Common chemical inducers include retinoic acid, cyclopamine and vismodegib (Table 1).

Retinoic acid-induced embryos show frontonasal process (FNP) and maxillary process (MXP) fusion dysfunction, which is caused by retinoic acid inhibition of the expression of SHH molecules. The lack of SHH causes the FNP and MXP to stop growing, resulting in bilateral cleft lip and palate²⁵.

Other SHH pathway-associated chemical inducers that cause OFCs in mice include cyclopamine and vismodegib. Both are antagonists of the SHH pathway and the induced mouse phenotype is CL/P. Cyclopamine directly binds Smo, changing its conformation to inhibit Hh pathway activation. Vismodegib can be chemically modified by cyclopamine; its principle is the same as cyclopamine but with a greater effect^{26,27}.

In addition to chemical modifications, transcription of target genes can also be blocked. Gli1, as the most common transcriptional activator activated by Smo, participates in the transcription of target genes and functions in craniofacial and finger development,

as well as central nervous system and gastrointestinal development, and is also involved in cell proliferation and differentiation through its role in SHH signalling, while cyclopamine is its common blocker. Stimulation of cranial neural crest cells (CNCCs) with SHH ligands causes significant upregulation of *Gli1* and *Foxf2* expression, which can be blocked completely by the addition of cyclopamine; outgrowth of the MNP is attenuated after blockade, leading to deficient frontonasal prominence-derived MNP, preventing contact with the MXP and subsequent fusion, which causes the CL/P phenotype²⁸.

Gene KO

KO techniques are used to construct OFC mouse models via deletion of target genes in mice by homologous recombination (Table 2).

The SHH-based mouse model of OFCs includes genes such as *Gli2*, *Gli3*, *Ihh*, *Ick* and *Tmem107*; the mouse phenotype is dominated by incomplete penetrant CPO.

Ihh is a ligand in the HH pathway that plays an important role in craniofacial development. It can form a negative feedback loop with parathyroid hormone-associated protein to indirectly regulate chondrocyte differentiation and affect chondrocyte proliferation and osteoblast specification. *Ihh* KO mice have the CPO phenotype^{30,31}. The proteins encoded by *Cdo* and *Boc* are

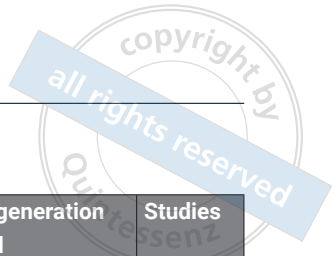


Table 1 Transgenic and chemical induction in SHH.

Gene	Approach	Phenotype and penetrance	Embryonic development period	Gene/protein expression	Cause of death	Model generation method	Studies
<i>Ptch1</i>	Transgenic	CPO	E14.5–15.5	E13.5: oral epithelium of the palatal shelves, with a corresponding gradient of <i>Ptch1</i> expression in the underlying mesenchyme	Perinatal lethality	EcoRI/HindIII double digest and pronuclear DNA injection of CBA/C56 BL6 embryos on E0.5. Isolating K14-SHH transgene	Cobourne et al ²²
<i>Hedgehog acyltransferase (Hhat)</i>	Transgenic	CPO	E9.5–14.5	The pharyngeal and midfacial hypoplasia evident in the form of a single nasal slit	Lymphatic and vascular anomalies	Hhat ⁺ /Creface	Dennis et al ²³
	Chemical induction	Bilateral CLP	NR	Endoderm of the first, second and third pharyngeal pouches, and ectodermal-endodermal boundaries	NR	Retinoic acid induction	Helms et al ²⁵
	Chemical induction	CL/P	GD17	Decreased snout length and mandible length and increased interocular distance	NR	Cyclopamine induction	Chen et al ²⁶ , Lipinski et al ²⁹
	Chemical induction	CL/P	GD7.0-8.25	Highly arched palate	NR	Vismodegib induction	Heyne et al ²⁷
<i>Gli1</i>	Chemical induction	CL/P	GD11.0–14.0	Medial nasal processes (MNPs)	NR	Cycloparamide induction of female mice on GD8.25–9.375, 120 mg/kg/day	Everson et al ²⁸

NR, not reported.

located in the cell membrane and both proteins act as SHH signal coreceptors to promote signal transduction. *Cdo/Boc* double heterozygous mice showed decreased SHH signalling, CPO and forebrain malformation phenotypes³². The protein encoded by *Gas1*, located in the cell membrane, can bind *Shh* together with *Ptch* and play an antagonistic role in the SHH pathway; however, *Gas1* can enhance the effect of SHH in early facial development. When the gene was knocked out, the mice developed CPO and miniature forebrain malformation^{33,34}.

Gli is another important transcriptional factor after *Ihh*. In the presence of *Shh*, *Smo* activation generates intracellular signals that induce dissociation of the *Gli-Sufu* complex and facilitate translocation of transcriptional activator *Gli* into the nucleus. *Gli2* is expressed in the palatal epithelium and mesenchyme; when knocked out, it blocks the SHH pathway, resulting in impaired palatal elevation (no elevation or partial elevation) or delayed fusion³⁵. *Gli3* functions as both an activator and a repressor; the phosphorylated full-length form acts as an activator, while *Gli3R*, a C-terminal truncated form, acts as a repressor. There is a proper balance between

Gli3 activator and inhibitor *Gli3R*. An imbalance will cause over- or underexpression of the SHH pathway, resulting in extensive separation of the palatal shelves from the underlying sphenoid bone, defects and incomplete mineralisation of the maxillary ramus, elevated palatal shelves and fusion disorders³⁶.

In addition to the above, cilia also have an impact on downstream genes. *Tmem107*, *Ick*, *Ift144*, *Bbs* and *Fuz* are related to the formation and function of cilia. Knockout of these genes causes changes in downstream genes, leading to the CPO model. *Tmem107* combined with *Gli2* and *Gli3* also plays a role in ciliogenesis and embryogenesis³⁷. *Ick* regulates intra-flagellar transport velocity and negatively regulates ciliary length. Knockout of *Ick* results in abnormal primary cilia and distribution of *Smo*, which affects conduction of the SHH pathway, resulting in CPO and other malformations³⁸. *Ift144*, which is related to ciliary transport, may mediate bone migration during development, such as fusion of the MNP and lateral nasal process as well as fusion with the MXP³⁹. *Bbs* can reduce the level of *Smo* in cilia but can also regulate the transformation

Table 2 Gene knockout in SHH.

Gene	Phenotype and penetrance	Embryonic development period	Gene/protein expression	Cause of death	Model generation method	Studies
<i>Ihh</i>	CPO	E13.5–17.5	Developing palatine bone	Murine lethality not mentioned	<i>Ihh</i> ^{+/-} ; <i>Ptc-lacZ</i>	Levi et al ³⁰ , Ohba ³¹
<i>Cdo, Boc</i>	CPO	E11.5–15.5	Dorsal regions of the developing CNS	Perinatal death, cause not mentioned	<i>Cdo</i> ^{+/-} : gene targeting in embryonic stem (ES) cells, deletion of exon 1 and addition of marker fragment <i>BOC</i> ^{+/-} : gene targeting of ES cells, deletion of exon 1 fragment and addition of marker gene fragment to exon 2	Zhang et al ³² , Cole and Krauss ⁴⁶
<i>Gas1</i>	CPO, 60%	E13.5–15.5	Early craniofacial region	Almost died within the first 3 days of life	<i>Gas1</i> gene was knocked out in ES cells, and recombinant positive cells were screened out to establish chimeric blastocysts	Lee et al ³³ , Seppala et al ³⁴
<i>Gli2</i>	CPO, 64%	13.5–14.5dpc	Epithelium and mesenchyme of jawbone	NR	<i>Gli2</i> zinc finger domain was isolated from a 129/Sv genomic library. Genomic DNA was digested with <i>EcoRV</i> and hybridised with a 0.7 kb <i>XbaI</i> - <i>BamHI</i> 5' probe, or with <i>BamHI</i> and hybridised with a 1.0-kb <i>XbaI</i> - <i>EcoRI</i> 3' probe	Mo et al ³⁵
<i>Gli3</i>	CPO	E13.5–14.0	Mesenchyma and epithelium of palatal shelves	NR	<i>Gli3</i> ^{+/-} mice with C57/BL6 genetic background	Huang et al ³⁶
<i>Tmem107</i>	CPO	E13.5–15.5	The front and middle of the palatal shelves	NR	<i>Tmem107</i> ^{-/-} mice (all 5 exons of <i>Tmem107</i> were replaced with a targeting cassette via homologous recombination)	Cela et al ³⁷
<i>Ick</i>	CPO	E15.5	Epithelial cells	Third trimester embryonic death	<i>Ick</i> ^{tm1a} (KOMP)Mbp allele (<i>Ick</i> ^{tm1a}) contains an embedded splice receptor sequence and a β-galactosidase reporter gene located between exons 5 and 6	Moon et al ³⁸
<i>Ift144</i>	CL/P, 84%	13.5–15.5dpc	Palatal shelves	NR	FVB/C57BL6 F1 <i>twf</i> ^{+/-} intercross or FVB/C57BL6 F1 <i>twf</i> ^{+/-} × FVB <i>twf</i> ^{+/-} backcross	Ashe et al ³⁹
<i>Bbs</i>	CPO	E12.5	<i>Bbs7</i> : endothelial cells, etc; <i>Ift88</i> : bronchial epithelial cells, etc	Prenatal death, double mutant embryos, pericardial oedema	Knockout of <i>Bbs7</i> combined with a hypomorphic <i>Ift88</i> allele (<i>orpk</i> as a model for SHH dysfunction)	Zhang et al ⁴⁰
<i>Fuz</i>	CPO	E18.5	Brain, spinal cord, eye, craniofacial, etc	Death after birth, cause not mentioned	Gene trap cassette inserted in the second exon of the <i>Fuz</i> gene	Gray et al ⁴¹

NR, not reported.

Table 3 Gene knock-in in SHH.

Gene	Phenotype and penetrance	Embryonic development period	Gene/protein expression	Cause of death	Model generation method	Studies
<i>Fgf</i>	CPO	E13.5	Posterior region and mesenchyme of the developing palate or nasal epithelium	NR	FGF-R1 recombinant virus with a hemagglutinin epitope tag	Crisera et al ⁴⁵
<i>Smo</i>	100% CPO	E14.5–15.5	Epithelial cells	The mice died shortly after birth for an undisclosed reason	K14-Cre; R26SmoM-2fl/+; <i>Gli1</i> -LacZ+/-	Li et al ⁴⁴

NR, not reported.



Table 4 CKO in SHH.

Gene	Phenotype and penetrance	Embryonic development period	Gene/protein expression	Cause of death	Model generation method	Studies
<i>Ptch1</i>	Complete cleft of the secondary palate	E13.5–16.5	Palate shelves and developing mandibles	NR	A reading frame of mouse <i>Shh</i> cloned downstream of a human K-14 promoter. EcoRI/HindIII double digest and pronuclear injection	Cobourne et al ²²
	CPO	E11.5–13.5	Palatal mesenchyme	NR	K14-Cre	Lan and Jiang ⁴⁹
<i>Kif3a</i>	CPO	E13.5	Palate shelves	NR	<i>Wnt1-Cre</i> ; <i>Kif3a</i> fl/fl	Li et al ⁵¹
	CPO	E11.5	Neural crest cells	NR	<i>Wnt1-Cre</i> ; <i>Kif3a</i> fl/fl	Liu et al ⁵²
<i>Ptch1</i>	CL	E10.5–11.5	Subfacial mesenchyme	Embryonic lethality at E12.0 (ubiquitous inactivation of <i>Ptch1</i> in mice leads to early embryonic lethality after 9.5 DPC)	<i>Wnt1-Cre</i> ; <i>Patch</i> fl/fl	Metzis et al ⁵⁰
<i>Ift88</i>	CL/P	E10.5–new-born	Palatal epithelium and mesenchyme	Death after birth, cause not mentioned	<i>Wnt1-Cre</i> ; <i>Ift88</i> fl/fl	Tian et al ⁴⁷
	CPO	E12.5–new-born	Palatal epithelium and mesenchyme	NR	<i>Osr2-Cre</i> ; <i>Ift88</i> fl/fl	Tian et al ⁴⁷
	CPO	E18.5	Palate shelves	NR	<i>Wnt1-Cre</i> ; <i>Ift88</i> fl/fl	Watanabe et al ⁴⁸
	CPO	E14.5	Palatal rugae	NR	<i>Shh-Cre</i> ; <i>Ift88</i> fl/fl	Nakaniwa et al ⁵³

NR, not reported.

of Smo from the inactive state to the activated state. SHH pathway activation in mouse embryonic fibroblast cells of *Bbs7* knockout and *Ift88/orpk* homozygous mice decreased by 20% to 30% in a study, showing the CPO phenotype⁴⁰. *Fuz* encodes a planar cell polarity protein involved in ciliogenesis and cargo transport between the base and the tip of the cilium. Knockout of this gene can lead to disorder of cilia development, downregulation of HH signalling and cilia malformation^{41,42}.

Gene knock-in

Gene knock-in, similar to knockout, involves the introduction of foreign functional genes into homologous sequences in cells and genomes via homologous recombination^{43,44} (Table 3).

FGF can induce epithelial cell proliferation and *Shh* expression at the very beginning of SHH signalling; the latter can lead to mesenchymal cell proliferation, thus FGF and SHH signalling have a synergistic effect. Recombinant FGF-R1 virus was transfected into mouse palatal shelf cells cut from E13.5 to induce CPO in this tissue *in vitro*⁴⁵.

HH signalling is gained in epithelial cells in the *K14-Cre*; *R26SmoM2* mouse model, which exhibits CPO. Normally, during palatal fusion, SHH signalling in MEE

cells must be downregulated to ensure palatal shelf fusion. This mouse model enhances HH signalling, leading to maintenance of p63, upregulation of p63 target genes, cell adhesion-associated genes and epithelial progenitor cell-associated genes, and persistence of MEE⁴⁴.

CKO

CKO can modify specific genes in certain development stages, tissues, and cells of mice, thereby improving specificity^{47,48}. Many OFC models are created in this way (Table 4).

The CKO mouse models of OFCs are relatively few, involving *Kif3a*, *Ift88* and *Ptch1*. *Ptch1* is a membrane receptor for *Shh*. Activation of the SHH pathway can be regulated by changing the expression levels of *Shh* or *Ptch1*. *Kif3a* and *Ift88* are both cilia-associated proteins that also regulate the SHH pathway.

Excessive activation of the SHH pathway leads to failure of secondary palate fusion. A mouse model of K14-induced overexpression of *Shh* in epithelial cells can be used to mimic the CKO model of *Ptch1*. Upregulation of *Shh* signals in epithelial cells of these mice results in severe bone and skin defects, as well as severe craniofacial deformities: a complete cleft of the secondary palate but an intact primary palate in K14-*Shh* mice.

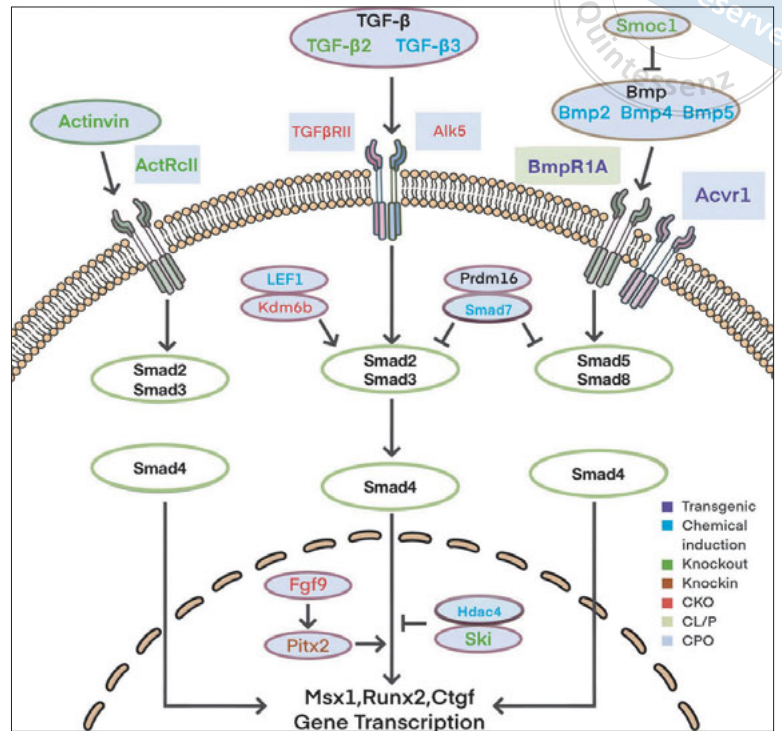


Fig 2 Genes associated with orofacial clefts in the TGF- β pathway.

K14 can also be used to induce *Shh* gene knockout in epithelial cells^{22,49}.

Besides K14-induced overexpression of *Shh* in epithelial cells, overactivation of the SHH pathway can also be achieved by direct CKO of *Ptch1*. Conditional *Ptch1* knockout mice in facial mesenchyme derived from neural crest cells were obtained using *Wnt1-Cre*, and exhibited cleft lip. Inhibitory signalling of Hedgehog by *Ptch1* is essential for formation of the nose and upper lip⁵⁰.

The bind of *Shh* and *Ptch1* is crucial for the formation and function of cilia. When *Shh* binds *Ptch1*, the latter loses its inhibitory effect on *Smo*. *Smo* localises to cilia to mediate downstream molecules. Thus, the SHH pathway can be regulated by altering cilia-associated proteins or inhibiting cilia-material transport. *Kif3a* is a microtubule-based anterograde transporter that functions in primary ciliogenesis; it is also required for ciliary basal formation and microtubule anchoring to centrioles. CKO mice show broad midface processes and nasal pits separated by fissures because of ciliary dyskinesia. At the same time, CNCCs do not extend primary cilia, and the bones of the palatal and ventral cranial midline (maxilla, trabecular lamina, palatal and sphenoid) are either laterally displaced or absent, exhibiting the CPO phenotype^{51,52}. *Kif3a* establishes crosstalk between the SHH and WNT pathways. After primary cilia are established, midline CNCCs require

Kif3a function to integrate and respond to WNT signals from the surrounding epithelium⁵².

Ift88 is involved in primary ciliogenesis and apoptosis and limits bone formation in the MXP. In SHH signalling, *Ift88* is located downstream of *Smo* and upstream of *Gli1*. In *Wnt1-Cre*-mediated *Ift88* knockout mice, the FNP was widened, the distance between nasal pits was increased, the medial nasal depression was rotated, proliferation of cells in the palatal shelves was decreased, proliferation of neural crest cells in the FNP was significantly decreased, apoptosis of cells in the palatal shelves was significantly increased, and proliferation was decreased. The mice showed the CL/P phenotype^{47,48,53,54}. *Osr2* is specifically expressed in the palatal shelves and mesenchyme from E12.5 to birth; *Osr2KI-Cre; Ift88^{fl/fl}* mice exhibited CPO⁴⁷.

TGF- β signalling pathway

The TGF- β signalling pathway is believed to have emerged early in multicellular evolution. TGF- β mainly mediates a variety of embryonic and adult signal functions, providing differentiation, proliferation and control of cell- or tissue-specific movement⁵⁵. In most cells, TGF- β combines with TGF- β receptor II and initiates downstream Smad protein-mediated signal transduction. Smad2 and Smad3 transcription factors in the cytoplasm form heteropolymer complexes and enter

Table 5 Transgenic and chemical induction in TGF- β .

Gene	Approach	Phenotype and penetrance	Embryonic development period	Gene/protein expression	Cause of death	Model generation method	Studies
<i>BmpRIA/Alk3</i>	Transgenic	CL/P	P0	Epithelium and mesenchyme of anterior palate, epithelium of posterior palate	All binary transgenic mice died shortly after birth	Wnt1-Cre mice were mated to pMes-caBmpRIa mice	Li et al ⁵⁸
<i>Acvr1</i>	Transgenic	Submucosal cleft palate, 100%	NR	Palatal epithelium	NR	Mice carrying the caACVR1 allele were mated with mice carrying the K14-Cre allele	Noda et al ⁵⁹
<i>TGF-β3</i>	Chemical induction	CPO	GD12.5, GD13.5, GD14.5, GD15.5, GD16.5	Pre-fusion palatal midline epithelium	NR	Pregnant mice were given tetrachlorodibenzo-p-dioxin on GD10 with or without folic acid. The control mice received sesame oil on GD10	Li et al ⁶⁰
<i>BMP I receptor</i>	Chemical induction	Partial anterior cleft palate or complete cleft palate	E16.5	NR	NR	Pregnant C57Bl/6J mice were intraperitoneally injected with LDN-193189 from E10.5 to E15.5 at a dose of 3, 6 or 9 mg/kg twice a day	Lai et al ⁶¹
<i>Bmp2,4,5 mRNA</i>	Chemical induction	CPO, 100%	E14-16	Many regions of the developing embryo	NR	BALB/c mice exposed to retinoic acid in E12	Lu et al ⁶²
<i>Smad7</i>	Chemical induction	CPO	E14.5	NR	NR	Retinoic acid induced C57BL/6 mice	Yu et al ⁶³ , Shu et al ⁶⁵
<i>Lef1</i>	Chemical induction	CPO	E14	NR	NR	Retinoic acid induced C57BL/6 mice	Yu et al ⁶³ , Shu et al ⁶⁵
<i>Smad3</i>	Chemical induction	CPO	E10.5-14.5	NR	NR	Retinoic acid induction	Kang et al ⁶⁴ , Shu et al ⁶⁶
<i>Hdac4</i>	Chemical induction	CPO	E10.5-14.5	NR	NR	Retinoic acid induction	Kang et al ⁶⁴ , Shu et al ⁶⁶

NR, not reported.

the nucleus, thus participating in various physiological and pathological processes (Fig 2).

TGF- β signalling regulates the proliferation, differentiation, migration and apoptosis of epithelial and mesenchymal cells in the lip and palate, thus affecting the fusion of facial prominences, the elevation and fusion of palatal shelves and the development of cartilage and bone^{56,57}. Pathway conduction disorder will lead to CPO and other abnormalities (Fig 2).

Transgenic

Transgenesis used in the TGF- β pathway mainly targets *BmpRIA* and *Acvr1*, which are receptors in this pathway (Table 5). OFC mouse models have been created using transgenic technology to overexpress *BmpRIA* and *Acvr1* in the TGF- β signalling pathway. Overexpression of *BmpRIA* in the cranial neural crest mediated by

WNT1-Cre leads to CL/P in mice. BMP signalling can regulate cell proliferation in the anterior palatal mesenchyme and maintain the integrity of the posterior palatal epithelium. *BmpRIA*-mediated BMP signalling activity is enhanced, the cell proliferation rate of the anterior palatal mesenchyme is changed, and ectopic expression of *Msx1* and *Shox2* in the posterior palatal mesenchyme leads to ectopic chondrogenesis and delayed palatal elevation, resulting in cleft palate formation⁵⁸. K14-Cre-mediated *Acvr1* overexpression in palatal epithelium also specifically enhances Smad-dependent BMP signalling, resulting in submucosal cleft palate⁵⁹.

Chemical induction

Chemical induction mainly targets TGF- β 3 and *Bmp*, which are ligands in the TGF- β pathway (Table 5). TGF- β 3, an important ligand of the TGF- β pathway, plays a domi-

nant role in palatogenesis and its fine-tuned expression is temporally and spatially correlated with the critical events surrounding palatal shelf adhesion. Tetrachlorodibenzo-p-dioxin can inhibit the expression of *TGF-β3* during palatine development and induce abnormal apoptosis in medial edge epithelial (MEE) cells, leading to CPO. Folic acid has no protective effect on 2,3,7,8-tetrachlorodibenzo-p-dioxin-induced cleft palate⁶⁰. Ldn-193189 can manipulate BMP signalling by selectively targeting the BMP/Smad signalling pathway, resulting in a significant reduction of BMP/Smad signalling (p-Smad1/5/8) and unchanged BMP noncanonical signalling (p-p38, p-Erk1/2); the palatal shelves thus fail to adhere properly, resulting in partial anterior or complete cleft palate⁶¹.

Bmp is also a ligand of the TGF-β pathway. Smads are signal transduction molecules downstream of the Bpm receptor. Following induction with retinoic acid, mice showed a CPO phenotype that was related to *Bmp-2/4/5*, *Smad7*, *Smad3* and *Hdac4*. The content of *Bmp-2/4/5* mRNA in both condensed and dispersed mesenchyme is reduced, and the ability of undifferentiated mesenchyme to differentiate into osteoblasts is also reduced, resulting in abnormal bone shape development⁶². Smad7 is an inhibitory signal transduction molecule downstream of TGF-β family receptors. Lef1 is a cofactor of the TGF-β pathway that forms a complex with Smad2/Smad4, corresponding to the TGF-β signal⁶³. Hdac4 acts as a co-repressor of TGF-β/Smad3-mediated Runx2 functional transcriptional repression in osteoblasts⁶⁴. Retinoic acid-induced reduction of *Smad7* and *Lef1* expression⁶⁵ and cis-element methylation of Smad3 and Hdac4⁶³ may be involved in CPO formation.

Gene knockout

In the TGF-β signalling pathway, knockout mouse models generally affect the elevation of mouse palatal shelves, leading to the occurrence of OFCs. The genes involved include *TGF-β2*, *Prdm16*, *Ctgf* and *Bmp7* (Table 6).

TGF-β2 is a ligand of the TGF-β family and plays a role in the epithelial-mesenchymal transition. *Bmp7* is a ligand of the BMP pathway. *Ctgf* mediates Smad-dependent TGF-β signalling to regulate mesenchymal cell proliferation during palatal development. At the same time, *Ctgf* is a downstream target of TGF-β signalling. The mechanism of CPO after *Tgf-β2*, *Bmp7* or *Ctgf* knockout is similar to that of *Prdm16*⁶⁷.

Prdm16 can bind Smads linked to TGF-β and BMP to regulate the transcription of downstream genes such as *Gdf6* and *Gsc*. Following knockout of *Prdm16*, the arch development of mice is defective, the tongue cannot be properly repositioned and the palatal shelves cannot

be properly elevated, leading to CPO (this gene model was also found in CKO, with a complete secondary cleft palate phenotype)⁶⁸.

Transcriptional repressors also work in the TGF-β pathway. Ski is a transcriptional repressor of the TGF-β pathway that can bind the Smad2/3/4 signal complex activated by TGF-β signalling and recruit nuclear receptor co-repressor (N-CoR) and the transcription corepressor Hdac. Hdac interacts directly with N-CoR/mSin3A to promote histone deacetylation; this leads to transcription shutdown⁶⁹. Loss of *Ski* function may lead to dysregulation of TGF-β pathway transcription, resulting in defects in craniofacial morphogenesis, abnormal neural tube and skeletal muscle formation and the CL/P phenotype⁷⁰.

In *Myf5^{-/-};MyoD^{-/-}* mice, *Tgfbr2* and *Bmp7* are downregulated. *Myf5* and *MyoD* are expressed in muscle tissue and participate in muscle paracrine signalling during palate development, affecting palatal shelf fusion. Knockout of *Myf5* and *MyoD* results in CPO. Furthermore, downregulation of *Gdf11* expression after *Myf5* and *MyoD* knockout may affect downstream genes, leading to CPO⁷¹.

Normal palatal development requires multiple mechanisms to balance the effects of agonists and antagonists on BMP signalling. *Smoc1* encodes a BMP antagonist, and knockout will affect stability of the BMP gradient. There may be an interaction between *Smoc1* and BMP4 leading to the cleft palate phenotype, but this will require experimental verification⁷².

Msx1 is a target of the WNT/β-catenin pathway and also regulates *Bmp4*⁷³. In *Msx1* knockdown mutants, angiogenesis of the MXP is disrupted and its growth is inhibited, which may lead to the cleft palate phenotype^{74,75}. Knockdown of *Msx1* also results in defective proliferation of anterior palatal mesenchymal cells, causing CPO. Several growth factors, including *Bmp2*, *Bmp4* and *Shh*, can be downregulated. Ectopic expression of *Bmp4* in palatal mesenchyme can restore normal cell proliferation and rescue the cleft palate phenotype. The authors hypothesised that *Msx1* regulates epithelial-mesenchymal interactions through a network of growth factors: in the anterior palatal shelves, *Msx1*, which is induced by *Bmp4*, is required for mesenchymal *Bmp4* expression, which in turn functions upstream of *Shh* and *Bmp2*, thereby regulating mammalian palate development⁷⁶. Frameshift mutations in *Msx* homeodomain 6 (MH6, the highly conserved C-terminal domain of *Msx1*) cause hypoplasia of mandibular incisor teeth with or without cleft palate in mice at embryonic day 16.5 (E16.5), highlighting the role of MH6 in tooth and palate development⁷⁷.



Table 6 Gene knockout in TGF-β.

Gene	Phenotype and penetrance	Embryonic development period	Gene/protein expression	Cause of death	Model generation method	Studies
<i>Prdm16</i>	CPO	GD14.5	Widely expressed	NR	<i>Prdm16</i> expression was inactivated by a gene-trap that inserted the gene for β-galactosidase between exons 1 and 2	Warner et al ⁶⁸
	CPO, 23%; skeletal abnormalities	E14	Widely expressed	Heart defect, pulmonary insufficiency	Blastocysts were prepared from C57BL/6J mice and the E14.1 ES cells were derived from 129/Ola blastocysts. Male germline chimeras were bred to outbred Black Swiss females (Taconic) to produce F1 offspring heterozygous for the TGF-β2 locus	Sanford et al ⁸⁵
<i>Bmp7</i>	CPO, 100%	E15.5	Palate, tongue, lower lip and other orofacial structures	NR	Delete a conditional <i>Bmp7</i> wt/flx allele by Cre-mediated recombination in the germline	Kouskoura et al ⁶⁷
<i>Ctgf</i>	CPO, 100%	E15.5	Lung, adipocyte, kidney, spleen and thyroid	NR	Replace a 500-bp <i>Sma</i> I fragment containing exon 1, the TATA box and the transcription start site with the neomycin resistance gene under the control of a PGK promoter	Ivkovic et al ⁸⁶
<i>Ski</i>	Facial fissures with abnormal formation of fingers and eyes; skeletal muscle defects	E14	Thyroid and pancreas	Death after birth, cause not mentioned	Specific mutation of the exon by targeted vector	Luo et al ⁶⁹ , Berk et al ⁷⁰
<i>Myf5, MyoD</i>	CPO	E18.5	Muscle	NR	<i>Myf5</i> cre allele is used to ablate <i>Myf5</i> -expressing cells in <i>Myf5</i> -NN/R-DTA embryos.	Rot and Kablar ⁷¹
<i>Gdf11</i>	CPO	E15.5	Maxillary, mandible, palate	NR	<i>Gdf11</i> ^{-/-} mice (null mutation)	Rot and Kablar ⁷¹
<i>Smoc1</i>	CPO	E14.5	Developing pharynx arch and frontal nasal region	Died at or shortly after birth, possibly related to CP	Mice with a targeted pre-conditional mutation in <i>Smoc1</i> containing a LacZ reporter allele	Rainger et al ⁷²
<i>Msx1</i>	NSCP, 100%(cleft secondary palate)	E14.5	Anterior palatal mesenchyme	NR	1. <i>Msx1</i> ^{-/-} mice (null mutation) 2. <i>Msx1</i> - <i>Bmp4</i> transgenic mice 3. <i>Msx1</i> ^{-/-} / <i>Tg</i>	Zhang et al ⁷⁶
<i>Msx homology domain 6 (MH6)</i>	Hypoplasia of lower incisors with or without cleft palate; hypoplasia of molars	E18.5, 4-week-old	Developing limb buds and craniofacial structures, dental papilla and follicle	NR	CRISPR/Cas-mediated genome editing	Mitsui et al ⁷⁷
<i>ActRcll</i>	CPO, 22%, Other deformities as mandibular dystrophy	E18.5	Mandibular component of the first branchial arch	NR	<i>ActRcll</i> -deficient mice. Mutating the <i>ActRcll</i> gene using ES cell technology to delete exon I, hybridisation of mutant heterozygotes. (activin-βA/βB double-mutant mice)	Matzuk et al ⁷⁸
<i>Activin</i>	Missing whiskers and lower incisors, defective second palate, including cleft palate	NR	Mesenchymal cells of the developing face, whiskers, hair follicles, heart and digestive tract	Developed to term but died within 24 hours of birth	1. Disrupted <i>activin</i> -βA allele by embryonic stem cell technology, hybridisation of mutant heterozygotes. (<i>Activin</i> -βA-deficient mice) 2. <i>Activin</i> -βA/βB double-mutant mice (hybridisation of mutant heterozygotes)	Matzuk et al ⁷⁹
<i>Runx2</i>	CPO with skeletal abnormalities, dental defects and failed eyelid fusion	P0	Dental mesenchyme	Died after birth due to respiratory failure	Mutations in ES cells were produced using a substitutional targeting vector. The correct targeted G418-resistant colonies were identified by southern blot analysis of the genomic DNA of SACC-digested ES cells	Lee et al ⁸⁰ , Afzal et al ⁸¹ , Aberg et al ⁸² , Otto et al ⁸⁷

NR, not reported.

Table 7 Gene knock-in in TGF- β .

Gene	Phenotype and penetrance	Embryonic development period	Gene/protein expression	Cause of death	Model generation method	Studies
<i>Pitx2</i>	CPO, with abnormal mandibular prominence and developmental arrest of the teeth	E14.5	Palatal mesenchyme	NR	Gene targeting by phage-mediated targeting vector	Iwata et al ⁸³ , Lu et al ⁸⁴

NR, not reported.

Activin is a TGF- β family ligand and a TGF- β pathway receptor. Knockdown of *ActRcll* results in mandibular dystrophy, Meckel cartilage abnormalities, craniofacial skeletal abnormalities, secondary cleft palate and loss of incisors in 22% of mice, but the main defect in most mice is in reproduction⁷⁸. By contrast, knockout of *Activin* leads to primary defects in the beard, lower incisors, eyelids and palate⁷⁹. The different phenotypes suggest that *ActRcll* is likely not a receptor in the Activin-mediated pathway.

Homozygous mutation of *Runx2* causes loss of function of Runx2, which is manifested as cleft palate accompanied by skeletal abnormalities, dental defects, eyelid fusion failure and death after birth. Runx2 is a downstream transcription factor of the TGF- β pathway⁸⁰. It can mediate the transcription of corresponding effector genes, and thus promotes the differentiation of mesenchymal precursor cells and induces the differentiation of osteoblasts and bone formation⁸¹. Loss of function of Runx2 leads to the inhibition of transcription of downstream effector genes of TGF- β /BMP2- and MAPK-dependent signals, as well as the blockage of signal transmission, which leads to inhibition of osteoblast differentiation and bone formation, failure of palatal fusion and CPO⁸².

Gene knock-in

Gene knock-in in the TGF- β pathway mainly targets *Pitx2* (Table 7). Gene targeting of *Pitx2* with phage-mediated targeting vectors results in gene loss; corresponding mouse models can be established, resulting in cleft palate with abnormal cardiac morphogenesis, abnormal maxillary and mandibular facial prominences and arrested tooth development. As a downstream transcription factor of the TGF- β pathway, *Pitx2* is widely expressed in epithelium and mesenchyme. The TGF- β -Fgf9-*Pitx2* signalling cascade involving *Pitx2* promotes the proliferation of mesenchymal cells in the process of palatal formation. As a downstream target of Fgf9, *Pitx2* can regulate cell proliferation by directly activating expression of the genes cyclin *D1* and *D3*⁸³. Loss of function of *Pitx2* may inhibit cell proliferation during palatal formation by blocking the TGF- β -Fgf9-*Pitx2* sig-

nalling cascade, leading to delayed palatal shelf elevation, extension failure and ultimately, CPO⁸⁴.

CKO

In CKO mouse models, dysfunctions of related genes affect various palatal development stages and finally lead to cleft palate and other OFCs (Table 8).

BmpRIA knockout in the MXP epithelium and stroma mediated by Nestin-Cre results in cleft lip, cleft palate and arrest of tooth development. *BmpRIA* is a receptor of the TGF- β pathway. Its deletion leads to downregulation of *Fgf8*, *P63* and *Pitx1* expression, and premature apoptosis of epithelial cells at the MNP margin results in cleft lip. Abnormal spatiotemporal expression of *Barx1* and *Pax9*, increased apoptosis of mesonasal ectoderm and mesenchymal cells, and defects in proliferation and anterior posterior patterning of maxillary mesenchymal cells lead to cleft palate⁸⁸. The growth and merger of the MNPs with each other and the MXP create the maxillomandibular segment consisting of the upper lip, maxilla and primary palate. Failure of adequate growth or fusion between the processes generates a spectrum of OFCs. Nestin-Cre-mediated knockdown of *Bmp4* in the marginal epithelium of the MNP and MXP results in delayed fusion of bilateral MNPs and the MXP, which leads to cleft lip. Eventually, however, most mutants spontaneously repair the cleft lip. *Bmp4* functions in the ectoderm of the nasal processes, and the authors hypothesised that *Bmp4*-*BmpRIA* signalling plays an important role in lip fusion⁸⁸.

Alk5 is a receptor of the TGF- β pathway. Wnt1-Cre-mediated knockout of *Alk5* results in craniomaxillofacial deformities including cleft palate. The authors observed significant changes in the expression of downstream genes *Msx1*, *Fgf8* and *Tgif*, abnormal apoptosis and cell proliferation in the palatal shelves, and abnormalities in other skeletal craniofacial structures that may also contribute to CPO⁸⁹.

Prdm16 is a transcriptional corepressor of TGF- β signalling that partly inhibits the differentiation of osteoblasts into osteocytes⁹⁰. *Prdm16* is also a Smads-binding protein that can form a complex with Smads2/3 and recruit Hdac1, thereby inhibiting TGF- β pathway



Table 8 CKO in TGF-β.

Gene	Phenotype and penetrance	Embryonic development period	Gene/protein expression	Cause of death	Model generation method	Studies
<i>BmpRIA/Alk3</i>	100% bilateral CLP; dental arrest	10.5 dpc, 11.5 dpc, 14.5 dpc, 18.5 dpc	Complete removal of BmpRIA from the epithelium and mesenchyme of the MXP by 10.5 dpc, and mosaic deletion in the epithelium of the mandibular and nasal processes	NR	<i>Nestin-Cre; BmpRIA^{null/flox}</i>	Liu et al ⁸⁸
<i>Bmp4</i>	CL	12.0 dpc, 14.5 dpc	<i>Bmp4</i> was deleted by 10.5 dpc in the edge epithelium of the MNP and MXP	NR	<i>Nestin-Cre; Bmp4^{null/flox(n/f)}</i>	Liu et al ⁸⁸
<i>Prdm16</i>	Complete secondary CP, 66%; middle ear defect with severe dysplasia of the tympanic ring, abnormal sex blastoid formation, and dysplasia of the incus and malleus, 100%	E18.5	The anterior part of the secondary palate, pharyngeal arch and head fold	NR	Transducing mice with a pln-ducer20 lentivirus23 expressing <i>Prdm16</i>	Zeng et al ⁹⁰ , Warner et al ⁹¹ , Shull et al ⁹²
<i>Bmp1 receptor/Alk2</i>	CPO; Mandibular dystrophy	E14, mutant palatal shelves fail to elevate, unilaterally or bilaterally	The first two pharyngeal arches	Death at birth or shortly after birth with multiple craniofacial defects	<i>Alk2/Wnt1-Cre-mediated</i>	Dudas et al ⁹³
<i>Fgf9</i>	Obvious secondary CP, 100%	E18.5	E9.5–E12.5: ectoderm of the craniofacial region, with spatiotemporal variation E13.5: palatal epithelium E14.5: epithelium and mesenchyme	Death after birth, cause not mentioned	<i>Ddx4-Cre</i>	Iwata et al ⁸³ , Li et al ⁹⁴
<i>TGFbr2</i>	Cleft secondary palate and cranial hypoplasia, 100%	E14.5–16.5 (palatal fusion failure)	Palatal mesenchyme	Defects of yolk sac hematopoiesis and vasculogenesis	<i>Wnt1-Cre; TGFbr2^{fl/fl}</i>	Ito et al ⁹⁵
	Cleft soft palate, submucosal cleft, and primary and secondary palate fusion failure, 100%	E14.5 (cell proliferation rate and Cyclin D1 were significantly reduced)	Palatal epithelium	Died shortly after birth, lack of milk in the stomach	<i>K14-Cre; TGFbr2^{fl/fl}</i>	Xu et al ⁹⁷
<i>Alk5</i>	CPO, 100% (especially anterior and posterior to the second palate)	E14, E14.5, E15, E17	Palatal epithelium	Died shortly after birth, lack of milk in the stomach	<i>K14-Cre-mediated</i>	Dudas et al ⁸⁹
	Cranial hypoplasia; oronasal cleft; micromandible; uvula; CPO	E10, E11, E14	Palatal mesenchyme	Severely disfigured, died shortly after birth	<i>Wnt1-Cre-mediated</i>	Dudas et al ⁸⁹
<i>Hdac3</i>	CPO	E17.5	E9.5–10: widely expressed in the head, including neural crest, ectoderm and endoderm	Cleft palate pups are unable to generate suction and suckling, and subsequently die at P0 from dehydration and air accumulation in the digestive tract	<i>Wnt1-Cre-mediated</i>	Singh et al ⁹⁶
<i>Kdm6b (Jmjd3)</i>	Complete secondary CP, 66% No CL/P	NR	Cranial neural crest-derived cells	NR	<i>Wnt1-Cre; Kdm6b^{fl/fl} Krt14-Cre; Kdm6b^{fl/fl}</i>	Guo et al ⁹⁸ , Fueyo et al ⁹⁹ , Lee et al ¹⁰⁰

NR, not reported.

signalling⁹¹. Prdm16 deficiency results in the failure of palatal shelf elevation to meet and fuse at the midline, eventually leading to CPO⁹². Wnt1-Cre-mediated knockout of *Alk2* leads to hypoplasia of the jaw; a smaller mouth obstructs normal movement of the tongue, which in turn results in delayed and unsynchronised palatal shelf elevation and secondary cleft palate⁹³.

Ddx4-Cre-mediated specific knockout of *Fgf9* in germ cells results in significant secondary cleft palate and death shortly after birth. *Fgf9* is widely expressed in epithelial and mesenchymal cells⁹⁴. It promotes palatal growth and timely elevation by regulating cell proliferation and accumulation of hyaluronic acid. By influencing tongue descent and morphology and mandibular growth, it ensures there is sufficient space for the process of palate elevation⁹⁴. TGF- β regulates cell proliferation through the *Fgf9*-Pitx2 signalling cascade during palate formation⁸³. The germ-specific knockdown of *Fgf9* may lead to obstruction of the *Fgf9*-Pitx2 signalling cascade and inhibition of palatal formation. At E18.5, the vertical growth of palatal shelves is small, elevation is delayed and contact fails, ultimately leading to CPO⁹⁴.

Loss of *Tgfb2* in palatal mesenchyme inhibited cyclin D1 expression and affected the proliferation of CNCCs in palatal mesenchyme and palatogenesis, resulting in impaired palatal shelf extension and failure of palatal shelf fusion. The mutant mice presented with cleft secondary palate and skull hypoplasia⁹⁵.

Neural crest cells show a demand for class I histone deacetylase *Hdac3* during craniofacial development. Following *Hdac3* knockout, G1/S arrest is caused by abnormal cell cycle regulation in mouse neural crest cells. Upregulation of *Msx1* and *Msx2* in the precranial mesenchyme leads to a marked increase in apoptosis and a decrease in proliferation without proper migration or proliferation. In addition, *Bmp4* upregulation results in failure of palatal shelf expansion and ultimately, cleft palate⁹⁶.

Progressive disintegration of the midline epithelial seam as well as removal of the transient epithelial seams begin following contact of the palatal shelves¹⁶. A mouse model of K14-Cre-mediated ectodermal epithelial-specific knockout of *Alk5* showed cleft palate. Loss of *Alk5* leads to the failure of palatal epithelial seam disappearance⁸⁹. TGF- β 2 is a receptor of the TGF- β pathway. K14-Cre-mediated knockout leads to the downregulation of *Irf6* and *Mmp13*, interfering with apoptosis in MEE⁹⁷.

Wnt1-Cre-mediated specific knockout of *Kdm6b* results in complete cleft palate with defects in the soft palate and death shortly after birth. *Kdm6b* is widely

expressed in the palate, but K14-Cre-mediated epithelial-specific knockout of *Kdm6b* did not cause CL/P, indicating that palate development depends on *Kdm6b* in CNCCs rather than epithelial cells⁹⁸. *Kdm6b* (*Jmjd3*) is a cofactor of the TGF- β pathway and is required for enhancer activation when TGF- β is stimulated⁹⁹. Ras-activated *Kdm6b* contributes to TGF- β I-induced *Smad2* and *Smad3* activation by promoting syntenin-mediated TGF- β RI/*Smad2/3* complex formation, thereby promoting TGF- β -induced epithelial-mesenchymal transition¹⁰⁰. A lack of *Kdm6b* leads to inhibition of the epithelial-mesenchymal transition, limited proliferation and differentiation of CNCCs and development failure, resulting in CPO⁹⁸.

Discussion

The present review offers a systematic summary of various mouse models of OFCs and focuses on elucidating the roles of defective genes involved in the SHH and TGF- β signalling pathways and the genetic aetiology of corresponding phenotypes.

Shh, *Ihh*, *Smo*, *Ptch1*, *Cdo*, *Boc* and *Glis* are among the Hedgehog signalling genes. Except for loss of *Gli1* and *Ptch1*, all mice defective in these genes exhibit CPO. *Gli1* knockout mice show CL/P, while *Ptch1* loss causes cleft lip. Deletion of *Ihh* affects osteogenesis of the secondary palate. Deletion of *Smo* leads to upregulation of *p63* and its target gene. Deletion of *Gli* is mainly related to failure of elevation and fusion of the palatal shelves. *Ptch1* is crucial to the formation of the original nose and upper lip. Hedgehog signalling during embryogenesis depends on primary cilia function and intra-flagellar transport. *Ick*, *Tmem107*, *Ift144*, *Ift88*, *Fuz* and *Kif3a* are closely related to the development of cilia. Deletion of these genes leads to a disorder of cilia development and blocks normal Hedgehog signalling. Except for *Ift144* deletion and *Wnt-1-Cre*-mediated *Ift88* CKO, other deletions lead to CPO. Ablation of *Gas1*, *FGF* and *Bbs*, which regulate Hedgehog signalling, results in CPO (Fig 1).

Among the TGF- β signalling molecules, members of the Smads family are important molecules that transmit extracellular signals to the nucleus. *Ctgf*, *Prdm16*, *Myf5*, *MyoD*, *Gdf11*, *Smoc1*, *Msx1*, *Kdm6b* and *Fgf9* regulate the signalling pathway. *Pitx2*, *Runx2*, *Ski* and *Hdac3* are targets. The loss of most molecules leads to CPO (Fig 2).

Conditional activation of *BmpR1A* mediated by *Wnt1-Cre* leads to CL/P. The *Bmp4-BmpR1A* pathway plays an important role in lip fusion. *Nestin-Cre*-mediated CKO of *BmpR1A* leads to CL and CP, while *Bmp4* leads

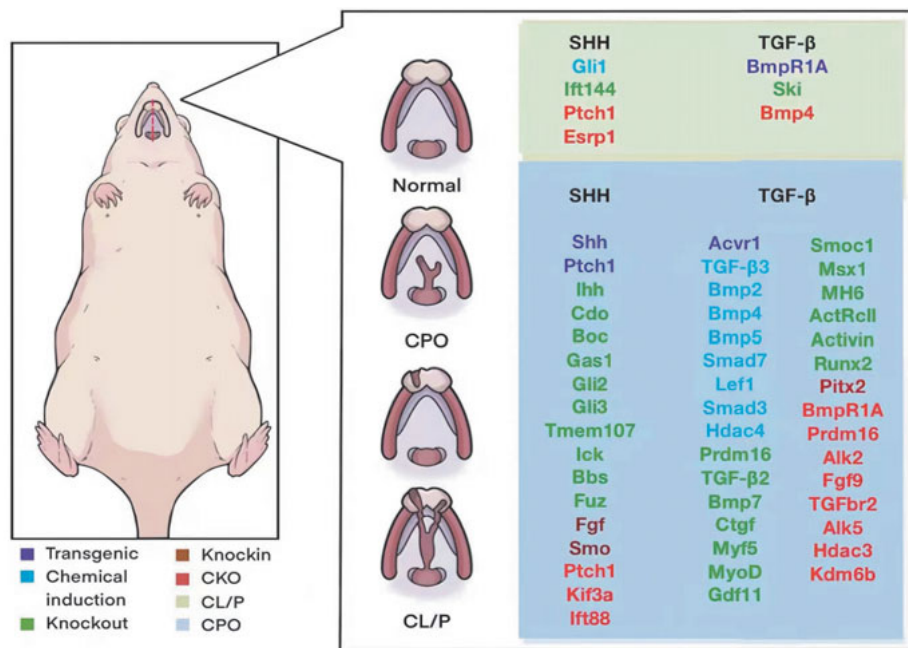


Fig 3 Phenotypic classification of OFC mouse models in the SHH and TGF-β pathways.

to CL, both causing MNP and MXP proliferation defect and fusion delay. Knockout of *Tgf-β2*, *Bmp7*, *Pitx2*, *Fgf9*, *Prdm16* and *Alk2* result in CPO due to delay or obstruction of palatal shelf elevation. Among these, loss of *Prdm16* and *Alk2* lead to mandibular development defects, resulting in an inability to reposition the tongue properly. In *Acvr1*, *TGF-β3* and *Alk5* KO mice and *K14-Cre; TGF-βR2* CKO mice, MEE cells fail to disappear. *Wnt1-Cre; TGFβ-R2* CKO and *Hdac3* defects affect the proliferation of CNCCs in the palatal mesenchyme, leading to failure of palatal shelf extension and fusion. Although the different *TGF-βR2* CKO models both show cleft palate, the affected stages differ because the knockout happens in the epithelium and mesenchyme, respectively. The loss of *Bmp-2/4/5*, *Ctgf*, *Runx2*, *Prdm16* and *Kdm6b* is related to the abnormal development of cartilage and bone, thus leading to CPO.

Knockout of different genes in the two pathways may lead to OFCs through similar mechanisms (such as palatal shelf elevation disorder or abnormal fusion of facial prominences) (Fig 3). The same gene can also function in multiple pathways. These signalling pathways do not act in isolation during lip and palate development; instead, they interact with each other through several important molecules including *p63*, *Fgfs*, *Msx1* and *Kif3a*.

Different modelling methods have their own characteristics. As the earliest method used in this field, chemical induction is relatively simple and intuitive, but the impact of the environment cannot be excluded, and the specific mechanism involved cannot be proven.

As in the TGF-β pathway, retinoic acid induction can lead to changes in several molecules, thereby weakening the correlation between any single molecule and OFCs. Knockout mice have improved these problems, but the important genes related to morphogenesis often play multiple roles in embryonic development. Even in the lip and palate, they may also have different functions in different parts and types of cells. Moreover, complete knockout in the embryo may lead to serious embryonic lethality and severe syndromes, which hampers in-depth research. As an improvement, knock-in enhances pertinence through site-directed mutagenesis; however, the abnormal phenotype may be hidden due to compensation. In recent years, CKO has solved the obstacle of early embryo lethality and greatly improved accuracy through tissue-specific gene knockout, thus gradually becoming the most powerful and most commonly used method.

The present study is not without limitations. Certain genes might possess multiple functions across both the lip/palate and other regions of the body, leading to severe syndromes and fatal malformations. This complexity hampers our ability to distinctly elucidate the specific mechanisms driving OFCs. Additionally, distinguishing primary OFCs from those secondary to other craniomaxillofacial malformations can pose challenges. The redundancy in gene function can also obscure certain abnormalities. While the present authors have comprehensively summarised gene mutation sites within the TGF-βs, SHH and WNT pathways in recent years, numerous mutation sites outside these

pathways remain unexplored. Other pathways relevant to OFCs, not discussed in this article, are also waiting to be uncovered and consolidated. Furthermore, our understanding of the intricate interconnections among genes in specific pathways is still incomplete, and we have yet to fully elucidate how, when and where signalling pathways intersect and converge. To advance our research, a more profound grasp of the intricate interactions governing lip/palate development through these signalling pathways is crucial.

The integration of single-cell multiomics into the study of mouse models of OFCs presents an innovative avenue for unravelling the complex pathogenic mechanisms underlying these congenital anomalies. By enabling high-resolution characterisation of gene expression patterns at the level of individual cells, single-cell multiomics techniques have the potential to offer unparalleled insights into the molecular and cellular events that contribute to the development of OFCs. The recent use of single-cell RNA sequencing (scRNA-seq) datasets in craniofacial research underscores the potency of this approach in deciphering the heterogeneity of cell populations during critical palate formation stages. This encompasses the identification of specific cell types, exploration of shared expression patterns across datasets and unveiling of potential regulatory networks involving pivotal candidate genes¹⁰¹. As we navigate the era of single-cell multiomics, future research should concentrate on refining data analysis methodologies to ensure precise cluster resolution and cross-dataset comparisons. Tackling technical challenges related to data integration, cell type annotation and noise reduction will be pivotal in unlocking the full potential of this technology. Additionally, coupling the application of single-cell multiomics with spatial transcriptomic analyses will help unveil the spatial organisation of gene expression within tissue structures, offering a holistic perspective on how molecular events impact tissue architecture during craniofacial development. Collaborative efforts between bioinformaticians, developmental biologists and clinicians will play a crucial role in translating these findings into clinically relevant insights, ultimately advancing our comprehension of the aetiology of CL/P and facilitating the development of targeted therapeutic interventions.

Currently, most mouse models primarily target functional gene regions. While the majority of attention has historically been directed towards protein-coding genes, emerging evidence underscores the pivotal role of ncRNA, particularly miRNA, in orchestrating gene expression networks that govern tissue development and differentiation, and homeostasis of the lip and pal-

ate¹⁰¹. Moving forward, the creation of mouse models for OFCs based on miRNA and other ncRNA mutations should be explored. Furthermore, given the growing recognition that non-coding RNAs often exhibit tissue- and developmental stage-specific expression patterns, mouse models offer a unique opportunity to investigate the context-dependent roles of miRNA in palate formation. By manipulating miRNA expression during distinct developmental stages, researchers can pinpoint critical windows of vulnerability and better understand how miRNA dysregulation contributes to the aetiology of OFCs. These insights hold promise for the development of targeted interventions that aim to normalise miRNA expression and restore proper craniofacial development. Additionally, innovative strategies for modulating miRNA activity, such as miRNA mimics or inhibitors, can be explored in mouse models to assess their potential as therapeutic interventions.

At present, clinical application of OFC pathogenic genes is mainly used to provide a basis for early screening of familial genetic disorders, and the treatment of OFCs is still mainly focused on traditional repair surgery. In the future, the application of small molecule inhibitors or specialised nutritional elements during early embryonic development could hold the potential to reverse the occurrence of OFCs. By targeting key signalling pathways and molecular processes implicated in craniofacial development, these interventions could potentially mitigate the disruptions that give rise to OFCs. This approach could address the underlying molecular and cellular disruptions that lead to cleft formation, offering the advantage of avoiding surgical procedures and their associated risks. Additionally, intervening at the embryonic stage might allow for more natural and holistic corrections in tissue development, potentially yielding better functional and aesthetic outcomes. However, while this concept holds great promise, its implementation requires careful consideration and extensive research. The precise identification of critical developmental time windows and the specific signalling pathways amenable to modulation are essential to maximise the effectiveness of such interventions. Rigorous preclinical studies using mouse models should be conducted to validate the safety, efficacy and potential long-term consequences of employing small molecule inhibitors or nutritional elements in altering embryonic development.

Conclusion

In summary, the horizon of research into OFCs is undergoing a transformative shift, propelled by the innovative

potential of mouse models. Alongside the traditional paradigms of functional gene targeting, emerging avenues such as single-cell multiomics and the exploration of ncRNA mutations are set to reshape the landscape of our understanding. The integration of single-cell multiomics techniques promises an unprecedented resolution in characterising gene expression patterns across individual cells, unravelling the intricate molecular events that shape CL/P development. Furthermore, the recognition of the role of miRNA and other ncRNA in the aetiology of CL/P has opened up a compelling avenue. Researchers will increasingly zero in on core target molecules within pathways, striving to elucidate comprehensive chains of events and crosstalk across diverse pathways. Having a deeper understanding of the intricate mechanisms and complex interactions that underpin OFCs will enhance prospects for treatment and prevention, ultimately fostering improved natal and prenatal care as well as nurturing practices. As a pivotal genetic disorder within the maxillofacial domain, OFC-related research has the potential to substantially mitigate the profound impact of birth defects on both individuals and society as a whole.

Conflicts of interest

The authors declare no conflicts of interest related to this study.

Author contribution

Drs Yu Chen LI, Le Ran LI, Zi Han GAO, Yi Ran YANG, Qian Chen WANG and Wei Yu ZHANG contributed to drafting the manuscript; Drs Tian Song XU, Li Qi ZHANG and Feng CHEN contributed to the review and revision of the manuscript; Dr Feng CHEN provided the idea and made the conceptual framework.

(Received Mar 09, 2023; accepted Sep 18, 2023)

References

1. Beames TG, Lipinski RJ. Gene-environment interactions: aligning birth defects research with complex etiology. *Development* 2020;147:dev191064.
2. Mai CT, Isenburg JL, Canfield MA, et al. National population-based estimates for major birth defects, 2010-2014. *Birth Defects Res* 2019;111:1420-1435.
3. Harris BS, Bishop KC, Kemeny HR, Walker JS, Rhee E, Kuller JA. Factors for birth defects. *Obstet Gynecol Surv* 2017;72:123-135.
4. Cobourne MT. The complex genetics of cleft lip and palate. *Eur J Orthod* 2004;26:7-16.
5. Martinelli M, Palmieri A, Carinci F, Scapoli L. Non-syndromic cleft palate: An overview on human genetic and environmental risk factors. *Front Cell Dev Biol* 2020;8:592271.
6. Chen S, Jia Z, Cai M, et al. SP1-mediated upregulation of long noncoding RNA ZFAS1 involved in non-syndromic cleft lip and palate via inactivating WNT/ β -catenin signaling pathway. *Front Cell Dev Biol* 2021;9:662780.
7. Gao L, Yin J, Wu W. Long non-coding RNA H19-mediated mouse cleft palate induced by 2,3,7,8-tetrachlorodibenzo-p-dioxin. *Exp Ther Med* 2016;11:2355-2360.
8. Fu C, Lou S, Zhu G, et al. Identification of new miRNA-mRNA networks in the development of non-syndromic cleft lip with or without cleft palate. *Front Cell Dev Biol* 2021;9:631057.
9. Garland MA, Sun B, Zhang S, Reynolds K, Ji Y, Zhou CJ. Role of epigenetics and miRNAs in orofacial clefts. *Birth Defects Res* 2020;112:1635-1659.
10. Sharp GC, Ho K, Davies A, et al. Distinct DNA methylation profiles in subtypes of orofacial cleft. *Clin Epigenetics* 2017;9:63.
11. Mouse Genome Sequencing Consortium, Waterston RH, Lindblad-Toh K, et al. Initial sequencing and comparative analysis of the mouse genome. *Nature* 2002;420:520-562.
12. Won HJ, Kim JW, Won HS, Shin JO. Gene regulatory networks and signaling pathways in palatogenesis and cleft palate: A comprehensive review. *Cells* 2023;12:1954.
13. Cai S, Si N, Wang Y, Yin N. Transcriptomic analysis of the upper lip and primary palate development in mice. *Front Genet* 2023;13:1039850.
14. Hu D, Helms JA. The role of sonic hedgehog in normal and abnormal craniofacial morphogenesis. *Development* 1999;126:4873-4884.
15. Jiang R, Bush JO, Lidral AC. Development of the upper lip: Morphogenetic and molecular mechanisms. *Dev Dyn* 2006;235:1152-1166.
16. Gritli-Linde A. The etiopathogenesis of cleft lip and cleft palate: Usefulness and caveats of mouse models. *Curr Top Dev Biol* 2008;84:37-138.
17. Ingham PW. Hedgehog signaling. *Curr Top Dev Biol* 2022;149:1-58.
18. Ingham PW, McMahon AP. Hedgehog signaling in animal development: paradigms and principles. *Genes Dev* 2001;15:3059-3087.
19. Kurosaka H. The roles of Hedgehog signaling in upper lip formation. *Biomed Res Int* 2015;2015:901041.
20. Abramyan J. Hedgehog signaling and embryonic craniofacial disorders. *J Dev Biol* 2019;7:9.
21. Kousa YA, Moussa D, Schutte BC. IRF6 expression in basal epithelium partially rescues Irf6 knockout mice. *Dev Dyn* 2017;246:670-681.
22. Cobourne MT, Xavier GM, Depew M, et al. Sonic hedgehog signalling inhibits palatogenesis and arrests tooth development in a mouse model of the nevoid basal cell carcinoma syndrome. *Dev Biol* 2009;331:38-49.
23. Dennis JF, Kurosaka H, Iulianella A, et al. Mutations in Hedgehog acyltransferase (Hhat) perturb Hedgehog signaling, resulting in severe acrania-holoprosencephaly-agnathia craniofacial defects. *PLoS Genet* 2012;8:e1002927.
24. Tao H, Manak JR, Sowers L, et al. Mutations in prickle orthologs cause seizures in flies, mice, and humans. *Am J Hum Genet* 2011;88:138-149.
25. Helms JA, Kim CH, Hu D, Minkoff R, Yhaller C, Eichele G. Sonic Hedgehog participates in craniofacial morphogenesis and is down-regulated by teratogenic doses of retinoic acid. *Dev Biol* 1997;187:25-35.

26. Chen JK, Taipale J, Cooper MK, Beachy PA. Inhibition of Hedgehog signaling by direct binding of cyclopamine to Smoothened. *Genes Dev* 2002;16:2743–2748.
27. Heyne GW, Melberg CG, Doroodchi P, et al. Definition of critical periods for Hedgehog pathway antagonist-induced holoprosencephaly, cleft lip, and cleft palate. *PLoS One* 2015;10:e0120517.
28. Everson JL, Fink DM, Yoon JW, et al. Sonic hedgehog regulation of Foxf2 promotes cranial neural crest mesenchyme proliferation and is disrupted in cleft lip morphogenesis. *Development* 2017;144:2082–2091.
29. Lipinski RJ, Holloway HT, O’Leary-Moore SK, et al. Characterization of subtle brain abnormalities in a mouse model of Hedgehog pathway antagonist-induced cleft lip and palate. *PLoS One* 2014;9:e102603.
30. Levi B, James AW, Nelson ER, et al. Role of Indian hedgehog signaling in palatal osteogenesis. *Plast Reconstr Surg* 2011;127:1182–1190.
31. Ohba S. Hedgehog signaling in skeletal development: Roles of Indian Hedgehog and the mode of its action. *Int J Mol Sci* 2020;21:6665.
32. Zhang W, Hong M, Bae GU, Kang JS, Krauss RS. Boc modifies the holoprosencephaly spectrum of Cdo mutant mice. *Dis Model Mech* 2011;4:368–380.
33. Lee CS, May NR, Fan CM. Transdifferentiation of the ventral retinal pigmented epithelium to neural retina in the growth arrest specific gene 1 mutant. *Dev Biol* 2001;236:17–29.
34. Seppala M, Depew MJ, Martinelli DC, Fan CM, Sharpe PT, Cobourne MT. Gas1 is a modifier for holoprosencephaly and genetically interacts with sonic hedgehog. *J Clin Invest* 2007;117:1575–1584.
35. Mo R, Freer AM, Zinyk DL, et al. Specific and redundant functions of Gli2 and Gli3 zinc finger genes in skeletal patterning and development. *Development* 1997;124:113–123.
36. Huang X, Goudy SL, Ketova T, Litingtung Y, Chiang C. Gli3-deficient mice exhibit cleft palate associated with abnormal tongue development. *Dev Dyn* 2008;237:3079–3087.
37. Cela P, Hampl M, Shylo NA, et al. Ciliopathy protein Tmem107 plays multiple roles in craniofacial development. *J Dent Res* 2018;97:108–117.
38. Moon H, Song J, Shin JO, et al. Intestinal cell kinase, a protein associated with endocrine-cerebro-osteodysplasia syndrome, is a key regulator of cilia length and Hedgehog signaling. *Proc Natl Acad Sci U S A* 2014;111:8541–8546.
39. Ashe A, Butterfield NC, Town L, et al. Mutations in mouse Ift144 model the craniofacial, limb and rib defects in skeletal ciliopathies. *Hum Mol Genet* 2012;21:1808–1823.
40. Zhang Q, Seo S, Bugge K, Stone EM, Sheffield VC. BBS proteins interact genetically with the IFT pathway to influence SHH-related phenotypes. *Hum Mol Genet* 2012;21:1945–1953.
41. Gray RS, Abitua PB, Wlodarczyk BJ, et al. The planar cell polarity effector Fuz is essential for targeted membrane trafficking, ciliogenesis and mouse embryonic development. *Nat Cell Biol* 2009;11:1225–1232.
42. Zhang Z, Wlodarczyk BJ, Niederreither K, et al. Fuz regulates craniofacial development through tissue specific responses to signaling factors. *PLoS One* 2011;6:e24608.
43. Doyle A, McGarry MP, Lee NA, Lee JJ. The construction of transgenic and gene knockout/knockin mouse models of human disease. *Transgenic Res* 2012;21:327–349.
44. Li J, Yuan Y, He J, et al. Constitutive activation of hedgehog signaling adversely affects epithelial cell fate during palatal fusion. *Dev Biol* 2018;441:191–203.
45. Crisera C, Teng E, Wasson KL, et al. Formation of in vitro murine cleft palate by abrogation of fibroblast growth factor signaling. *Plast Reconstr Surg* 2008;121:218–224.
46. Cole F, Krauss RS. Microform holoprosencephaly in mice that lack the Ig superfamily member Cdon. *Curr Biol* 2003;13:411–415.
47. Tian H, Feng J, Li J, et al. Intraflagellar transport 88 (IFT88) is crucial for craniofacial development in mice and is a candidate gene for human cleft lip and palate. *Hum Mol Genet* 2017;26:860–872.
48. Watanabe M, Kawasaki M, Kawasaki K, et al. Ift88 limits bone formation in maxillary process through suppressing apoptosis. *Arch Oral Biol* 2019;101:43–50.
49. Lan Y, Jiang R. Sonic hedgehog signaling regulates reciprocal epithelial-mesenchymal interactions controlling palatal outgrowth. *Development* 2009;136:1387–1396.
50. Metzis V, Courtney AD, Kerr MC, et al. Patched1 is required in neural crest cells for the prevention of orofacial clefts. *Hum Mol Genet* 2013;22:5026–5035.
51. Li S, Jin S, Jin C. The correlative hypotheses between Pitchfork and Kif3a in palate development. *Med Hypotheses* 2019;126:23–25.
52. Liu B, Chen S, Johnson C, Helms JA. A ciliopathy with hydrocephalus, isolated craniosynostosis, hypertelorism, and clefting caused by deletion of Kif3a. *Reprod Toxicol* 2014;48:88–97.
53. Nakaniwa M, Kawasaki M, Kawasaki K, et al. Primary cilia in murine palatal rugae development. *Gene Expr Patterns* 2019;34:119062.
54. Schock EN, Struve JN, Chang CF, et al. A tissue-specific role for intraflagellar transport genes during craniofacial development. *PLoS One* 2017;12:e0174206.
55. Tzavlaki K, Moustakas A. TGF- β signaling. *Biomolecules* 2020;10:487.
56. Nawshad A, LaGamba D, Hay ED. Transforming growth factor beta (TGFbeta) signalling in palatal growth, apoptosis and epithelial mesenchymal transformation (EMT). *Arch Oral Biol* 2004;49:675–689.
57. Wan M, Cao X. BMP signaling in skeletal development. *Biochem Biophys Res Commun* 2005;328:651–657.
58. Li L, Wang Y, Lin M, et al. Augmented BMPRIA-mediated BMP signaling in cranial neural crest lineage leads to cleft palate formation and delayed tooth differentiation. *PLoS ONE* 2013;8:e66107.
59. Noda K, Mishina Y, Komatsu Y. Constitutively active mutation of ACVR1 in oral epithelium causes submucous cleft palate in mice. *Dev Biol* 2016;415:306–313.
60. Li C, He W, Meng T, Lu S, Shi B. Tetrachlorodibenzo-p-dioxin-induced cleft palate because of partial loss of cell polarity to interfere with apoptosis during early developmental stage [in Chinese]. *Zhonghua Kou Qiang Yi Xue Za Zhi* 2014;49:719–723.
61. Lai Y, Xie C, Zhang S, Gan G, Wu D, Chen W. Bone morphogenetic protein type I receptor inhibition induces cleft palate associated with micrognathia and cleft lower lip in mice. *Birth Defects Res A Clin Mol Teratol* 2016;106:612–623.
62. Lu H, Jin Y, Tipoe GL. Alteration in the expression of bone morphogenetic protein-2,3,4,5 mRNA during pathogenesis of cleft palate in BALB/c mice. *Arch Oral Biol* 2000;45:133–140.
63. Yu W, Ruest LB, Svoboda KK. Regulation of epithelial-mesenchymal transition in palatal fusion. *Exp Biol Med (Maywood)* 2009;234:483–491.
64. Kang JS, Alliston T, Delston R, Derynck R. Repression of Runx2 function by TGF-beta through recruitment of class II histone deacetylases by Smad3. *EMBO J* 2005;24:2543–2455.

65. Shu X, Shu S, Cheng H. A novel lncRNA-mediated trans-regulatory mechanism in the development of cleft palate in mouse. *Mol Genet Genomic Med* 2019;7:e00522.
66. Shu X, Shu S, Zhai Y, Zhu L, Ouyang Z. Genome-wide DNA methylation profile of gene cis-acting element methylations in all-trans retinoic acid-induced mouse cleft palate [ePub ahead of print 2 October 2018]. *DNA Cell Biol* doi: 10.1089/dna.2018.4369.
67. Kouskoura T, Kozlova A, Alexiou M, et al. The etiology of cleft palate formation in BMP7-deficient mice. *PLoS One* 2013;8:e59463.
68. Warner DR, Wells JP, Greene RM, Pisano MM. Gene expression changes in the secondary palate and mandible of Prdm16(-/-) mice. *Cell Tissue Res* 2013;351:445–452.
69. Luo K, Stroschein SL, Wang W, et al. The Ski oncoprotein interacts with the Smad proteins to repress TGFbeta signaling. *Genes Dev* 1999;13:2196–2206.
70. Berk M, Desai SY, Heyman HC, Colmenares C. Mice lacking the ski proto-oncogene have defects in neurulation, craniofacial, patterning, and skeletal muscle development. *Genes Dev* 1997;11:2029–2039.
71. Rot I, Kablar B. Role of skeletal muscle in palate development. *Histol Histopathol* 2013;28:1–13.
72. Rainger J, van Beusekom E, Ramsay JK, et al. Loss of the BMP antagonist, SMOC-1, causes Ophthalmic-acromelic (Waardenburg Anophthalmia) syndrome in humans and mice. *PLoS Genet* 2011;7:e1002114.
73. Song L, Li Y, Wang K, et al. Lrp6-mediated canonical Wnt signaling is required for lip formation and fusion. *Development* 2009;136:3161–3171.
74. Satokata I, Maas R. Msx1 deficient mice exhibit cleft palate and abnormalities of craniofacial and tooth development. *Nat Genet* 1994;6:348–356.
75. Medio M, Yeh E, Popelut A, Babajko S, Berdal A, Helms JA. Wnt/beta-catenin signaling and Msx1 promote outgrowth of the maxillary prominences. *Front Physiol* 2012;3:375.
76. Zhang Z, Song Y, Zhao X, Zhang X, Fermin C, Chen Y. Rescue of cleft palate in Msx1-deficient mice by transgenic Bmp4 reveals a network of BMP and Shh signaling in the regulation of mammalian palatogenesis. *Development* 2002;129:4135–4146.
77. Mitsui SN, Yasue A, Masuda K, et al. Novel human mutation and CRISPR/Cas genome-edited mice reveal the importance of C-terminal domain of MSX1 in tooth and palate development. *Sci Rep* 2016;6:38398.
78. Matzuk MM, Kumar TR, Bradley A. Different phenotypes for mice deficient in either activins or activin receptor type II. *Nature* 1995;374:356–360.
79. Matzuk MM, Kumar TR, Vassalli A, et al. Functional analysis of activins during mammalian development. *Nature* 1995;374:354–356.
80. Lee KS, Hong SH, Bae SC. Both the Smad and p38 MAPK pathways play a crucial role in Runx2 expression following induction by transforming growth factor-beta and bone morphogenetic protein. *Oncogene* 2002;21:7156–7163.
81. Afzal F, Pratap J, Ito K, et al. Smad function and intranuclear targeting share a Runx2 motif required for osteogenic lineage induction and BMP2 responsive transcription. *J Cell Physiol* 2005;204:63–72.
82. Aberg T, Cavender A, Gaikwad JS, et al. Phenotypic changes in dentition of Runx2 homozygote-null mutant mice. *J Histochem Cytochem* 2004;52:131–139.
83. Iwata J, Tung L, Urata M, et al. Fibroblast growth factor 9 (FGF9)-pituitary homeobox 2 (PITX2) pathway mediates transforming growth factor beta (TGFbeta) signaling to regulate cell proliferation in palatal mesenchyme during mouse palatogenesis. *J Biol Chem* 2012;287:2353–2363.
84. Lu MF, Pressman C, Dyer R, Johnson RL, Martin JF. Function of Rieger syndrome gene in left-right asymmetry and craniofacial development. *Nature* 1999;401:276–278.
85. Sanford LP, Ormsby I, Gittenberger-de Groot AC, et al. TGF-beta2 knockout mice have multiple developmental defects that are non-overlapping with other TGFbeta knockout phenotypes. *Development* 1997;124:2659–2670.
86. Ivkovic S, Yoon BS, Popoff SN, et al. Connective tissue growth factor coordinates chondrogenesis and angiogenesis during skeletal development. *Development* 2003;130:2779–2791.
87. Otto F, Thornell AP, Crompton T, et al. Cbfa1, a candidate gene for cleidocranial dysplasia syndrome, is essential for osteoblast differentiation and bone development. *Cell* 1997;89:765–771.
88. Liu W, Sun X, Braut A, et al. Distinct functions for Bmp signaling in lip and palate fusion in mice. *Development* 2005;132:1453–1461.
89. Dudas M, Kim J, Li WY, et al. Epithelial and ectomesenchymal role of the type I TGF-beta receptor ALK5 during facial morphogenesis and palatal fusion. *Dev Biol* 2006;296:298–314.
90. Zeng HC, Bae Y, Dawson BC, et al. MicroRNA miR-23a cluster promotes osteocyte differentiation by regulating TGF-beta signalling in osteoblasts. *Nat Commun* 2017;8:15000.
91. Warner DR, Horn KH, Mudd L, Webb CL, Greene RM, Pisano MM. PRDM16/MEL1: A novel Smad binding protein expressed in murine embryonic orofacial tissue. *Biochim Biophys Acta* 2007;1773:814–820.
92. Shull LC, Sen R, Menzel J, Goyama S, Kurokawa M, Artinger KB. The conserved and divergent roles of Prdm3 and Prdm16 in zebrafish and mouse craniofacial development. *Dev Biol* 2020;461:132–144.
93. Dudas M, Sridurongrit S, Nagy A, Okazaki K, Kaartinen V. Craniofacial defects in mice lacking BMP type I receptor Alk2 in neural crest cells. *Mech Dev* 2004;121:173–182.
94. Li R, Sun Y, Chen Z, et al. The fibroblast growth factor 9 (Fgf9) participates in palatogenesis by promoting palatal growth and elevation. *Front Physiol* 2021;12:653040.
95. Ito Y, Yeo JY, Chytil A, et al. Conditional inactivation of Tgfb2 in cranial neural crest causes cleft palate and calvaria defects. *Development* 2003;130:5269–5280.
96. Singh N, Gupta M, Trivedi CM, Singh MK, Li L, Epstein JA. Murine craniofacial development requires Hdac3-mediated repression of Msx gene expression. *Dev Biol* 2013;377:333–344.
97. Xu X, Han J, Ito Y, Bringas P Jr, Urata MM, Chai Y. Cell autonomous requirement for Tgfb2 in the disappearance of medial edge epithelium during palatal fusion. *Dev Biol* 2006;297:238–248.
98. Guo T, Han X, He J, et al. KDM6B interacts with TFDP1 to activate P53 signaling in regulating mouse palatogenesis. *Elife* 2022;11:e74595.
99. Fueyo R, Iacobucci S, Pappa S, et al. Lineage specific transcription factors and epigenetic regulators mediate TGF-beta-dependent enhancer activation. *Nucleic Acids Res* 2018;46:3351–3365.
100. Lee SH, Kim O, Kim HJ, Hwangbo C, Lee JH. Epigenetic regulation of TGF-beta-induced EMT by JMJD3/KDM6B histone H3K27 demethylase. *Oncogenesis* 2021;10:17.
101. Siewert A, Reiz B, Guergo, et al. Analysis of candidate genes for cleft lip ± cleft palate using murine single-cell expression data. *Front Cell Dev Biol* 2023;11:1091666.

Effect of Intact Periosteum on Alveolar Ridge Contour Stability after Horizontal Guided Bone Regeneration in the Posterior Region: a Retrospective and Radiographical Cohort Study

Deng Hui DUAN¹, Hom Lay WANG², En Bo WANG¹

Objective: To radiographically evaluate the effect of intact periosteum in guided bone regeneration (GBR) for the treatment of peri-implant ridge defects in posterior region.

Methods: Twenty-eight patients who satisfied the criteria were included in this study. Buccal dehiscence defects were regenerated using demineralised bovine bone mineral (DBBM). Subjects were divided into two groups: the control group (conventional GBR, buccal trapezoidal flap and DBBM with collagen membrane coverage, $n = 14$) and the test group (modified GBR, buccal pouch and DBBM with collagen membrane coverage, $n = 14$). CBCT images obtained immediately after and 3 to 7 months following GBR were used to assess buccal bone thickness (BBT) at a level of 0, 2, 4 and 6 mm below the implant platform.

Results: Immediately after surgery, BBT at 0 mm and 2 mm below the implant platform presented a significant difference between the two groups ($P < 0.05$) with significantly thicker buccal bone in the control group in terms of BBT-0 (3.83 ± 1.01 mm) and BBT-2 (4.88 ± 1.15 mm) than in the test group (2.33 ± 0.66 mm and 3.60 ± 1.10 mm, $P = 0.000$ and $P = 0.008$, respectively). After 3 to 7 months of healing, the BBT at all levels showed no significant difference between the two groups ($P > 0.05$), but more bone graft resorption (BBR) in the control group in terms of BBR-0 (2.45 ± 1.14 mm), BBR-2 (2.09 ± 0.94 mm) and BBR-0% ($65.37\% \pm 26.62\%$) than the test group (BBR-0 1.07 ± 0.51 mm, $P = 0.001$; BBR-2, 1.22 ± 0.63 mm, $P = 0.008$; BBR-0% $45.70\% \pm 15.52\%$, $P = 0.024$).

Conclusion: In the short term, all treatment modalities achieved similar coronal BBT and the intact periosteum had a positive effect on keeping ridge dimensions even.

Key words: alveolar ridge augmentation, bone regeneration, CBCT, dental implants
Chin J Dent Res 2023;26(4):227–233; doi: 10.3290/j.cjdr.b4784067

Guided bone regeneration (GBR) using particulate bone graft with a collagen membrane is commonly employed to resolve peri-implant ridge defects¹⁻³; however, the stability of alveolar ridge contour after GBR surgery is unpre-

dictable, as up to 68.9% of the augmented alveolar ridge dimension may collapse horizontally.⁴⁻⁷ The potential mechanisms were apical displacement of bone graft^{5,8,9} and its accelerated resorption^{10,11} for an unstable mechanical environment in the augmented implant sites generated due to pressure from the perioral muscles.

The periosteum is a specialised, vascularised connective tissue anchored to the surface of bone and has two distinct layers: the outer fibrous layer containing fibroblasts, nerves, vessels and Sharpey fibres, and the inner cambium layer containing the osteoprogenitors¹²⁻¹⁵. Due to the lower elasticity of its fibrous layer, a buccal trapezoidal mucoperiosteal flap with a periosteal incision at the mesial, distal and apical sites is needed to achieve primary tension-free wound closure in GBR surgery^{16,17}. Consequently, the buccal

1 Department of Oral and Maxillofacial Surgery, Peking University School and Hospital of Stomatology, National Clinical Research Centre for Oral Diseases & National Engineering Research Centre of Oral Biomaterials and Digital Medical Device, Beijing Key Laboratory of Digital Stomatology, Beijing, P.R. China.

2 Department of Periodontics and Oral Medicine, School of Dentistry, University of Michigan, Ann Arbor, MI, USA.

Corresponding author: Dr En Bo WANG, Department of Oral and Maxillofacial Surgery, Peking University School and Hospital of Stomatology, #22, Zhongguancun South Avenue, HaiDian District, Beijing, 100081, P.R. China. Tel: 86-10-82195382; Fax: 86-10-62173402. Email: ebwang-hlg@163.com.

trapezoidal flap cannot withstand the pressure from the perioral muscles, forcing the bone graft materials to be displaced apically during healing^{5,8,9}. In addition, the mesio, distal and apical tension-releasing incisions not only increase the postoperative reaction and nerve injury complications¹⁸, but also reduce the blood supply from the buccal soft tissue flap to the bone graft material underneath.

The application of a buccal trapezoidal mucoperiosteal flap has been challenged recently by the subperiosteal tunnelling technique¹⁹⁻²² and the intrabony defect reconstruction associated with peri-implantitis²³⁻²⁵, through which successful bone regeneration has been achieved with a punch flap^{19,20,23-25}. Successful bone regeneration may be attributed to the intact periosteal fibrous layer in the tunnelling technique and the intrabony defect within peri-implantitis to confine the bone graft within the pocket or defect.

To take advantage of the properties of the periosteum to perform GBR in a minimally invasive manner, this study proposes a modified GBR procedure: after making an incision at the bone crest, a mucoperiosteal flap is elevated buccally to form a pouch between the buccal bone plate and the elevated periosteum. The particulate bone graft with collagen membrane is grafted into the pocket after implant placement. The mucoperiosteal flap is sutured with a transmucosal healing abutment. The purpose of the present study was to retrospectively and radiographically investigate the role of the intact periosteum on the stability of alveolar ridge contour after GBR; that is, whether there were differences in ridge contour between the conventional GBR procedure (control group) and the modified GBR procedure (test group).

Materials and methods

Patient selection

All patients were informed of the treatment protocol and signed an informed consent form. The study was conducted in accordance with the 1975 Declaration of Helsinki as revised in 2013. The study protocol was approved by the Institutional Review Board of Peking University School and Hospital of Stomatology, Beijing, China (approval no. PKUSSIRB-202385015), and the Strengthening the Reporting of Observational Studies in Epidemiology (STROBE) guidelines were followed.

A total of 61 consecutive patients who underwent GBR during implant placement at the Department of Oral and Maxillofacial Surgery of Peking University

School and Hospital of Stomatology in Beijing, China from January 2019 to April 2023 were included in this retrospective study. The inclusion criteria were as follows:

- aged 19 years or older;
 - a single missing maxillary or mandibular posterior tooth with intact mesial and distal adjacent teeth;
 - a buccal dehiscence defect at the time of implant placement;
 - three sets of CBCT data available (T0, preoperative; T1, immediately after dental implantation and GBR surgery; and T2, 3 to 7 months after surgery).
- The exclusion criteria were as follows:
- more than one missing tooth at the surgical site;
 - combined horizontal and vertical peri-implant defect at the buccal site;
 - palatal or lingual peri-implant bone defect;
 - CBCT data with severe artifacts or not available;
 - ongoing use of immunosuppressants, corticosteroids or bisphosphonates;
 - smoking more than 10 cigarettes per day.

GBR procedures

All surgical procedures in this study were performed by one oral surgeon (Duan DH). In the control group, GBR was performed using a conventional trapezoidal flap with vertical and periosteal releasing incisions. After local infiltration anaesthesia, a mid-crestal incision was made at the edentulous site, and vertical releasing incisions were placed at the line angles of the immediately adjacent mesial and distal teeth. Full-thickness buccal and oral flaps were raised. According to the manufacturer's instructions, a 10-mm-long tissue-level implant (Standard Plus, Straumann, Basel, Switzerland) was placed in a prosthetically driven position with a cover screw placed. A collagen membrane (Bio-Gide, Geistlich, Wolhusen, Switzerland) was trimmed, placed buccal to the ridge and fixed apically with a minimum of two titanium tacks. Deproteinised bovine bone mineral (DBBM) (Bio-Oss, Geistlich) was placed over the buccal dehiscence defect up to the smooth-rough implant interface. The membrane was stretched tightly over the graft and fixed with titanium pins. Periosteal releasing incisions were made along the buccal flap to achieve passive primary wound closure along with resorbable sutures (Jiahe Medical Materials, Changsha, China) (Fig 1).

In the test group, a buccal pouch design without periosteal or vertical releasing incisions was used. After administering local infiltration anaesthesia, a mid-crestal incision was made at the edentulous site, and a minimally invasive full-thickness buccal flap was

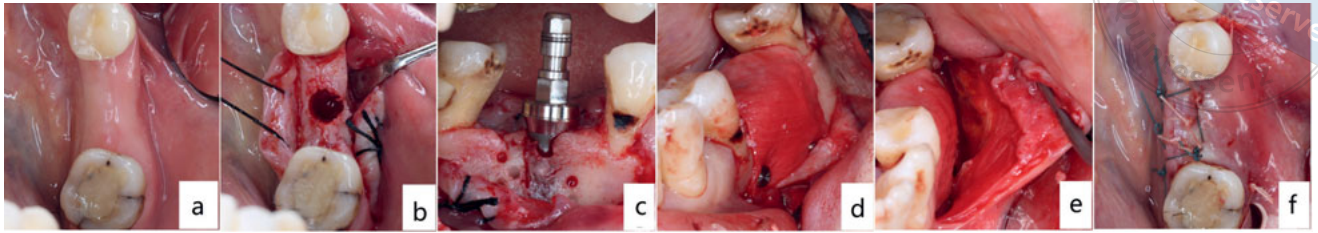


Fig 1 Surgical protocol for the control group. (a) Occlusal view of the mandibular left first molar implant site. (b) Thin buccal bone plate after implant osteotomy site preparation. (c) Buccal dehiscence defect after implant placement. (d) Bone graft covered by collagen membrane. (e) Buccal trapezoidal flap with periosteal releasing incision. (f) Primary wound closure with resorptive suture.

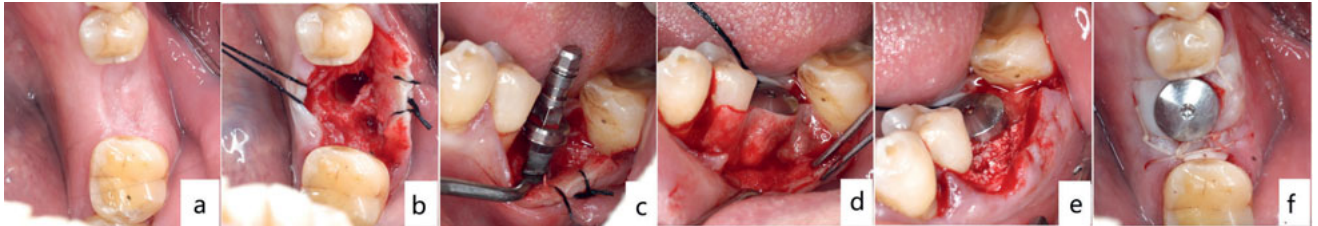


Fig 2 Surgical protocol for the test group. (a) Occlusal view of the mandibular left first molar implant site. (b) Buccal bone defect after implant osteotomy site preparation. (c) Buccal dehiscence defect after implant placement. (d) Collagen membrane inserted into the buccal pouch. (e) Bone graft covered with collagen membrane and restricted within the buccal pouch. (f) Non-primary wound closure with resorbable suture.

elevated mesially, distally and apically to form a pouch with an approximate dimension of 12 mm (apicocoronal) by 15 mm (mesiodistal). Following the manufacturer's instructions, a 10-mm-long tissue-level implant was placed in a prosthetically driven position (Standard Plus), and a 3-mm-tall healing abutment was placed. The buccal dehiscence defect was grafted over with DBBM up to the smooth-rough implant interface. A collagen membrane (Bio-Gide) was inserted between the flap and the graft. The site was sutured (Vicryl Rapide, Ethicon, Somerville, MA, USA), leaving the healing abutment exposed (Fig 2).

Following surgery, patients were prescribed an antibiotic (500 mg amoxicillin, p.o, b.i.d) and an analgesic (600 mg ibuprofen p.o, t.i.d) for 7 days. They were instructed to rinse twice daily for 30 seconds with 0.12% chlorhexidine gluconate. Sutures were removed 7 to 14 days after surgery. Patients were recalled on a monthly basis after implantation to monitor healing. In the control group, re-entry surgery was performed after 3 to 7 months, and taller healing abutments were placed as needed. All patients were referred to their prosthetic dental practitioner for restoration 3 to 7 months after surgery.

Radiographic evaluation

CBCT scans were taken of all sites using a CBCT machine (3DX Accuitomo, Morita, Kyoto, Japan) with a field of

view (FOV) with a diameter of 10 cm and height of 5.6 cm, acceleration voltage of 90 kV, beam current of 8.0 mA and voxel size of 0.2 mm at three different time points: preoperatively (T0), immediately after implant placement/GBR (T1) and 3 to 7 months after implant placement/GBR (T2) (Fig 3). The data were exported as DICOM files and a CBCT measurement protocol was established. To determine the preoperative alveolar ridge contour with respect to the implant position, the T1 DICOM data set was transferred to Mimics software (version 15.0, Materialise, Leuven, Belgium). After segmentation, the 3D models of the arch and implant were exported as stereolithography (STL) files and superimposed with the T0 DICOM data to calculate the implant-relative buccal contour at T0. A reference plane was set at the smooth-rough implant interface (Fig 4).

The following variables were measured on the bucco-oral cross-section perpendicular to the central axis of the implant^{26,27}:

- Buccal bone thickness (BBT-0 to BBT-6), which was the bone thickness buccal to the implant surface at 0, 2, 4 and 6 mm coronal to the reference plane), measured at T0, T1 and T2. Negative values were used for alveolar positions palatal or lingual to the buccal implant surface at T0.
- Buccal bone level (BBL), which was the vertical distance from the reference plane to the alveolar crest at the mid-buccal implant surface, measured at T0, T1 and T2. The virtually derived implant was used for the

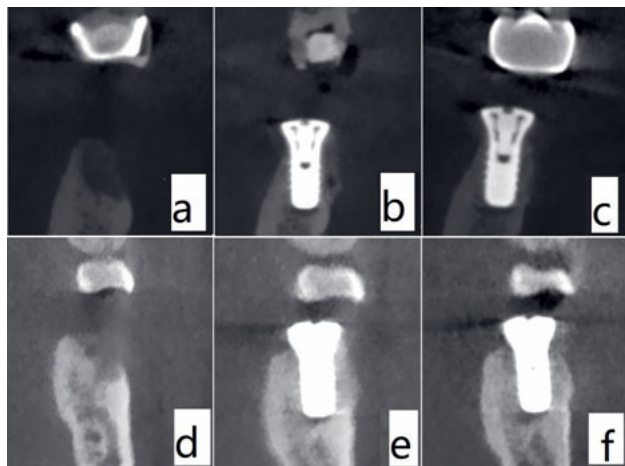


Fig 3 Alveolar ridge contour on the bucco-oral section at T0 (a and d), T1 (b and e) and T2 (c and f) in the control group (a to c) and test group (d to f).

T0 measurement. Negative values were used for hard tissue levels coronal to the reference plane.

- Buccal bone resorption (BBR-0 to BBR-6), which was the change in BBT from T1 to T2 at 0, 2, 4 and 6 mm coronal to the reference plane.
- BBL change (BBLC), which was the change in BBL from T1 to T2.

An experienced and calibrated assessor (Duan DH) performed the CBCT measurements, which were repeated twice and then averaged. Calibration was performed using 20 implant sites. The coefficients of intra-examiner repeatability for BBT and BBL were at least 0.90.

Statistical evaluation

Data from a previous study²⁸ were used to calculate the necessary sample size. In that study, the final horizontal bone thickness at 6 months was 1.66 mm in the membrane group and 1.02 mm in the non-membrane group²⁸. Using a free online calculator (<http://powerandsamplesize.com/Calculators/Compare-2-Means/2-Sample-Equality>) with a significance level of 0.05, standard deviation of 0.59 and a power of 80%, the number of patients per group required in this study was determined to be 14, to give a total of 28 patients.

Statistical analysis was performed using SPSS software (version 22.0, IBM, Armonk, NY, USA). The mean and standard deviation (SD) for each parameter were calculated for each of the three treatment groups. Parametric (Student *t* test, one-way analysis of variance [ANOVA]) or non-parametric tests (Mann-Whitney) were used to test the differences between the two groups, depending on the normal distribution of data. For cat-

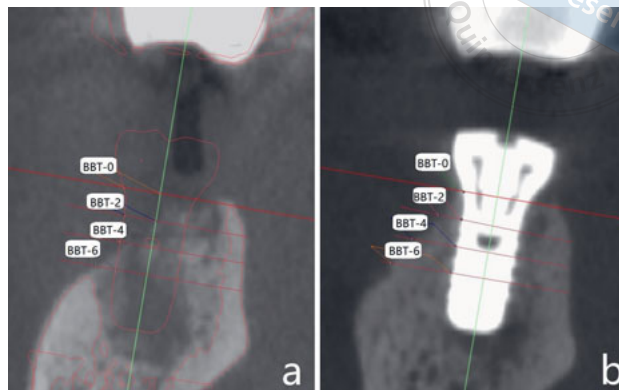


Fig 4 Measurement of the thickness of the buccal bone plate at different levels below the smooth-rough implant interface. (a) Measurement before surgery (registration with the CBCT mandible and implant model immediately after surgery). (b) measurement immediately and 5 months after surgery.

egorical variables, a chi-square analysis was used. The level of statistical significance was set at $P < 0.05$.

Results

The flowchart for the experiment is shown in Fig 5. A total of 61 patients were included in the initial screening, but 33 were excluded due to incompatibility with the eligibility criteria. A total of 28 patients with 28 implants were included for statistical analysis (control group, $n = 14$; test group, $n = 14$). The study population included 10 men (35.71%) and 18 women (64.29%), with a mean age of 44.11 ± 11.91 years (range 24 to 74 years) and a mean T1 to T2 interval of 5.21 ± 1.50 months (range 3 to 7 months) showing no significant differences between the two groups ($P > 0.05$). There were no significant differences in age, sex or healing time between the two groups ($P > 0.05$). Of the 28 dental implants, two were placed in maxillary molar sites (control group, $n = 0$; test group, $n = 2$), four in mandibular premolar sites (control group, $n = 1$; test group, $n = 3$), and 22 in mandibular molar sites (control group, $n = 13$; test group, $n = 9$); there were no significant differences in implant site distribution between the groups.

Table 1 presents the outcomes at each time point. At baseline (T0), there were no significant differences in BBT at any level or in BBL ($P > 0.05$) between the groups. The mean BBT-0 was -1.28 ± 0.91 mm in the control group and -1.37 ± 1.38 mm in the test group. The corresponding values for BBT-2 were 0.62 ± 0.90 mm and -0.30 ± 1.50 mm, respectively. The BBL, equivalent to the dehiscence length (apicocoronally), was -2.15 ± 2.45 mm in the control group and -1.53 ± 4.56 mm in the test group.

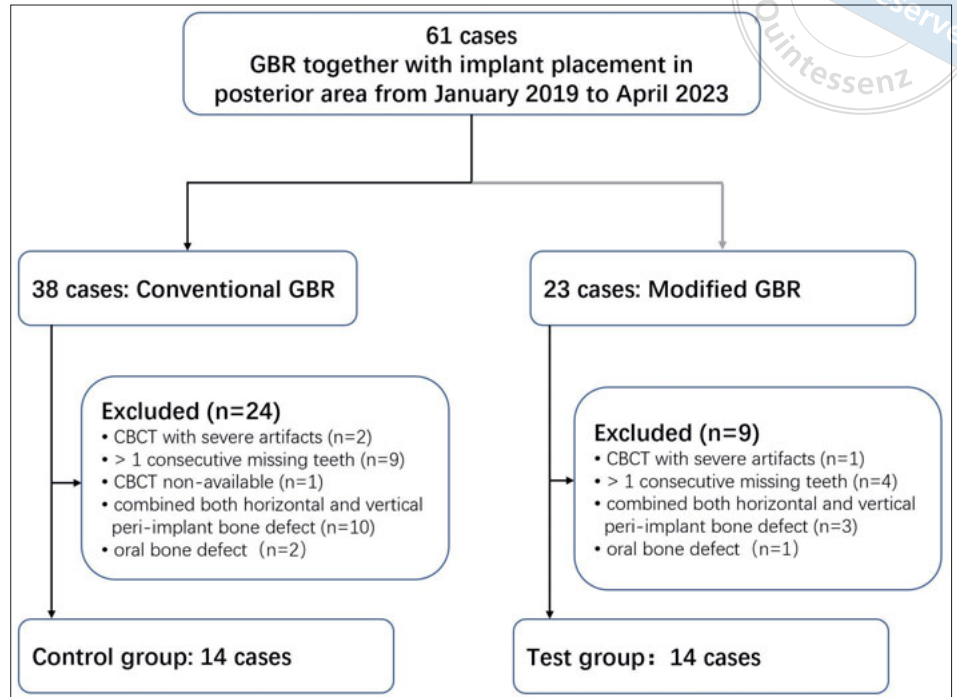


Fig 5 Experimental flowchart.

Table 1 Mean alveolar ridge dimensions at different time points.

Time point	Variable	Control group (n = 14)	Test group (n = 14)	Difference between groups	P value
T0	BBT-0, mm	-1.28 ± 0.91	-1.37 ± 1.38	0.10	0.828
	BBT-2, mm	0.62 ± 0.90	-0.30 ± 1.50	0.91	0.063
	BBT-4, mm	1.67 ± 1.29	0.94 ± 1.58	0.72	0.197
	BBT-6, mm	2.70 ± 1.61	1.74 ± 1.84	0.96	0.156
	BBL, mm	-2.15 ± 2.45	-1.53 ± 4.56	-0.62	0.661
T1	BBT-0, mm	3.83 ± 1.01	2.33 ± 0.66	1.50	0.000**
	BBT-2, mm	4.88 ± 1.15	3.60 ± 1.10	1.28	0.006**
	BBT-4, mm	5.34 ± 1.34	4.40 ± 1.44	0.93	0.088
	BBT-6, mm	5.18 ± 1.67	4.51 ± 1.63	0.67	0.292
	BBL, mm	1.80 ± 1.22	1.38 ± 0.59	0.42	0.266
T2	BBT-0, mm	1.38 ± 1.24	1.26 ± 0.55	0.11	0.755
	BBT-2, mm	2.79 ± 1.16	2.38 ± 0.94	0.41	0.318
	BBT-4, mm	3.97 ± 1.43	3.51 ± 1.32	0.46	0.388
	BBT-6, mm	4.39 ± 1.80	3.91 ± 1.48	0.48	0.450
	BBL, mm	0.49 ± 0.76	0.77 ± 0.71	-0.27	0.335
T1-T2	BBR-0, mm	2.45 ± 1.14	1.07 ± 0.51	1.38	0.001**
	BBR-2, mm	2.09 ± 0.94	1.22 ± 0.63	0.87	0.008**
	BBR-4, mm	1.36 ± 1.14	0.89 ± 0.75	0.48	0.202
	BBR-6, mm	0.79 ± 1.46	0.60 ± 0.55	0.19	0.649
	BBLC, mm	1.31 ± 1.10	0.62 ± 0.67	0.69	0.057
	BBR-0%	65.37 ± 26.62	45.70 ± 15.52	19.67	0.024*
	BBR-2%	43.49 ± 15.55	34.86 ± 15.39	8.62	0.152
	BBR-4%	25.56 ± 19.22	20.75 ± 15.43	4.81	0.472
BBR-6%	12.46 ± 33.63	12.74 ± 11.54	-0.29	0.976	

*P < 0.05, **P < 0.01

Immediately after surgery (T1), BBT-0 and BBT-2 were significantly different between groups ($P < 0.05$), with the control group showing statistically significantly greater BBT-0 (3.83 ± 1.01 mm) and BBT-2 (4.88 ± 1.15 mm) than the test group (2.33 ± 0.66 mm and 3.60 ± 1.10 mm, respectively). There was no significant difference in BBL between the groups at T1.

After 3 to 7 months (T2), there were no differences in BBT at any level or BBL between the groups ($P > 0.05$). From T1 to T2, the control group demonstrated statistically greater graft resorption in millimetres (BBR-0, 2.45 ± 1.14 mm and BBR-2, 2.09 ± 0.94 mm) and as a percentage (BBR-0% $65.37\% \pm 26.62\%$) than the test group (BBR-0 1.07 ± 0.51 mm, BBR-2 1.22 ± 0.63 mm, BBR-0% $45.70\% \pm 15.52\%$; $P = 0.001$, 0.008 and 0.024 , respectively); however, there were no differences in the percentage of buccal graft resorption or in BBL between the groups.

Discussion

This retrospective cohort study investigated the impact of intact periosteum on buccal ridge dimensions in the short term after simultaneous GBR and implant placement in single posterior sites. The conservative buccal pouch approach, introduced in this study, successfully increased BBT and resolved dehiscence defects, similar to the conventional flap design.

Designing flaps with vertical and periosteal releasing incisions for the purpose of achieving primary wound closure has been the preferred approach to GBR^{16,17}; however, incising the periosteum may have negative effects on GBR as it is composed of two layers: an inner cambium layer containing vascular and osteogenic cells, and an outer inelastic fibrous layer¹²⁻¹⁵. Additionally, violating the periosteal outer layer can result in a flap that is too weak to withstand pressure from the perioral muscles, potentially leading to apical graft displacement^{5,8,9}. Thus, surgeons may try to over-augment sites to compensate for bone graft resorption or use rigid support structures such as tenting screws, titanium plates and titanium mesh to mitigate bone graft displacement^{10,29,30}.

In the present study, over-augmentation in the test group was restricted due to the taut nature of the intact periosteal fibrous layer compared with the control group. This was reflected by significantly thicker buccal bone in the control group in terms of BBT-0 (3.83 ± 1.01 mm) and BBT-2 (4.88 ± 1.15 mm) than in the test group (2.33 ± 0.66 mm and 3.60 ± 1.10 mm, $P = 0.0000$ and $P = 0.006$, respectively); however, after 3 to 7 months of healing (T2), the BBT at all levels showed no significant

difference between the two groups with BBT-0 of less than 2 mm (1.38 ± 1.24 mm and 1.26 ± 0.55 mm in the control group and test group, respectively) and BBT-2 more of than 2 mm (2.79 ± 1.16 and 2.38 ± 0.94 mm in the control group and test group, respectively). From T1 to T2, patients with periosteal tension-reducing incisions (control group) showed more bone graft resorption in terms of BBR-0 (2.45 ± 1.14 mm), BBR-2 (2.09 ± 0.94 mm) and BBR-0% ($65.37 \pm 26.62\%$) than the test group (BBR-0 1.07 ± 0.51 mm, $P = 0.001$; BBR-2 1.22 ± 0.63 mm, $P = 0.008$; BBR-0% $45.70 \pm 15.52\%$, $P = 0.024$). These results indicated that the modified GBR technique could achieve comparable BBT, with less over-augmentation but in a minimally invasive manner, compared with the conventional approach. This difference in resorption could be due to the greater vascularisation and protection of the graft from the elements provided by an intact and inflexible periosteum.

As the present study was retrospective and non-randomised, with a limited number of patients, varying healing time intervals due to a delay in follow-ups caused by the COVID-19 pandemic and a disproportionate distribution of mandibular versus maxillary sites, caution is advised when interpreting the results. Additionally, the short follow-up period and lack of evaluation after re-entry further limit the study's findings. Thus, future randomised controlled trials with larger sample sizes and longer follow-up periods are needed to validate these findings and provide more conclusive evidence.

Conclusion

GBR can be performed using a surgically simple buccal pouch to treat dehiscence defects during implant placement in single posterior sites, and this technique may augment sites as well as GBR using a conventional flap; however, before recommending this technique for daily practice, long-term data after functional loading are necessary.

Conflicts of interest

The authors declare no conflicts of interest related to this study.

Author contribution

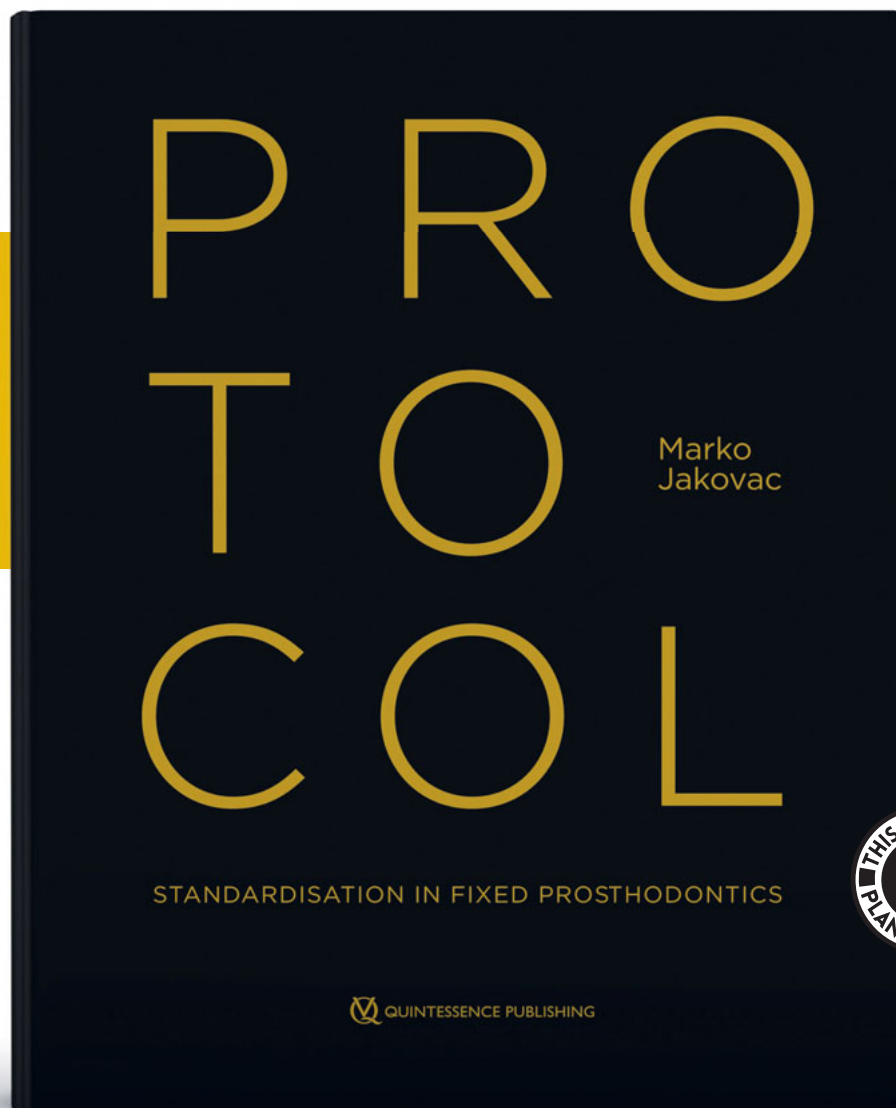
Dr Deng Hui DUAN performed the study and drafted the manuscript; Dr Hom Lay WANG revised the manuscript; Dr En Bo Wang supervised the study and all the authors approved the final submission.

(Received May 21, 2023; accepted Aug 21, 2023)

References

- Jung RE, Fenner N, Hämmerle CHF, Zitzmann NU. Long-term outcome of implants placed with guided bone regeneration (GBR) using resorbable and non-resorbable membranes after 12-14 years. *Clin Oral Implants Res* 2013;24:1065-1073.
- Thoma DS, Bienz SP, Figuero E, Jung RE, Sanz-Martin I. Efficacy of lateral bone augmentation performed simultaneously with dental implant placement: A systematic review and meta-analysis. *J Clin Periodontol* 2019;46(suppl 21):257-276.
- Hämmerle CHF, Jung RE, Feloutzis A. A systematic review of the survival of implants in bone sites augmented with barrier membranes (guided bone regeneration) in partially edentulous patients. *J Clin Periodontol* 2002;29(suppl 3):226-231; discussion 32-33.
- Fu JH, Oh TJ, Benavides E, Rudek I, Wang HL. A randomized clinical trial evaluating the efficacy of the sandwich bone augmentation technique in increasing buccal bone thickness during implant placement surgery: I. Clinical and radiographic parameters. *Clin Oral Implants Res* 2014;25:458-467.
- Benic GI, Thoma DS, Jung RE, et al. Guided bone regeneration with particulate vs. block xenogenic bone substitutes: a pilot cone beam computed tomographic investigation. *Clin Oral Implants Res* 2017;28:e262-e270.
- Jung EH, Jeong SN, Lee JH. Augmentation stability and early wound healing outcomes of guided bone regeneration in peri-implant dehiscence defects with L- and I-shaped soft block bone substitutes: A clinical and radiographic study. *Clin Oral Implants Res* 2021;32:1308-1317.
- Ye GH, Duan DH, Wang EB. Ridge volume stability of maxillary anterior implants placed with simultaneous lateral guided bone regeneration during healing: A radiographic analysis. *Chin J Dent Res* 2021;24:251-256.
- Mir-Mari J, Wui H, Jung RE, Hämmerle CHF, Benic GI. Influence of blinded wound closure on the volume stability of different GBR materials: An in vitro cone-beam computed tomographic examination. *Clin Oral Implants Res* 2016;27:258-265.
- Araújo MG, Carmagnola D, Berglundh T, Thilander B, Lindhe J. Orthodontic movement in bone defects augmented with Bio-Oss. An experimental study in dogs. *J Clin Periodontol* 2001;28:73-80.
- Duan DH, Wang HL, Xiao WC, Liu Z, Wang EB. Bone regeneration using titanium plate stabilization for the treatment of peri-implant bone defects: A retrospective radiologic pilot study. *Clin Implant Dent Relat Res* 2022;24:792-800.
- Nagy P, Molnar B, Nemes B, Schupbach P, Windisch P. Histologic evaluation of human intrabony periodontal defects treated with deproteinized bovine bone mineral in combination with orthodontic tooth movement: A case series. *Int J Periodontics Restorative Dent* 2019;40:321-330.
- Simon TM, Van Sickle DC, Kunishima DH, Jackson DW. Cambium cell stimulation from surgical release of the periosteum. *J Orthop Res* 2003;21:470-480.
- Al-Qtaitat A, Shore RC, Aaron JE. Structural changes in the ageing periosteum using collagen III immuno-staining and chromium labelling as indicators. *J Musculoskelet Neuronal Interact* 2010;10:112-123.
- Siems WF, Viehland LA, Hill HH Jr. Improved momentum-transfer theory for ion mobility. I. Derivation of the fundamental equation. *Anal Chem* 2012;84:9782-9791.
- Lin Z, Fateh A, Salem DM, Intini G. Periosteum: biology and applications in craniofacial bone regeneration. *J Dent Res* 2014;93:109-116.
- Arnal HM, Angioni CD, Gaultier F, Urbinelli R, Urban IA. Horizontal guided bone regeneration on knife-edge ridges: A retrospective case-control pilot study comparing two surgical techniques. *Clin Implant Dent Relat Res* 2022;24:211-221.
- Benic GI, Thoma DS, Muñoz F, Sanz Martin I, Jung RE, Hämmerle CHF. Guided bone regeneration of peri-implant defects with particulated and block xenogenic bone substitutes. *Clin Oral Implants Res* 2016;27:567-576.
- Urban IA, Sommer C, Wang IC, Wang HL. Periosteum classification and flap advancement techniques around the mental foramen. *Int J Periodontics Restorative Dent* 2022;42:753-759.
- Lee EA. Subperiosteal minimally invasive aesthetic ridge augmentation technique (SMART): A new standard for bone reconstruction of the jaws. *Int J Periodontics Restorative Dent* 2017;37:165-173.
- Kakar A, Kakar K, Sripathi Rao BH, et al. Lateral alveolar ridge augmentation procedure using subperiosteal tunneling technique: A pilot study. *Maxillofac Plast Reconstr Surg* 2018;40:3.
- Block MS, Degen M. Horizontal ridge augmentation using human mineralized particulate bone: Preliminary results. *J Oral Maxillofac Surg* 2004;62:67-72.
- Jeong SM, Choi BH, Li J, Xuan F. Simultaneous flapless implant placement and peri-implant defect correction: An experimental pilot study in dogs. *J Periodontol* 2008;79:876-880.
- Regidor E, Ortiz-Vigón A, Romandini M, Dionigi C, Derks J, Sanz M. The adjunctive effect of a resorbable membrane to a xenogeneic bone replacement graft in the reconstructive surgical therapy of peri-implantitis - A randomized clinical trial. *J Clin Periodontol* 2023;50:765-783.
- Monje A, Pons R, Vilarrasa J, Nart J, Wang HL. Significance of barrier membrane on the reconstructive therapy of peri-implantitis: A randomized controlled trial. *J Periodontol* 2023;94:323-335.
- Roos-Jansäker AM, Renvert H, Lindahl C, Renvert S. Surgical treatment of peri-implantitis using a bone substitute with or without a resorbable membrane: A prospective cohort study. *J Clin Periodontol* 2007;34:625-632.
- Benic GI, Bienz SP, Song YW, et al. Randomized controlled clinical trial comparing guided bone regeneration of peri-implant defects with soft-type block versus particulate bone substitutes: Six-month results of hard-tissue changes. *J Clin Periodontol* 2022;49:480-495.
- Jiang X, Zhang Y, Di P, Lin Y. Hard tissue volume stability of guided bone regeneration during the healing stage in the anterior maxilla: A clinical and radiographic study. *Clin Implant Dent Relat Res* 2018;20:68-75.
- Park SH, Lee KW, Oh TJ, Misch CE, Shotwell J, Wang HL. Effect of absorbable membranes on sandwich bone augmentation. *Clin Oral Implants Res* 2008;19:32-41.
- César Neto JB, Cavalcanti MC, Sapata VM, et al. The positive effect of tenting screws for primary horizontal guided bone regeneration: A retrospective study based on cone-beam computed tomography data. *Clin Oral Implants Res* 2020;31:846-855.
- Naenni N, Schneider D, Jung RE, Hüsler J, Hämmerle CHF, Thoma DS. Randomized clinical study assessing two membranes for guided bone regeneration of peri-implant bone defects: clinical and histological outcomes at 6 months. *Clin Oral Implants Res* 2017;28:1309-1317.

ENHANCE YOUR EXPERTISE



Marko Jakovac

Protocol: Standardisation in Fixed Prosthodontics

732 pages, 1,200 illus.

ISBN 978-1-78698-117-2, €300



Fixed prosthodontic therapy is one of the most demanding disciplines in dentistry. This avenue is usually pursued only after other options have been exhausted, often when teeth are missing or show reduced durability, or in the presence of conditions that cannot be treated conservatively. Enhance your expertise with this comprehensive text that presents the key steps to success at every stage of therapy: planning, execution, manufacturing, and finalization. Discover the importance of meticulous treatment planning to meet patients' short- and long-term requirements; learn key principles and techniques for effective

and minimally invasive tooth preparation; avoid mistakes caused by performing procedures without proper guidance; embrace the latest techniques and technologies for creating high-quality prosthetic restorations; explore the intricacies of cementation for optimal adhesion and retention; and learn how to strategize to maintain restoration success and oral health. Whether you are an experienced clinician or a dental professional seeking to expand your practice, the protocol-driven approach advocated in this text will equip you to achieve consistent and exceptional results with fixed prosthodontic therapy.



www.quint.link/protocol



books@quintessenz.de



+49 (0)30 761 80 667

 QUINTESSENCE PUBLISHING

Sixteen Cellular Senescence-associated DNA Methylation Signature Predicts Overall Survival in Patients with Head and Neck Squamous Cell Carcinoma

Ming Han YE¹, Xin Yi HUANG², Chun Jie LI^{1,3}, Qian Ju WU^{4,5}, Fei LIU¹

Objective: To construct a cellular senescence-related DNA methylation model to act as an independent prognosis predictor for patients with head and neck squamous cell carcinoma (HNSCC).

Methods: Methylome, transcriptome and clinical information for 499 HNSCC patients were received from The Cancer Genome Atlas (TCGA) as a training set. An extra independent methylation dataset of 54 patients with oral squamous cell carcinoma (OSCC) was downloaded from the NCBI Gene Expression Omnibus (GEO) database as the validation set. To assess the cellular senescence level of each sample, the senescence score (SS) of each patient was calculated using the transcriptome data via single-sample gene set enrichment analysis (ssGSEA). Least absolute shrinkage and selection operator (LASSO) Cox regression analyses were conducted to confirm Cytosine, phosphoric acid and Guanine (CpG) sites for the development of a cellular senescence-related DNA methylation signature.

Results: Based on the SS of each HNSCC patient in the TCGA cohort, the patients were divided into high- and low-SS subgroups. The high-SS group showed a better prognosis than the low-SS group. Moreover, 3,261 differentially methylated CpG sites (DMCs) were confirmed between the two groups. Among them, 16 DMCs were included to develop a 16-DNA methylation signature for evaluation of HNSCC prognosis using LASSO and multivariate Cox regression analysis.

Conclusion: A novel cellular senescence-related 16-DNA methylation signature was determined, which can be used as an independent index to evaluate the prognosis of HNSCC patients and select appropriate treatment strategies.

Key words: cellular senescence, diagnostic predictor, DNA methylation signature, head and neck squamous cell carcinoma, oral squamous cell carcinoma

Chin J Dent Res 2023;26(4):235–248; doi: 10.3290/j.cjdr.b4784007

1 The State Key Laboratory of Oral Diseases, National Clinical Research Centre for Oral Diseases, West China Hospital of Stomatology, Sichuan University, Chengdu, Sichuan Province, P.R. China.

2 School and Hospital of Stomatology, Cheeloo College of Medicine, Shandong University & Shandong Key Laboratory of Oral Tissue Regeneration & Shandong Engineering Laboratory for Dental Materials and Oral Tissue Regeneration, Jinan, P.R. China.

3 Department of Head and Neck Oncology, West China Hospital of Stomatology, Sichuan University, Chengdu, P.R. China.

4 Stomatological Hospital of Xiamen Medical College, Xiamen Key Laboratory of Stomatological Disease Diagnosis and Treatment, Xiamen, P.R. China.

5 Shanghai Ninth People's Hospital, School of Medicine, Shanghai Jiao Tong University, Shanghai, P.R. China.

Corresponding authors: Dr Qian Ju WU, Stomatological Hospital of Xiamen Medical College, Xiamen Key Laboratory of Stomatological Disease Diagnosis and Treatment, Xiamen 361008, P.R. China. Tel: 86-592-2678557. Email: qianjuwu@163.com

Head and neck squamous cell carcinoma (HNSCC) is the sixth most common malignancy worldwide with a significant death rate and originates from the oral cavity, larynx and pharynx¹. According to the 2020 Global Cancer Report, there more than 600,000 new HNSCC cases are diagnosed each year². HNSCC is characterised as a heterogeneous malignancy with inter- and intra-tumour

Dr Fei LIU, State Key Laboratory of Oral Diseases, National Clinical Research Centre for Oral Diseases, National Centre for Stomatology, West China School of Stomatology, Sichuan University, Chengdu 610041, P.R. China. Tel: 86-15680820580. Email: liufei.hxkq@scu.edu.cn

The present work was supported by the Department of Science and Technology of Sichuan Province (grant number: 2021JDR0166) and the China Postdoctoral Science Foundation (grant number: 2020M683329).

differences³⁻⁵. Nowadays, although multiple therapies for HNSCC have developed significantly, the overall 5-year survival rate for HNSCC is still around 50%, which is far from satisfactory⁶. Accumulated evidence proved that early diagnosis of HNSCC leads to a higher 5-year survival rate and a better prognosis⁶. Hence, the discovery of trustworthy prognostic biomarkers is crucial to identify HNSCC at an early stage, offer patients effective therapy and improve their prognosis.

Cellular senescence is a permanent process of cell proliferation termination. It plays a pertinent role in tumour initiation growth, and metastasis, which is related to the activation of senescence-associated secretory phenotype (SASP), a key parameter generated by senescent cells⁷⁻⁹. Cellular senescence and SASP are a Jekyll and Hyde alteration, which means they facilitate suppression of the division of abnormal cells transforming into tumours while activating tumour cell growth and distant metastasis, particularly in tumours with higher SASP⁹⁻¹⁰. Studies have described how cellular senescence also plays a vital role in the resistance of HNSCC against radiotherapy and chemotherapy¹¹⁻¹³. Investigating the particular mechanism underlying the regulation of cellular senescence on the HNSCC could lead to a new way of detecting HNSCC at an early stage and offering timely therapy. Thus, further research on cellular senescence in HNSCC is urgently needed.

DNA methylation is one of the most widely explored epigenetic modifications, exhibiting a tight correlation to tumours¹⁴. Recently, emerging evidence has supported the idea that DNA methylation regulates cellular senescence and expression level of cellular senescence-related genes (CSRGs) in HNSCC patients^{12,15}. Accordingly, the exploration of DNA methylation and cellular senescence in HNSCC is potentially worthwhile.

Machine learning-based models show giant potential in evaluating tumour prognosis and improving the efficiency of immunotherapy in the treatment of tumours like HNSCC¹⁶. Recently, Wang et al¹⁷ developed a cellular senescence-related prognosis model to predict the HNSCC survival rate. Nevertheless, to the best of the present authors' knowledge, there is no HNSCC cellular senescence-related prognosis model constructed based on the methylome data.

The flowchart of the study workflow is shown in Fig 1. In the present study, in order to construct a cellular senescence-related DNA methylation model as a biomarker for the prediction of the prognosis of HNSCC patients, the methylome, transcriptome and clinical data for HNSCC patients were downloaded from the Cancer Genome Atlas (TCGA) to construct a prediction

model of HNSCC prognosis. Sixteen DMCs were determined to develop a 16-DNA methylation signature for HNSCC prognosis evaluation by way of a least absolute shrinkage and selection operator (LASSO) and multivariate Cox regression analysis. This cellular senescence-related DNA methylation signature has been proven to be a significant independent prediction factor in the prognosis of HNSCC patients and the identification of a subgroup that is more suited for immunotherapy. The discovery made in the present study may offer a better understanding of the role that cellular senescence plays in the prognosis of HNSCC and provide new strategies to identify subgroups and offer accurate therapy for HNSCC.

Materials and methods

Data collection and pre-processing

The data of HNSCC patients included in this study were obtained from UNSC Xena (<https://xena.ucsc.edu/>). The online database provided the transcriptome (RNA-seq, HTSeq-Counts/FPKMs) and methylome (Illumina Human Methylation 450, HM450) data containing 566 samples along with corresponding phenotype information. A total of 499 HNSCC patients and 44 normal controls with complete corresponding survival data were selected as the training set. The expression value (FPKM) was then normalised by quantile normalisation. An extra independent methylation dataset including 54 OSCC samples was downloaded from the NCBI Gene Expression Omnibus (GEO) database (access no. GSE75537)¹⁸. The GEO dataset was downloaded for external verification as a validation set.

Inference of senescence score (SS) and survival analysis investigating the relationship between SS and HNSCC prognosis

A total of 279 cellular senescence-related genes (CSRGs) were collected from the CellAge database including 28 oncogene-induced, 232 replicative and 34 stress-induced genes¹⁹. Five of these were both oncogene-induced and replicative, and ten were both stress-induced and replicative. To further understand the role played by cellular senescence in HNSCC and to investigate the methylation sites associated with cellular senescence and the relationship between cellular senescence and patient prognosis, the SS model was introduced. Firstly, a univariate Cox survival analysis was performed to confirm the CSRGs of which the expression level showed positive

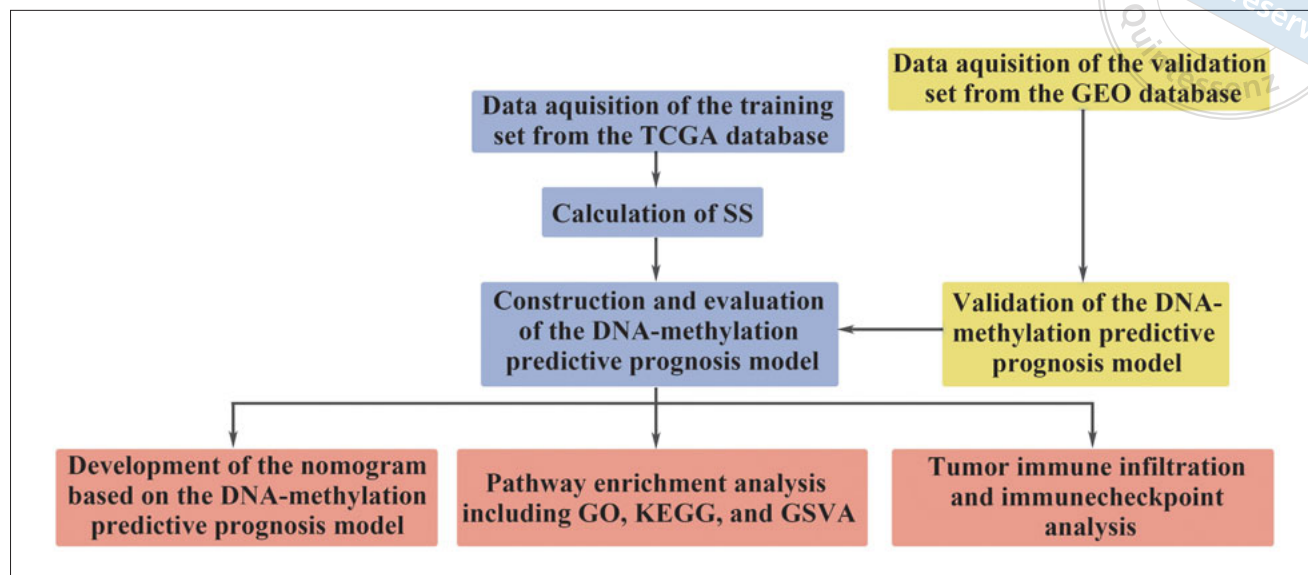


Fig 1 Flowchart for the present study.

and negative correlations with HNSCC patient prognosis, which were then defined as the senescence-positive and negative gene sets, respectively. The SSs were then inferred according to the method described in two previous reports²⁰⁻²¹. Enriched SSs based on the two gene sets above were computed by applying ssGSEA in the Gene Set Variation Analysis (GSVA) R package²², and the enriched score of senescence-positive components minus that of senescence-negative components was calculated and defined as the SS for each HNSCC individual. To verify the relationship between SS and HNSCC prognosis, patients in the training set were divided into high- and low-SS groups, which were confirmed by the median SS of the 499 TCGA HNSCC patients. In this study, a higher SS represented higher cellular senescence activity.

The survival status, survival time and phenotype data including the age, gender, sex and race of TCGA HNSCC patients were extracted to determine whether cellular senescence is related to the prognosis of patients with HNSCC via univariate and multivariate Cox proportional hazards analyses using the survival R package. Kaplan-Meier (KM) survival curves were drawn using the “survfit” function of the survminer R package to show the difference in the prognosis of HNSCC patients between the high- and low-SS groups.

Analysis of DMCs related to tumorigenesis and HNSCC prognosis

DMCs between tumour and normal samples in the training set were initially extracted using the limma R

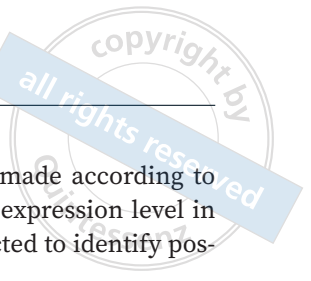
package, then the DMCs between the high- and low-SS subgroups were confirmed. The DMCs between HNSCC samples and normal samples were determined with a P value < 0.01 and $|\logFC| > 1.2$. The DMCs between high- and low-SS groups were determined with a P value < 0.01 and $|\logFC| > 1.1$.

Construction and validation of the predictive model of HNSCC prognosis

To develop a prognosis signature, the survival time, survival status and methylome data of DMCs included in the previous section were integrated to conduct a LASSO Cox regression analysis using the glmnet R package. By way of 10-fold cross-validation, the appropriate coefficient value was calculated to create the following predictive model of HNSCC prognosis:

$$\text{Risk score} = \sum_{i=1}^n \text{coef}(i) * \text{expr}(i).$$

coef was the coefficient value of each corresponding DMC, and expr was the expression level of each corresponding DMC. To validate the prediction efficacy of the predictive model, the validation set from the GEO database was selected. Specifically, the risk score for each patient in the validation set was calculated and divided into high- and low-risk score groups according to the median risk score. In both the training set and the validation set, KM and ROC analyses were performed to examine the prediction ability. ROC analysis was carried out based on the pROC R package to obtain the area under the ROC curve (AUC) at 1, 3 and 5 years.



Development of a nomogram

Using the “rms” R package, the survival time, survival status and eight clinical features were integrated to develop a nomogram and calibration curves. The nomogram is available when evaluating the prognosis significance of each variable. Total points can be calculated by adding up all the values of the corresponding features in this nomogram to evaluate patients' prognoses. ROC curves were drawn to confirm the prediction ability of this nomogram to act as an independent predictor. The method of ROC analysis was described in the previous section.

Gene function enrichment analysis

To explore the potential biomolecular mechanisms underlying the regulation of the CSRGs on the prognosis of HNSCC patients, GO, KEGG and GSVA analyses were performed. First, differential expression analysis was conducted to identify differentially expressed genes (DEGs) between the high- and low-risk groups. Genes with $P < 0.01$ and $|\log FC| > 1.5$ met the criteria. To extract essential pathways that were closely correlated to the DEGs, GO and KEGG gene function enrichment analysis were performed in clusterProfiler. GO analysis is a widely popular method that annotates genes and downstream products with three groups: molecular function (MF), biological pathways (BP) and cellular components (CCs)²³. GO annotation information was extracted from org.Hs.eg.db. KEGG is a powerful and comprehensive database developed for the systematic investigation of gene function pathways²⁴⁻²⁵ based on the newest KEGG pathway annotation from KEGG rest API (<https://www.kegg.jp/kegg/rest/keggapi.html>). To evaluate the influence of the expression level of each DEG, GSVA analysis²² was performed based on GO and KEGG terms downloaded from the Molecular Signatures Database separately²⁶.

Assessment of tumour immune infiltration and immune checkpoints in HNSCC

To clarify the tumour immune purity in HNSCC, the tumour microenvironment in each TCGA HNSCC sample was then explored. ESTIMATE²⁷ and TIMER²⁸ methods were used to clarify tumour immune purity in detail via the IOBR R package²⁹.

Considering the potential prospect of immune checkpoints in immunotherapy for HNSCC, a list of

known immune checkpoints were made according to the previous literature³⁰, and their expression level in high- and low-risk groups was detected to identify possible therapeutic targets.

Statistical analysis

In the current research, the online data analysis platform Sangerbox 3.0 (<http://vip.sangerbox.com/>) was used to conduct the aforementioned statistical analysis and result visualisation. Sangerbox 3.0 is a comprehensive, interaction-friendly website platform for bioinformatics analysis that makes it possible to perform a series of customized bioinformatics analyses and visualisation mapping based on the R packages mentioned above, and corresponding results can be downloaded from the platform³¹.

Results

SSs of HNSCC patients were associated with their prognosis

To investigate the role of cellular senescence in the genesis of HNSCC, the CSRGs were retrieved from the CellAge database¹⁹. Next, 11 and 9 genes (Table 1) were distinguished showing better and worse overall survival in the TCGA cohort, respectively, between expression level and overall survival ($P < 0.01$). The two gene sets were defined as senescence-positive and senescence-negative. Based on the expression levels of the two gene sets using ssGSEA, the SSs of HNSCC patients were calculated. SS represents the cellular senescence activity of different individuals to assess whether there is a relationship between cellular senescence and HNSCC patients, and was used in the subsequent section for screening of differentially expressed DNA methylation sites. The SSs ranged between -0.61 and 1.00 and the median was 0.16 . Next, the HNSCC patients were separated into high- and low-SS groups by the median SS and a KM survival analysis was conducted. Using a log-rank test, the findings indicated that low-SS HNSCC patients had poor overall survival ($P < 0.01$; Fig 2a). After adjusting for the effects of variables, such as age, sex, race and clinical stage, a multivariate Cox model analysis was performed and the relationship between SSs and survival of patients with HNSCC was verified (Fig 2b). These results revealed that SSs of the TCGA HNSCC samples were associated with their prognosis.

Table 1 CSRGs related to HNSCC survival confirmed by the training set.

Genes (ensemble ID)	Hazard ratio (HR) (95% CI for HR)	P value	
Senescence-positive gene sets	MAP2K7 (ENSG00000076984.16)	0.895 (0.843–0.951)	0.0003729
	MXD4 (ENSG00000123933.13)	0.937 (0.905–0.971)	0.0006764
	MAP3K6 (ENSG00000142733.13)	0.967 (0.948–0.986)	0.0009821
	CDKN2A (ENSG00000147889.15)	0.982 (0.971–0.992)	0.0010847
	MAP4K1 (ENSG00000104814.11)	0.877 (0.807–0.952)	0.0017620
	BTG3 (ENSG00000154640.13)	0.974 (0.956–0.990)	0.0021045
	LGALS3 (ENSG00000131981.14)	0.995 (0.991–0.998)	0.0021653
	DUSP16 (ENSG00000111266.7)	0.943 (0.907–0.981)	0.0037633
	BLK (ENSG00000136573.11)	0.600 (0.420–0.857)	0.0038601
	MOB3A (ENSG00000172081.12)	0.976 (0.959–0.993)	0.0068108
	EHF (ENSG00000135373.11)	0.991 (0.984–0.998)	0.0091848
Senescence-negative gene sets	PCGF2 (ENSG00000277258.3)	1.055 (1.025–1.086)	0.0003175
	FXR1 (ENSG00000114416.16)	1.035 (1.015–1.055)	0.0004351
	MAP2K1 (ENSG00000169032.8)	1.038 (1.015–1.061)	0.0011761
	SLC13A3 (ENSG00000158296.12)	1.484 (1.147–1.921)	0.0026281
	PSMD14 (ENSG00000115233.10)	1.050 (1.016–1.085)	0.0037126
	SMURF2 (ENSG00000108854.14)	1.130 (1.040–1.228)	0.0037972
	AURKA (ENSG00000087586.16)	1.031 (1.009–1.053)	0.0062148
	ERRF1 (ENSG00000116285.11)	1.013 (1.003–1.022)	0.0075066
	TERF2 (ENSG00000132604.9)	1.123 (1.029–1.226)	0.0093966

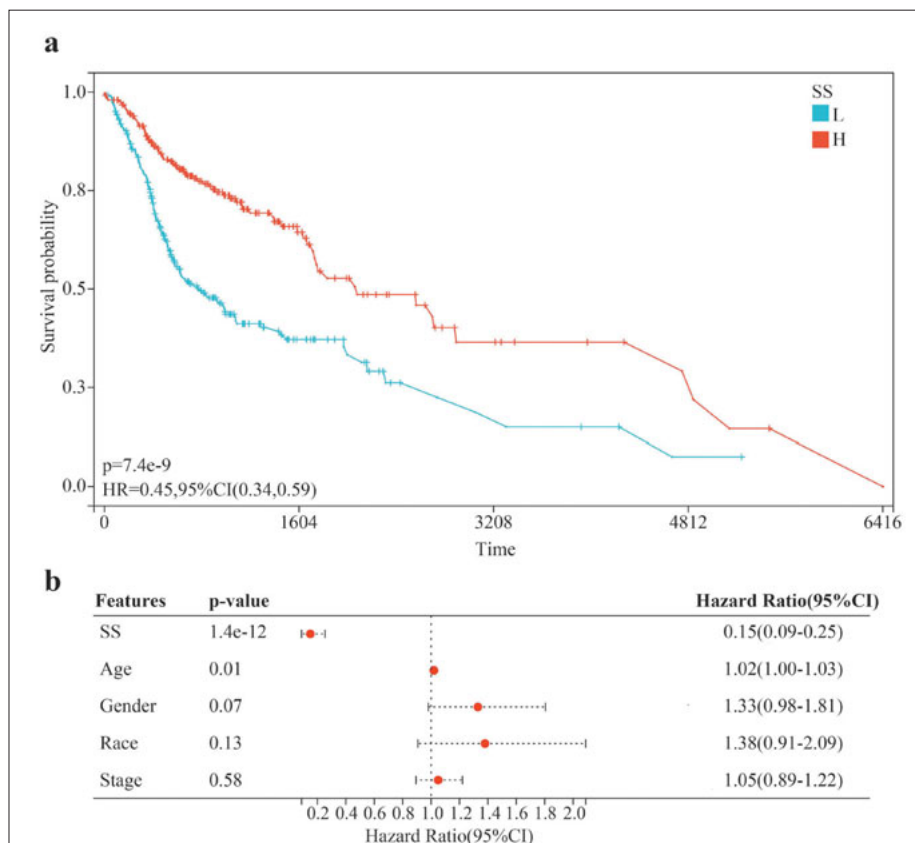


Fig 2 Relationships between SS and HNSCC overall survival. **(a)** KM curves of HNSCC with high- and low-SS subgroups in the training set. **(b)** Forest plot of the relationship between SS and HNSCC survival based on a multivariate Cox analysis.

The predictive prognosis model based on 16 cellular senescence-related DMCs was developed based on HNSCC overall survival

In the TCGA cohort, 12,046 DMCs were initially uncovered between HNSCC patients and normal samples ($P < 0.01$ and $|\logFC| > 1.2$). Ulteriorly, 3,261 DMCs were identified between high- and low-SS subgroups ($P < 0.01$ and $|\logFC| > 1.1$).

Next, the prognosis value of the 3,261 DMCs in the training set was evaluated using the LASSO Cox regression model. Through ten-fold cross-validation, the optimal lambda value was selected and then the range of DMCs was condensed in order to find a DNA methylation signature for the prediction of overall survival in HNSCC. As a result, a total of 16 CpG sites were included to construct the predictive prognosis model (Figs 3a and b). Using each CpG site's coefficient value and methylation status, a risk score model was developed as follows: RiskScore = $(0.4921997969551 * \text{cg}01995815) + (0.24140263854671 * \text{cg}02409878) + (-0.0746925257634289 * \text{cg}03424345) + (-0.185126888295284 * \text{cg}06459070) + (-0.084858590961658 * \text{cg}06879746) + (0.0240142978934278 * \text{cg}06903569) + (-0.405194167436796 * \text{cg}07768107) + (-0.061251172529722 * \text{cg}08106706) + (-0.0491305887218784 * \text{cg}12298745) + (0.430730131248078 * \text{cg}12389461) + (0.153090807571048 * \text{cg}13757826) + (-0.0119448628610951 * \text{cg}14170959) + (0.301928975546258 * \text{cg}16123269) + (0.243110636620704 * \text{cg}19239041) + (-0.0744088213742415 * \text{cg}20711812) + (-0.978573233155824 * \text{cg}21230425)$. To elucidate the efficacy of the influence of each CpG site included in the predictive prognosis model in the overall survival of HNSCC, multivariate and univariate Cox analyses were conducted. The multivariate Cox model was then used to compute the coefficient values of these 16 CpG sites (Fig 3c). Additionally, using univariate Cox regression, the relationship between each CpG site and HNSCC survival was assessed (Fig 3d). Based on the results of the multivariate and univariate Cox models, the methylation of the 16 CpG sites was strongly linked with HNSCC survival. A Pearson correlation analysis was also performed to investigate whether risk scores and SSs of the HNSCC patients in the training set were significantly related. A significant negative correlation was observed between the risk scores calculated by the 16-DNA methylation predictive prognosis model and SSs in the TCGA dataset ($P = 4.2e-37$; Fig 3e).

The potential impact of the 16 CpG sites of the DNA methylation signature on the 20 CSRGs associated with HNSCC survival was also investigated. A Pearson correlation analysis was conducted to investigate the relationship between the 16 CpG sites and 20 CSRGs

impacting HNSCC prognosis. The results revealed that all the DMCs selected were significantly correlated with several CSRGs ($P < 0.01$; Fig 3f). Among them, the methylation level of cg21230425 significantly correlated with the maximum number of CSRGs amounted to 16, whereas that of cg14170959 correlated with the minimum of the CSRGs amounted to 2. These results imply that the 16 DMCs probably regulate CSRG transcription either directly or mediately.

The 16-DMC predictive prognosis model is an independent predictor for the prognosis of HNSCC patients

Each HNSCC patient's risk score was calculated and then the patients were separated into high- and low-risk subgroups according to the median score to analyse the survival prognosis model. Following this, a KM survival analysis was performed, and found that HNSCC patients in the high-risk subgroup had a significantly worse probability of survival ($P = 3.4e-12$; Fig 4a), suggesting that the risk score model could be a reliable prognostic predictor. As shown in Fig 4b, compared to the low-risk subgroup, more deaths occurred in the high-risk subgroup. The heatmap visualised the methylation value of the 16 DMCs in the risk score signature. To assess the prediction ability of the predictive prognosis model, an ROC analysis was conducted. For patients with HNSCC from the training set, this model was quite effective at predicting survival, with AUC of 0.69, 0.73 and 0.75 for predicting 1-, 3- and 5-year survival rate, respectively (Fig 4c). In summary, using the TCGA cohort, the 16-DMC predictive prognosis model was confirmed to be an independent parameter for the prognosis of HNSCC patients.

16-DMC predictive prognosis model is validated in the OSCC GEO dataset

As described above, a 16-DNA methylation signature with an authentic effect in predicting the prognosis of HNSCC patients was constructed based on the TCGA database. Since OSCC is the main disease type of HNSCC, methylation and survival data from the OSCC dataset GSE75537 were downloaded from the GEO database (<https://www.ncbi.nlm.nih.gov/geo/>) to further verify the risk model. As expected, OSCC patients in the GEO dataset with higher risk scores had a worse prognosis ($P < 0.01$; Fig 5a). Based on the developed prognostic model, heatmap visualisation of different DMCs for patients and survival distribution in the GEO dataset also showed a similar pattern as in the TCGA dataset (Fig 5b), with an

Fig 3 Constructing a prognostic model. (a) LASSO regression coefficients. (b) Lambda value was selected to identify genes and develop a prognosis model. (c) A multivariate Cox analysis showed the correlation between methylation values. (d) A univariate Cox analysis showed the correlation between the methylation value of the 16 DMCs and TCGA HNSCC patients' survival. (e) A Pearson correlation analysis showed the relevance between SS and risk score in the training set. (f) Relevance between methylation value of the 16 DMCs selected to construct the prognosis signature and expression level of CSRGs impacting HNSCC survival.

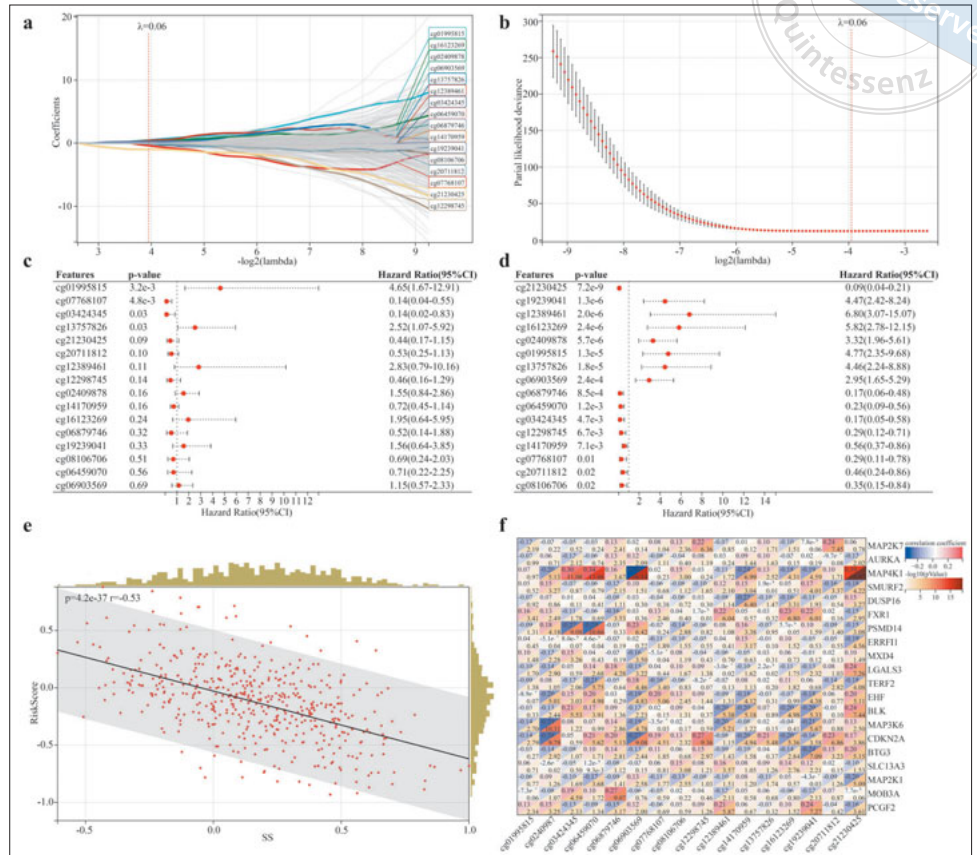
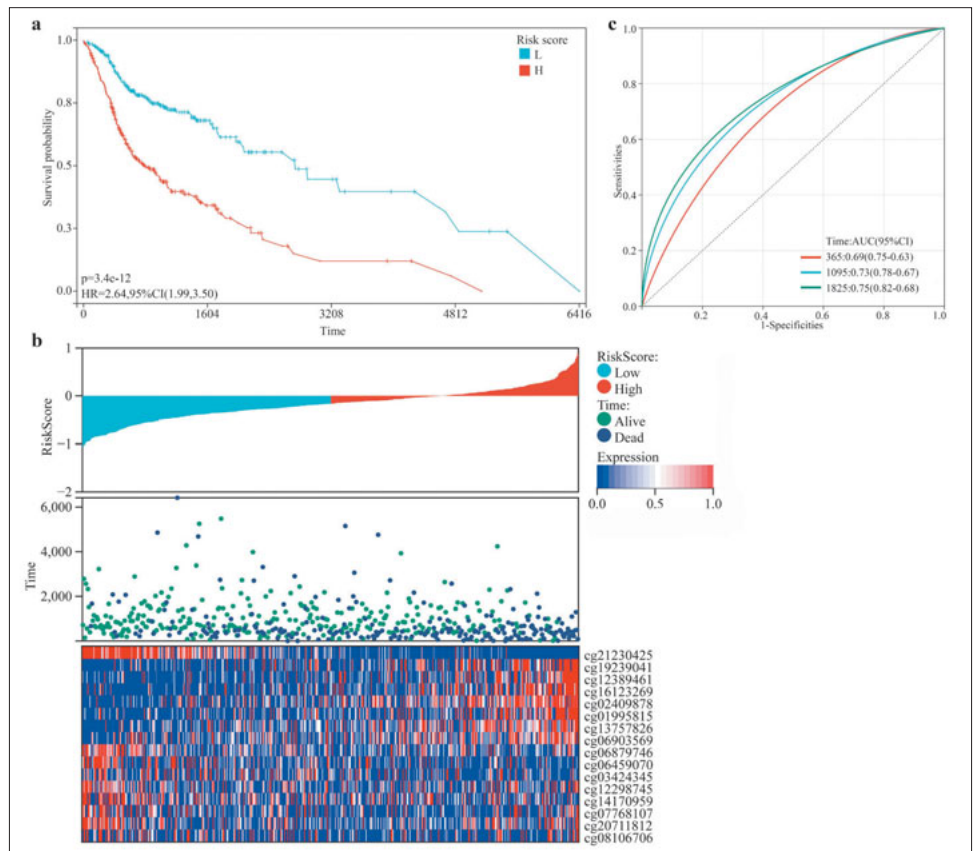


Fig 4 Development of cellular senescence-related DNA methylation prognosis model based on methylation level of 16 DMCs in the training set. (a) KM curves for high- and low-risk subgroups in the training set. (b) Risk survival status plot and heatmap of the methylation level of the 16 DMCs model in TCGA HNSCC patients with high- and low-risk scores. (c) AUCs for the prediction of 1-, 3- and 5-year overall survival of HNSCC.



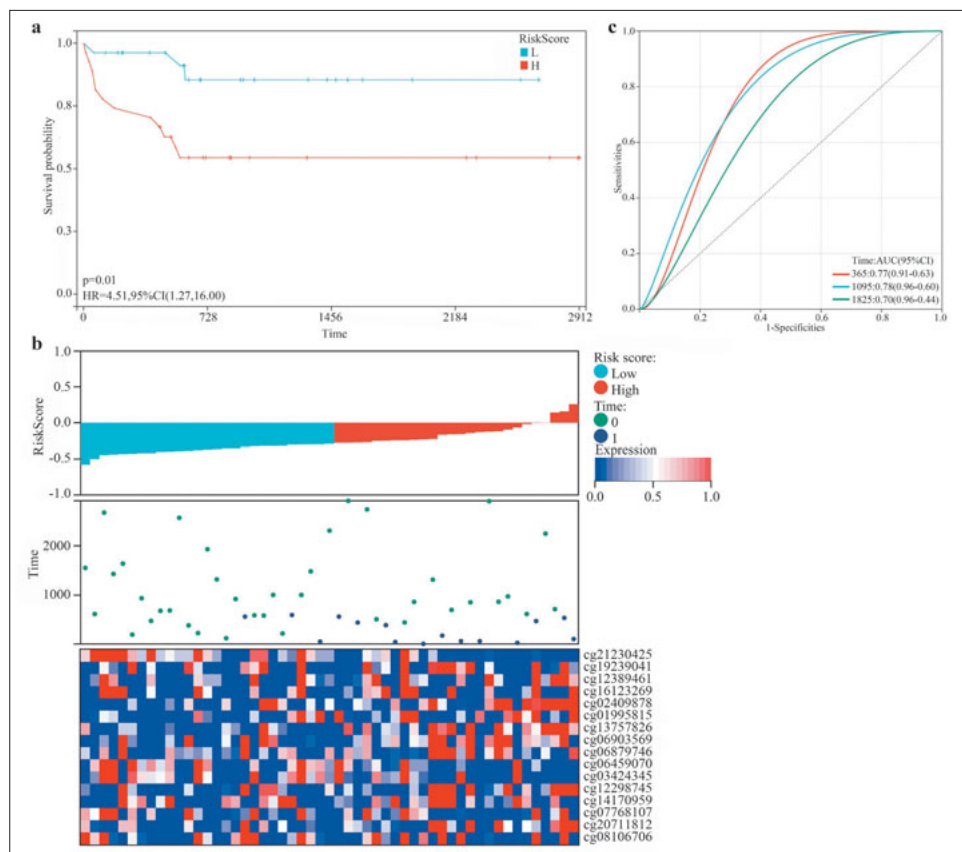


Fig 5 Validation of cellular senescence-related DNA methylation prognosis model based on methylation level of 16 DMCs in the validation set. **(a)** KM curves for high- and low-risk subgroups in the GEO cohort. **(b)** Risk survival status plot and heatmap of the methylation level of 16 DMCs model in GEO OSCC patients with high- and low-risk scores. **(c)** AUCs for the prediction of 1-, 3- and 5-year overall survival of OSCC.

AUC of 0.77 at 1 year, 0.78 at 3 years and 0.70 at 5 years, respectively (Fig 5c). Thus, the validation results indicate that the model is sufficiently stable to be applicable to a broader HNSCC population.

Establishment of a nomogram based on the model with predictive efficacy in HNSCC prognosis

To thoroughly predict HNSCC patients' survival based on both risk score and clinical factors, a nomogram was developed by age, sex, grade, clinical stage, clinical T stage, clinical M stage, clinical N stage and risk score (Fig 6a). When the total points were 53.06, the predicted survival probability was more than 0.90 at 1 year, more than 0.80 at 3 years and more than 0.75 at 5 years. Subsequently, it was proved that the observed survival probability and predicted survival probability were almost in congruity on the 3- and 5-year calibration curves (Fig 6b). The result proved that this nomogram is highly accurate in predicting the survival probability of HNSCC patients. ROC curves were then depicted (Fig 6c). The 1-, 3- and 5- year AUCs were 0.69, 0.75 and 0.77, respectively. This validated the excellent survival rate prediction ability of the nomogram.

Discovery of differential pathways related to immune function between the high- and low-risk subgroups of HNSCC

Subsequently, differential expression analysis using the limma package was conducted; thus, 4,673 DEGs were uncovered in the two subgroups ($P < 0.01$, $|\logFC| > 1.5$). GO and KEGG enrichment analyses were performed to crystallise the function and mechanisms of the preceding DEGs. The enrichment results were visualised in bubble plots and the findings of the GO analysis included three different function types: BP, CC and MF (Figs 7a to d).

In the BP sections, the previous DEGs exhibited enrichment in “response to stress”, “immune system process” and “immune response”. For CC, the most significantly enriched terms contained “cytosol”, “endo-membrane system” and “vesicle”. In MF terms, the DEGs were significantly enriched in “catalytic activity” and “enzyme binding” along with “identical protein binding”. Additionally, the bubble plot for the KEGG analysis revealed that these genes were enriched in the top 10 pathways, among which “cell adhesion molecules (CAMs) signalling pathway”, “Th17 cell differentiation signalling pathway”, “hematopoietic cell lineage

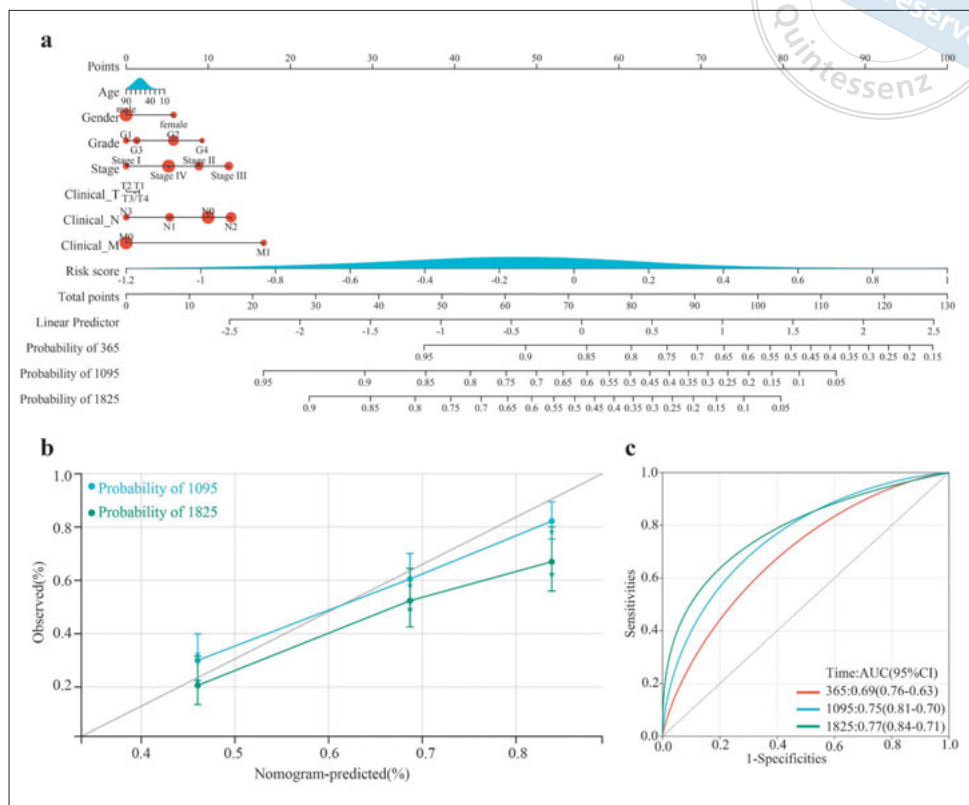


Fig 6 Development of a nomogram for survival prediction. **(a)** Nomogram with sufficient predictive efficacy. **(b)** 3- and 5-year calibration curves of the nomogram. **(c)** ROC curves of the nomogram.

signalling pathway” and “primary immunodeficiency signalling pathway” were closely related to immunity function.

Considering the expression level of DEGs may influence the enrichment results, GSEA analysis was performed to further clarify the role these DEGs played in the HNSCC patients. The heatmap contained the top 20 KEGG signalling pathways enriched by GSEA (Fig 7e). According to the analysis, signalling pathways such as “Glycosphingolipid biosynthesis-ganglio series”, “Glycosaminoglycan biosynthesis-chondroitin sulphate”, “Glycosaminoglycan biosynthesis-keratan sulphate” and “Glycosaminoglycan biosynthesis-heparan sulphate” were significantly active in HNSCC patients in the high-risk subgroup, suggesting the genesis and development of HNSCC were accompanied by an abnormal change in glycan biosynthesis and metabolism. Meanwhile, pathways related to the immune system, such as the “B cell receptor signalling pathway” and “intestinal immune network for IgA production and T cell receptor signalling pathway” were significantly suppressed. All the pathway enrichment results indicated the possibility that abnormal immune system function plays an important role in the prognosis of HNSCC patients.

Immune infiltration CSRG transcription/DNA methylation is correlated with HNSCC

Given the crosstalk between cellular senescence and tumour immune infiltration, the authors then investigated whether the cellular senescence-related 16-DMCs model played a role in immune cell infiltration of HNSCC patients. ESTIMATE and TIMER algorithms were used to clarify the tumour purity and immune infiltration level in the HNSCC tumour microenvironment. The immune infiltration level between the high- and low-risk subgroups was compared and violin plots were drawn to elucidate whether the discrepancies found in ESTIMATE and TIMER immune scores existed between the two groups (Figs 8a and 8b). As shown in Fig 8a, the immune score and ESTIMATE score were significantly lower in the high-risk group compared to the low-risk group ($P < 0.01$). Meanwhile, there was no significant difference in the stromal score found in the two groups ($P = 0.77$). These findings revealed that immune cell infiltration may decrease in the tumour microenvironment in HNSCC patients. These results were in accordance with the TIMER analysis. As shown in Fig 8b, five types of immune cells except macrophages exhibited significantly lower infiltration in the high-risk subgroup ($P < 0.01$). These indications supported the possibility that

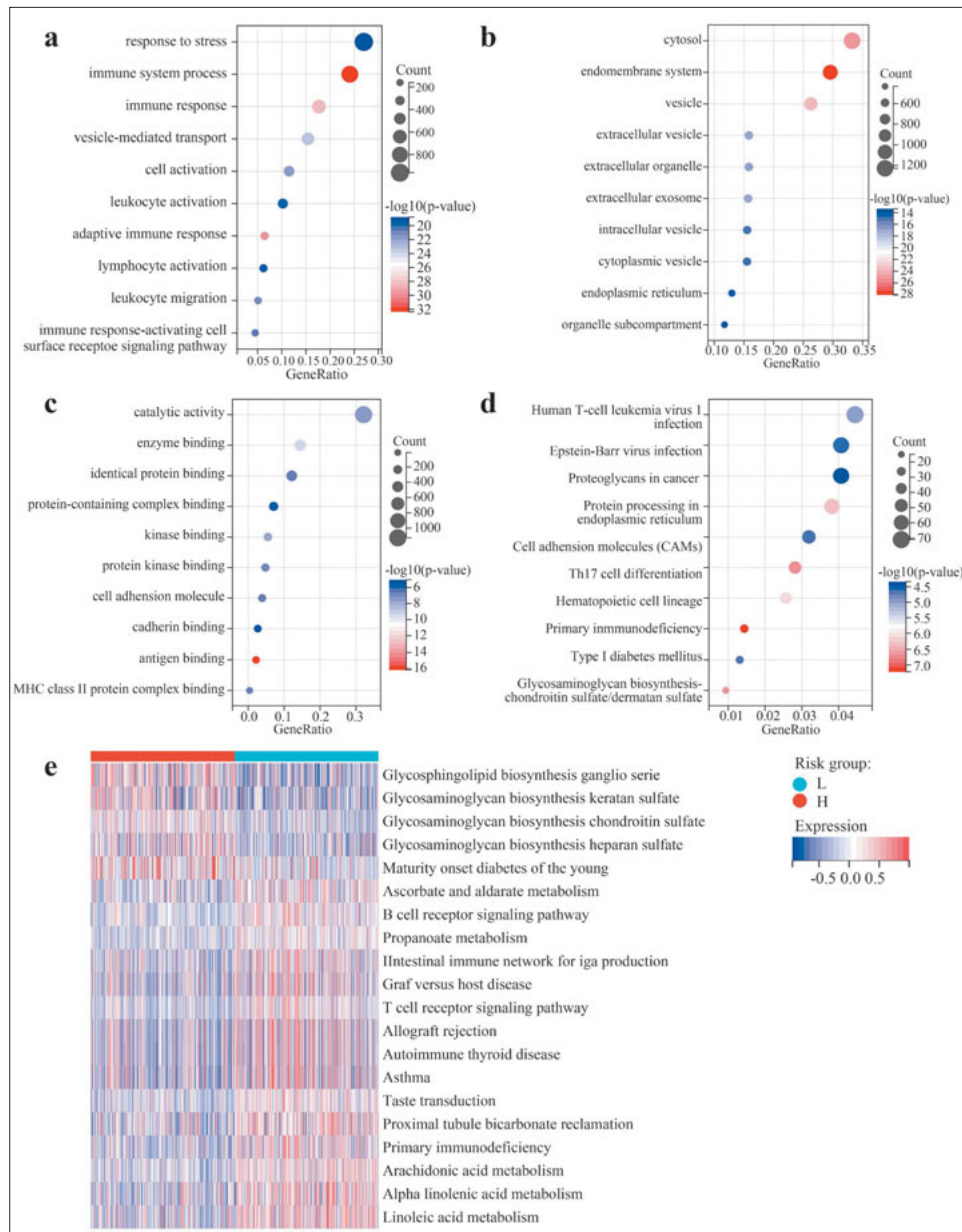


Fig 7 GO and KEGG analysis of the DEGs. **(a)** Results of GO-BP. **(b)** Results of GO-CC. **(c)** Results of GO-MF. **(d)** Results of KEGG. **(e)** Results of GSVA.

immune infiltration influences the prognosis of HNSCC patients.

To further confirm this, a Pearson correlation analysis was performed to evaluate the relationship between risk score and immune infiltration level (Figs 8c and 8d). With the exception of the stromal score calculated using the ESTIMATE algorithm and the macrophage infiltration score calculated using the TIMER algorithm, the results demonstrated a significantly negative relationship between risk score and all the immune scores ($P < 0.01$). Thus, the present research proved that the 16-DMCs prognosis signature played an indispensable role in decreasing the infiltration level of immune cells in the tumour microenvironment in HNSCC,

which shed a light on immune therapy for HNSCC.

The variation in immune checkpoint expression between the two subgroups was also investigated in light of the significance of checkpoint-based immunotherapies. A list of immune checkpoints was retrieved from previous studies to compare their expression levels in the two groups (Fig 8e)³⁰. Of the 11 immune checkpoints, 9 checkpoints (BTLA, HAVCR2, LAG3, LILRB2, PDCD1, SIGLEC7, SIRPA, TIGHT and VSIR) were confirmed to express significantly lower levels in the high-risk subgroup, which may provide a new immunotherapy strategy that involves choosing effective targeted medicine.

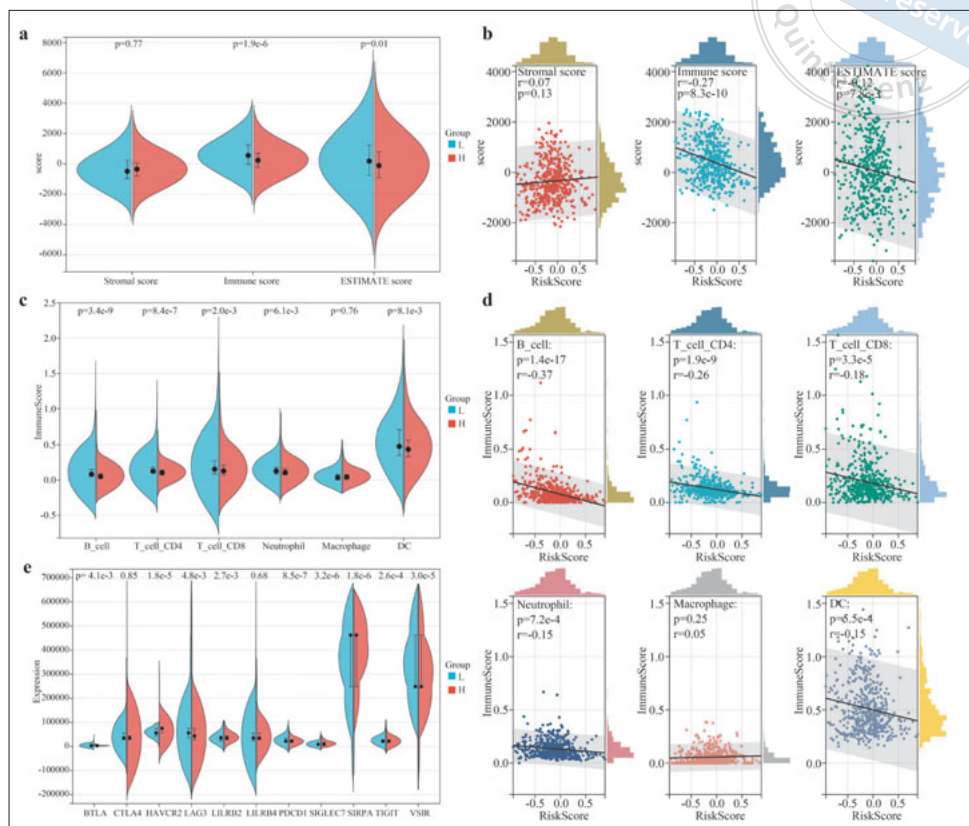


Fig 8 Immune infiltration and immune checkpoint analysis. **(a)** Immune infiltration analysis result by ESTIMATE. **(b)** Immune infiltration analysis result by TIMER. **(c)** A Pearson correlation analysis showed the relevance between risk score and ESTIMATE immune infiltration level in TCGA HNSCC patients. **(d)** A Pearson correlation analysis showed the relevance between risk score and TIMER in HNSCC patients. **(e)** Expression level of immune checkpoints in low- and high-risk subgroups.

Discussion

Since the discovery of cellular senescence¹⁹, the phenomenon has been widely investigated and has been proven to be involved in oncogene activation and tumour suppression³²⁻³³. The most recent research has demonstrated that senescent cancer cells are heterogeneous due to various variables, manifesting both pro- and anti-tumour effects, suggesting that cellular senescence may lead to novel treatment strategies³⁴⁻³⁵. DNA methylation, a well-studied form of epigenetic modification involving the attachment of a methyl group onto the C5 position of the cytosine to synthesize 5-methylcytosine, influences the transcription of corresponding genes (like lysine methyltransferases [KMTs]) in various tumour types, which alter cellular senescence in tumour tissue and may serve as biomarkers in HNSCC prognosis³⁶⁻³⁸. In the present study, the 16-DNA methylation HNSCC predictive prognosis model was first developed based on the SS and was further validated. Further analysis showed that immune system function change and tumour immune microenvironment alteration occur in HNSCC, which is related to HNSCC prognosis and cellular senescence. The results indicate that the 16 DMCs related to cellular senescence may regulate the local lesion by affecting immune function. The present

results could be profound in the HNSCC therapy area.

First, the methylome and transcriptome data were collected from the TCGA database for HNSCC patients. Based on the expression of 20 CSRGs and HNSCC survival, a unique SS was first derived for each HNSCC patient. The method used to infer sample scores followed that employed in previous articles on the relationship between cancer and another biological process^{39,40}. Among the CSRGs involved, several genes have been confirmed that participate in cellular senescence and tumorigenesis. For instance, FXR1 is considered a promoter for enhancing cellular senescence⁴¹, and its regulation activity is conducive to tumour growth in different cancer tissues including HNSCC⁴²⁻⁴⁴; CDKN2A is commonly altered in human tumours, which influences tumour-immune microenvironments⁴⁵ and plays an important role in in vivo aging via the p19(Arf)-p53 pathway⁴⁶. The KM survival analysis revealed that HNSCC patients with higher SS had a poorer prognosis ($P < 0.01$), indicating a strong correlation between SS and HNSCC survival.

To create a DNA methylation predictive prognosis model for the diagnosis and prediction of HNSCC, 3,261 DMCs were next identified between the high- and low-SS groups in the TCGA. Ultimately, 16 DMCs were included via the LASSO Cox regression method. Based

on this model, the risk score for each HNSCC patient was calculated. The Pearson correlation analysis showed a significant negative relationship between SS and risk score. ROC curves revealed that the DNA methylation model was able to predict HNSCC prognosis reliably. Its prediction accuracy and stability were validated via a further investigation in the dataset GSE75537¹⁸. Furthermore, the DMCs used in model construction were proven to be closely related to the expression of the aforementioned CSRGs, thus indicating the possible interaction with CSRGs in cancer tissue. To include the effect of clinical variables and increase the accuracy in prognosis prediction, a nomogram was constructed based on the 16-DNA methylation risk model. ROC curves and calibration curves both confirmed the accurate evaluation ability in HNSCC patients.

To further clarify the concrete mechanism in HNSCC, GO²³ and KEGG^{24,25} analyses were conducted to enrich signaling pathways using DEGs in high- and low-risk subgroups. The results proved that immune system function change may be involved in tumorigenesis and disease development, like “immune system process”, and “immune response” in GO terms. Through GO enrichment, several terms were identified, some of which have been reported in the previous literature to regulate cellular senescence in tumours. For instance, extracellular vesicle (EV) has been discovered that expresses higher in tumour tissue than adjacent normal tissue⁴⁷ and can capture cell-free DNA⁴⁸, which is essential in the tumour microenvironment, thus EV may be a biomarker in tumour senescence detection⁴⁹. KEGG analysis also suggested that there is a difference in immune function between the two risk groups identified by the risk model, as immunity-related KEGG signalling pathways like “Proteoglycans in cancer”, “Th17 cell differentiation” and “Primary immunodeficiency” were significantly enriched. To assess the expression level of the DEGs additionally, GSEA analysis²² was conducted and the heatmap revealed the top 20 KEGG signalling pathways. The result of the analysis was consistent with the GO and KEGG analyses, suggesting change in immune function plays an important role in the prognosis of HNSCC. Several immune system-related KEGG signalling pathways, such as “Primary immunodeficiency”, “T cell receptor signalling pathway”, “Intestinal immune network for IgA production” and “B cell receptor signalling pathway”, were found to be significantly suppressed in the high-risk group. Among them, “Primary immunodeficiency” was evaluated with the top absolute value of fold change, which was identified in an autophagy-related HNSCC prognosis model by Ren et al⁵⁰. Interestingly, KEGG analysis strongly

inhibits the upregulation of glycan biosynthesis and metabolism, indicating that active glycan metabolism levels may be a positive factor in the prognosis of HNSCC. This opinion was corroborated by previous studies⁵¹⁻⁵⁴.

Research in the present study indicated that immune system function influences the prognosis of HNSCC patients, suggesting the potential participation of the tumour microenvironment. The tumour microenvironment plays a pivotal role in tumour progression and metastasis. Its unique composition and subtype in individuals result in different therapeutic outcomes⁵⁵. Thus, the evaluation of immune cell infiltration in the HNSCC tumour microenvironment was valuable. The IOBR package by R²⁹ was used to evaluate the tumour immune purity of each sample via ESTIMATE²⁷ and TIMER²⁸. According to the ESTIMATE analysis, the HNSCC patients in the high-risk group presented with significantly lower immune scores and ESTIMATE scores, indicating that higher immune scores and ESTIMATE scores are distinct positive predictors of HNSCC prognosis, which is not consistent with other cancer types like lung adenocarcinoma⁵⁶, gastric cancer⁵⁷ and clear cell renal cell carcinoma⁵⁸. Next, the infiltration level of six immune cells was evaluated via the TIMER algorithm. Significantly decreasing infiltration levels were noted in the high-risk group of each immune cell type except macrophage. In summary, the integrated evaluation suggested immunotherapy may benefit low-risk HNSCC patients, but may not be suitable for high-risk patients.

The present study has some limitations. First, the analysis was retrospective and dependent on publicly accessible databases, and it was challenging to account for the regional difference, which limited the application of the risk model in the clinic. Second, it is favourable to evaluate immune and stromal components systematically in the centre of the tumour and at the invasive margin given that the microenvironment may vary in each individual and tumour site. The various tumour regions could not be considered because the transcriptome profiles employed in the present investigation were all generated from a core sample of tumour tissue. Thus, there is a lack of consideration of the heterogeneity of different tumour sites within an individual, which may weaken the accuracy of the prognostic model to some extent. Therefore, further validation of cellular or animal models in the future will help to increase the credibility of the study. Meanwhile, a carefully planned, prospective, multicentre clinical trial that is conducted internationally is anticipated. Third, the authors used a GEO dataset for validation. Although having more data-

sets for validation would increase the persuasiveness of the findings, eligible validation sets are difficult to obtain. In the future, further tests on HNSCC clinical samples are needed to assess methylation site changes in HNSCC more comprehensively.

Conclusion

In conclusion, the present authors first established a 16-DNA methylation predictive HNSCC prognosis model associated with cellular senescence that may be utilised to select treatment for HNSCC patients. The selected 16 CpG sites that were identified as participating in cellular senescence were potential biofunction targets, revealing a novel research direction in the strategy for tumour therapy.

Acknowledgements

The analysis was supported by Sangerbox (Shanghai, China). The authors express their gratitude to the public databases TCGA and GEO.

Conflicts of interest

The authors declare no conflicts of interest related to this study.

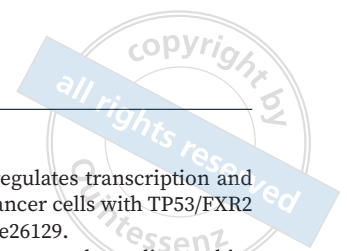
Author contribution

Dr Ming Han YE contributed to the investigation, methodology, data interpretation, statistical analysis and manuscript draft; Dr Xin Yi HUANG contributed to the investigation and methodology; Drs Chun Jie LI, Qian Ju WU and Fei LIU contributed to the conceptualisation, project administration and supervision. All the authors approved the final version.

(Received May 11, 2023; accepted Aug 09, 2023)

References

- Johnson DE, Burtneß B, Leemans CR, Lui VWY, Bauman JE, Grandis JR. Head and neck squamous cell carcinoma. *Nat Rev Dis Primers* 2020;6:92.
- Sung H, Ferlay J, Siegel RL, et al. Global Cancer Statistics 2020: GLOBOCAN Estimates of Incidence and Mortality Worldwide for 36 Cancers in 185 Countries. *CA Cancer J Clin* 2021;71:209–249.
- Cancer Genome Atlas Network. Comprehensive genomic characterization of head and neck squamous cell carcinomas. *Nature* 2015;517:576–582.
- Chung CH, Parker JS, Karaca G, et al. Molecular classification of head and neck squamous cell carcinomas using patterns of gene expression. *Cancer Cell* 2004;5:489–500.
- Leemans CR, Snijders PJF, Brakenhoff RH. The molecular landscape of head and neck cancer. *Nat Rev Cancer* 2018;18:269–282.
- Bhat GR, Hyole RG, Li J. Head and neck cancer: Current challenges and future perspectives. *Adv Cancer Res* 2021;152:67–102.
- Birch J, Gil J. Senescence and the SASP: Many therapeutic avenues. *Genes Dev* 2020;34:1565–1576.
- Calcinotto A, Kohli J, Zagato E, Pellegrini L, Demaria M, Alimonti A. Cellular senescence: Aging, cancer, and injury. *Physiol Rev* 2019;99:1047–1078.
- Coppé JP, Patil CK, Rodier F, et al. Senescence-associated secretory phenotypes reveal cell-nonautonomous functions of oncogenic RAS and the p53 tumor suppressor. *PLoS Biol* 2008;6:2853–2868.
- Demirci D, Dayanc B, Mazi FA, Senturk S. The Jekyll and Hyde of cellular senescence in cancer. *Cells* 2021;10:208.
- Schoetz U, Klein D, Hess J, et al. Early senescence and production of senescence-associated cytokines are major determinants of radioresistance in head-and-neck squamous cell carcinoma. *Cell Death Dis* 2021;12:1162.
- Lee M, Nam HY, Kang HB, et al. Epigenetic regulation of p62/SQSTM1 overcomes the radioresistance of head and neck cancer cells via autophagy-dependent senescence induction. *Cell Death Dis* 2021;12:250.
- Ahmadinejad F, Bos T, Hu B, et al. Senolytic-mediated elimination of head and neck tumor cells induced into senescence by Cisplatin. *Mol Pharmacol* 2022;101:168–180.
- Klutstein M, Nejman D, Greenfield R, Cedar H. DNA methylation in cancer and aging. *Cancer Res* 2016;76:3446–3450.
- Loughran O, Malliri A, Owens D, et al. Association of CDKN2A/p16INK4A with human head and neck keratinocyte replicative senescence: relationship of dysfunction to immortality and neoplasia. *Oncogene* 1996;13:561–568.
- Howard FM, Kochanny S, Koshy M, Spiotto M, Pearson AT. Machine learning-guided adjuvant treatment of head and neck cancer. *JAMA Netw Open* 2020;3:e2025881.
- Wang J, Zhou CC, Sun HC, et al. Identification of several senescence-associated genes signature in head and neck squamous cell carcinoma. *J Clin Lab Anal* 2022;36:e24555.
- Krishnan NM, Dhas K, Nair J, et al. A minimal DNA methylation signature in oral tongue squamous cell carcinoma links altered methylation with tumor attributes. *Mol Cancer Res* 2016;14:805–819.
- Avelar RA, Ortega JG, Tacutu R, et al. A multidimensional systems biology analysis of cellular senescence in aging and disease. *Genome Biol* 2020;21:91.
- Liu Z, Zhao Q, Zuo ZX, et al. Systematic analysis of the aberrances and functional implications of ferroptosis in cancer. *iScience* 2020;23:101302.
- Xu Y, Hong M, Kong D, Deng J, Zhong Z, Liang J. Ferroptosis-associated DNA methylation signature predicts overall survival in patients with head and neck squamous cell carcinoma. *BMC Genomics* 2022;23:63.
- Hänzelmann S, Castelo R, Guinney J. GSEA: Gene set variation analysis for microarray and RNA-seq data. *BMC Bioinformatics* 2013;14:7.
- Gene Ontology Consortium, Blake JA, Dolan M, et al. Gene Ontology annotations and resources. *Nucleic Acids Res* 2013;41:D530–D535.



24. Kanehisa M, Furumichi M, Tanabe M, Sato Y, Morishima K. KEGG: New perspectives on genomes, pathways, diseases and drugs. *Nucleic Acids Res* 2017;45:D353–D361.
25. Kanehisa M, Goto S. KEGG: Kyoto encyclopedia of genes and genomes. *Nucleic Acids Res* 2000;28:27–30.
26. Liberzon A, Subramanian A, Pinchback R, Thorvaldsdóttir H, Tamayo P, Mesirov JP. Molecular signatures database (MSigDB) 3.0. *Bioinformatics* 2011;27:1739–1740.
27. Yoshihara K, Shahmoradgoli M, Martínez E, et al. Inferring tumour purity and stromal and immune cell admixture from expression data. *Nat Commun* 2013;4:2612.
28. Li B, Severson E, Pignon JC, et al. Comprehensive analyses of tumor immunity: implications for cancer immunotherapy. *Genome Biol* 2016;17:174.
29. Zeng D, Ye Z, Shen R, et al. IOBR: Multi-omics immuno-oncology biological research to decode tumor microenvironment and signatures. *Front Immunol* 2021;12:687975.
30. Shibru B, Fey K, Fricke S, et al. Detection of immune checkpoint receptors - A current challenge in clinical flow cytometry. *Front Immunol* 2021;12:694055.
31. Schabath MB, Cote ML. Cancer progress and priorities: Lung cancer[J]. *Cancer Epidemiol Biomarkers Prev* 2019;28:1563–1579.
32. Almangush A, Mäkitie AA, Triantafyllou A, et al. Staging and grading of oral squamous cell carcinoma: An update. *Oral Oncol* 2020;107:104799.
33. Hayflick L, Moorhead PS. The serial cultivation of human diploid cell strains. *Exp Cell Res* 1961;25:585–621.
34. Gorgoulis V, Adams PD, Alimonti A, et al. Cellular senescence: Defining a path forward. *Cell* 2019;179:813–827.
35. Di Micco R, Krizhanovsky V, Baker D, d'Adda di Fagagna F. Cellular senescence in ageing: From mechanisms to therapeutic opportunities. *Nat Rev Mol Cell Biol* 2021;22:75–95.
36. Prasanna PG, Citrin DE, Hildesheim J, et al. Therapy-induced senescence: Opportunities to improve anticancer therapy. *J Natl Cancer Inst* 2021;113:1285–1298.
37. Moore LD, Le T, Fan G. DNA methylation and its basic function. *Neuropsychopharmacology* 2013;38:23–38.
38. Ramu D, Shan TW, Hirpara JL, Pervaiz S. Cellular senescence: Silent operator and therapeutic target in cancer. *IUBMB Life* 2021;73:530–542.
39. Rao VK, Pal A, Taneja R. A drive in SUVs: From development to disease. *Epigenetics* 2017;12:177–186.
40. Brown R, Curry E, Magnani L, Wilhelm-Benartzi CS, Borley J. Poised epigenetic states and acquired drug resistance in cancer. *Nat Rev Cancer* 2014;14:747–753.
41. Majumder M, House R, Palanisamy N, et al. RNA-binding protein FXR1 regulates p21 and TERC RNA to bypass p53-mediated cellular senescence in OSCC. *PLoS Genet* 2016;12:e1006306.
42. Qie S, Majumder M, Mackiewicz K, et al. Fbxo4-mediated degradation of Fxr1 suppresses tumorigenesis in head and neck squamous cell carcinoma. *Nat Commun* 2017;8:1534.
43. Fan Y, Yue J, Xiao M, et al. FXR1 regulates transcription and is required for growth of human cancer cells with TP53/FXR2 homozygous deletion. *Elife* 2017;6:e26129.
44. Cao S, Zheng J, Liu X, et al. FXR1 promotes the malignant biological behavior of glioma cells via stabilizing MIR17HG. *J Exp Clin Cancer Res* 2019;38:37.
45. Adib E, Nassar AH, Akl EW, et al. CDKN2A alterations and response to immunotherapy in solid tumors. *Clin Cancer Res* 2021;27:4025–4035.
46. Baker DJ, Jin F, van Deursen JM. The yin and yang of the Cdkn2a locus in senescence and aging. *Cell Cycle* 2008;7:2795–2802.
47. Lázaro-Ibáñez E, Sanz-García A, Visakorpi T, et al. Different gDNA content in the subpopulations of prostate cancer extracellular vesicles: Apoptotic bodies, microvesicles, and exosomes. *Prostate* 2014;74:1379–1390.
48. Kustanovich A, Schwartz R, Peretz T, Grinshpun A. Life and death of circulating cell-free DNA. *Cancer Biol Ther* 2019;20:1057–1067.
49. Ou HL, Hoffmann R, González-López C, Doherty GJ, Korkola JE, Muñoz-Espín D. Cellular senescence in cancer: From mechanisms to detection. *Mol Oncol* 2021;15:2634–2671.
50. Ren Z, Zhang L, Ding W, et al. Development and validation of a novel survival model for head and neck squamous cell carcinoma based on autophagy-related genes. *Genomics* 2021;113(1 Pt 2):1166–1175.
51. Zhao X, Brusadelli MG, Sauter S, et al. Lipidomic profiling links the Fanconi anemia pathway to glycosphingolipid metabolism in head and neck cancer cells. *Clin Cancer Res* 2018;24:2700–2709.
52. Reiss M, Maniglia CA, Sartorelli AC. Modulation of cell shedding and glycosaminoglycan synthesis of human malignant keratinocytes by all-trans-retinoic acid and hydrocortisone in vitro. *J Invest Dermatol* 1986;86:683–688.
53. Skandalis SS, Theocharis AD, Papageorgakopoulou N, Vynios DH, Theocharis DA. The increased accumulation of structurally modified versican and decorin is related with the progression of laryngeal cancer. *Biochimie* 2006;88:1135–1143.
54. Vynios DH, Theocharis DA, Papageorgakopoulou N, et al. Biochemical changes of extracellular proteoglycans in squamous cell laryngeal carcinoma. *Connect Tissue Res* 2008;49:239–243.
55. Wu T, Dai Y. Tumor microenvironment and therapeutic response. *Cancer Lett* 2017;387:61–68.
56. Wu J, Li L, Zhang H, et al. A risk model developed based on tumor microenvironment predicts overall survival and associates with tumor immunity of patients with lung adenocarcinoma. *Oncogene* 2021;40:4413–4424.
57. Wang H, Wu X, Chen Y. Stromal-immune score-based gene signature: A prognosis stratification tool in gastric cancer. *Front Oncol* 2019;9:1212.
58. Xu WH, Xu Y, Wang J, et al. Prognostic value and immune infiltration of novel signatures in clear cell renal cell carcinoma microenvironment. *Aging (Albany NY)* 2019;11:6999–7020.

Evaluation of Sealer Remnants Using a Bioceramic Sealer Single-cone Technique after Post Space Preparation and its Influence on the Adhesion of Fibre Posts *in vitro*

Di QIAO¹, Meng Meng ZHU¹, Jie PAN¹

Objective: To compare calcium silicate-based endodontic sealer and epoxy resin-based sealer remnants on root canal walls after post space preparation and their influence on the bond strength of fibre posts fixed with a dual-cured resin cement.

Methods: Thirty-six extracted single-root mandibular premolars were instrumented and divided randomly into two equal groups with different endodontic sealers. iRoot SP (Innovative BioCeramix, Vancouver, Canada) was employed in the experimental group and AH Plus (Dentsply Sirona, Charlotte, NC, USA) was used in the control group. Sealer remnants were observed under an endodontic microscope after root canal therapy and post space preparation. Fibre posts were fixed with dual-cured resin cement. Specimens were taken at each third of the post space. The push-out bond strength was measured using a universal testing machine and fracture modes were assessed. Statistical analysis was performed using an independent samples *t* test and one-way analysis of variance.

Results: There was no statistically significant difference in bond strength of fibre posts between the control and experimental group ($P > 0.05$); however, sealer remnants were observed in 38.9% of the samples treated with iRoot SP and none of the samples treated with AH Plus. The major fracture mode in samples treated with iRoot SP was adhesive failure between the resin cement and the post, and no adhesive failure between the resin cement and dentine occurred at the site of the sealer remnant. The presence of iRoot SP remnants on the root canal walls after post space preparation did not interfere with bonding.

Conclusion: iRoot SP is a viable option for root canal obturation before fibre post cementation.

Key words: AH Plus, bond strength, calcium silicate-based sealer, endodontic sealer, fibre post, iRoot SP

Chin J Dent Res 2023;26(4):249–256; doi: 10.3290/j.cjdr.b4784043

Fibre posts are recommended for ensuring retention of teeth that have been compromised by extensive coronal destruction and treated endodontically^{1,2}. Resin cement

is commonly used to fix fibre posts in place; however, one of the main concerns with this technique is the uncertain nature of the bond strength between the fibre post and dentine, which is closely related to the high sensitivity of the adhesive technique³.

Endodontic sealer is commonly used during root canal obturation; thus, careful consideration of the endodontic sealer used during the obturation process but before fibre post cementation is required, as adhesion of the resin cement to the root dentine may be affected by the endodontic sealer, which may impact retention of the fibre post after treatment^{4,5}. It is commonly accepted that eugenol-based sealers should be avoided because the eugenol may inhibit polymerisation of the resin-based cement or modify the surface of the polymerised resin⁶, decreasing the bond strength of fibre posts to the root dentine⁶⁻¹⁰. In addition, sealers

1 Department of General Dentistry, Peking University School and Hospital of Stomatology & National Centre for Stomatology & National Clinical Research Centre for Oral Diseases & National Engineering Research Centre of Oral Biomaterials and Digital Medical Devices, Beijing, P.R. China.

Corresponding author: Dr Jie PAN, Department of General Dentistry, Peking University School and Hospital of Stomatology & National Centre for Stomatology & National Clinical Research Centre for Oral Diseases & National Engineering Research Centre of Oral Biomaterials and Digital Medical Devices, #22 Zhongguancun South Avenue, Haidian District, Beijing 100081, P.R. China. Tel: 86-10-8219586; Fax: 86-10-82195586. Email: panjie72@sina.com

This study was supported by a grant from the Programme for New Clinical Techniques and Therapies of Peking University School and Hospital of Stomatology (grant no. PKUSSNCT-17B04).

containing calcium hydroxide are difficult to remove from dentinal walls, and can also reduce the bond strength^{11,12}.

AH Plus (Dentsply Sirona, Charlotte, NC, USA) is an epoxy resin-based sealer that is considered the gold standard due to its excellent adhesive properties, sealing ability and non-interference with the bond strength of fibre posts fixed using adhesive resin cements^{13,14}. For this reason, the performance of new endodontic sealers is often compared against that of AH Plus. In recent years, iRoot SP (Innovative BioCeramix, Vancouver, Canada), a calcium silicate-containing, injectable, premixed sealer with good physicochemical and biological properties, has become an increasingly popular alternative sealant for root canal obturation¹⁵⁻¹⁷.

During the setting process, iRoot SP can form tag-like structures consisting of either sealer itself, or crystals formed by the reaction of calcium hydroxide present in iRoot SP with phosphate ions present in the dentine¹⁸⁻²⁰, producing a high bonding capacity between the dentine and the filling material, which consequently means removal is more difficult^{21,22}. It has been shown that iRoot SP can penetrate dentine tubules to a depth of more than 1 mm^{6,23}, and any sealer remnants in the dentine tubules might affect the bond strength since bonding is mainly based on micromechanical retention through the diffusion of monomers into the dentinal tubule²⁴. Besides the sealer in the dentine tubules, large amounts of sealer may still remain on the root canal walls even after fibre post preparation, because the material becomes very hard when set and is difficult to remove²⁵. Thus, the influence of sealer remnants on the adhesion of fibre posts must be evaluated.

Few studies have examined the influence of iRoot SP sealer on the adhesion of fibre posts^{4,9,10,26}; however, the results were conflicting. Some studies found that fibre posts displayed lower bond strength when iRoot SP was used compared with AH Plus^{4,9,10}, whereas others found that both sealers showed equal bond strength^{26,27}. These conflicting results may be due to the different morphology of the root canals, differences in treatment and the use of different cement resins. Therefore, whether the bond strength of fibre posts can reach the same level of bond strength after using iRoot SP or AH Plus as endodontic sealer remains inconclusive. There have also not been any reports on whether large amounts of sealer remnants on the root canal walls after post space preparation affects the adhesion of fibre posts.

The purpose of this *in vitro* study was to assess the effect of the calcium silicate-based endodontic sealer

iRoot SP on the push-out bond strength of fibre posts cemented with a dual-cured resin cement and observe the relationship between the sealer remnants and the debonding of fibre posts. The null hypothesis was that the type of endodontic sealer would have no influence on the adhesion of fibre posts, even if there might be large amounts of sealer remnants on the root canal wall.

Materials and methods

Experimental design

This study was approved by the Biomedical Ethics Committee of Peking University School of Stomatology under the protocol PKUSSIRB-201734051. The sample size was calculated based on the following formulae: $n = f(\alpha, \beta/2) \times 2 \times \sigma^2 / d^2$, where σ is the standard deviation, and $f(\alpha, \beta) = [\Phi^{-1}(\alpha) + \Phi^{-1}(\beta)]^2$, where Φ^{-1} is the cumulative distribution function of a standardised normal deviate. The power was set at 80% and the level of statistical significance was set at 0.05. The minimum sample size was determined to be 18 samples in each group. Each procedure in the study was performed by a trained operator.

A total of 36 human permanent mandibular premolars extracted for orthodontic reasons were collected and immersed in 0.1% thymol solution. All the selected teeth had a straight root with a single canal with a fully formed apical foramen and were free of caries lesions and cracks (Fig 1a). The teeth were decoronated below the cemento-enamel junction with a high-speed bur (TR-13; MANI, Utsunomiya, Japan) under water to obtain a standard root length of 14 mm (Fig 1b). The roots were observed under an endodontic microscope (Carl Zeiss, Gottingen, Germany) to make sure there were no cracks. The initial apical width was no more than the diameter of a size 20 K-file (MANI) in order to reduce the variation in size between the root canals. The diameters (buccal-lingual and mesial-distal) of the root canals at orifice level were measured with digital calipers (Mitutoyo, Kawasaki, Kanagawa, Japan) and the length-width ratio was calculated for each specimen.

The specimens were divided randomly into two groups by way of a coin toss according to different endodontic sealers and corresponding obturation techniques. Group 1 ($n = 18$, experimental group) used iRoot SP sealer with the single-cone technique (Fig 1c), and Group 2 ($n = 18$, control group) used AH Plus sealer with the warm vertical condensation technique (Fig 1d).

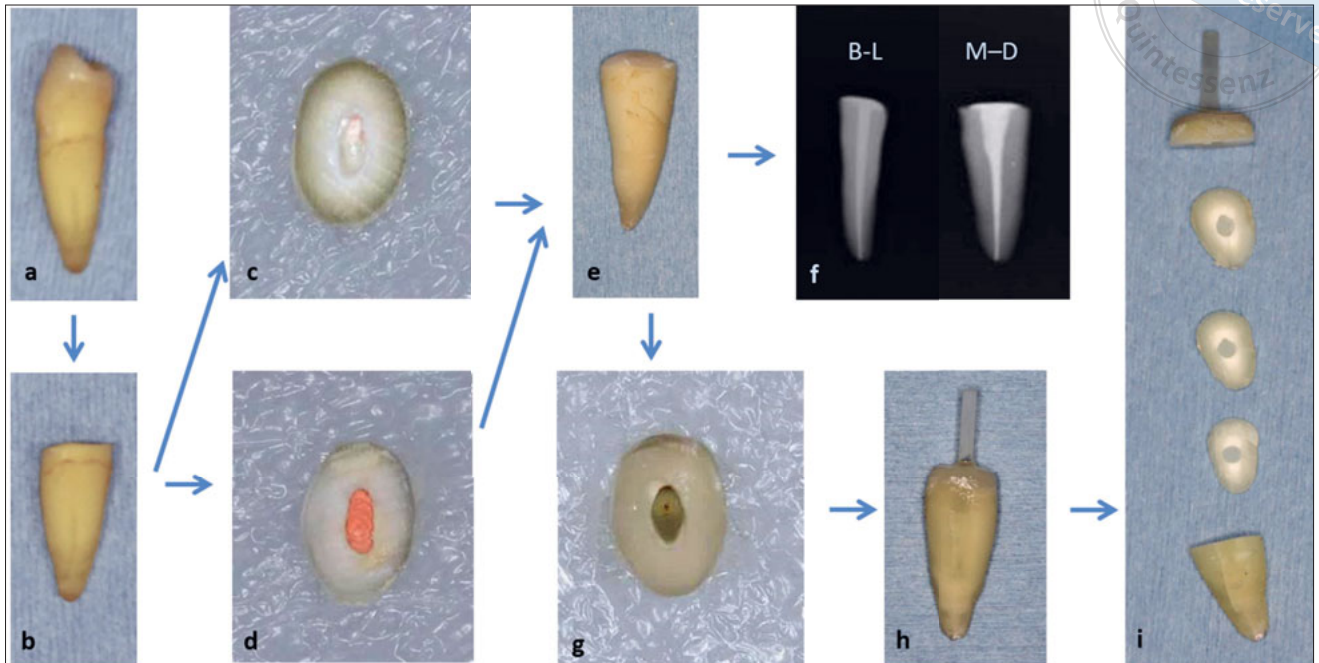


Fig 1 Operation procedure. (a) Mandibular premolar; (b) decoronated; (c) root canal obturation with iRoot SP using the single-cone technique; (d) root canal obturation with AH Plus using the warm vertical condensation technique; (e) coronal access cavity sealed with resin; (f) radiographs showing buccal-lingual (B-L) and mesial-distal (M-D) expansion; (g) post space preparation; (h) fibre post adhesion; (i) three specimens for each tooth.

Both groups had several round (length-width ratio < 1.2) and oval root canals (length-width ratio \geq 1.2). In Group 1, there were 7 round root canals and 11 oval root canals, and in Group 2, there were 6 round root canals and 12 oval root canals.

Endodontic treatment

The working length was set as 1 mm shorter than the length of a size 10 K-file (MANI) in the tooth when its tip is placed at the apical foramen. The canals were instrumented with ProTaper Next rotary instruments (Dentsply Sirona) up to X3, with 2.5% sodium hypochlorite (NaOCl) irrigation (1 ml, after using each file) through a side-vented needle (239; Paikedun, Suzhou, China), followed by treatment in an ultrasonic bath (P5 Newtron; Satelec, Merignac, France) with 2.5% NaOCl for 20 seconds, three times. Subsequently, the canals were immersed in 17% ethylenediaminetetraacetic acid for 1 minute, followed by a final flush with 5 ml of 2.5% NaOCl, and then dried with absorbent paper points (Dayading, Beijing, China).

In Group 1, iRoot SP was inserted with the syringe provided by the manufacturer in the middle third of the canal, and then one 35#/0.04 gutta-percha point (Dayading) was covered with a thin layer of sealer and

slowly inserted. The gutta-percha point was cut off at the root canal orifice with a heat carrier (B&L Biotech, Ansan, South Korea). In Group 2, AH Plus was prepared according to the manufacturer's recommendations and the warm vertical condensation technique was applied. Each root canal was obturated with one 35#/0.04 gutta-percha point covered with AH Plus and several 25#/0.02 gutta-percha points (Dayading) if necessary to ensure that the apical 4 mm was tightly filled. The gutta-percha points were removed 4 mm from the apical foramen with a heat carrier, and then the root canal was back-filled with warm gutta-percha.

Finally, for all specimens, Clearfil SE Bond (Kuraray Medical, Tokyo, Japan) and P60 resin (3M ESPE, St Paul, MN, USA) were used to seal the coronal access cavity (Fig 1e), and radiographs were taken from both the buccal-lingual and mesial-distal expansions to ensure there was no vacuole within the root filling materials (Fig 1f). The specimens were stored at 37°C under 100% humidity for 7 days.

Fibre post cementation

After storage, the P60 resin was removed with a diamond bur. The gutta-percha and its surrounding sealer material was removed with 1# to 3# Peeso reamers

(MANI), leaving 4 mm of filling material in the apical third. Post spaces were prepared to a depth of 9 mm with a blue size (diameter of 1.2 mm) post space preparation drill (RTD, St Egeven, France) (Fig 1g). The post spaces were then observed under an endodontic microscope, and if sealer remained in the canals, this was recorded. Before cementation, the post spaces were treated in an ultrasonic water bath for 1 minute and then dried with absorbent paper points. The CORECEM adhesive resin cement system (RTD) was injected into the post spaces with a syringe until the resin cement spilled out of the root canal orifice. Fibre posts (RTD) with a diameter of 1.2 mm were inserted to full depth with bulldog forceps and finger pressure. Excess cement was removed and the cement was cured for 40 seconds with an ultraviolet-light-emitting diode (UV-LED) curing light (Fig 1h). The roots were then incubated in 100% humidity at 37°C for 24 hours.

Push-out test

Each root specimen was sectioned transversally with a cutting machine (Isomet 1000 Precision Saw; South Bay Technology, San Clemente, CA, USA) under water irrigation, and slices with a thickness of 1 mm at the cervical, middle and apical thirds of the created post space were obtained at depths of 2.0, 4.5 and 7.0 mm from the root canal orifice, respectively (Fig 1i). Images of both sides of the slice were captured with a camera attached to an endodontic microscope. Slices with evident bubbles or voids were discarded from the study.

The push-out bond strength was measured using a universal testing machine (Instron 5969; Instron, Norwood, MA, USA). Loading was performed at a cross-head speed of 0.5 mm/min, with a metallic plunger with a diameter of 0.8 mm in the crown-to-apex direction until the post was completely dislodged from the slice, which is in line with a previous study²⁸. The maximum force at failure (F) was recorded in Newtons (N), and the thickness of the slice (H) was measured in mm with digital calipers. The push-out bond strength (P) in megapascals (MPa) of each slice was calculated using the following equations: $P = F/S$; $S = C \times H$ and $C = \pi \times D$, where S is the area of the bonded interface (mm^2); C is the periphery of the post (mm) and D is the diameter of the post (mm).

Fracture mode analysis

All push-out specimens were assessed under 16× magnification with an endodontic microscope for the fracture analysis. The fracture modes were divided into four cat-

egories (Figs 2a to d): adhesive failure between resin cement and dentine (the post was enveloped by resin cement); adhesive failure between resin cement and the post (no cement visible around the post); cohesive failure in the post, i.e., the fracture occurred in the fibre post; and mixed failure i.e. post, cement and dentine visible on the debonded area.

Scanning electron microscopy (SEM) (S-4800; Hitachi, Tokyo, Japan) was used to observe the bonding interface and fracture surface. The specimens were immersed in 2.5% glutaraldehyde for 24 hours at 4°C and a gradient of dehydration in 30%, 50%, 70% and 90% ethanol for 10 minutes each and finally immersed in 100% ethanol for 30 minutes. Subsequently, the samples were dried naturally and fixed with electrically conductive silicone for examining.

Statistical analysis

Statistical analysis was conducted with an independent samples t test and one-way analysis of variance (ANOVA), using a factorial design with the type of sealer (AH Plus and iRoot SP) and the root canal region (cervical, middle and apical), followed by post-hoc Tukey multiple comparisons using SPSS statistics software (version 20.0; SPSS, Armonk, NY, USA) for Windows. The level of significance was set at $\alpha = 0.05$. The results were considered statistically significant when $P < 0.05$.

Results

The mean bond strength values (in MPa) and standard deviation values for fibre posts that were cemented in the root canals previously obturated with different sealers at the cervical, middle and apical regions were determined (Table 1). Within the same root canal region, there was no statistically significant difference in bond strength between the two sealers, whether in the cervical, middle or apical portion ($P = 0.67$, $P = 0.14$ and $P = 0.78$ for the cervical, middle and apical portions, respectively). When using the same sealer, the highest bond strength was obtained in the cervical portion for both AH Plus and iRoot SP (22.78 ± 3.80 MPa and 23.88 ± 4.15 MPa, respectively), which was significantly higher than for the middle portion (19.74 ± 3.49 MPa and 20.90 ± 4.03 MPa, respectively) ($P = 0.030$ and $P = 0.048$ for AH Plus and iRoot SP, respectively) and the apical portion (18.96 ± 4.86 MPa and 18.82 ± 4.55 MPa, respectively) ($P = 0.07$ and $P < 0.001$ for AH Plus and iRoot SP, respectively).

In the AH Plus group, there were two major fracture modes: adhesive failure between the resin cement and

Table 1 Mean bond strengths (MPa) and standard deviations for the sealers in different canal regions.

Group	Root canal region			Overall
	Cervical	Middle	Apical	
AH Plus	22.78 ± 3.80 ^{aA}	19.74 ± 3.49 ^{aB}	18.96 ± 4.86 ^{aB}	20.49 ± 4.34 ^a
iRoot SP	23.88 ± 4.15 ^{aA}	20.90 ± 4.03 ^{aB}	18.82 ± 4.55 ^{aB}	21.24 ± 4.64 ^a

Uppercase letters correspond to the comparison in the rows (among root canal regions) and lowercase letters correspond to the comparison in the columns (among sealers). The same letters indicate no significant differences between the compared groups ($P > 0.05$) and vice versa.

Table 2 Mode failure percentages for each group (n = 18).

Sealer	Region	Failure mode			
		Adhesive cement–dentine	Adhesive cement–post	Cohesive in post	Mixed
AH Plus	Cervical	0.0%	33.3%	27.8%	38.9%
	Middle	5.6%	44.4%	16.7%	33.3%
	Apical	16.7%	38.9%	5.6%	38.9%
iRoot SP	Cervical	0.0%	50.0%	33.3%	16.7%
	Middle	0.0%	50.0%	27.8%	22.2%
	Apical	5.6%	50.0%	5.6%	38.9%

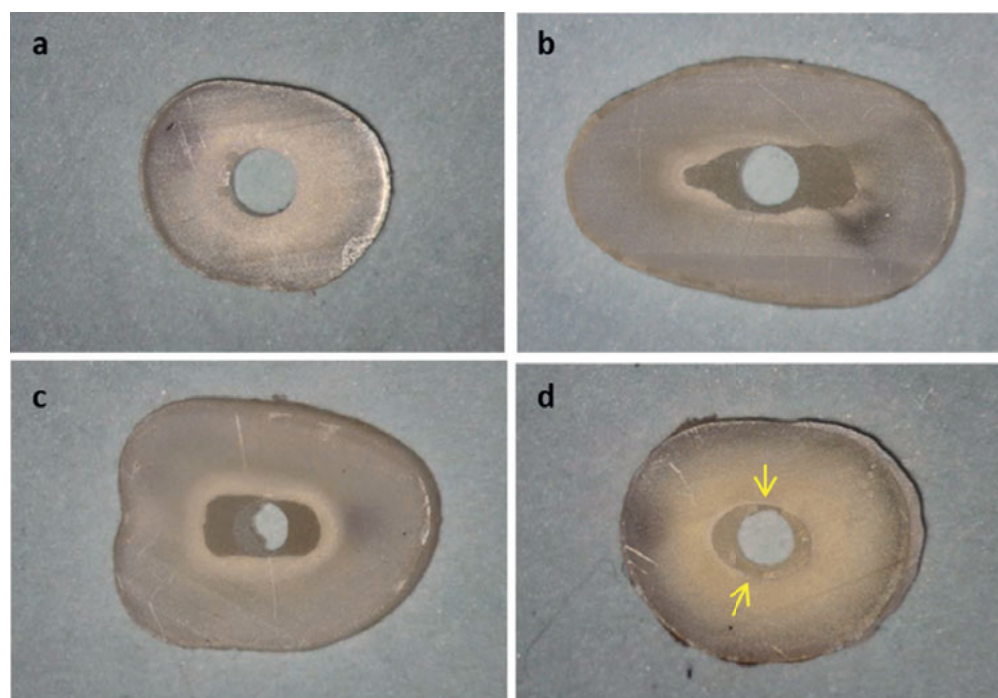


Fig 2 Fracture mode categories. (a) Adhesive failure between resin cement and dentine. (b) Adhesive failure between resin cement and the post. (c) Cohesive failure in the post. (d) Mixed failure (arrows indicate the location for debonding between the adhesive resin and dentine).

the post, and mixed failure. In the iRoot SP group, the major fracture mode was adhesive failure between the resin cement and the post (Table 2). In both the AH Plus and iRoot SP groups, compared with the cervical and middle specimens, there were more adhesive failures between the cement and dentine and fewer cohesive failures in the post in the apical specimens. In the specimens that showed mixed failure, the most common location for debonding between the adhesive resin and the dentine was where the adhesive resin was thin and weak, as shown by the arrows in Fig 2d.

After post space preparation, sealer could still be seen on the root canal walls in 38.9% (7/18) of root canals with iRoot SP obturation (Fig 3a), whereas no sealer was seen in the AH Plus group. All seven of the root canals containing sealer remnants were oval, with the location of the remnants being near the vertex of the long axis of the ellipse. Of these seven root canals, six had sealer remnants in the cervical portion, seven in the middle portion, and three in the apical portion. The adhesive resin was also found to combine tightly with the sealer (Fig 3b), and there was no debonding

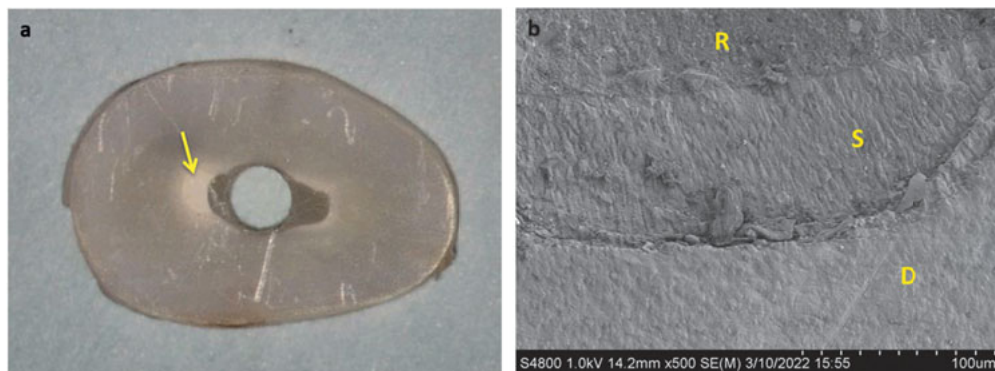


Fig 3 Sealer remnants on root canal walls after post space preparation in the iRoot SP group.

(a) Sealer remnants were located near the vertex of the long axis of the ellipse (arrow point).

(b) The adhesive resin (R), the sealer (S) and the dentine (D) were bound tightly together after push-out testing.

of adhesive resin on the root canal wall where sealer remnants were present.

Discussion

To evaluate the bond strength of materials, several techniques can be used, including conventional tensile strength testing, as well as pull-out and push-out tests. The push-out test is widely used when evaluating the bond strength of fibre posts and was employed in the present study, since it can be used in confined areas such as root canal walls and give a precise indication of the location(s) in which failures occurred^{8, 29}.

The present study has shown that it is difficult to remove excess iRoot SP completely from the root canal system after post space preparation, whereas all excess AH Plus can be removed. iRoot SP was seen in each third of the root canal, mainly in the cervical and middle regions. From the cervical to the apical region, the shape of the cross-section of the root canal changes gradually from oval to circular, the diameter of the root canal becomes progressively smaller and the penetration depth of the sealer in the dentine tubule gradually becomes less³⁰, making it easier to remove the sealer in the apical region.

Most previous studies have demonstrated that iRoot SP has a negative influence on the bond strength of fibre posts^{9,10,31,32}, and that any sealer remnants could prevent contact between the resin cement and the collagen matrix in dentine and change the wettability, permeability, pH and reactivity of the dentine, affecting the resin-dentine bond strength⁹; however, this was not shown to be the case in the present study, and the authors did not observe any difference in the bond strength to root dentine whether iRoot SP or AH Plus sealer was used, which is in line with the findings reported by He et al²⁶ and Özcan et al²⁷. One possible explanation for this could be the use of different study designs and methodologies in the present study and others, for example in relation to

the obturation technique, post space irrigation methods, and brand of cement and fibre post used³³. The retention of fibre posts depends mainly on adhesion, including the adhesion between cement and dentine and between cement and the post. In the present study, most dislocations occurred between cement and the post, which means that as long as the bond strength between the cement and dentine was greater than that between the cement and the post, there would be no difference in bond strength of fibre posts between the iRoot SP and AH Plus groups, even if there was some difference in bond strength between cement and dentine between the two groups. Although sealer remnants were found along the root canal walls, it may not be enough to have an impact on the bond strength of fibre posts cemented with the CORECEM adhesive resin system.

This study showed that the bond strength of the fibre posts in the cervical portion was higher than that in the middle and apical portions when both AH Plus and iRoot SP were used, which is consistent with previous studies^{8,10,34,35}. One possible explanation for this is the morphological differences within the dentine along the canal, such as the reduction in the number, density and diameter of dentine tubules from the cervical to the apical portion^{36,37}. Since adhesion relies mainly upon micromechanical retention, higher bond strength is expected to be achieved in the cervical portion^{10,27}. Another factor that may explain the lower bond strength in the deepest portion of the root canal is the difficulty accessing this area. For example, insertion of the acid etching solution and adhesive system was impaired³⁸ and there was likely poor UV curing of the resin composite in regions distant from the light source, with incomplete curing likely contributing to the diminished bond strength of fibre posts^{5,26,38}.

Finally, the major fracture modes with AH Plus were found to be adhesive failure between the resin cement and the post and mixed failure, whereas with iRoot SP, half of the specimens experienced adhesive fracture

between the resin cement and the post, implying that this group had better adhesion with the dentine walls, which is in accordance with Özcan et al²⁷ but in contrast with the majority of previous studies, where most failures were either of the adhesive at the cement–dentine interface^{8,9,26} or mixed failure³⁰. The possible explanations for the different distribution of fracture mode include the type of luting cements used, the approach taken to treatment of the post space, and difference in the pre-treatment of the fibre post. Fibre posts that have been airborne-particle abraded and pre-treated with silane might experience fewer adhesive failures between the cement and posts, although this warrants further investigation^{39–41}.

The main limitation of the present study was the fact that different obturation techniques were used for different sealers; however, the study design is based on clinical application. AH Plus with the warm vertical condensation technique is considered the gold standard^{13,14}, whereas warm vertical condensation was not advised in conjunction with iRoot SP by some researchers⁴². The single-cone technique is employed by most dental practitioners when iRoot SP is used¹⁷, as the technique is easy and fast and the most important is the clinical success rate. The success rate of root canal therapy using a single-cone technique with iRoot SP was 90.9%, which fell within the range found in previous studies⁴³. To eliminate the influence of different obturation techniques, another group with the use of iRoot SP in conjunction with the warm vertical condensation technique could be added; however, this approach is rarely used in clinical settings and might have limited clinical significance.

Conclusion

Within the limitations of the present in vitro study, it can be concluded that the presence of remnants of iRoot SP sealer after post space preparation has a limited effect on the bond strength of fibre posts to dentine. iRoot SP used with the single-cone technique is a viable option for root canal obturation before fibre post cementation.

Conflicts of interest

The authors declare no conflicts of interest related to this study.

Author contribution

Drs Di QIAO and Meng Meng ZHU contributed to the experiments, data collection and analysis. Dr Di QIAO

drafted the manuscript; Drs Jie PAN and Di QIAO contributed to the study design. All the authors approved the manuscript.

(Received May 08, 2023; accepted Aug 22, 2023)

References

- Boone KJ, Murchison DF, Schjndler WG, Walker WA. Post retention: The effect of sequence of post-space preparation, cementation time, and different sealers. *J Endod* 2001;27:768–771.
- Iaculli F, Rengo C, Lodato V, Patini R, Spagnuolo G, Rengo S. Fracture resistance of endodontically-treated maxillary premolars restored with different type of posts and direct composite reconstructions: A systematic review and meta-analysis of in vitro studies. *Dent Mater* 2021;37:e455–e484.
- Pulido CA, de Oliveira Franco APG, Gomes GM, et al. An in situ evaluation of the polymerization shrinkage, degree of conversion, and bond strength of resin cements used for luting fiber posts. *J Prosthet Dent* 2016;116:570–576.
- Nesello R, Silva IA, Bem IA, et al. Effect of bioceramic root canal sealers on the bond strength of fiber posts cemented with resin cements. *Braz Dent J* 2022;33:91–98.
- Teixeira CS, Pasternak-Junior B, Borges AH, Paulino SM, Sousa-Neto MD. Influence of endodontic sealers on the bond strength of carbon fiber posts. *J Biomed Mater Res B Appl Biomater* 2008;84B:430–435.
- Altmann AS, Leitune VC, Collares FM. Influence of eugenol-based sealers on push-out bond strength of fiber post luted with resin cement: Systematic review and meta-analysis. *J Endod* 2015;41:1418–1423.
- Bohrer TC, Fontana PE, Wandscher VF, et al. Endodontic sealers affect the bond strength of fiber posts and the degree of conversion of two resin cements. *J Adhes Dent* 2018;20:165–172.
- Dos Santos GL, Cardoso IV, Suzin SM, Ballarin A, Lopes GC, Teixeira CS. Influence of different endodontic sealers on bond strength of fiber posts to weakened roots after resin restoration. *Clin Oral Investig* 2021;25:4125–4135.
- Vilas-Boas DA, Grazziotin-Soares R, Ardenghi DM, et al. Effect of different endodontic sealers and time of cementation on push-out bond strength of fiber posts. *Clin Oral Investig* 2018;22:1403–1409.
- Soares IMV, Crozeta BM, Pereira RD, Silva RG, da Cruz-Filho AM. Influence of endodontic sealers with different chemical compositions on bond strength of the resin cement/glass fiber post junction to root dentin. *Clin Oral Investig* 2020;24:3417–3423.
- Skupien JA, Sarkis-Onofre R, Cenci MS, Moraes RR, Pereira-Cenci T. A systematic review of factors associated with the retention of glass fiber posts. *Braz Oral Res* 2015;29:1–8.
- Escobar PM, Lopes FC, Carvalho K, et al. Influence of different calcium hydroxide removal protocols on the bond strength of epoxy resin-based sealer in long oval root canals. *Microsc Res Tech* 2022;85:781–788.
- Cecchin D, Farina AP, Souza MA, Carlini-Júnior B, Ferraz CC. Effect of root canal sealers on bond strength of fibreglass posts cemented with self-adhesive resin cements. *Int Endod J* 2011;44:314–320.

14. Resende LM, Rached-Junior FJ, Versiani MA, et al. A comparative study of physicochemical properties of AH plus, epiphany, and epiphany SE root canal sealers. *Int Endod J* 2009;42:785–793.
15. Donnermeyer D, Bürklein S, Dammaschke T, Schäfer E. Endodontic sealers based on calcium silicates: A systematic review. *Odontology* 2019;107:421–436.
16. Silva Almeida LH, Moraes RR, Morgental RD, Pappen FG. Are premixed calcium silicate-based endodontic sealers comparable to conventional materials? A systematic review of in vitro studies. *J Endod* 2017;43:527–535.
17. Guivarc'h M, Jeanneau C, Giraud T, et al. An international survey on the use of calcium silicate-based sealers in non-surgical endodontic treatment. *Clin Oral Investig* 2020;24:417–424.
18. Loushine BA, Bryan TE, Looney SW, et al. Setting properties and cytotoxicity evaluation of a premixed bioceramic root canal sealer. *J Endod* 2011;37:673–677.
19. Han L, Okiji T. Bioactivity evaluation of three calcium silicate-based endodontic materials. *Int Endod J* 2013;46:808–814.
20. Chen X, Liu H, He Y, Luo T, Zou L. Effects of endodontic sealers and irrigation systems on smear layer removal after post space preparation. *J Endod* 2018;44:1293–1297.
21. Oltra E, Cox TC, LaCourse MR, Johnson JD, Paranjpe A. Retreatability of two endodontic sealers, EndoSequence BC Sealer and AH Plus: A micro-computed tomographic comparison. *Restor Dent Endod* 2017;42:19–26.
22. Yang R, Tian J, Huang X, et al. A comparative study of dentinal tubule penetration and the retreatability of EndoSequence BC sealer HiFlow, iRoot SP, and AH plus with different obturation techniques. *Clin Oral Investig* 2021;25:4163–4173.
23. El Hachem R, Khalil I, Le Brun G, et al. Dentinal tubule penetration of AH plus, BC sealer and a novel tricalcium silicate sealer: a confocal laser scanning microscopy study. *Clin Oral Investig* 2019;23:1871–1876.
24. Zicari F, Couthino E, De Munck J, et al. Bonding effectiveness and sealing ability of fiber-post bonding. *Dent Mater* 2008;24:967–977.
25. Yang R, Han Y, Liu Z, Xu Z, Liu H, Wei X. Comparison of the efficacy of laser-activated and ultrasonic-activated techniques for the removal of tricalcium silicate-based sealers and gutta-percha in root canal retreatment: A microtomography and scanning electron microscopy study. *BMC Oral Health* 2021;21:275.
26. He Y, Wu J, Ji M, et al. The effect of two endodontic sealers and interval before post-preparation and cementation on the bond strength of fiber posts. *Clin Oral Investig* 2021;25:6211–6217.
27. Özcan E, Çapar İD, Çetin AR, Tunçdemir AR, Aydınbelge HA. The effect of calcium silicate-based sealer on the push-out bond strength of fibre posts. *Aust Dent J* 2012;57:166–170.
28. Chen WP, Chen YY, Huang SH, Lin CP. Limitations of push-out test in bond strength measurement. *J Endod* 2013;39:283–287.
29. Goracci C, Tavares AU, Fabianelli A, et al. The adhesion between fiber posts and root canal walls: comparison between microtensile and push-out bond strength measurements. *Eur J Oral Sci* 2004;112:353–361.
30. Chen H, Zhao X, Qiu Y, Xu D, Cui L, Wu B. The tubular penetration depth and adaption of four sealers: A scanning electron microscopic study. *Biomed Res Int* 2017;2017:2946524.
31. do Nascimento AL, Pereira JR, Pamato S, et al. The influence of endodontic sealer dentine penetration on fibreglass post retention. *Int J Adhes Adhes* 2019;88:26–33.
32. Dibaji F, Mohammadi E, Farid F, Mohammadian F, Sarraf P, Kharrazifard MJ. The effect of BC Sealer, AH-Plus and Dorifill on push-out bond strength of fiber post. *Iran Endod J* 2017;12:443–448.
33. Wang ZJ. Bioceramic materials in endodontics. *Endodontic Topics* 2015;32:3–30.
34. Menezes MS, Queiroz EC, Campos RE, Martins LR, Soares CJ. Influence of endodontic sealer cement on fibreglass post bond strength to root dentine. *Int Endod J* 2008;41:476–484.
35. Peña Bengoa F, Magasich Arze MC, Macchiavello Noguera C, Moreira LFN, Kato AS, Bueno CEDS. Effect of ultrasonic cleaning on the bond strength of fiber posts in oval canals filled with a premixed bioceramic root canal sealer. *Restor Dent Endod* 2020;45:e19.
36. Mjör IA, Nordahl I. The density and branching of dentinal tubules in human teeth. *Arch Oral Biol* 1996;41:401–412.
37. Ferrari M, Mannocci F, Vichi A, Cagidiaco MC, Mjör IA. Bonding to root canal: structural characteristics of the substrate. *Am J Dent* 2000;13:255–260.
38. Vichi A, Grandini S, Davidson CL, Ferrari M. An SEM evaluation of several adhesive systems used for bonding fiber posts under clinical conditions. *Dent Mater* 2002;18:495–502.
39. Ubaldini ALM, Benetti AR, Sato F, et al. Challenges in luting fibre posts: Adhesion to the post and to the dentine. *Dent Mater* 2018;34:1054–1062.
40. Elnaghy AM, Mandorah A, Hassan AH, Elshazli A, Elsaka S. Effect of surface treatments on push-out bond strength of calcium silicate-based cements to fiber posts. *BMC Oral Health* 2021;21:131.
41. Niu DL, Xie JF, Liu C, Ni SL, Liu H. The influence of different treatments on fiber post and root canal to bond strength of fiber post. *J Adhes Sci Technol* 2021;35:928–940.
42. Qu W, Bai W, Liang YH, Gao XJ. Influence of warm vertical compaction technique on physical properties of root canal sealers. *J Endod* 2016;42:1829–1833.
43. Chybowski EA, Glickman GN, Patel Y, Fleury A, Solomon E, He J. Clinical outcome of non-surgical root canal treatment using a single-cone technique with Endosequence bioceramic sealer: A retrospective analysis. *J Endod* 2018;44:941–945.

Comparison of Powered versus Manual Tooth Brushing for Safety and Efficacy in Patients with Gingivitis: A Randomised, Multicentre Clinical Trial in China

Dan Ying TAO¹, Yan SI², Tao HU³, Shu Guo ZHENG², Han JIANG⁴, Ye TAO⁵, Yan ZHOU⁵, Fang Zhi ZHU³, Bao Jun TAI⁴, Xi Ping FENG¹

Objective: To evaluate the effects of powered and manual tooth brushing on gingival inflammation in a Chinese population with mild to moderate gingivitis.

Methods: The present randomised, single-blind, parallel clinical trial was conducted in five cities in China. Generally healthy participants aged 18 to 65 years, who were non-smokers and had at least 20 sites of gingival bleeding, were included as eligible subjects. The subjects were randomly assigned to either the powered tooth brushing (PTB) group or standard manual tooth brushing (MTB) group. All subjects were supplied with a fluoride-containing toothpaste. Gingival Bleeding Index (GBI), Modified Gingival Index (MGI) and the Turesky modification of the Quigley-Hein Plaque Index (MPI) were used to evaluate the outcomes.

Results: A total of 235 subjects completed the study, 118 in the PTB group and 117 in the MTB group. The mean age and sex distribution for the PTB and MTB groups were 34.40 ± 9.99 years, 89 women and 29 men, and 34.20 ± 10.14 years, 82 women and 35 men, respectively. After 6 months, the percentage decrease in MGI was $26.150\% \pm 26.897\%$ for the PTB group and $14.768\% \pm 38.544\%$ for the MTB group ($P = 0.0092$). Statistically significant differences between types of tooth brushing were also observed at 6 months for GBI, and at all time points for MPI.

Conclusion: Tooth brushing with a powered toothbrush twice a day was shown to be more effective than use of a manual toothbrush in reducing gingival inflammation, gingival bleeding and surface plaque after a 6-month period. Both kinds of toothbrushes were safe for the oral tissues.

Key words: dental hygiene, gingivitis, oral hygiene, public health

Chin J Dent Res 2023;26(4):257–264; doi: 10.3290/j.cjdr.b4784023

- 1 Department of Preventive Dentistry, Shanghai Ninth People's Hospital, Shanghai Jiao Tong University School of Medicine; College of Stomatology, Shanghai Jiao Tong University, Shanghai, P.R. China.
- 2 Department of Preventive Dentistry, Peking University School and Hospital of Stomatology, Beijing, P.R. China.
- 3 Department of Preventive Dentistry, West China Hospital of Stomatology, Sichuan University, Chengdu, P.R. China.
- 4 Department of Preventive Dentistry, Wuhan University School of Stomatology, Wuhan, P.R. China.
- 5 Department of Preventive Dentistry, Guanghua School of Stomatology, Hospital of Stomatology, Sun Yat-sen University, Guangzhou, P.R. China.

Corresponding authors: Dr Xi Ping FENG, Department of Preventive Dentistry, Shanghai Ninth People's Hospital, Shanghai Jiao Tong University School of Medicine, #500 Quxi Road, Huangpu District, Shanghai 200011, P.R. China. Tel: 86-21-33183424. Email: fengxi ping9h@163.com

The role of home oral hygiene practices has been studied extensively, with the efficacy and safety of home-use methods, toothbrushes and interproximal cleaning devices being well-documented¹⁻⁴; however, there is limited evidence from clinical trials available to evaluate their impact with a multicentre design and a longer duration. The Fourth National Oral Health Survey of

Dr Bao Jun TAI, Department of Preventive Dentistry, Wuhan University School of Stomatology, #237 Luoyu Road, Hongshan District, Wuhan 430079, P.R. China. Tel: 86-27-87686110. Email: taibaojun@126.com

This study was funded by the Society of Preventive Dentistry Chinese Stomatological Association and the Shanghai Clinical Research Centre for Oral Diseases (no. 19MC1910600).

China showed a high prevalence of periodontal disease in China, with reported rates of 52.8%, 69.3% and 64.6% in the age groups of 35 to 44 years, 55 to 64 years and 65 to 74 years, respectively⁵. This is important across the entire spectrum of periodontal status, as adequate prevention may reduce the prevalence of periodontal disease and adequate maintenance may minimise its severity. It is important to evaluate the preventative effects of tooth brushing in patients who have not yet experienced periodontitis⁶. The present study aimed to compare the effects of powered versus manual toothbrush use on gingivitis to provide valuable information to help prevent periodontitis.

Materials and methods

Subjects

This was a multicentre study conducted on generally healthy adult volunteers aged 18 to 65 years. The Clinical Study Ethics Committee of Shanghai Ninth People's Hospital, Shanghai, China, approved the protocol (SH9H-2018-T60-1) and the trial was registered at chictr.org (ChiCTR2100050706). Subjects' rights were protected by the Ethics Committee and written informed consent was obtained.

The inclusion criteria were as follows:

- routine manual toothbrush users;
- non-smokers;
- at least 20 natural teeth;
- informed consent provided voluntarily with agreement to fulfil study visits and complete procedures over a 12-month period;
- mild to moderate gingivitis with at least 20 sites of gingival bleeding as assessed by the Gingival Bleeding Index (GBI);
- minimum plaque score of at least 1.5 according to the Turesky modification of the Quigley-Hein Plaque Index (MPI) following an oral hygiene abstention period lasting 8 to 16 hours⁸⁻¹⁰.

The exclusion criteria were as follows:

- fixed orthodontic appliances;
- removable dentures;
- untreated caries lesions;
- significant evidence of periodontal disease and general health problems;
- dental students, dental professionals and others with potential conflicts of interest.

Study sites and examiners

The study was conducted in five cities in China: Beijing, Shanghai, Chengdu, Wuhan and Guangzhou. All the investigators were oral clinicians with at least 2 years' practice experience.

Interventions and home hygiene instructions

Two interventions were planned in this home oral hygiene study. The subjects were divided randomly into two groups and provided with either a powered toothbrush (Sonicare DiamondClean Smart used in Gum Health mode with Premium Gum Care brush head [both Philips, Amsterdam, The Netherlands], PTB group) or a manual toothbrush (American Dental Association reference toothbrush with flat-trim nylon bristles, MTB group). All subjects used the assigned toothbrush twice daily, once in the morning and once in the evening, with a standardised fluoride-containing toothpaste. The subjects assigned to the PTB group brushed their teeth according to the instructions provided by the product manufacturer, whereas those assigned to the MTB group brushed their teeth according to their routine habits. All other oral hygiene measures were prohibited. Compliance with the assigned tooth brushing regimen was tracked in a home diary record that was supplied to each subject and reviewed at each study visit by designated staff.

Outcome measurement

Modified Gingival Index (MGI) was evaluated at four sites on the gingival margin and papillary units of each tooth, with severity rated on a scale of 0 to 4. Gingival Bleeding was assessed using a Community Periodontal Index (CPI) probe. Severity was rated as binary, i.e., bleeding present or not. GBI is part of the empirical clinical algorithm¹¹. MPI was scored at six sites, including the labial and lingual side (mesial/centric/distal). All teeth were stained with plaque disclosing dye and then scored.

Description of study procedures

The subjects attended eight visits to complete the study over a 12-month follow-up period and were enrolled from February 2019 to July 2020. Table 1 presents the study visit intervals and the procedures conducted at each visit.

Table 1 Timing of study visits and procedures carried out.

Visit 1: Screening (up to day 14)	Informed consent, medical and dental history, concomitant medications, oral examination, preliminary eligibility assessment, enrolment
Visit 2: Baseline/day 0	Oral examination, adverse events/concomitant medications, MGI, GBI and MPI ^a for final eligibility determination, randomisation, product dispensation and instruction, issuing diary
Visit 3: Day 5	Oral examination, adverse events/concomitant medications, compliance review, MPI, dispensing new diary
Visit 4: Week 6	Oral examination, adverse events/concomitant medications, compliance review, MGI, GBI, MPI, dispensing new diary, product use questionnaire
Visit 5: Month 3	Oral examination, adverse events/concomitant medications, compliance review, MGI, GBI, MPI, dispensing new diary, dispensing new brush head or MTB, product use questionnaire
Visit 6: Month 6	Oral examination, adverse events/concomitant medications, compliance review, MGI, GBI, MPI, dispensing new diary, dispensing new brush head or MTB, product use questionnaire
Visit 7: Month 9	Adverse events/concomitant medications, compliance review, dispensing new diary, dispensing new brush head or MTB
Visit 8: Month 12 ^b	Oral examination, adverse events/concomitant medications, compliance review, MGI, GBI, MPI, product use questionnaire

^aSubjects were required to abstain from administering oral hygiene between 8 and 16 hours prior to each visit at which MPI was assessed.

^bThe clinical measurements of MGI, GBI and MPI were not collected due to the COVID-19 outbreak preceding the scheduled visit.

Sample size determination

The sample size determination was based on the results of a prior study with similar eligibility criteria in which the primary efficacy endpoint, MGI, was measured in a comparison between a powered toothbrush and a manual toothbrush¹². After adjustment according to the linear model, the difference in percentage decrease between treatments at week 6 was 46.50%¹².

In the absence of pilot data for any of the planned clinical sites used, the present authors adopted a conservative estimate of a difference between products of 10% at month 3 (standard deviation 20%, 0.05 significance level, with 90% power). Based on these assumptions, the minimum sample size required to detect the proposed difference was 86 subjects per group, to give a total of 172 subjects. To allow for a 15% dropout rate, the sample size was increased conservatively to enrol 240 subjects (120 per group).

Randomisation

Subjects were randomised at visit 2 by designated unblinded study personnel. These personnel were not responsible for any efficacy and safety endpoint assessment. As this was a multicentre study, enrolment and randomisation were independent among sites. Each site aimed to enrol 50 subjects (25 per group), except for one site, where the target was 40 subjects (20 per group). Each site's randomisation schedule was paper-based and was provided by a third-party research organisa-

tion. Randomisation was stratified by age: 18 to 34 years and 35 to 65 years.

Explanation of any interim analyses or withdrawal/termination criteria

There were no planned interim analyses for this study. All subjects were able to withdraw voluntarily at any time. In addition, the principal investigator at each site was able to terminate a subject's participation for any intercurrent concerning safety issue, or as related to significant non-compliance. Withdrawn subjects were not replaced.

Blinding

Given the nature of the test products, this was a single-blind study. All examiners of the clinical indices were blinded to the treatment assignment of subjects. Designated unblinded study personnel performed randomisation, product dispensing and instruction, and diary dispensing and review. The study data were merged with randomisation following database lock. Statistical analysis was conducted thereafter.

Repeatability

Repeat examinations for MGI assessments of three participants were carried out by examiners at each site and a reference examiner at baseline and during the visit at month 3 to evaluate inter-examiner repeatabil-



Screened subjects (N=579)		
Enrolled subjects (N=241)		Screen failures (N=338)
Randomized to PTB (N=121)	Randomized to MTB (N=120)	Lost follow up or withdraw (N=6)
Completion PTB (N=118)	Completion MTB (N=117)	

Fig 1 Subject screening, enrolment and completion.

ity. Replicate GBI examinations were not conducted for the influence of the first examination on the replication. Assessments of each tooth performed at each visit were cross-tabulated and a Kappa coefficient (κ) was calculated. Repeatability was compared according to pre-defined values as fair to good if it was between 0.40 and 0.75. The Kappa scores for MGI with regard to five examiners were 0.56–0.62 at baseline and 0.57–0.61 at the 3-month visit.

Statistical methods

The primary efficacy analysis was conducted including all randomised subjects with a baseline and MGI evaluation at month 3 (modified intention to treat [MITT]). The safety analysis included all randomised subjects who were exposed to treatment. All variables were summarised by descriptive statistics. Standard subject demographics (e.g., age, sex, ethnicity) and baseline characteristics were summarised for all randomised subjects, and for MITT subjects. For continuous subject characteristics, means were compared using a one-way analysis of variance (ANOVA). The incidence of categorical variables was compared using a chi-square test or Fisher exact test, where appropriate.

For each visit, an ANOVA model was used to evaluate product comparisons for efficacy variables. The reduction from the baseline percentage of each efficacy variable (MPI, MGI and GBI) was used as the response variable of the model; the group was used as the independent variable. A sensitivity analysis was performed for central effects. In addition, the time effect of efficacy was tested using a linear mixed-effect model, which considered both time effect and time-group interaction effect.

Deviations from the planned protocol and analysis

Clinical examinations were not performed at any of the five clinical sites at month 12 due to the COVID-19 pandemic at that time. Thus, the final efficacy endpoints for MPI, GBI and MGI were analysed with outcomes as recorded at month 6. A telephone interview was completed at month 12 to assess safety. These data are included in the final analysis.

Results

Study subjects: enrolment, randomisation and completion

A total of 579 subjects were screened for inclusion in this study. Of these, 338 did not meet the inclusion criteria and 241 were enrolled, with 121 randomised to the PTB group and 120 to the MTB group. Upon completion at month 12, there were 118 subjects in the PTB group and 117 in the MTB group. Figure 1 presents the flow of subjects from screening to completion. The baseline values depicting the distribution of age, sex, ethnicity, MGI, GBI and MPI between treatment groups, across all five sites, are presented in Table 2.

Efficacy outcomes

Gingival inflammation was found to improve for both treatment groups over the study period. At week 6, both treatment groups had made a modest improvement compared to baseline; however, no statistical intergroup difference was observed, with mean percentage decrease values of $7.206\% \pm 17.310\%$ and $7.184\% \pm 22.232\%$ for the PTB and MTB group, respectively. At month 3, the reduction trend continued, with percentage decrease values of $17.490\% \pm 33.525\%$ for the PTB group and $11.260\% \pm 35.725\%$ for the MTB group ($P = 0.1693$). In month 6, the reduction trend continued and a statistically significant intergroup difference was observed, with outcomes of $26.150\% \pm 26.897\%$ for the PTB group and $14.770\% \pm 38.544$ for the MTB group ($P = 0.0092$).

GBI was also found to reduce compared to baseline for both treatment groups. No statistical difference was observed between groups, however, until month 6, as was also the case for MGI, above. At month 6, the percentage decrease outcomes were $48.660\% \pm 31.849\%$ for the PTB group and $31.750\% \pm 39.960\%$ for the MTB group ($P = 0.0004$).

As is customary in Chinese dental practice, an early indication of product efficacy for plaque reduction was

Table 2 Baseline demographics and clinical values.

Indicator		Study group (PTB), n = 118	Control group (MTB), n = 117	P value
Age, y	Mean ± standard deviation	34.40 ± 9.99	34.20 ± 10.14	0.8778
	Median	33.5	33.0	
	Range	18–63	18–59	
Sex	Female	89 (75.4%)	82 (70.1%)	0.3580
	Male	29 (24.6%)	35 (29.9%)	
Ethnic group	Han Chinese	115 (97.5%)	112 (95.7%)	0.3135
	Manchu	0 (0.0%)	3 (2.6%)	
	Hui	2 (1.7%)	1 (0.9%)	
	Nakhi	0 (0.0%)	1 (0.9%)	
	Mongol	1 (0.8%)	0 (0.0%)	
Baseline MGI	Mean ± standard deviation	1.8264 ± 0.4223	1.8237 ± 0.4328	0.9617
	Median	1.7464	1.8018	
	Range	0.7755–2.9196	0.6667–2.8661	
Baseline GBI	Mean ± standard deviation	0.4676 ± 0.2140	0.4530 ± 0.2138	0.6016
	Median	0.4073	0.3929	
	Range	0.1818–0.9811	0.1786–0.9107	
Baseline MPI	Mean ± standard deviation	3.3110 ± 0.6758	3.3347 ± 0.6704	0.7875
	Median	3.3097	3.3286	
	Range	1.7357–4.8053	1.7071–4.9643	

evaluated on day 5. A reduction from baseline plaque levels was observed at all time points for both groups. In addition, between-group differences were observed to be statistically significant at each time point. The mean percentage decreases were 11.320% ± 14.212% for the PTB group and 6.287% ± 12.904% for the MTB group ($P = 0.0049$) at day 5; 7.030% ± 14.929% for the PTB group and 3.208% ± 14.171% for the MTB group ($P = 0.045$) at week 6; 13.576% ± 20.842% for the PTB group and 7.792% ± 18.472% for the MTB group ($P = 0.0253$) at month 3; and 16.777% ± 20.151% for the PTB group and 5.469% ± 19.409% for the MTB group ($P < 0.0001$) at month 6. Figure 2 presents the trend for the three outcome variables over time.

Sensitivity and correlation analysis

Sensitivity analysis was conducted for the percentage reduction in MGI, GBI and MPI to investigate the impact of multiple factors, such as age, time and clinical site. There was no statistical difference between the two age groups (18 to 34 years and 35 to 65 years) for reductions in MGI, GBI and MPI at any of the visits, except for MPI reduction at 5 days. The interaction between time and study group was statistically significant ($P < 0.05$), with both groups exhibiting different trends at each visit. Additionally, an interaction was observed between site and group ($P < 0.05$), with the clinical efficacy of both treatment groups in Wuhan found to be inconsistent with those at the other four sites.

Further, correlation analysis of the percentage reduction in MGI, GBI and MPI with the Pearson method indicates that there was a positive correlation among these three efficacy variables at 3 and 6 months. The correlation coefficient among MGI, GBI and MPI reduction was between 0.25 and 0.45 ($P < 0.0001$) (Table 3). At 6 weeks, the percentage reduction in MPI appeared to correlate with the percentage reduction in GBI, but not MGI.

Safety outcomes

Over the 12-month period, one adverse event occurred that was possibly related to the study product in each treatment group, both indicated as mild in severity. Neither group reported a severe or greater adverse event possibly related to the study products. A total of 55 subjects reported 69 adverse events that were not related to the study: 27 subjects in the PTB group had 32 adverse events, and 28 subjects in the MTB group had 37 adverse events. There was no statistically significant difference between the two groups.

Subject deviations

In general, subjects were highly compliant. The most common deviation reported was incidents of missed brushing. Such incidents were infrequent, and therefore deemed insufficiently serious to interfere with the efficacy or safety endpoints.

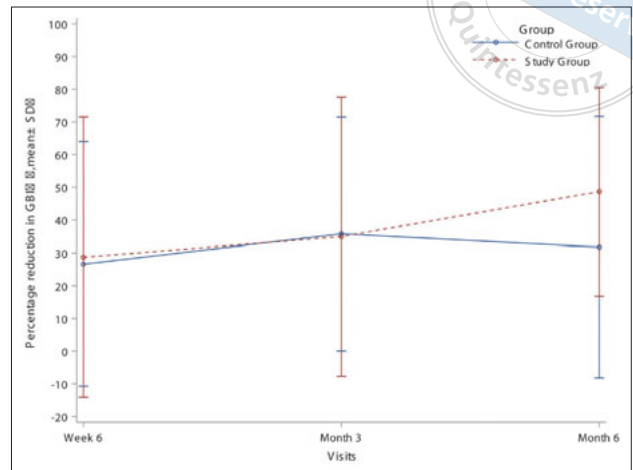
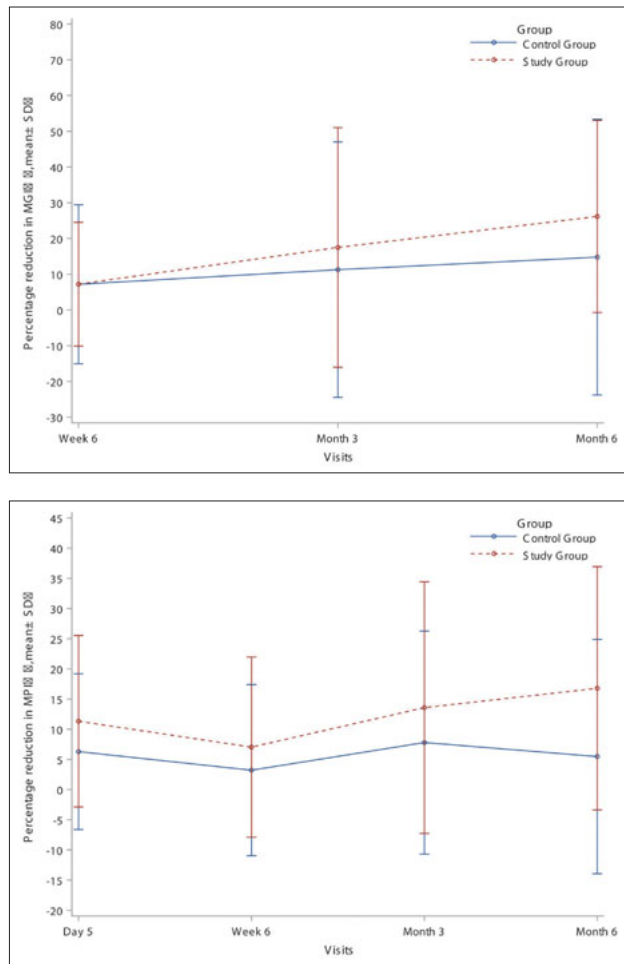


Fig 2 Mean percentage decrease for the (a) MGI, (b) GBI and (c) MPI.

Discussion

The fourth National Oral Health Survey of China reported high prevalence and severity of periodontal disease among adults in mainland China¹³. The constituents of biofilm are implicated as the source of pathogenesis of periodontal inflammation and disease^{14,15}. Adequate home oral hygiene care, such as regular and effective tooth brushing, is necessary for primary periodontal disease prevention. Many individuals use manual toothbrushes as part of their standard home care regimen. Recently published long-term epidemiological research conducted in Germany has shown that use of powered toothbrushes, compared to manual toothbrushes, was found to be significantly associated with a greater number of retained teeth (19.5%), reduced progression of mean pocket depth and reduced clinical attachment level, over an 11-year study period¹⁶.

The design attributes of powered toothbrushes may help to account for the differences observed in long-term outcomes. In the present study, the PTB group

was found to have gained substantial benefits regarding plaque levels as early as day 5, compared to the MTB group, with gingival inflammatory status observed to improve as well, up to month 6. It is important to note the positive correlation between reduction in dental plaque and gingival bleeding or in dental plaque and gingival inflammation.

The present study corroborates previously published clinical trial outcomes and meta-analyses that show that powered tooth brushing has a clinically measurable benefit on gingival health and plaque management compared to manual tooth brushing¹⁷⁻²⁰. In addition to corroborating previously observed effectiveness outcomes, the low incidence of adverse events also adds important evidence to demonstrate that powered tooth brushing is safe for long-term use.

Many of the published prospective trials comparing powered and manual toothbrushes are single-centre²¹⁻²³. The present study had a multicentre design. The five sites involved in the study represent distinct regions of mainland China. Indeed, there may be

Table 3 Correlation analysis results of percentage reduction in MGI, GBI and MPI.

Visit	Percentage reduction	MGI correlation coefficient	GBI correlation coefficient	MPI correlation coefficient
Week 6	MGI	1.00000	0.04829	0.06468
	GBI	0.04829 ($P = 0.4613$)	1.00000	0.25984
	MPI	0.06468 ($P = 0.3235$)	0.25984 ($P < 0.0001$)	1.00000
Month 3	MGI	1.00000	0.26167	0.40981
	GBI	0.26167 ($P < 0.0001$)	1.00000	0.29966
	MPI	0.40981 ($P < 0.0001$)	0.29966 ($P < 0.0001$)	1.00000
Month 6	MGI	1.00000	0.42481	0.39357
	GBI	0.42481 ($P < 0.0001$)	1.00000	0.31771
	MPI	0.39357 ($P < 0.0001$)	0.31771 ($P < 0.0001$)	1.00000

Note: The correlation analysis of percentage reduction in MGI, GBI and MPI at 6 weeks, 3 months and 6 months was conducted using the Pearson method.

population-based differences between sites, but inter-examiner variation must also be considered. We recommend that subsequent multicentre study designs plan to conduct periodic recalibration exercises during the study period to minimise elements of bias or variation.

However, while the multicentre nature of the study may have presented its own challenges and limitations, the present authors are confident in the value of the generalisability of the observed results. Intragroup statistical differences were observed compared to baseline and intergroup statistical differences were evident. While the control available in a single-centre study may limit variation, such a model may lack the generalisability that a multicentre study affords.

Finally, we acknowledge the limitation presented by the interruption caused to this study by the COVID-19 pandemic. Lacking the data for month 12 makes it difficult to fully capture the drivers of the observed differences. Looking at the study data trends, between-group differences were more marked over time. The difference may also reflect that there is a delay between sustained lowered plaque levels introduced by powered tooth brushing and a subsequent reduction in gingival inflammatory status.

Conclusion

Within the limits and design of the present study, performing oral hygiene twice a day with a powered toothbrush was shown to reduce plaque levels significantly in the short and long term compared to use of a manual toothbrush. There was a positive correlation among the three efficacy variables (MPI, GBI and MGI) at months 3 and 6. There was a very low incidence of adverse events across all sites, demonstrating the long-term safety of the use of powered and manual toothbrushes among the population.

Acknowledgements

The authors express their sincere thanks to all participants in this study.

Conflicts of interest

The authors declare no conflicts of interest related to this study.

Author contribution

Drs Dan Ying TAO, Yan SI, Bao Jun TAI, Xi Ping FENG, Tao HU, Shu Guo ZHENG and Han JIANG designed the study and drafted the manuscript; Drs Ye TAO, Yan ZHOU and Fang Zhi ZHU collected the data and revised the manuscript. All the authors read and approved the final version.

References

- van der Weijden GA, Timmerman MF, Reijerse E, et al. The long-term effect of an oscillating /rotating electric toothbrush on gingivitis. An 8-month clinical study. *J Clin Periodontol* 1994;21:139–145.
- Delaurenti M, Ward M, Souza S, et al. The effect of use of a sonic power toothbrush and a manual toothbrush control on plaque and gingivitis. *J Clin Dent* 2017;28(1 Spec No A):A1–A6.
- Kotsakis GA, Lian Q, Ioannou AL, Michalowicz BS, John MT, Chu H. A network meta-analysis of interproximal oral hygiene methods in the reduction of clinical indices of inflammation. *J Periodontol* 2018;89:558–570.
- Figueró E, Roldán S, Serrano J, Escribano M, Martín C, Preshaw PM. Efficacy of adjunctive therapies in patients with gingival inflammation: A systematic review and meta-analysis. *J Clin Periodontol* 2020;47:125–143.
- Jiao J, Jing W, Si Y, et al. The prevalence and severity of periodontal disease in Mainland China: Data from the Fourth National Oral Health Survey (2015-2016). *J Clin Periodontol* 2021;48:168–179.

6. Chapple IL, Van der Weijden F, Doerfer C, et al. Primary prevention of periodontitis: Managing gingivitis. *J Clin Periodontol* 2015;42(suppl 16):S71–S76.
7. Silness J, Løe H. Periodontal disease in pregnancy. *Acta Odontol Scand* 1963;21:533–551.
8. Ainamo J, Bay I. Problems and proposals for recording gingivitis and plaque. *Int Dent J* 1975;25:229–235.
9. Quigley GA, Hein JW. Comparative cleansing efficiency of manual and power brushing. *J Am Dent Assoc* 1962;65:26–29.
10. Turesky S, Gilmore ND, Gickman I. Reduced plaque formation by the chloromethyl analogue of vitamin C. *J Periodontol* 1970;41:41–43.
11. Tonetti MS, Sanz M. Implementation of the new classification of periodontal diseases: Decision-making algorithms for clinical practice and education. *J Clin Periodontol* 2019;46:398–405.
12. Jenkins W, Souza S, Ward M, Defenbaugh J, Milleman KR, Milleman JL. An evaluation of plaque and gingivitis reduction following home use of sonicare flexcare platinum with premium plaque control brush head and a manual toothbrush. *J Clin Dent* 2017;28(1 Spec No A):A7–A12.
13. Sun HY, Jiang H, Du MQ, et al. The prevalence and associated factors of periodontal disease among 35 to 44-year-old Chinese adults in the 4th National Oral Health Survey. *Chin J Dent Res* 2018;21:241–247.
14. Tonetti MS, Eickholz P, Loos BG, et al. Principles in prevention of periodontal diseases: Consensus report of group 1 of the 11th European Workshop on Periodontology on effective prevention of periodontal and peri-implant diseases. *J Clin Periodontol* 2015;42(suppl 16):S5–S11.
15. Theilade E, Wright WH, Jensen SB, Løe H. Experimental gingivitis in man. II. A longitudinal clinical and bacteriological investigation. *J Periodontol Res* 1966;1:1–13.
16. Pitchika V, Pink C, Völzke H, Welk A, Kocher T, Holtfreter B. Long-term impact of powered toothbrush on oral health: 11-year cohort study. *J Clin Periodontol* 2019;46:713–722.
17. Yaacob M, Worthington HV, Deacon SA, et al. Powered versus manual toothbrushing for oral health. *Cochrane Database Syst Rev* 2014;2014:CD002281.
18. de Jager M, Rmaile A, Darch O, Bikker JW. The effectiveness of manual versus high-frequency, high-amplitude sonic powered toothbrushes for oral health: A meta-analysis. *J Clin Dent* 2017;28(1 Spec No A):A13–A28.
19. Clark-Perry D, Levin L. Systematic review and meta-analysis of randomized controlled studies comparing oscillating-rotating and other powered toothbrushes. *J Am Dent Assoc* 2020;151:265–275.e6.
20. Wang P, Xu Y, Zhang J, et al. Comparison of the effectiveness between power toothbrushes and manual toothbrushes for oral health: A systematic review and meta-analysis. *Acta Odontol Scand* 2020;78:265–274.
21. Starke EM, Mwatha A, Ward M, et al. A comparison of the effects of a powered and manual toothbrush on gingivitis and plaque: A randomized parallel clinical trial. *J Clin Dent* 2019;30(Spec No A):A24–A29.
22. Ainamo J, Xie Q, Ainamo A, Kallio P. Assessment of the effect of an oscillating/rotating electric toothbrush on oral health. A 12-month longitudinal study. *J Clin Periodontol* 1997;24:28–33.
23. Cronin M, Dembling W, Warren PR, King DW. A 3-month clinical investigation comparing the safety and efficacy of a novel electric toothbrush (Braun Oral-B 3D Plaque Remover) with a manual toothbrush. *Am J Dent* 1998;11(Spec No):S17–S21.

Clear Cell Renal Cell Carcinoma Metastatic to the Mandible: a Unique Case Report and Literature Review

Xiao Fei HUANG¹, Zi Li YU²

Renal cell carcinoma (RCC) is often diagnosed in advanced stages and a third of patients have distant metastasis at diagnosis. Metastasis may be the first evidence of clear cell RCC in many cases. RCC most often metastasises to the lung, liver, bone, brain and thyroid; however, metastatic disease to the oral cavity, especially the mandible, is rare. The purpose of this study is to report a case of clear cell RCC metastatic to the mandible and review the literature. The mandible lesion underwent radical excision in this case. Notably, no metastatic lesions were detected in the lungs and liver in this patient until 15 months after the mandibulectomy. The patient lived for around 2.5 years after the diagnosis of RCC.

Key words: mandible, mandibular metastasis, renal cell carcinoma (RCC)
Chin J Dent Res 2023;26(4):265–270; doi: 10.3290/j.cjdr.b4784061

Renal cell carcinoma (RCC) is a cause of significant morbidity and mortality that accounts for 2% to 3% of all adult cancers, with 77,410 new cases and 46,345 deaths in China in 2022^{1,2}. A severe smoking habit has been associated with its development³. Clear cell RCC, which represents 85% to 90% of all RCC cases, is the predominant histological type^{1,4,5}. Since RCC is resistant to both traditional chemotherapy and radiation therapy and a third of patients have distant metastatic disease at diagnosis^{6–8}, the prognosis for RCC is usually unfavourable and the median overall survival time is approximately 12 months. Clear cell RCC accounts for 94% of cases of metastatic RCC^{1,2}. The most common sites of metastasis are the lung (50% to 70%), liver (30% to 40%), bone (30% to 40%), brain (9% to 17%) and thyroid (25%)²; however, metastasis of RCC to the oral cavity is relatively rare, with a reported incidence of 15%⁹. The present case report describes a 48-year-old man who suffered meta-

static clear cell RCC to the left mandible and lived for 2.5 years after his diagnosis.

Case presentation

This study was approved by the review board of the Ethics Committee of Hospital of Stomatology, Wuhan University, Wuhan, China. The use of human tissues was in accordance with the National Institutes of Health guidelines, and written consent to publish this information was obtained from the study participants.

In August 2016, a 48-year-old man was admitted to the Department of Oral and Maxillofacial Surgery, School and Hospital of Stomatology, Wuhan University, with a chief complaint of swelling of the gingiva and mobility of molars in the left mandible. The gingival masses were noticed 4 years previously and he had experienced fluctuations in size for 4 years. One month previously, the gingival swelling and numbness of his left lower lip had become increasingly severe. He had a history of smoking 2.5 packs of cigarettes per day for 30 years, and alcohol consumption of 250 ml every day for 30 years. The patient denied experiencing any odontogenic symptoms before the appearance of the mandibular swelling. His medical history showed that he had had clear cell renal cell carcinoma (RCC) in the right kidney and had undergone a right nephrectomy to treat it in September 2015. He attended follow-up

1 Department of Stomatology, General Hospital of the Yangtze River Shipping, Wuhan, P.R. China.

2 Department of Oral and Maxillofacial Surgery, School & Hospital of Stomatology, Wuhan University, Wuhan 430079, P. R. China.

Corresponding author: Dr Zi Li YU, Department of Oral and Maxillofacial Surgery, School & Hospital of Stomatology, Wuhan University, #237 Luoyu Road, Wuhan 430079, P.R. China. Tel: 86-27-87686215. Email: zili09@whu.edu.cn

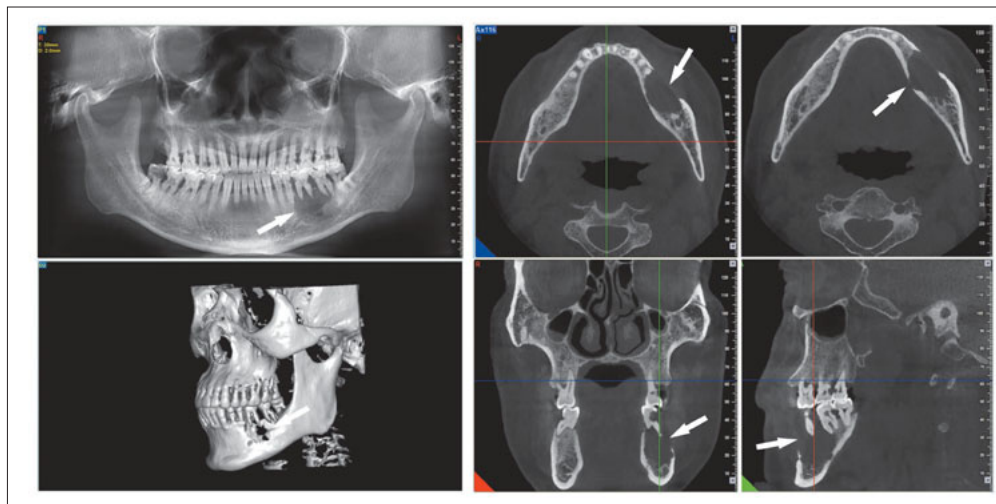


Fig 1 CBCT images of mandible lesion. The arrow indicates the location of the lesion.

visits for nearly 1 year and no metastasis was detected in the lungs, liver or left kidney. The physical examination showed a mass measuring 2 cm × 1 cm × 1 cm on the gingiva on the buccal side in the mandibular left molar region with no trismus. The mass was soft to the touch, fluctuant and tender. The mandibular left first and second molars displayed significant mobility. No ulceration was observed on the mass, and no cervical lymph node was palpable.

On the CBCT examination, a radiolucent, ill-defined lesion with dimensions of around 3.1 cm × 1.7 cm × 2.3 cm with no clear margin was observed at the apex of the mandibular left second premolar to second molar (Fig 1). The bone cortex on the buccal side of these teeth had disappeared and the bone continuity of the lingual side was interrupted. The chest radiograph did not show any abnormalities. The laboratory examination revealed no abnormalities except for increased uric acid (UA, 579 μmol/L). Considering the aforementioned clinical features, the patient was presumptively diagnosed with a malignant tumour of the left mandible. A biopsy specimen was taken of the gingival mass to identify the pathological nature of the mandible lesion. To the present authors' surprise, inflammatory cell infiltration was observed in the gingival swelling (Fig 2a) and there were no carcinoma cells in the gingival lesion. Confronted with this contradiction, we realised that the result of the biopsy specimen taken of the gingival mass might not represent the pathological nature of the mandibular lesion. After considering the results of the CBCT examination (a radiolucent, ill-defined lesion) and symptoms, such as numbness of the left lower lip, a decision was made to take an excisional biopsy specimen. The mandibular lesion was excised surgically in its entirety via mandibulectomy.

The surgical steps were as follows:

1. Extraction of the mandibular right central incisor;
2. Sectioning of the mandible near the extraction site;
3. Cutting of the associated muscles;
4. Opening of the temporomandibular joint capsule;
5. Complete removal of the patient's left mandible.

The patient was discharged 8 days after surgery for home care. Six months after the diagnosis of the mandible metastasis, he did not present any signs of recurrence.

Haematoxylin and eosin (H&E) staining showed that the lesions were composed of extensive areas of carcinoma cells forming small nests or clusters (Fig 2b). These cells have clear intracytoplasmic vacuoles and are arranged in nests that are invested by fibrous tissue, frequently small-calibre blood vessels and a small lake of erythrocytes. The nuclei of carcinoma cells are small, hyperchromatic and round. The histological characteristics of the left mandibular lesion met the diagnostic criteria for clear cell RCC¹⁰. Moreover, the lesion was located in the cancellous supporting bone and did not involve alveolar bone proper, compact supporting bone, periodontium or mucosa (Fig 2c).

Additional immunohistochemistry (IHC) staining revealed that the carcinoma cells were positive for vimentin, CD10, cytokeratin-19 (CK-19) and PCK but negative for CK-5/6, CK-7, CK-20, P63, smooth muscle actin (SMA) and calponin (Fig 3). The Ki-67 proliferation index was 30%. Considering these findings, this lesion was diagnosed as clear cell RCC metastasis to the left mandible. H&E staining was also used to evaluate the relationship between the gingival mass and metastatic carcinoma. As shown in Fig 4, inflammatory cell infiltration was observed in the gingival swelling. The inflammatory lesions and metastatic clear cell RCC

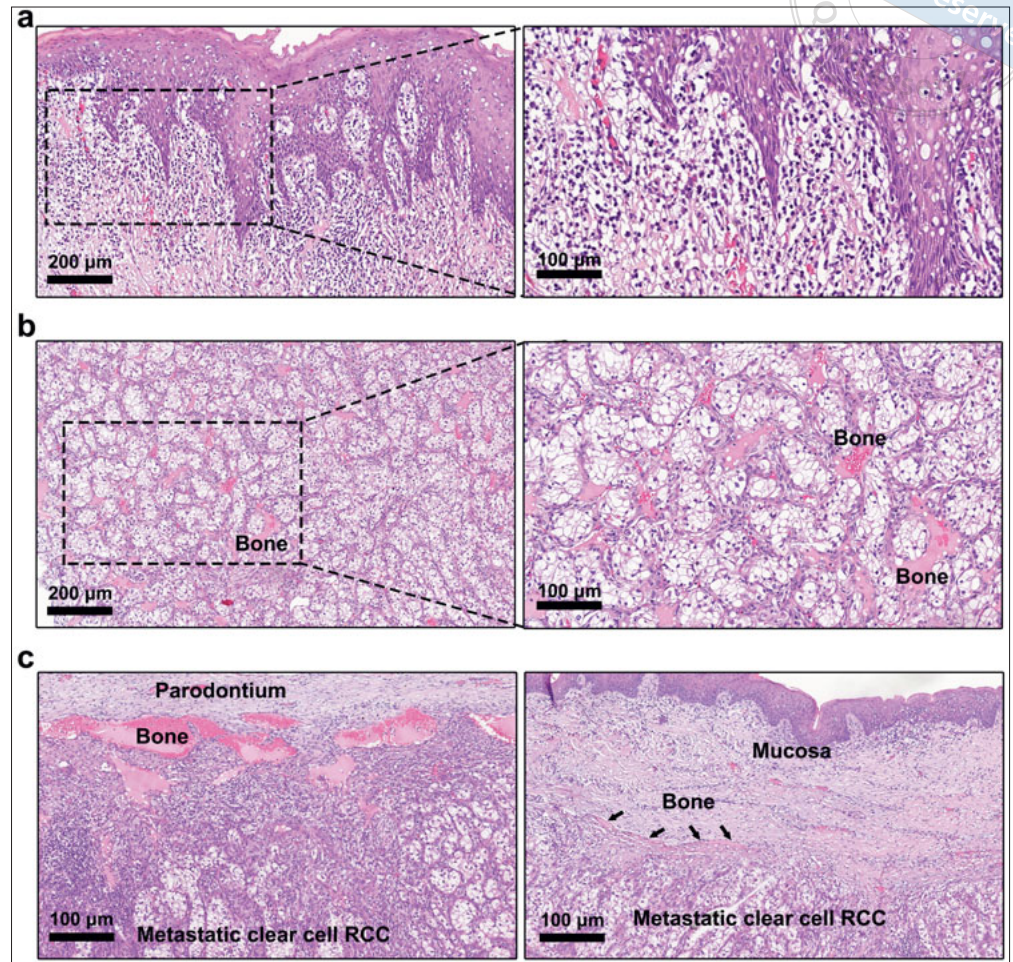


Fig 2 Results of the biopsy specimens taken of the gingival mass and mandibular lesion. The pathological nature of the (a) gingival mass and (b) mandibular lesion was determined by H&E staining. (c) Mandibular lesion located in the cancellous supporting bone.

were separated by compact supporting bone, indicating that the gingival inflammation had no direct connection with metastatic carcinoma.

Discussion

Metastatic cancer of the oral cavity is extremely rare¹¹, estimated to account for only around 1% of all diagnosed oral malignancies^{12,13}, and only 16% of these reported cases originate from the kidneys¹⁴. In many cases, metastasis is the first indication of clear cell RCC¹². Approximately one-third of clear cell RCC patients have distant metastatic disease at diagnosis. The most common sites of metastasis are the lung, liver, bone, brain and thyroid. Metastatic disease of the oral cavity is rare, but in the present patient, no metastasis was detected in the lungs, and a live, metastatic lesion was only observed in the left mandible. A severe smoking habit has been associated with the development of RCC. The present patient had a history of consistent smoking,

having consumed 2.5 packs of cigarettes per day for 30 years. The present authors speculate that the patient's mandibular metastatic cancer may be associated with his long-term history of heavy smoking.

A review of the scientific literature published in English reported five cases of metastatic clear cell RCC in the mandible (Table 1). The present authors report one more case. In the six cases, patients' age ranged from 48 to 71 years (mean 56.3 years). Oral metastasis was more frequent in men (four cases) than women (two cases), with a male/female ratio of 2:1. Among these six cases, three patients were identified to have simultaneous metastasis in the ribs, femur and ilium, along with metastasis in the mandible¹⁵; however, in two patients, including the patient in the present study, no metastasis was found in any bones apart from the mandible. Carcinoma cells were found in the gingival lesion in only one patient, indicating that mandibular metastasis does not typically involve the gingiva. According to the existing literature, metastasis of RCC to the gingiva

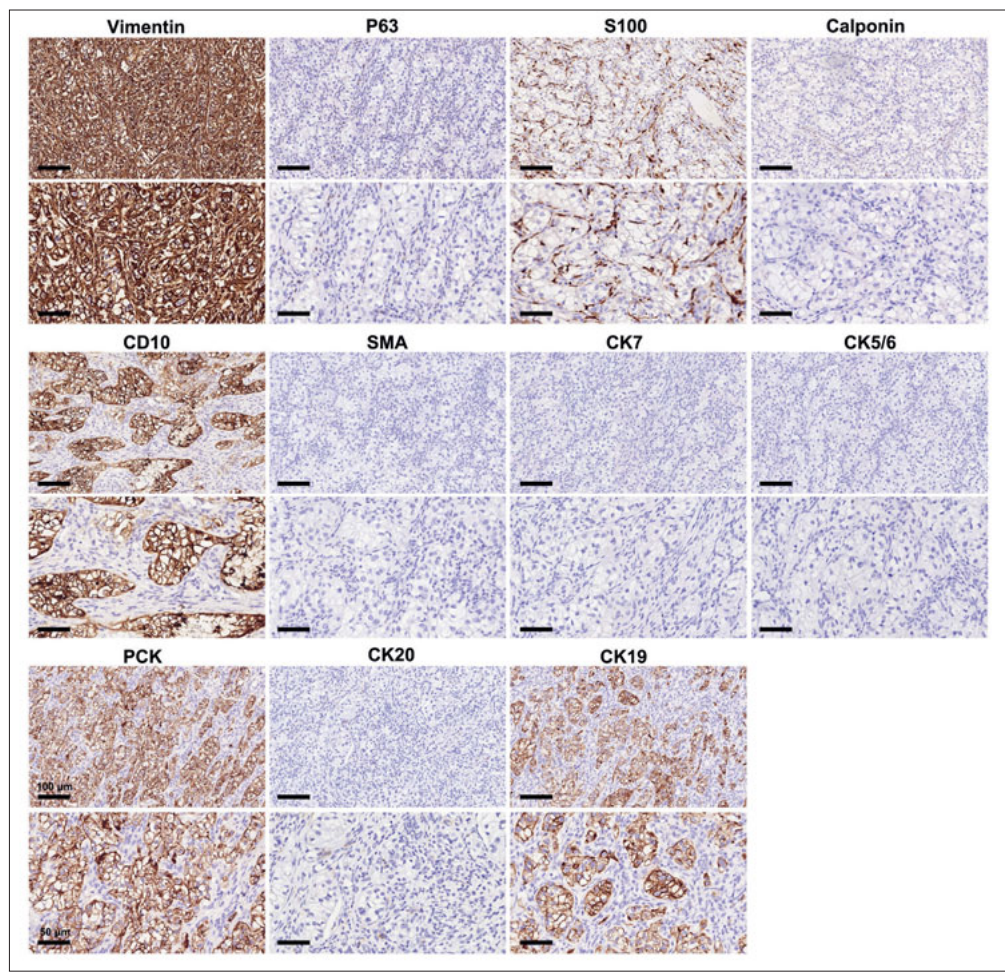


Fig 3 IHC staining images of the mandibular lesion.

is extremely rare, and the exact mechanism behind this phenomenon remains unclear. The phenomenon is that cancer cells are mainly located in the cancellous bone. First, tumour cells disseminate through the bloodstream and reach the trabecular bone. Once they reach the trabecular bone, they become trapped, which hinders their ability to reach the gingival tissue. Second, in contrast to the trabecular bone, the gingival mucosa is regularly exposed to external stimuli, leading to a more active mucosal immune system. This heightened immune activity is unfavourable for metastatic tumour growth in the gingival mucosa.

The diagnosis of metastatic RCC should ideally involve a comparison of the tissue acquired outside the site of primary disease to the primary histology. Histological evaluation should include common markers of RCC, including paired box gene 8 (PAX8) and carbonic anhydrase IX (CAIX). Clear cell RCC consists predominantly of clear cells, and these carcinomas can be difficult to distinguish from a wide variety of other clear cell tumours that may also involve the arches,

such as salivary gland (mucoepidermoid tumour, acinic cell tumour) and odontogenic tumours (calcifying epithelial odontogenic tumour, clear cell odontogenic carcinoma). IHC staining helps in this distinction. Clear cell odontogenic carcinoma immunohistochemically showed positive staining for CK-19 and epithelial membrane antigen (EMA), but negative for vimentin, SMA and S-100 protein. CK-19 has been proven to react with all kinds of odontogenic epithelial cells¹⁶. Both clear cell odontogenic carcinoma and clear cell RCC showed positive immunoreactivities in the cytoplasm for CK-19 and negative for SMA; however, most clear cell RCCs are positive for vimentin¹². CK-7 staining became negative and there was a strong reaction for vimentin, which rules out salivary gland tumours¹⁷. Additionally, the previous medical history of clear cell RCC was very helpful for diagnosing a metastatic lesion to the mandible of renal origin.

Tissue biopsy specimens are extremely useful for disease diagnosis. Because the gingival mass was in the region of the mandibular lesion, it would have

been easy to assume that the gingival mass originated from the mandibular lesion and thus had the same pathological characteristics; however, the pathological characteristic of the gingival mass was chronic inflammatory cell infiltration. The biopsy specimen taken of the gingival mass does not represent the pathological characteristics of the mandibular lesion and may even lead to misdiagnosis of such lesions. The present case shows that the biopsy sites play a crucial role in the diagnosis of lesions. As a result, multiple biopsy sites are encouraged¹⁸.

The prognosis for patients with oral metastases of RCC is usually poor¹². Most patients diagnosed with metastatic RCC to the oral cavity succumb to the disease within the first year, highlighting the fact that oral metastases often imply the presence of multiple metastatic sites¹⁹; however, no metastatic lesions were detected in the present patient's lungs or liver. To optimise the therapeutic effect and improve the survival rate, the mandibular lesion was excised radically in this case. After surgery, the patient was monitored diligently for 6 months, with three essential follow-up appointments scheduled. No complications or local oral recurrence were found. Regrettably, the patient chose not to attend any further examinations at the hospital. To ensure his well-being, the present authors maintained regular communication with him via phone to inquire about his condition and provide necessary support. The patient was still alive 1 year after diagnosis of the mandibular metastasis. Subsequently, metastasis was detected in the left leg and the patient died 15 months after mandibulectomy, having lived for around 2.5 years after the diagnosis of RCC.

According to the ASCO Guideline, all patients with metastatic RCC who require systemic therapy in the first-line setting should undergo risk stratification into risk grade: favourable (0), intermediate (1 to 2) and poor (3+) risk groups²⁰. For first-line systemic treatment of metastatic RCC, patients with intermediate- or poor-risk disease should be offered combination treatment with two immune checkpoint inhibitors (ICIs) or an ICI in combination with a vascular endothelial growth factor receptor r (VEGFR) tyrosine kinase inhibitor (TKI). Patients with favourable-risk disease who require systemic therapy may be offered an ICI in combination with a VEGFR TKI. For optimal second- or later-line systemic treatment, nivolumab or cabozantinib should be offered to patients who experienced progression on a VEGFR TKI alone. Patients progressing on combination immunotherapy should be offered a VEGFR TKI, and those who progress after initial therapy combining VEGFR TKI with an ICI may be offered an alter-

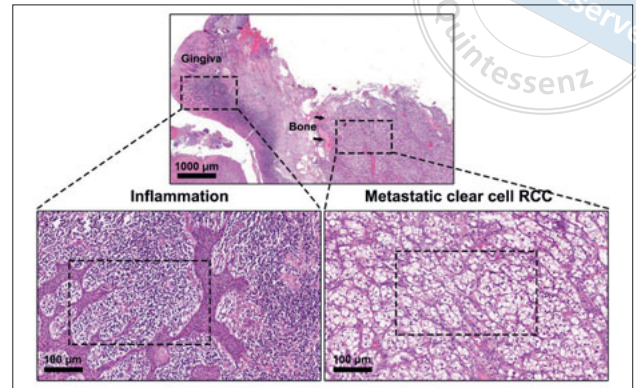


Fig 4 Pathological characteristics of the gingival mass.

nate VEGFR TKI as a single agent. Patients with bone metastases from metastatic RCC should be offered a bone resorption inhibitor when clinical concern for fracture or skeletal-related events is present. In the present case, the metastatic mandibular lesion was excised completely, which is in accordance with the ASCO guideline that recommends surgical resection for patients with low-volume metastatic RCC. There is no recommendation regarding optimal systemic treatment for metastatic RCC patients with bone metastasis. The present patient did not receive postoperative anti-tumour medication treatment.

Conclusion

Although oral metastatic tumours only represent approximately 1% of oral tumours, oral oncologists should be aware of and fully understand the patient's medical history.

Conflicts of interest

The authors declare no conflicts of interest related to this study.

Author contribution

Drs Xiao Fei HUANG and Zi Li YU analysed the data, performed the reference search, and drafted and revised the manuscript. Both authors read and approved the final manuscript.

(Received May 14, 2023; accepted Aug 10, 2023)



Table 1 Data on cases of clear cell RCC in the mandible.

Study	Histological type	Sex	Age, y	Location	Metastasis in other tissue
Pick et al ¹⁵	RCCC	Male	71	Left mandible	Ribs/cervical lymph node
Jones et al ¹⁴	CCRC	Female	62	Right mandible and gingiva	Femur/brain
Jones et al ¹⁴	CCRC	Female	52	Right mandible	Ilium
Van der Waal et al ¹³	RCCC	Male	48	Mandible	Not available
Ahmadnia et al ⁸	RCCC	Male	57	Right mandible	No
Huang et al (present study)	RCCC	Male	48	Left mandible	No

CCRC, clear cell renal carcinoma; RCCC, renal clear cell carcinoma.

References

- Xia C, Dong X, Li H, et al. Cancer statistics in China and United States. 2022: Profiles, trends, and determinants. *Chin Med J (Engl)* 2022;135:584–590.
- Bukavina L, Bensalah K, Bray F, et al. Epidemiology of renal cell carcinoma: 2022 update. *Eur Urol* 2022;82:529–542.
- Sheikh M, Mukeriya A, Zahed H, et al. Smoking cessation after diagnosis of kidney cancer is associated with reduced risk of mortality and cancer progression: A prospective cohort study. *J Clin Oncol* 2023;41:2747–2755.
- Ryan CW, Tangen CM, Heath EI, et al. Adjuvant everolimus after surgery for renal cell carcinoma (EVEREST): A double-blind, placebo-controlled, randomised, phase 3 trial. *Lancet* 2023;S0140-6736(23) 00913-3.
- He T, Zhang Q, Xu P, et al. Extracellular vesicle-circEHD2 promotes the progression of renal cell carcinoma by activating cancer-associated fibroblasts. *Mol Cancer* 2023;22:117.
- Rosellini M, Marchetti A, Mollica V, Rizzo A, Santoni M, Massari F. Prognostic and predictive biomarkers for immunotherapy in advanced renal cell carcinoma. *Nat Rev Urol* 2023;20:133–157.
- Mickisch GH. Multimodality treatment of metastatic renal cell carcinoma. *Expert Rev Anticancer Ther* 2002;2:681–685.
- Ahmadnia H, Amirmajidi NM, Mansourian E. Renal cell carcinoma presenting as mandibular metastasis. *Saudi J Kidney Dis Transpl* 2013;24:789–792.
- Nisi M, Izzetti R, Graziani F, Gabriele M. Renal cell carcinoma metastases to the oral cavity: Report of 2 cases and review of literature. *J Oral Maxillofac Surg* 2020;78:1557–1571.
- Edmondson EF, Hess AM, Powers BE. Prognostic significance of histologic features in canine renal cell carcinomas: 70 nephrectomies. *Vet Pathol* 2015;52:260–268.
- Owosho AA, Xu B, Kadempour A, et al. Metastatic solid tumors to the jaw and oral soft tissue: A retrospective clinical analysis of 44 patients from a single institution. *J Craniomaxillofac Surg* 2016;44:1047–1053.
- Makos CP, Psomadakis K. A literature review in renal carcinoma metastasis to the oral mucosa and a new report of an epulis-like metastasis. *J Oral Maxillofac Surg* 2009;67:653–660.
- van der Waal RI, Buter J, van der Waal I. Oral metastases: Report of 24 cases. *Br J Oral Maxillofac Surg* 2003;41:3–6.
- Jones GM, Telfer MR, Eveson JW. Metastatic renal clear cell carcinoma of the jaws. Two cases illustrating clinical and pathological diagnostic problems. *Br J Oral Maxillofac Surg* 1990;28:172–175.
- Pick JB, Wagner RM, Indresano AT. Initial appearance of renal cell carcinoma as a metastatic mass in the mandible. *J Am Dent Assoc* 1986;113:759–761.
- Kumamoto H, Yamazaki S, Sato A, Yamaguchi T, Tezuka F, Ooya K. Clear cell odontogenic tumor in the mandible: Report of a case with duct-like appearances and dentinoid induction. *J Oral Pathol Med* 2000;29:43–47.
- Abbaszadeh-Bidokhty H, Motallebnejad M, Rajabi-Moghaddam M. Metastatic renal cell carcinoma presenting as a clear-cell tumor in tongue: A case report. *Iran J Otorhinolaryngol* 2014;26:185–190.
- Albuquerque RPP, Richards A. Squamous-cell carcinoma of the tongue. *N Engl J Med* 2016;374:e32.
- Hatziotis JC, Constantinidou H, Papanayotou PH. Metastatic tumors of the oral soft tissues. Review of the literature and report of a case. *Oral Surg Oral Med Oral Pathol* 1973;36:544–550.
- Rathmell WK, Rumble RB, Van Veldhuizen PJ, et al. Management of metastatic clear cell renal cell carcinoma: ASCO guideline. *J Clin Oncol* 2022;40:2957–2995.

Guideline for the Diagnosis and Clinical Management of Oral Submucous Fibrosis

Society of Oral Medicine, Chinese Stomatological Association

Oral submucous fibrosis (OSF) is a chronic, progressive and potentially malignant oral mucosal disease. Patients often have a habit of chewing betel nuts. Areca catechu has been listed as a Class 1 carcinogen by the International Agency for Research on Cancer (IARC), and its main active component, arecoline, is classified as a Group 2B carcinogen by the IARC. The World Health Organization (WHO) categorises OSF as an oral potentially malignant disorder (OPMD). The present guideline describes the risk factors, clinical symptoms and clinical signs of OSF. Clinical staging, auxiliary examination methods, basis for diagnosis and differential diagnosis and the need to improve bad lifestyle habits are proposed and addressed, and local treatment drugs, therapies, dosage and course of treatment, possible adverse reactions, and oral treatment drugs, dosage and course of treatment are proposed. The guideline also addresses the indications for surgical treatment, alternative non-drug treatment methods, selection of treatment plans for different clinical stages, criteria for efficacy evaluation, and preventive measures.

Key words: carcinogenic, chewing betel nut, oral potentially malignant disorders, oral submucous fibrosis, risk factors

Chin J Dent Res 2023;26(4):271–285; doi: 10.3290/j.cjdr.b4784075

Preface

This document was prepared in accordance with the GB/T 1.1-2020 Structure and Drafting Rules for Standardisation Documents. It was proposed by the Chinese Society of Oral Medicine and is under the jurisdiction of the Chinese Stomatological Association.

Oral submucous fibrosis (OSF) is a chronic, progressive and potentially malignant oral mucosal disease. It is associated with various factors, and most patients who suffer from it have a habit of chewing betel nut, a chewing stimulant that is used widely in regions such as Hunan, Hainan and Taiwan in China, as well as in Southeast Asian countries like India, Pakistan and Vietnam. It has been classified as a Class 1 carcinogen by the International Agency for Research on Cancer

(IARC), and its main active component, arecoline, is classified as a Group 2B carcinogen by the IARC. The World Health Organization (WHO) categorises OSF as an oral potentially malignant disorder (OPMD)¹.

The clinical manifestations of OSF mainly include burning pain when eating, formation of oral submucous fibrous cords and limited mouth opening. At present, no evidence-based guidelines relating to OSF have been published in the field of stomatology in China. To standardise the diagnosis and clinical management of OSF, an expert group and working group for the development of guidelines for the diagnosis and clinical management of OSF were established under the leadership of Peking University School and Hospital of Stomatology and Xiangya Hospital of Central South University in conjunction with 22 colleges and universities and units nationwide after the approval of the group standard development project of the Chinese Stomatological Association (CHSA approval number: T/CHSA 044-2022). The working group followed the methodological system design of the second edition of the WHO handbook for guideline development issued in 2014, conducted a comprehensive search and careful evaluation of the relevant literature on OSF at home and abroad based on the Grading of Recommendations

Corresponding authors: Dr Hong Wei LIU, Department of Oral Medicine, Peking University, School and Hospital of Stomatology, #22, Zhong-guancun South Avenue, HaiDian District, Beijing 100081, P.R. China. Tel: 86-10-82195362. Email: hongweil2569@163.com.

Dr Xin Chun JIAN, Department of Oral and Maxillofacial Surgery, Xiangya Hospital, Central South University, #87 Xiangya Road, Changsha 410008, Hunan Province, P.R. China. Tel: 86-731-88908030. Email: drjianxin-chun@163.com

**Table 1** GRADE quality of evidence grading system description.

Level of evidence	Description
High (A)	Very confident, the observed value is close to the true value and further study will not change the credibility of the assessment results of this intervention.
Medium (B)	Moderate power for an observed value; the observed value is likely to be close to the true value but may vary widely; further research is likely to affect the credibility of the assessment results of this intervention and may alter them.
Low (C)	The power for an observation is limited and it is likely that the observation is very different from the true value; further research is very likely to affect the credibility of the assessment results of this intervention and is likely to change them.
Very low (D)	Little power is given to the observed value, which can be very different from the true value; any assessment is very uncertain.

Assessment, Development and Evaluation (GRADE) evidence quality grading system, and developed the exposure draft of the Guidelines for the Diagnosis and Clinical Management of OSF over 2 years. The guideline development process refers to the specifications of the Appraisal of Guidelines for Research and Evaluation (AGREE)-China quality evaluation standard system for clinical practice guidelines; the writing process refers to the requirements set out in the Reporting Items for Practice Guidelines in Health Care (RIGHT) guideline writing specifications to meet the trend of methodological development of current clinical practice guidelines.

The recommendations set out in the guidelines are divided into two major parts: the first concerns diagnosis of OSF, and the second part addresses its clinical management.

Scope

The target population of this guideline is patients in China who meet the diagnosis set out in the fifth edition of the 13th Five-Year Plan textbook “Oral Mucosal Diseases”². The International Classification of Diseases (ICD) code for the disease is ICD-11 DA02.2.

This guideline gives recommendations for the clinical diagnosis and treatment of OSF, and the user population comprises clinicians, dental practitioners, nursing staff, laboratory personnel, policy formulation and management personnel and other relevant professionals in various medical institutions at all levels in China.

Normative references

There are no normative references to this document.

Terms and definitions

The following terms and definitions are applicable to this document.

Abbreviation

OSF: this is a chronic, progressive oral mucosal disease with a tendency to become cancerous that is due to areca nut chewing, and is clinically characterised by burning pain in the oral mucosa, pain when eating irritating foods, loss of elasticity of the oral mucosa or formation of submucous fibrous cords, progressive limited mouth opening and dysphagia. The WHO lists OSF as a potential malignant disease of the oral cavity.

Coefficient of variation (CV)

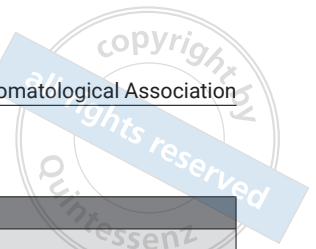
The absolute value reflecting the degree of data dispersion; taking the coefficient of variation (CV) = standard deviation/mean value in this Delphi method, it is believed that $CV > 0.3$ indicates that there is disagreement in expert opinions.

Guideline recommendations

General

The literature was screened according to the inclusion and exclusion criteria and the GRADE system was used as the evaluation criteria. The quality of evidence is shown in Table 1, in which systematic reviews and randomised controlled trials were used as high-quality evidence (downgraded as appropriate); cohort studies were considered medium-quality evidence (upgraded or downgraded as appropriate); case-control studies and case series analyses were used as low-quality evidence; and individual case reports and expert opinions were listed as very low-quality evidence. This guideline did not use the results of animal and in vitro experiments as evidence.

The recommendations for intervention measures are based on the Evidence to Decision (EtD) framework

**Table 2** Evidence to Recommendation (EtD) framework.

Content	Description
Prioritisation of issues	Prioritisation of issues
Benefit or risk	Degree of potential benefit (efficacy) to patients and the degree of possible risks (side effects, adverse reactions, etc.) to patients
Credibility of evidence	How credible the evidence population is
Importance of outcome measures	Whether there is significant uncertainty or variability in the judgment of primary outcome measures
Pros and cons balance	Judge whether the results tend to support the intervention or control from the perspective of the benefits and risks of the recommended intervention
Resource utilisation	How resource-intense an option is, if it is cost-effective and if there is incremental benefit. The more advantageous or clearly disadvantageous these resource implications are, the more likely is a strong recommendation
Equity	Impact on health-related equity
Acceptability	Whether the intervention is acceptable to stakeholders and meets the values or general wishes of the target population
Feasibility	Whether the intervention is possible to implement or whether the implementation process has the necessary prerequisites

Table 3 Recommendation strength description.

Recommended strength	Description
Strong	Clear support for the intervention, showing that the benefits outweigh the risks, and expert voting in Delphi, i.e., mean score > 7 and CV ≤ 0.3
Weak	The pros and cons of interventions are uncertain, or are comparable regardless of the quality of evidence, which may outweigh the pros and cons, with expert voting in Delphi averaging 5 to 7 and CV < 0.4
Good practice statement (GPS)	Recommendations based on non-direct evidence or expert opinion/experience, expert voting in Delphi, mean score 4 to 5 or CV > 0.4 with limited clinical reference

(Table 2), taking into account factors such as literature quality, socio-economic costs, values and willingness of users and target populations, feasibility and accessibility. Three rounds of Delphi questionnaire surveys, one face-to-face expert discussion and two online expert discussions were used to form recommendations. The recommendation strength of the intervention was based on the evaluation results of the body of evidence using the GRADE system and on the recommendations formed using the above EtD framework, referring to the mean score from the expert recommendation voting in the Delphi method questionnaire survey to form a graded recommendation intensity. (Table 3).

Guidelines for the diagnosis and treatment of OSF, part 1: Diagnosis

Risk factors for OSF

Recommendation

Areca nut chewing is a major risk factor for OSF (level of evidence, high; strength of recommendation, strong),

and the occurrence of OSF may also be related to genetics, smoking and autoimmunity (level of evidence, very low; strength of recommendation, good practice statement [GPS]).

Evidence overview

Previous reviews³⁻¹² and results of four epidemiological surveys¹³⁻¹⁶ showed that the prevalence of OSF in people who chew areca nut was higher than that in the normal population; from the above review, potential risk factors for OSF were selected and included in the two rounds of Delphi analysis by 52 experts.

Recommendation notes

The present recommendation is based on previous reviews, epidemiological surveys, and expert opinions and experience, because OSF mainly occurs in people with an areca nut chewing habit and in regions where this is common, and the incidence is higher in people who chew areca nut, so the history of this habit is one of the important foundations for the diagnosis of OSF.



Genetics, smoking, autoimmunity and other factors may also promote the occurrence of OSF.

Clinical symptoms of OSF

Recommendation

The clinical symptoms of OSF mainly include burning pain in the oral mucosa and when eating irritating food, inability to bulge the cheeks or whistle due to mucosal tightness (evidence level, very low; recommendation intensity, strong). Possible symptoms include limited tongue movement with dysphagia, dysphonia, dry mouth, hypogeusia and tongue numbness (evidence level, very low; recommendation intensity, weak).

Evidence overview

Clinical symptoms that may occur in OSF were screened from previous systematic reviews^{3,12,17-20} and clinical physician recommendations. After two rounds of Delphi analysis by 52 experts, the above symptoms were included.

Recommendation notes

This recommendation is based mainly on the comments from the expert group involved in the development of previous reviews and guidelines. Patients with OSF may present with different clinical symptoms at different stages of the disease, which has certain value for diagnosis.

Clinical signs of OSF

Recommendation

Clinical signs of OSF mainly include pale mucosa, decreased mucosal elasticity and hardening, fibrous strip formation, reduced mouth opening, mucosal blister or ulcer formation, impaired secretion of minor salivary glands ("blisters" when eating irritating foods, which can gradually subside; mucocele formation in severe cases) (level of evidence, high; strength of recommendation, strong). Possible signs of OSF include atrophy of the lingual papillae, shortening of the lingual palatal arch/pharyngeal palatal arch, uvula shrinkage, lip tissue atrophy (lip redness thinning, scar contraction, mouth fissure narrowing), fibrosis of the soft palate and uvula (may be associated with velopharyngeal insufficiency, mild nasal sounds or language disorders), narrowing of the tongue morphology or atrophy of the

lingual muscle (level of evidence, very low; strength of recommendation, weak).

Evidence overview

Clinical signs that may appear in OSF were selected from previous systematic reviews^{3,12,17-20} and clinicians' recommendations and included in the aforementioned clinical signs by two rounds of Delphi analysis by 52 experts.

Recommendation notes

This recommendation is mainly based on the comments of the guideline development expert group. Patients with OSF with lesions at different stages may present with different clinical signs, which has certain value for diagnosis. When measuring mouth opening, it is advisable to use the distance between the incisal edges of the central incisors as the standard. The reference measurement method is to ask the patient to actively open their mouth as wide as possible and use a vernier caliper to measure the distance between the incisal edges of the maxillary and mandibular central incisors. If there is a dentition defect, measure the interdental distance closest to the middle and with the occlusal relationship.

Clinical staging of OSF

Recommendations

See Table 4 for details (level of evidence, high; strength of recommendation, strong).

Evidence overview

The clinical staging criteria refer to Professor Jian Xinchun's 2009 OSF diagnostic criteria published in 2009²¹ and Khanna-Andrade²² staging, from which several representative clinical symptoms or signs were selected and summarised into clinical stages with mouth opening as the main reference standard, which was statistically passed by Delphi method in two rounds by 52 experts.

Recommendation notes

The clinical staging of OSF has guiding significance for treatment. Defining the clinical stages of OSF can provide an objective reference standard for future clinical research and treatment.

**Table 4** Clinical staging criteria for OSF.

Phase	Description
Phase I	When mouth opening is ≥ 30 mm, the oral mucosa shows local or scattered white changes; the texture is not changed or rough, and the elasticity is not significantly changed
Phase II	Mouth opening is 20 to 30 mm, the colour of mucosa shows a flaky white appearance or strip formation; the texture becomes hard and the elasticity decreases
Phase III	Mouth opening is 10 to 20 mm, the oral mucosa is widely white changed and stripes are formed; the texture becomes hard, with a plate- or leather-like appearance upon palpation, and poor elasticity
Stage IV	Mouth opening ≤ 10 mm, with leucoplakia or oral squamous cell carcinoma

Note: 1. The symptoms and signs that may occur in each phase include burning sensation, pain and ulceration (if there are no other symptoms or signs, it is classified as phase I). One of the manifestations listed in each stage can be classified as phase I.

2. Scope of lesions: The oral mucosa is divided into five regions: lip and perioral; buccal mucosa and transitional sulcus; tongue; floor of mouth; and soft palate, tongue and palate arch, and uvula. Stage I involves one to two regions; phase II involves three regions; and phase III involves four to five regions.

3. Patients with leucoplakia/oral squamous cell carcinoma, regardless of the above findings, are classified as phase IV.

4. If the clinical manifestations in different regions are in different phases, diagnose according to more advanced phases.

Auxiliary examination method for OSF

Recommendation

Histopathological examination is the gold standard for the diagnosis of OSF (level of evidence, high; strength of recommendation, strong). For patients with leucoplakia/epithelial dysplasia, histopathological examination is recommended. At the same time, the results of autofluorescence examination, toluidine blue staining, exfoliative cell smear and other precancerous lesion examinations can be referred to diagnosis of leucoplakia/epithelial dysplasia (level of evidence, high; strength of recommendation, weak).

Evidence overview

Auxiliary examination methods that may be used for OSF were selected from previous systematic reviews²²⁻²⁶ and clinician recommendations and passed two rounds of Delphi analysis by 52 experts.

Recommended statement

Histopathological examination is the most reliable method for the diagnosis of OSF in clinical practice and has been widely used in previous randomised controlled trials, cohort studies and case-control studies. For patients with leucoplakia/epithelial dysplasia, histopathological examination is required to determine the progression status of the disease and the need for early surgical intervention.

Differential diagnosis of OSF

Recommendation

OSF needs to be differentiated from leucoplakia of oral mucosa (level of evidence, low; strength of recommendation, weak), lichen planus (level of evidence, low; strength of recommendation, weak), keratosis alba (level of evidence, low; strength of recommendation, weak) and white oedema (level of evidence, low; strength of recommendation, GPS).

Evidence overview

Diseases that may require differential diagnosis with OSF were selected from previous systematic reviews²²⁻²⁶ and clinician recommendations and passed two rounds of Delphi analysis by 52 experts.

Recommendation notes

This recommendation is based on previous reviews^{3,12,17-20} and the comments from the expert group that developed the guideline. The main diseases that need to be differentiated from OSF are those characterised primarily by white lesions.

Diagnosis basis of OSF

Recommendation

The diagnosis of OSF should be based on the following criteria:



- history of areca nut chewing (level of evidence, high; strength of recommendation: strong);
- typical clinical symptoms or signs (level of evidence, high; strength of recommendation, strong);
- histopathological findings (level of evidence, high; strength of recommendation: strong);
- auxiliary examinations suggestive of carcinogenesis: autofluorescence examination, toluidine blue staining, exfoliated cell smear (level of evidence, low; strength of recommendation, weak).

Evidence overview

Taking into account aforementioned the risk factors, clinical symptoms, clinical signs, and auxiliary examination methods for OSF, the items that may be used as the basis for the diagnosis of OSF were selected and 52 experts conducted and passed two rounds of Delphi analysis.

Recommendation notes

This recommendation is based on the opinion of the guideline development panel. A diagnosis of OSF can be made mainly with reference to the patient's history of areca nut chewing, typical clinical symptoms or signs and histopathological examination results.

Part 2: Clinical management

Patients with OSF need to improve their bad lifestyle habits

Recommendations

Patients need to abstain from areca nut chewing (level of evidence, high; strength of recommendation, strong), stop smoking (level of evidence, moderate; strength of recommendation, strong) and abstain from alcohol prior to treatment (level of evidence, moderate; strength of recommendation, weak). Stopping consuming betel nuts, smoking and drinking alcohol and reducing intake of spicy, irritating and rough foods are effective preventive measures against OSF (level of evidence, moderate; strength of recommendation, weak).

Evidence overview

Based on the above-mentioned risk factors for OSF combined with clinicians' suggestions, the measures that may be taken for the management of patients with OSF

were selected and 52 experts conducted and passed two rounds of Delphi analysis.

Recommendation notes

This recommendation is based primarily on the opinion of the Expert Group on Epidemiological Surveys, Cohort Studies and Guideline Development. OSF is one of the potential malignant diseases of the oral cavity, and bad habits that are not conducive to treatment such as areca nut chewing, smoking and alcohol consumption can be first corrected in patients prior to treatment. Abstaining from these and reducing intake of spicy, irritating and rough foods are effective preventive measures for OSF.

Drugs and therapies, dose and course of treatment available for local treatment of OSF

Recommendations

- Local injection of triamcinolone acetonide + lidocaine (10 mg/ml triamcinolone acetonide suspension 2 to 3 ml + 1 ml lidocaine, bilateral submucosal multi-point injection) (level of evidence, high; strength of recommendation, strong);
- Local injection of triamcinolone acetonide + lidocaine + salvia miltiorrhiza or tanshinone (50 mg triamcinolone acetonide + 2 ml lidocaine, 4 ml after shaking, 2 ml bilateral submucosal multi-point injection, followed by 2 mg salvia miltiorrhiza or tanshinone solution on each side) (level of evidence, high; strength of recommendation, strong);
- Local injection of triamcinolone acetonide (2 to 40 mg, bilateral submucosal multi-point injection) (level of evidence, high; strength of recommendation, weak);
- Hyaluronidase + triamcinolone acetonide injection (topical injection of 1500 IU hyaluronidase every 1 to 2 weeks, mixed with 10 mg triamcinolone acetonide) (level of evidence, high; strength of recommendation, weak).

Local injection treatment should be administered once every 1 to 2 weeks, with a treatment course lasting 4 to 10 weeks. The specific dosage and number of courses of treatment should be determined based on the individual patient's condition. There should be an interval of 1 to 2 months between each treatment course (level of evidence, high; strength of recommendation, strong).



Evidence overview

Two meta-analyses^{27,28} and 14 randomised controlled studies²⁹⁻⁴² showed that Danshen injection combined with steroid therapy could increase maximum mouth opening significantly and reduce the burning sensation of the oral mucosa in patients and reduce the area of oral mucosal lesions without increasing adverse reactions. According to the aforementioned literature and based on clinical experience, the local injection drugs and treatment courses that may be used for OSF were selected and passed by Delphi method in two rounds by 52 experts.

Recommendation description

This recommendation is mainly based on meta-analysis, randomised controlled trials and the opinions of expert groups in guideline development. The above operation mode and dose are only used as references, and the clinical operation should be adjusted according to patients' specific circumstances. In addition to the above recommendations, the local therapeutic drugs recommended by experts for OSF include compound Danshen tablets made into sublingual paste, topical application of epidermal growth factor, topical application of triamcinolone acetonide oral ointment and other doses for treatment. Due to insufficient evidence or a lack of consensus among experts, they are not included in this guideline.

Possible adverse reactions to drugs for topical treatment of OSF

Recommendations

Possible adverse reactions to tanshinone injection include allergy (shock, laryngeal oedema, dyspnoea, palpitation), transient elevated blood pressure, local pain and headache (level of evidence, high; strength of recommendation, weak). Potential reactions to triamcinolone acetonide include glucocorticoid-related adverse reactions (Cushing syndrome, calcium and potassium loss, induced or aggravated infection, or neurological symptoms such as agitation, insomnia and seizures) (level of evidence, high; strength of recommendation, weak).

Evidence overview

The adverse reactions that may occur in the use of related drugs were summarised from the drug instructions

and expert experience, which were passed by Delphi method in 2 rounds by 52 experts.

Recommendation notes

This recommendation is based mainly on the comments from the expert group for the development of drug instructions and guidelines. Adverse reactions shall be based on those indicated in the package insert. The possible adverse reactions should be explained to patients prior to local treatment. Patients' medical history should be taken before treatment to determine whether they have any systemic diseases or general conditions that may affect treatment or lead to an intolerance to treatment. For patients with poor control of hypertension and diabetes, glucocorticoids can be used with caution.

Drugs, dosage and course available for oral treatment of OSF

Recommendations

Danshen dripping pills can be used for systemic treatment of OSF. The recommended dose is 540 mg daily for 12 weeks (level of evidence, high; strength of recommendation, strong), and lycopene can be employed at a recommended dose of 6 to 24 mg daily for 3 to 6 months (level of evidence, high; strength of recommendation, weak).

Traditional Chinese medicine (TCM) can be used to treat OSF, which is differentiated according to individual conditions (level of evidence, moderate; strength of recommendation, weak). Vitamins and trace elements can be used for adjuvant treatment of OSF, and the recommended dose is vitamin A (25,000 IU once daily) combined with zinc agents (such as zinc gluconate, used with reference to the instructions) for 4 months (level of evidence, moderate; strength of recommendation, weak).

Evidence overview

A randomised controlled trial found that multi-point injection of triamcinolone acetonide acetate along with use of sublingual compound Danshen dripping pills was more effective than local injection of hormones only⁴³. Combined with the above literature, relevant reviews⁴⁴⁻⁵⁷ and clinicians' suggestions, the drugs that may be used for oral treatment of OSF were selected and passed by Delphi method in two rounds by 52 experts.

Recommended instructions

This recommendation is based mainly on randomised controlled clinical studies and was formed in combination with the comments of an expert group. In the aforementioned studies, oral drugs except TCM were used in combination with local injection drugs, and few clinical studies used oral drugs alone, suggesting that the treatment of OSF can focus mainly on local treatment at present and be supplemented by oral medication. Vitamins and trace elements may be used as adjunctive therapeutic agents.

Indications for surgical treatment of OSF

Recommendations

Indications include pooled heterogeneous leucoplakia (level of evidence, moderate; strength of recommendation, strong) and other symptoms that seriously affect patients' quality of life (such as pharyngeal arch adhesion affecting eating) (level of evidence, moderate; strength of recommendation, strong).

Histopathological examination revealed epithelial dysplasia (level of evidence, moderate; strength of recommendation, strong). This was combined with impacted third molars, recurrent ulcers and a wound surface higher than the mucosal surface (level of evidence, moderate; strength of recommendation, strong).

Limited mouth opening affects oral therapy (e.g., extraction of impacted the third molar, implant restorations) (level of evidence, moderate; strength of recommendation, weak). Mouth opening is less than 10 mm (level of evidence, medium; strength of recommendation, weak). Patients needed rapid improvement in mouth opening limitation (level of evidence, moderate; strength of recommendation: weak) and requested surgery and signed an informed consent (level of evidence, moderate; strength of recommendation, weak).

Evidence overview

Seven case reports⁵⁸⁻⁶³ and six reviews⁶⁴⁻⁶⁹ showed that surgical treatment improved mouth opening significantly and rapidly in patients with OSF.

Recommendation description

This recommendation is mainly based on case reports and expert opinions. Surgical treatment is an effective means to relieve the limitation of mouth opening in patients with OSF, but because it was reported at the

end of the last century that patients with OSF had limited mouth opening again after surgical treatment due to scar contracture, implantation of artificial skin materials and other reasons, the exploration of surgical treatment of OSF gradually slowed down. In recent years, due to the development of surgical techniques and artificial skin materials, the incidence of postoperative recurrence of limited mouth opening has been reduced compared with in the past. After expert discussion, it is believed that patients with heterogeneous leucoplakia, severely impacted quality of life, epithelial dysplasia and third molar impaction are recommended for surgical treatment, and patients with limited mouth opening affecting oral treatment, mouth opening < 10 mm, and who need rapid improvement of mouth opening undergo surgical treatment as appropriate. An informed consent form was required before surgery, and the risk of recurrence of limited mouth opening was explained to the patient.

Other non-pharmacological treatments for OSF

Recommendations

Other treatments for OSF include mouth opening training (level of evidence, high; strength of recommendation, strong), hyperbaric oxygen therapy (level of evidence, low; strength of recommendation, weak), photodynamic therapy (level of evidence, very low; strength of recommendation, weak) and laser therapy (level of evidence, very low; strength of recommendation, weak).

Evidence overview

One case observation⁷¹ and one systematic review⁷² showed that mouth opening training has an effect on improving mouth opening and maintaining therapeutic effects in patients with OSF. (numbers in superscript) Five case observations showed an effect of hyperbaric oxygen therapy helps to improve symptoms of OSF⁷²⁻⁷⁶. It was passed by Delphi method by 52 experts.

Recommendation notes

This recommendation is mainly based on the opinions of randomised controlled studies, case observations and consensus of expert groups. Mouth opening training is an effective way to improve mouth opening in patients with OSF and has a significant effect on the maintenance of therapeutic effects. Hyperbaric oxygen therapy,

photodynamic therapy and laser therapy play a role in relieving the symptoms of OSF and can be used as an adjunct to treatment.

Selection of treatment plans for different clinical stages of OSF

Recommendations

- Phase I: observation after education, local injection drug therapy, oral drug therapy (combined with local injection or used alone) and other therapies (such as hyperbaric oxygen therapy);
- Phase II: education, local injection drug therapy (can be combined with oral drug therapy) and other therapies (photodynamic therapy, hyperbaric oxygen therapy, mouth opening training, laser therapy, etc.);
- Phase III: education, local injection drug therapy (can be combined with oral drug therapy), other therapies (photodynamic therapy, hyperbaric oxygen therapy, mouth opening training, laser therapy, etc.), surgery as appropriate;
- Phase IV: education, surgical treatment, local injection drug therapy (can be combined with oral drug therapy) and other treatments (photodynamic therapy, hyperbaric oxygen therapy, mouth opening training, laser therapy, etc.).

Evidence overview

Referring to the above clinical symptoms, signs, staging and treatment options for OSF combined with clinician recommendations, 52 experts passed two rounds of Delphi method analysis.

Recommended instructions

The treatment options for patients with different stages of OSF may vary. Clinicians need to select the treatment that is appropriate to patients' specific circumstances. Some experts believe that patients without obvious symptoms in the first stage can only be educated, and if the lesion progresses, further treatment with medication, surgery and so on can be performed.

Efficacy criteria for the treatment of patients with OSF

Recommendations

- Recovered: mouth opening returned to > 30 mm or normal, oral mucosal elasticity recovered, pale mu-

cosa disappeared, oral submucosal fibrous cords disappeared, burning pain in general and when eating disappeared, symptoms of mucosal "tightness" disappeared (bulging cheeks or whistling were possible) (level of evidence, high; strength of recommendation, strong);

- Significantly effective (or significantly improved): partial recovery of mouth opening (amount recovered > 20 mm or recovered to > 25 mm), increased elasticity of oral mucosa, reduction/disappearance of mucosal pallor, reduction/disappearance of oral submucosal fibrous cords, reduction/disappearance of burning pain in general and when eating, reduction/disappearance of symptoms of mucosal "tightness" (level of evidence, high; strength of recommendation, strong);
- Improvement: minimal recovery of mouth opening (recovery > 10 mm or to > 20 mm), increased elasticity of oral mucosa, decreased paleness of mucosa, decreased fibrous cords in oral submucosa, reduced burning pain in general and when eating, reduced symptoms of mucosal "tightness" (level of evidence, high; strength of recommendation, strong);
- Ineffective: no improvement in limitation of mouth opening (amount recovered < 10 mm or recovered to < 15 mm), carcinogenesis, no improvement in oral mucosal elasticity, no improvement in the degree of mucosal pallor, no reduction in oral submucosal fibrous cords, no relief of burning pain in general and when eating, and no improvement in symptoms of mucosal "tightness" (level of evidence, high; strength of recommendation, strong).

Evidence overview

Referring to the above clinical symptoms, signs and staging of OSF combined with clinicians' suggestions, four criteria for the efficacy of treatment of OSF were proposed and passed by Delphi method in two rounds by 52 experts.

Recommendation notes

This recommendation is mainly based on the comments from the guideline development expert group. The objective evaluation of the therapeutic effect takes the degree of mouth opening as the main standard, which referred to other indicators. If the items are in different classifications, the grade with the best efficacy should prevail (if there are both recovered and significantly effective items, the final treatment efficacy is recovered).

Prevention of OSF

Suggestions for stopping areca nut chewing

Recommendations

Suggestions for stopping areca nut chewing for the public include:

- Strengthening popular science and education: publicising the harm that areca nut chewing can cause and resisting the transmission of areca nut;
- Controlling the placement of betel nuts: prohibiting placing them in easily accessible locations and advertising them;
- Not adding opioids, nicotine, ephedra and other addictive substances to areca nut;
- Placing a warning on products regarding the consumption of areca nut (for example, warning: chewing areca nut may cause oral cancer).

Summary of evidence

Based on expert opinions and referring to relevant policies and measures for stopping smoking, the evidence was discussed and adopted by Delphi method.

Recommendation notes

This recommendation is mainly based on the comments from the guideline development expert group. Experts believe that areca nut can cause substance dependence, but there is still disagreement regarding whether it is a psychoactive substance. The State Radio and Television Administration of China issued a notice in September 2021 to stop radio and television and online audiovisual programmes being used to publicise and promote areca nut and its products. Experts did not achieve a consensus on whether increasing the price of areca nut products helps individuals to stop consuming them.

Measures for stopping areca nut chewing

Recommendations

The measures to quit areca nut that can be used for individuals are as follows:

- Identifying the hazards of areca nut chewing: recognising that areca nut chewing may lead to OSF and/or oral cancer;
- Stopping chewing areca nut and using chewing substitutes, such as gum and liquorice;
- Diverting attention, exercising when wanting to chew areca nut, etc.;

- Being supervised by relatives and friends: asking family members, relatives and friends to offer supervision and dissuade from chewing areca nut.

Summary of evidence

Based on expert opinion, relevant policies and measures for stopping smoking were discussed and evidence was adopted by Delphi method.

Recommendation notes

This recommendation is mainly based on the comments from the guideline development expert group. The above measures can be used as a reference for people who need to stop chewing areca nut. In addition, with regard to the possible reactions during withdrawal from chewing areca nut, the large differences between individuals mean that more clinical observation is required. There are also significant differences in expert opinions, which are not included in this guideline for the time being.

Advantages and disadvantages of guideline implementation

Favourable factors

Further attention will be paid to the standardised diagnosis and treatment of OSF; medical institutions at all levels in all regions can select a reasonable clinical management plan according to their own actual situation and patients' wishes, values and preferences.

Adverse factors

As a chronic progressive disease, OSF may have a carcinogenic outcome, and this guideline does not discuss the relevant parts of malignancy. There are relatively few references in some parts of this guideline, and recommendations are formed based on the opinions of the expert group.

Limitations and deficiencies of the guideline

This guideline is intended for the Chinese population, but does not distinguish the ethnic characteristics of the population. There may be some deviations in the application process for the guideline of different ethnic groups. The clinical data derived from the Chinese population are concentrated in Hunan and Taiwan, and



there may be some deviations in the application process in other regions.

Appendix

Specific method for preparing the guidelines: Guideline development methodology

This guideline was prepared by referring to the relevant methodological standards in the WHO handbook for guideline development issued in 2015, as well as the contents of the guideline for developing the Report Checklist of AGREE-China, and according to the RIGHT Items statement.

Composition of the working group on guidelines

A guideline development expert group and working group were formed in April 2019. The working group is composed of young and middle-aged physicians engaged in the clinical diagnosis and treatment of oral mucosal diseases in Hunan, Hainan, Beijing and other regions who are especially familiar with the diagnosis and treatment of OSF, and the group leader is Professor Wu Yingfang. The expert group is composed of the members superior to the standing committee level of the Specialised Committee of Oral Mucosal Diseases, Chinese Stomatological Association and senior experts familiar with the diagnosis and treatment of OSF in China. The members specialise in oral mucosal diseases, oral and maxillofacial surgery and TCM, and the leader is Professor Liu Hongwei. Patients' values and wishes (for example, acceptance of invasive testing methods) were considered in the development of clinical questions and recommendations.

Collection and selection of clinical questions

Through systematic inquiry into published literature and systematic reviews on OSF, based on the population, intervention, control and outcome (PICO) principle of clinical study and combined with interviews with intended users of guidelines such as clinicians, this working group preliminarily drafted a list of clinical problems of interest and created a list of clinical problems in this guideline through analysis, classification and combination, with a total of seven diagnostic problems and ten clinical management problems.

Evidence retrieval, synthesis and evaluation

This guideline deconstructs the clinical questions and outcome measures included according to the PICO prin-

ciples, develops inclusion and exclusion criteria and conducts the relevant literature search.

Inclusion and exclusion criteria

The inclusion criteria were as follows:

- Study subjects: patients with OSF or OSF accompanied by oral leucoplakia and/or oral squamous cell carcinoma;
- Interventions and comparative measures: not limited;
- Outcome measures: not limited;
- Type of study: retrieval of case reports, observational studies, clinical studies, systematic reviews, meta-analyses and consensus or guidelines related to OSF.

The exclusion criteria were duplicate publications and proposals.

Data sources

The data sources were Chinese databases (CNKI, Wanfang Database, Chinese Biomedical Literature Database and VIP Database), English databases (PubMed, Cochrane Library and EMBASE) and data resources related to guidelines (American Clinical Guideline Center, National Institute for Health and Clinical Excellence, Scottish Intercollegiate Guideline Network and Yimaitong), and supplementary searching was performed using Baidu Scholar, Google Scholar, etc. The search period spanned from 1968 to 2021.

Search keywords

The search keywords included oral submucosal fibrosis, diagnosis, treatment or management. Foreign language databases searched the MeSH vocabulary for relevant topics, listing the following subject headings/keywords and their combined forms: oral submucous fibrosis, oral; oral submucous fibrosis; disease management; management; therapeutic; therapy; clinic; treatment; treatments; examinations; examinations; diagnosis, diagnosis; diagnosis.

Quality assessment

This guideline uses A Measurement Tool to Assess Systematic Reviews (AMSTAR)⁷⁷, Cochrane Risk of Bias (ROB)⁷⁸ and Quality Assessment of Diagnostic Accuracy Studies (QUADAS-2)⁷⁹ to evaluate the methodological quality of the included systematic reviews/meta-analyses, randomised controlled trials, diagnostic studies



and observational studies. The evaluation process was completed independently by two individuals, and any disagreements were resolved through discussion or consultation with a third party. Evidence and recommendations were graded using the GRADE Quality of Evidence Evaluation System⁸⁰⁻⁸² (Tables 1 and 3).

Form recommendation

Based on the evidence bodies related to various clinical problems, and with reference to relevant guideline evidence and expert opinions for some problems, the guideline working group also considered the diagnosis and treatment wishes of the Chinese patient population, human and economic costs, and the actual situation of medical institutions at all levels in all regions, focused on the risks/benefits of intervention measures, universal accessibility and feasibility in China, and formulated 17 recommendation opinions. The recommendations of this guideline were finally formed after three rounds of a Delphi questionnaire, one face-to-face expert discussion and two expert discussions.

Dissemination and implementation

The exposure draft of the guidelines was improved and revised, and then submitted to the expert steering committee for review. After further review and approval by the relevant administrative authorities of the Chinese Society of Stomatology, the formal release version will be created and released to the public. After the issuance of the formal version, the sponsor of these guidelines will disseminate and promote them in the following ways:

- By introducing and interpreting the guidelines at relevant academic conferences;
- By published the guidelines in professional academic journals and guideline databases;
- By disseminating the guidelines through the official publicity platform of each initiator (such as public number);
- By publicising the guidelines in all types of continuing education training at all levels so they can be interpreted by dental practitioners nationwide.

Update of guidelines

The guideline working group plans to update these guidelines 3 to 5 years after they are issued, or based on actual clinical needs and major research progress in this field at home and abroad. The updated method is performed according to the updated process of the guidelines.

Author contribution

This document was drafted by experts from Peking University School and Hospital of Stomatology; Xiangya Hospital of Central South University; Beijing Hospital; Changsha Stomatological Hospital; Hospital of Stomatology, Guangxi Medical University; Affiliated Stomatological Hospital of Guizhou Medical University; Haikou People's Hospital; Hainan General Hospital; The Second Affiliated Hospital of Hainan Medical University; The First Affiliated Hospital of Hainan Medical University; School of Stomatology of Hainan Medical University; Stomatological Hospital of Hebei Medical University; The First Hospital of Hunan University of Chinese Medicine; The Third Affiliated Hospital of Air Force Military Medical University; Affiliated Stomatological Hospital of Kunming Medical University; Affiliated Stomatological Hospital of Nanchang University; Qingdao Stomatological Hospital; Affiliated Stomatological Hospital of Nanjing University School of Medicine; Sanya People's Hospital; Sanya Central Hospital; Shanxi Medical University Stomatological Hospital; The Ninth People's Hospital of Shanghai Jiaotong University School of Medicine; Shanghai Tongji University Stomatological Hospital; Capital Medical University Beijing Stomatological Hospital; West China Stomatological Hospital of Sichuan University; Affiliated Stomatological Hospital of Tongji University; Stomatological Hospital of Wuhan University; Affiliated Stomatological Hospital of Southwest Medical University; Xiangtan Stomatological Hospital; The Second Affiliated Hospital of Zhejiang University School of Medicine; Stomatology Hospital, Zhejiang University School of Medicine; Affiliated Stomatological Hospital of China Medical University; Xiangya Stomatological Hospital of Central South University; The Second Xiangya Hospital of Central South University; Affiliated Stomatological Hospital of Sun Yat-sen University.

The main drafters of this document were Drs Wu Yingfang*, Wang Yutian*, Huang Guodong, Liu Zijian, Jian Xinchun and Liu Hongwei.

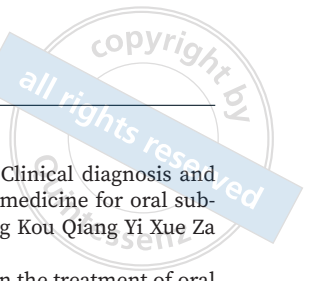
The individuals involved in the formulation/drafting of this document, listed in alphabetical order based on the first letter of their pinyin names, were as follows: Cai Yang, Zeng Xin, Chen Chen, Chen Jun, Chen Qianming, Chen Lizhong, Cheng Bin, Dan Hongxia, Du Yongxiu, Fang Changyun, Feng Hui, Fu Qiya, Gao Xing, Gao Yijun, Guan Xiaobing, Han Ying, He Shengteng, He Yuan, Hong Yun, Hu Yanjia, Huang Xieshan, Jiang Lu, Jiang Canhua, Jiang Weiwen, Li Chuanzhen, Li Ming, Li Ning,

* Drs Wu Yingfang and Wang Yutian contributed equally to the drafting of this document.

Li Pengcheng, Li Yanli, Li Yuancong, Ling Tianyong, Liu Binjie, Liu Deyu, Liu Li, Liu Yiping, Liu Zhiwen, Ma Liwei, Min Anjie, Nie Minhai, Peng Jieying, Su Tong, Tan Jin, Tang Guoyao, Tang Jieqing, Tao Renchuan, Wang Hong, Wang Hui, Wang Jinling, Wang Wanchun, Wang Xiang, Wang Xinwen, Wu Lan, Xiehui, Xie Xiaoyan, Xu Chunjiao, Yan Zhimin, Zhang fang, Zhang Jing, Zhang Ying, Zhang Yuxing, Zhao Danping, Zhou Gang, Zhu Lilei and Zong Juanjuan.

References

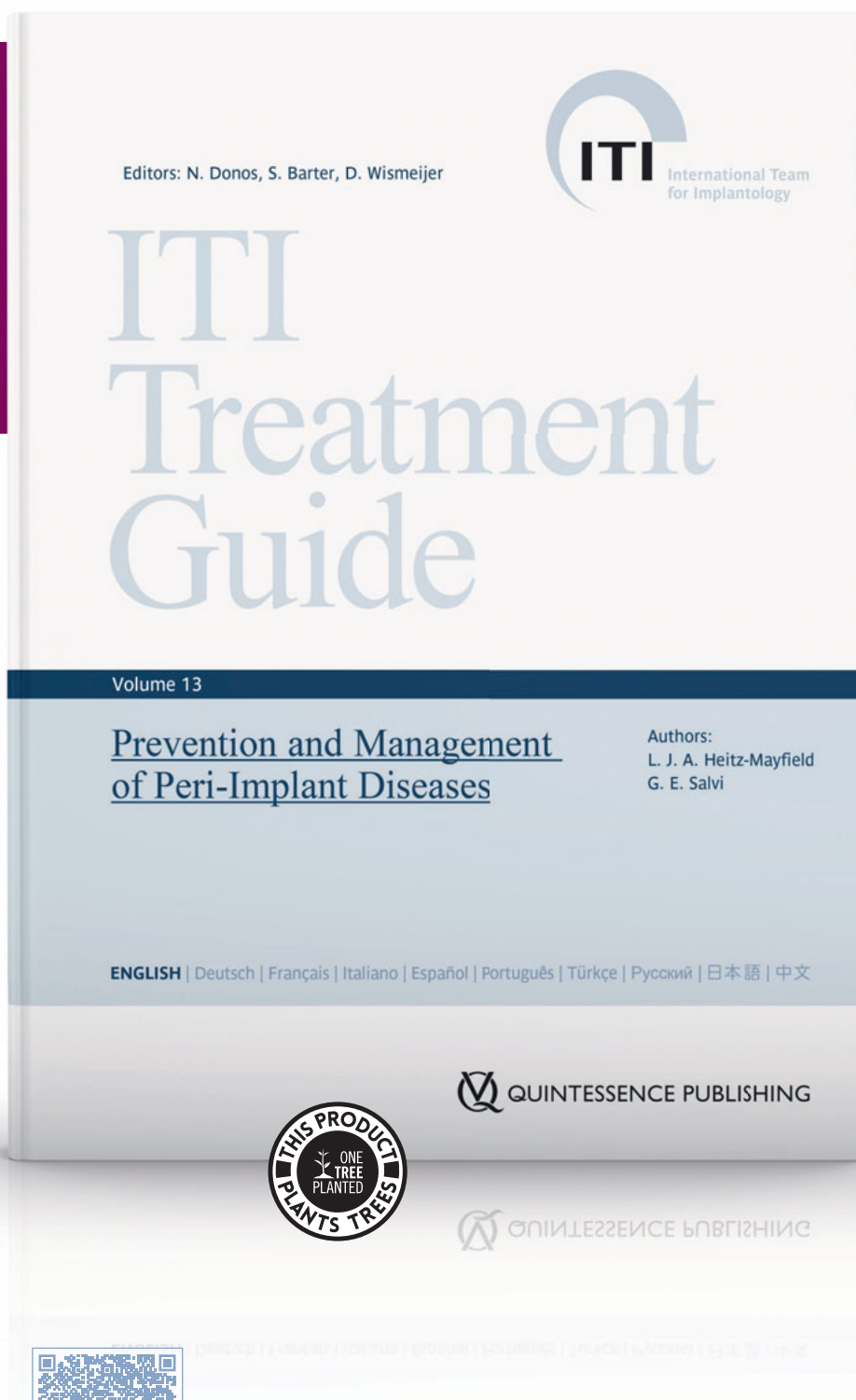
- Warnakulasuriya S, Kujan O, Aguirre-Urizar JM, et al. Oral potentially malignant disorders: A consensus report from an international seminar on nomenclature and classification, convened by the WHO Collaborating Centre for Oral Cancer. *Oral Dis* 2021;27:1862–1880.
- Chen QM. *Diseases of Oral Mucosa*, ed 5 [in Chinese]. Beijing: People's Medical Publishing House, 2020.
- He FQ, Wang HF, Xu CJ. Trace elements and oral submucosal fibrosis [in Chinese]. *Lin Chuang Kou Qiang Yi Xue Za Zhi* 2019;35:124–127.
- Gao YJ, Yin XM. Research progress on pathogenic factors of oral submucosal fibrosis [in Chinese]. *Zhongguo Yi Shi Za Zhi* 2015;17:1309–1313.
- Jian XC, Zhang Y. Research progress on chewing betel nut and oral submucosal fibrosis and oral cancer [in Chinese]. *Zhonghua Kou Qiang Yi Xue Yan Jiu Za Zhi (Dian Zi Ban)* 2011;5:229–234.
- Xiao YB, Yin XM, Gao YJ. Analysis of risk factors related to malignant transformation of oral submucosal fibrosis [in Chinese]. *Zhongguo Xian Dai Yi Xue Za Zhi* 2011;21:2648–2651.
- Gao YJ, Yin XM. Research progress on pathogenic factors of oral submucosal fibrosis [in Chinese]. *Zhongguo Shi Yong Kou Qiang Ke Za Zhi* 2011;4:68–72.
- Shih YH, Wang TH, Shieh TM, Tseng YH. Oral submucosal fibrosis: A review on etiopathogenesis, diagnosis, and therapy. *Int J Mol Sci* 2019;20:2940.
- Sharma A, Kumar R, Johar N, Sabir H. Oral submucous fibrosis: An etiological dilemma. *J Exp Ther Oncol* 2017;12:163–166.
- Arakeri G, Rai KK, Hunasgi S, Merx MAW, Gao S, Brennan PA. Oral submucous fibrosis: An update on current theories of pathogenesis. *J Oral Pathol Med* 2017;46:406–412.
- Pillai R, Balaram P, Reddiar KS. Pathogenesis of oral submucous fibrosis. Relationship to risk factors associated with oral cancer. *Cancer* 1992;69:2011–2020.
- Thomas G, Hashibe M, Jacob BJ, et al. Risk factors for multiple oral premalignant lesions. *Int J Cancer* 2003;107:285–291.
- Tang JQ, Jian XF, Gao ML, Ling TY, Zhang KH. Epidemiological study on oral submucosal fibrosis in Xiangtan, Hunan, China [in Chinese]. *Zhongguo Yi Shi Za Zhi* 2015;17:1290–1295.
- Du YX, Jian XC, Zhou T, et al. Clinical investigation and analysis of 123 cases of oral submucosal fibrosis in Haikou area [in Chinese]. *Zhongguo Yi Shi Za Zhi* 2015;17:1286–1289.
- Gao YJ, Ling TY, Liu L, Li WH, Li X. Epidemic trends of oral submucosal fibrosis in Hunan province: A retrospective study of 278 cases [in Chinese]. *Lin Chuang Kou Qiang Yi Xue Za Zhi* 2004;20:117–119.
- Pindborg JJ, Mehta FS, Gupta PC, Daftary DK. Prevalence of oral submucous fibrosis among 50,915 Indian villagers. *Br J Cancer* 1968;22:646–654.
- Xiao X, Wu YF, Peng JY, Xie D, Li M, Song XL. Clinical and pathological analysis of 74 cases of oral submucosal fibrosis coexisting with leukoplakia [in Chinese]. *Guo Ji Kou Qiang Yi Xue Za Zhi* 2015;42:273–275.
- Jian XC. Past, present and future of oral submucous fibrosis research in Chinese Mainland [in Chinese]. *Zhonghua Kou Qiang Yi Xue Yan Jiu Za Zhi (Dian Zi Ban)* 2008;2:545–552.
- Panchbhai A. Effect of oral submucous fibrosis on jaw dimensions. *Turk J Orthod* 2019;32:105–109.
- Kerr AR, Warnakulasuriya S, Mighell AJ, et al. A systematic review of medical interventions for oral submucous fibrosis and future research opportunities. *Oral Dis* 2011;17(suppl 1):42–57.
- Jian XC. Diagnostic criteria for oral submucosal fibrosis (trial draft) [in Chinese]. *Zhonghua Kou Qiang Yi Xue Za Zhi* 2009;44:130–131.
- Khanna JN, Andrade NN. Oral submucous fibrosis: A new concept in surgical management. Report of 100 cases. *Int J Oral Maxillofac Surg* 1995;24:433–439.
- Peng JY, Meng QY, Li JJ. Research progress in the diagnosis of oral submucosal fibrosis [in Chinese]. *Zhongguo Shi Yong Kou Qiang Ke Za Zhi* 2011;4:72–75.
- Jian XC, Zheng L. Research progress in oral submucosal fibrosis [in Chinese]. *Zhongguo Shi Yong Kou Qiang Ke Za Zhi* 2011;4:65–68.
- He H. Research progress in oral submucosal fibrosis [in Chinese]. *Lin Chuang Kou Qiang Yi Xue Za Zhi* 2002;18:234–236.
- Jian XC, Liu SF, Shen ZH, Yang YH. Histomorphological observation of epithelial tissue in cases of oral submucosal fibrosis [in Chinese]. *Hua Xi Kou Qiang Yi Xue Za Zhi* 1988;6:227–228.
- Yang B, Tang ZG. Meta analysis of salvia miltiorrhiza combined with triamcinolone acetonide acetate injection in the treatment of oral submucosal fibrosis [in Chinese]. *Zhong Cheng Yao* 2018;40:2165–2169.
- Cai XJ, Huang JH, Yao ZG, et al. Meta analysis of local injection of Danshen combined with triamcinolone acetonide in the treatment of oral submucosal fibrosis [in Chinese]. *Kou Qiang Ji Bing Fang Zhi* 2018;26:374–378.
- Deng T, Ling L. Evaluation of the efficacy of tanshinone combined with triamcinolone acetonide in the treatment of oral submucosal fibrosis [in Chinese]. *Shi Jie Zui Xin Yi Xue Xin Xi Wen Zhai* 2019;19:254–255.
- Lu C, Jian XC. Evaluation of the efficacy of triamcinolone acetonide combined with tanshinone solution in the treatment of submucosal fibrosis of the soft palate [in Chinese]. *Zhong Nan Da Xue Xue Bao (Yi Xue Ban)* 2019;44:801–804.
- Zhang YY. Evaluation of the efficacy of triamcinolone acetonide and tanshinone injection in the treatment of oral submucosal fibrosis [in Chinese]. *Quan Ke Kou Qiang Yi Xue Dian Zi Za Zhi* 2019;6:44,47.
- Zeng NB, Ye YY, Wang D, Ding DL. Analysis of the therapeutic effect of triamcinolone acetonide and tanshinone injection on oral submucosal fibrosis [in Chinese]. *Quan Ke Kou Qiang Yi Xue Dian Zi Za Zhi* 2019;6:53–54.
- Chen HX, Zhong ZQ. Study on the efficacy of Danshen injection combined with local injection of triamcinolone acetonide in the treatment of oral submucosal fibrosis [in Chinese]. *Shanxi Zhong Yi* 2019;40:97–99.
- Li JP, Chen ZQ, Tang ZG. Clinical study on the combination of tanshinone solution and triamcinolone acetonide in the treatment of oral submucosal fibrosis [in Chinese]. *Lin Chuang Jun Yi Za Zhi* 2018;46:1235–1236,1238.



35. Chen GY. Evaluation of the efficacy of triamcinolone acetonide and tanshinone injection in the treatment of oral submucosal fibrosis [in Chinese]. *Zhong Guo Xian Dai Yao Wu Ying Yong* 2018;12:1-3.
36. Jian XC, Zheng L, Zhu R, Wang BP, Zhou T, Du YX. Evaluation of the efficacy of triamcinolone acetonide and tanshinone injection in the treatment of oral submucosal fibrosis [in Chinese]. *Zhonghua Kou Qiang Yi Xue Za Zhi* 2017;52:16-21.
37. Su Y. Observation on the effect of combining Danshen injection and triamcinolone acetate injection in treating oral submucosal fibrosis [in Chinese]. *Dang Dai Yi Yao Lun Cong* 2016;14:94-95.
38. Gou RD. Analysis of the therapeutic effect of Danshen combined with local injection of triamcinolone acetonide on oral submucosal fibrosis [in Chinese]. *Quan Ke Kou Qiang Yi Xue Dian Zi Za Zhi* 2015;2:36-37.
39. Jiang LH, Dong Y, Xie LN, Yan CG, Jing XD. Clinical observation on the treatment of oral submucosal fibrosis with Danshen injection [in Chinese]. *Xin Zhong Yi* 2014;46:144-145.
40. Shi YZ. Clinical analysis of the combined treatment of salvia miltiorrhiza and prednisolone in 50 patients with oral submucosal fibrosis (OSF) [in Chinese]. *Qi Qi Ha Er Yi Xue Yuan Xue Bao* 2014;35:655-656.
41. Su W, Sun YM, Gan Q, Zheng HZ. Observation on the therapeutic effect of Danshen combined with prednisolone on oral submucosal fibrosis [in Chinese]. *Guangxi Yi Xue* 2013;35:921-922,925.
42. Yang F, Luo HP, Li Q, Xiong XY. Clinical study on the treatment of oral submucosal fibrosis by local injection of Danshen combined with triamcinolone acetonide [in Chinese]. *Guangdong Ya Bing Fang Zhi* 2010;18:206-209.
43. Zuo WX, Li XY, Cai GY, Liu K. Clinical study on the treatment of oral submucosal fibrosis with compound Danshen dropping pills and triamcinolone acetate [in Chinese]. *Shi Yong Kou Qiang Yi Xue Za Zhi* 2014;30:846-848.
44. Wang FF, Cai Y. Progress in drug therapy for oral submucosal fibrosis [in Chinese]. *Lin Chuang Kou Qiang Yi Xue Za Zhi* 2019;35:760-762.
45. Liu JL, Chen FM, Jiang L. Progress in drug treatment of oral submucosal fibrosis [in Chinese]. *Guo Ji Kou Qiang Yi Xue Za Zhi* 2017;44:325-331.
46. Yang CX, Jian XC, Pan YY, Qiu RN, Du YX. Progress in the treatment of oral submucosal fibrosis [J/OL] [in Chinese]. *Hai Nan Yi Xue* 2017;28:3376-3378.
47. Zhang SS, Ling TY. Research progress in the treatment of oral submucosal fibrosis [in Chinese]. *Kou Qiang Yi Xue* 2013;33:351-352.
48. Wu YF. Research progress in the treatment of oral submucosal fibrosis [in Chinese]. *Zhongguo Shi Yong Kou Qiang Ke Za Zhi* 2011;4:76-80.
49. Gao YJ. Research progress in the treatment of oral submucosal fibrosis [in Chinese]. *Lin Chuang Kou Qiang Yi Xue Za Zhi* 2004;20:253-254.
50. Guo JC, Xie H. Clinical research progress in the treatment of oral submucosal fibrosis with traditional Chinese medicine [in Chinese]. *Kou Qiang Yi Xue Yan Jiu* 2019;35:423-426.
51. Liu YP, Wen Q, Tan J. Experience in traditional Chinese medicine diagnosis and treatment of oral submucosal fibrosis [in Chinese]. *Hunan Zhong Yi Za Zhi* 2019;35:38-39,47.
52. Zou XH, Tao ZJ. Clinical diagnosis and treatment plan of traditional Chinese medicine for oral submucosal fibrosis [in Chinese]. *Quan Ke Kou Qiang Yi Xue Dian Zi Za Zhi* 2019;6:22.
53. Li YC, Tan J, Wen Q, Luo M, Tang Y. Clinical diagnosis and treatment plan of traditional Chinese medicine for oral submucosal fibrosis [in Chinese]. *Shi Yong Kou Qiang Yi Xue Za Zhi* 2018;34:838-840.
54. Cai H, Song LW. Clinical observation on the treatment of oral submucosal fibrosis with modified licorice xiexin and simiao yong'an tang [in Chinese]. *Zhonghua Zhong Yi Yao Xue Kan* 2016;34:1486-1488.
55. Sun Y. The therapeutic effect of combined traditional Chinese and Western medicine on oral submucosal fibrosis [in Chinese]. *Quan Ke Kou Qiang Yi Xue Dian Zi Za Zhi* 2016;3:44-45.
56. Wu YF, Peng JY, Que GY, Xu CJ, Yin XM. The therapeutic effect of combining traditional Chinese and Western medicine on oral submucosal fibrosis [in Chinese]. *Zhong Nan Da Xue Xue Bao (Yi Xue Ban)* 2010;35:358-364.
57. Li YC, Wu CH. Research progress of oral submucosal fibrosis in traditional Chinese and Western medicine [in Chinese]. *Zhongguo Zhong Yi Yao Xin Xi Za Zhi* 2003;10(S1):78-79.
58. Chen J, Jiang CH, Chen LC, et al. Modified nasolabial flap for repairing anterior buccal mucosal defect [in Chinese]. *Zhongguo Xiu Fu Chong Jian Wai Ke Za Zhi* 2015;29:582-585.
59. Jiang CH, Li C, Shi FQ, Chen XQ, Tang ZG, Jian XC. Application of xenogeneic acellular dermal matrix repair membrane in the surgical treatment of oral submucosal fibrosis [in Chinese]. *Shanghai Kou Qiang Yi Xue* 2011;20:273-277.
60. Zhang JG, Huang YQ, Tang Z, Liu Q. Application of buccal fat pad flap in the repair of defects after oral submucosal fibrosis surgery [in Chinese]. *Lin Chuang Kou Qiang Yi Xue Za Zhi* 2010;26:432-434.
61. Jiang C, Guo F, Li N, Huang P, Jian X, Munnee K. Tripaddled anterolateral thigh flap for simultaneous reconstruction of bilateral buccal defects after buccal cancer ablation and severe oral submucosal fibrosis release: A case report. *Microsurgery* 2013;33:667-671.
62. Mehrotra D, Pradhan R, Gupta S. Retrospective comparison of surgical treatment modalities in 100 patients with oral submucosal fibrosis. *Oral Surg Oral Med Oral Pathol Oral Radiol Endod* 2009;107:e1-e10.
63. Ramanujam S, Venkatachalam S, Subramanian M, Subramanian D. Platysma myocutaneous flap for reconstruction of intraoral defects following excision of oral submucosal fibrosis: A report of 10 cases. *J Pharm Bioallied Sci* 2015;7(suppl 2):S708-S711.
64. Kshirsagar R, Mohite A, Gupta S, Patankar A, Sane V, Raut P. Complications in the use of bilateral inferiorly based nasolabial flaps for advanced oral submucosal fibrosis. *Natl J Maxillofac Surg* 2016;7:115-121.
65. Kamath VV. Surgical Interventions in oral submucosal fibrosis: A systematic analysis of the literature. *J Maxillofac Oral Surg* 2015;14:521-531.
66. Rai A, Datarkar A, Rai M. Is buccal fat pad a better option than nasolabial flap for reconstruction of intraoral defects after surgical release of fibrous bands in patients with oral submucosal fibrosis? A pilot study: A protocol for the management of oral submucosal fibrosis. *J Craniomaxillofac Surg* 2014;42:e111-e116.
67. Kumar NG, Thapliyal GK. Free dermal fat graft for restoration of soft tissue defects in maxillofacial surgery. *J Maxillofac Oral Surg* 2012;11:319-322.
68. Prashanth R, Nandini GD, Balakrishna R. Evaluation of versatility and effectiveness of pedicled buccal fat pad used in the reconstruction of intra oral defects. *J Maxillofac Oral Surg* 2013;12:152-159.

69. Mokal NJ, Raje RS, Ranade SV, Prasad JS, Thatte RL. Release of oral submucous fibrosis and reconstruction using superficial temporal fascia flap and split skin graft—A new technique. *Br J Plast Surg* 2005;58:1055–1060.
70. Lambade P, Dawane P, Thorat P. Oral submucous fibrosis—A treatment protocol based on clinical study of 100 patients in central India. *Oral Maxillofac Surg* 2015;19:201–207.
71. Sharma M, Radhakrishnan R. Limited mouth opening in oral submucous fibrosis: Reasons, ramifications, and remedies. *J Oral Pathol Med* 2017;46:424–430.
72. Yao YB, Li LL, Shi LL, Ren YY. Analysis of the effect of hyperbaric oxygen combined with medication in the treatment of oral submucosal fibrosis [in Chinese]. *Shi Yong Yi Yao Za Zhi* 2020;37:130–131.
73. Zhao H, Wang YQ, Chen WM. Observation on the therapeutic effect of hyperbaric oxygen on oral submucosal fibrotic lesions [in Chinese]. *Lin Chuang Kou Qiang Yi Xue Za Zhi* 2016;32:346–348.
74. Zhou HW. Experience in the treatment of 20 cases of oral submucosal fibrosis with hyperbaric oxygen therapy [in Chinese]. *Xiang Nan Xue Yuan Xue Bao* 2006;8:58–59.
75. Li XM, Tang JQ, Ling TY, Long AF. Clinical observation on hyperbaric oxygen therapy for oral submucosal fibrosis [in Chinese]. *Zhonghua Kou Qiang Yi Xue Za Zhi* 1999;34:340.
76. Ling TY, Liu ZW, Tang JQ. Hyperbaric oxygen therapy for oral submucosal fibrosis: A case report [in Chinese]. *Zhongguo Xian Dai Yi Xue Za Zhi* 1997;7:51–52.
77. Shea BJ, Grimshaw JM, Wells GA, et al. Development of AMSTAR: A measurement tool to assess the methodological quality of systematic reviews. *BMC Med Res Methodol* 2007;7:10.
78. Higgins JPT, Altman DG, Gtzsche PC, et al. The Cochrane Collaboration's tool for assessing risk of bias in randomised trials. *BMJ* 2011;343(oct18 2):d5928.
79. Whiting PF, Rutjes AW, Westwood ME, et al. QUADAS-2: A revised tool for the quality assessment of diagnostic accuracy studies. *Ann Intern Med* 2011;155:529–536.
80. Schünemann HJ, Wiercioch W, Brozek J, et al. GRADE Evidence to Decision (EtD) frameworks for adoption, adaptation, and de novo development of trustworthy recommendations: GRADE-ADOLOPMENT. *J Clin Epidemiol* 2017;81:101–110.
81. Chen YL, Yao L, Susan N, et al. The necessity and precautions of GRADE application in system evaluation [in Chinese]. *Zhongguo Xun Zheng Yi Xue Za Zhi* 2013;13:1401–1404.
82. Deng T, Han F, Wang Y, Li BH, Jin YH, Wang XH. The application of EtD framework in the formulation of clinical practice guidelines [in Chinese]. *Zhongguo Xue Zheng Xin Xue Guan Yi Xue Za Zhi* 2019;11:516–520,525.

LATEST EVIDENCE-BASED INFORMATION



Nikolaos Donos | Stephen Barter
Daniel Wismeijer (Eds.)
Lisa J. A. Heitz-Mayfield | Giovanni E. Salvi

Prevention and Management of Peri-Implant Diseases


ITI Treatment Guide Volume 13

200 pages, 280 illus.
ISBN 978-1-78698-111-0

€86

Dental implants are used routinely throughout the world to replace missing teeth. With the broadening of treatment options and an increasing number of clinicians that provide implant therapy, it is important to ensure that the treatment methods used meet the highest clinical standards. The ITI Treatment Guide series is a compendium of evidence-based implant-therapy techniques in daily practice. Written by renowned clinicians and supported by contributions from expert practitioners, the ITI Treatment Guides provide a comprehensive overview of the various indicated treatment options. The management of different clinical situations is discussed with an emphasis on sound diagnostics, evidence-based treatment concepts, and predictable treatment outcomes with minimal risk to the patient. Volume 13 of the ITI Treatment Guide series provides clinicians with the latest evidence-based information on the prevention and management of peri-implant diseases. This information is based in part on the proceedings of the 6th ITI Consensus Conference held in Amsterdam in 2018, as well as on a review of the current literature. Seventeen clinical cases presented by experienced clinicians from all over the world illustrate the diagnosis and treatment of peri-implant diseases.



 QUINTESSENZ PUBLISHING

 QUINTESSENZ PUBLISHING



www.quint.link/iti13



books@quintessenz.de



+49 (0)30 761 80 667

 QUINTESSENZ PUBLISHING

A COMPREHENSIVE GUIDE



Konrad Wangerin
Caroline Fedder (Eds)

Optimizing Orthognathic Surgery

Diagnosis, Planning, Procedures

416 pages, 1,450 illus

ISBN 978-1-78698-121-9

€228

OPTIMIZING ORTHOGNATHIC SURGERY

Diagnosis • Planning • Procedures

KONRAD WANGERIN
CAROLINE FEDDER (EDS)

NEW

This book presents interdisciplinary treatment approaches for dysgnathia correction based on considerations of both orofacial function and facial esthetics. Written by international experts with over 30 years of surgical experience, valuable insights are shared through close collaboration with experts from various fields of dentistry and medicine. The integration of intraoral distraction surgery into orthognathic procedures is explored with a special focus on severe cases. The wealth of treatment strategies and solutions presented will navigate readers through the intricate pathways of managing complex craniofacial malformations.

QUINTESSENZ PUBLISHING



QUINTESSENZ PUBLISHING



